

**Alma Mater Studiorum – Università di Bologna**

**DOTTORATO DI RICERCA**

**INGEGNERIA ELETTROTECNICA**

Ciclo XX

Settore scientifico disciplinare di afferenza:  
**ING – INF/07 MISURE ELETTRICHE E ELETTRONICHE**

**DEVELOPMENT AND CHARACTERIZATION OF A  
DISTRIBUTED MEASUREMENT SYSTEM FOR  
THE EVALUATION OF VOLTAGE QUALITY  
IN ELECTRIC POWER NETWORKS**

**Presentata da: ELISA SCALA**

Coordinatore Dottorato

PROF. FRANCESCO NEGRINI

Relatore

PROF. LORENZO PERETTO

---

**Esame finale anno 2008**



<b>1. Introduction</b> .....	<b>1</b>
<b>2. Power quality in Electrical Systems</b> .....	<b>3</b>
<b>2.1. Introduction</b> .....	<b>3</b>
<b>2.2. Power Quality Degrading Phenomena</b> .....	<b>5</b>
<b>2.2.1. Steady state Voltage Characteristics</b> .....	<b>5</b>
<b>2.2.2. Transients</b> .....	<b>5</b>
<b>2.2.3. Harmonic Distortion</b> .....	<b>6</b>
<b>2.2.4. Short Duration Voltage Variations</b> .....	<b>7</b>
<b>2.3. Power Quality Evaluation</b> .....	<b>10</b>
<b>2.3.1. Research and Standardization Activity</b> .....	<b>11</b>
<b>2.3.2. Basic Definitions of Voltage Parameters</b> .....	<b>13</b>
<b>2.3.3. Overview of Power Quality Indices</b> .....	<b>15</b>
<b>2.3.4. Standard Measurement Methods of PQ Parameters</b> .....	<b>19</b>
<b>2.3.5. Non conventional Parameters for PQ measurement</b> .....	<b>28</b>
<b>2.4. European Scenario: Standard, Guides and PQ level</b> .....	<b>30</b>
<b>2.4.1. Reliability Regulation</b> .....	<b>34</b>
<b>2.4.2. Voltage Quality Regulation</b> .....	<b>37</b>
<b>2.4.3. Monitoring the Voltage Quality within EU</b> .....	<b>38</b>
<b>2.4.4. Minimum Standards</b> .....	<b>40</b>
<b>2.4.5. Incentive Schemes</b> .....	<b>42</b>
<b>References</b> .....	<b>44</b>
<b>3. Electromagnetic Transients in Power Distribution Networks</b> .....	<b>47</b>
<b>3.1. Transients</b> .....	<b>49</b>
<b>3.1.1. Lightning</b> .....	<b>51</b>
<b>3.1.2. Direct Flashes to Overhead Lines</b> .....	<b>52</b>
<b>3.1.3. Induced Overvoltages on Overhead Lines</b> .....	<b>53</b>
<b>3.1.4. Overvoltages caused by coupling with other systems</b> .....	<b>53</b>
<b>3.1.5. Lightning surges transferred from MV systems</b> .....	<b>54</b>
<b>3.1.6. Surge magnitude and propagation in MV systems</b> .....	<b>54</b>
<b>3.1.7. Surge transfer to the Low Voltage System</b> .....	<b>55</b>
<b>3.2. Transmission Lines</b> .....	<b>56</b>
<b>3.2.1. Travelling Waves</b> .....	<b>66</b>

3.2.2. Modal Transformation .....	67
3.3. Time Frequency Representation of Signals .....	69
3.3.1. The Wavelet Transform .....	71
3.3.2. The Discrete time Wavelet Transform .....	73
3.3.3. Filter Banks .....	75
3.3.4. Wavelets and Filter Banks .....	77
3.4. Fault Location Methods for Distribution Networks .....	80
3.4.1. Signal Analysis of Fundamental Frequency Components .....	82
3.4.2. Signal Analysis of High Frequency Components .....	83
3.4.3. Artificial Neural Network Techniques .....	87
3.5. Distributed Measurement System detecting Transient Disturbances and Method to locate the Transient Source .....	89
3.5.1. Procedure to locate the Source of a transient .....	90
3.6. Fault Location Method integrating the Distributed Measurement System and Wavelet Analysis .....	93
References .....	97
4. Analysis of the performance featured by the fault location method based on distributed simultaneous measurements - simulations of distribution networks in EMTP-RV environment .....	101
4.1. Implementation of an IEEE Std. test network affected by bolt faults .....	101
4.1.1. Experimental Results .....	105
4.1.1.1. Line to line short circuit .....	105
4.1.1.2. Line to ground short circuit .....	106
4.1.1.3. Insertion of capacitor bank .....	107
4.2. Implementation of a distribution network operating in actual conditions – variation of fault parameters .....	111
4.2.1. Improvements in the Procedure .....	111
4.2.2. Test conditions: non ideal faults and network elements .....	112
4.2.3. Models of Power Distribution and Measurement Systems .....	114
4.2.4. Simulation Results .....	119
4.2.4.1. Direct Lightning .....	120
4.2.4.2. Phase to ground short circuit – Transposed lines .....	121
4.2.4.3. Phase to ground short circuit – Untransposed lines .....	121
4.2.4.4. Phase to phase short circuit – Untransposed lines .....	126
4.2.4.5. Variations in the Network Topology .....	126

4.3. Implementation of a radial distribution network to test the version of the fault location procedure integrated with DWT analysis .....	129
References .....	132
5. The distributed measurement system for transients detection .....	133
5.1. The Voltage Transducer .....	135
5.2. The Event Detection Block .....	136
5.3. The GPS based device .....	139
5.3.1. What is GPS? .....	139
5.3.2. The GPS station .....	140
5.4. The DAQ board .....	142
5.5. The GSM protocol .....	144
5.5.1. The GPRS protocol .....	146
5.6. Metrologic characterization of the measurement system - The Supplement 1 to the G.U.M. ....	148
5.6.1. Main stages of uncertainty evaluation .....	149
5.6.2. Propagation of Distributions .....	150
5.6.3. Monte Carlo Approach to the propagation .....	152
5.7. Evaluation of the combined uncertainty on the position of the transient source .....	157
5.7.1. Metrological characterization of the voltage transducer .....	157
5.7.2. Metrological Characterization of the Event Detection Block..	160
5.7.3. Metrological Characterization of the GPS station .....	162
5.7.4. Monte Carlo Method to evaluate the combined uncertainty on the Fault Location .....	162
5.7.5. Experimental Results .....	163
5A. Appendix: Uncertainty Contribution of the Analog Conditioning Block in DSP- based Instruments .....	165
5A.1. The calibration Method .....	166
5A.2. Characterization Indices .....	167
5A.3. Application Example .....	170
5A.4. An Equipment for Voltage Transducers Calibration .....	173
5A.5. Uncertainty sources in the Equipment .....	176
References .....	183
6. Design and Characterization of an Electric field based Medium Voltage Transducer .....	185

<b>6.1. Voltage Transducers.....</b>	<b>185</b>
<b>6.2. Electric field strength meters .....</b>	<b>188</b>
6.2.1. Free body meter .....	189
6.2.2. Ground reference Type meter .....	191
6.2.3. Electro-optic meter .....	192
6.2.4. Calibration of Electric field strength meters .....	194
6.2.5. Main sources of measurement uncertainty .....	195
<b>6.3. The Voltage Transducer .....</b>	<b>197</b>
6.3.1. Operating principle .....	197
6.3.2. prototype realization .....	197
6.3.3. Experimental setup .....	200
6.3.3.1. voltage error .....	201
6.3.3.2. phase error .....	203
6.3.3.3. bandwidth .....	205
6.3.3.4. immunity to other electric field contributions .....	207
<b>References .....</b>	<b>209</b>
<b>7. Conclusions .....</b>	<b>211</b>

## 1. Introduction

The research activity carried out during the PhD course in Electrical Engineering belongs to the branch of electric and electronic measurements. The main subject of the present thesis is a distributed measurement system to be installed in Medium Voltage power networks, as well as the method developed to analyze data acquired by the measurement system itself and to monitor power quality. In chapter 2 the increasing interest towards power quality in electrical systems is illustrated, by reporting the international research activity inherent to the problem and the relevant standards and guidelines emitted. The aspect of the quality of voltage provided by utilities and influenced by customers in the various points of a network came out only in recent years, in particular as a consequence of the energy market liberalization. Usually, the concept of quality of the delivered energy has been associated mostly to its continuity. Hence the reliability was the main characteristic to be ensured for power systems. Nowadays, the number and duration of interruptions are the “quality indicators” commonly perceived by most customers; for this reason, a short section is dedicated also to network reliability and its regulation. In this contest it should be noted that although the measurement system developed during the research activity belongs to the field of power quality evaluation systems, the information registered in real time by its remote stations can be used to improve the system reliability too.

Given the vast scenario of power quality degrading phenomena that usually can occur in distribution networks, the study has been focused on electromagnetic transients affecting line voltages. The outcome of such a study has been the design and realization of a distributed measurement system which continuously monitor the phase signals in different points of a network, detect the occurrence of transients superposed to the fundamental steady state component and register the time of occurrence of such events. The data set is finally used to locate the source of the transient disturbance propagating along the network lines.

Most of the oscillatory transients affecting line voltages are due to faults occurring in any point of the distribution system and have to be seen before protection equipment intervention. An important conclusion is that the method can improve the monitored network reliability, since the knowledge of the location of a fault allows the energy manager to reduce as much as possible both the area of the network to be disconnected for protection purposes and the time spent by technical staff to recover the abnormal condition and/or the damage.

The part of the thesis presenting the results of such a study and activity is structured as follows: chapter 3 deals with the propagation of electromagnetic transients in power

systems by defining characteristics and causes of the phenomena and briefly reporting the theory and approaches used to study transients propagation. Then the state of the art concerning methods to detect and locate faults in distribution networks is presented. Finally the attention is paid on the particular technique adopted for the same purpose during the thesis, and the methods developed on the basis of such approach.

Chapter 4 reports the configuration of the distribution networks on which the fault location method has been applied by means of simulations as well as the results obtained case by case. In this way the performance featured by the location procedure firstly in ideal then in realistic operating conditions are tested.

In chapter 5 the measurement system designed to implement the transients detection and fault location method is presented. The hardware belonging to the measurement chain of every acquisition channel in remote stations is described. Then, the global measurement system is characterized by considering the non ideal aspects of each device that can concur to the final combined uncertainty on the estimated position of the fault in the network under test. Finally, such parameter is computed according to the Guide to the Expression of Uncertainty in Measurements, by means of a numeric procedure.

In the last chapter a device is described that has been designed and realized during the PhD activity aiming at substituting the commercial capacitive voltage divider belonging to the conditioning block of the measurement chain. Such a study has been carried out aiming at providing an alternative to the used transducer that could feature equivalent performance and lower cost. In this way, the economical impact of the investment associated to the whole measurement system would be significantly reduced, making the method application much more feasible.



## 2. Power quality in electrical systems

### 2.1. *Introduction*

Electrical energy is a product and, like any other product, should satisfy the proper quality requirements. If electrical equipment is to operate correctly, it requires electrical energy to be supplied at a voltage that is within a specified range around the rated value. A significant part of the equipment in use today, especially electronic and computer devices, requires good power quality (PQ). However, the same equipment often causes distortion of the voltage supply in the installation, because of its non-linear characteristics, i.e. it draws a non-sinusoidal current with a sinusoidal supply voltage. Thus, maintaining satisfactory PQ is a joint responsibility for the supplier and the electricity user.

All customers have to make sure that they obtain an electricity supply of satisfactory quality to avoid the high cost of equipment failures; electrical equipment must also be capable of functioning as required when small disturbances occur. Customers are granted to be safe only if the limits within which power quality may vary can be specified. According to the technical context, such limits should be fixed by standards, by the national regulator, by the customer by means of a power quality contract, by the manufacturer in a device manual or by the grid operator in a guideline. The defined limits must be meaningful, consistent and easy to compare to actual power quality levels. All these different limits have to be accomplished, on the one hand to prevent devices or installations from malfunctioning, on the other hand for clear communication about the quality of supply that is provided or demanded. The starting point for the definition of the supply-voltage quality is the set of limits defined by the National Regulator and to be met at the point of common coupling with the customer. At the moment, there is no standard for the current quality relevant to that point, in fact the main document dealing with requirements concerning the supplier's side is standard EN 50160 [1], which characterizes voltage parameters. This is a European standard on electrical energy in public distribution systems, completed in some regions or countries by other supplemental standards.

According to [1] the *supplier* is the party who provides electricity via a public distribution system, and the user or *customer* is the purchaser of electricity from a supplier. The user is entitled to receive a suitable quality of power from the supplier. In practice, the level of PQ is a compromise between user and supplier. Where the available PQ is not sufficient for the user's needs, PQ improvement measures are needed and a cost-benefit analysis should be carried out. However, the cost of poor PQ usually exceeds the cost of measures required for improvement - it is estimated that losses caused by power quality degradation cost EU industry and commerce about € 10 billion per annum.

The electric system, characterized in the past by an high level of vertical integration, is the subject of a recent liberalization process which separates the energy production, the management of the transmission network and the power distribution among a plurality of subjects. Beside the classic boundary between the distributor and the user (in high, medium or low voltage systems), all the other new boundaries must be taken into account. This applies in particular to voltage quality, which has to be defined, at least for the main parameters, not only at supply points to the end users, but also at the other boundaries. In facts, the final voltage quality depends on the operating conditions at all levels of the whole process.

However, electrical energy is a very specific product. The possibility for storing electricity in any significant quantity is very limited, so it is consumed at the same instant it is generated. Measurement and evaluation of the quality of the supplied power has to be made at the instant of its consumption. The measurement of PQ is complex, since the supplier and user, whose sensitive electrical equipment is also a source of disturbances, have different perspectives.

The interaction between voltage and current makes it hard to separate the customer as receiving and the network company as supplying a certain level of PQ. The voltage quality (for which the network is often considered responsible) and current quality (for which the customer is often considered responsible) are affecting each other by mutual interaction. The effects of insufficient PQ are normally expressed in terms of emission, immunity and compatibility. The emission is defined as the causal disturbance, such as the offset of a voltage from its nominal value. The immunity is the degree at which the equipment will be able to function as planned in spite of the emission. The compatibility level is the level at which the risk of the equipment malfunctioning is sufficiently low. On the user's side, it is the quality of power available to the user's equipment that is important. Correct equipment operation requires the level of electromagnetic influence on equipment to be maintained below certain limits. Equipment is influenced by disturbances on the supply and by other equipment in the installation, as well as itself influencing the supply. These problems are summarized in the EN 61000 series [7-15] of EMC standards, in which limits of conducted disturbances are characterized.

## **2.2. Power Quality degrading phenomena**

Power quality variations fall into two basic categories:

1. Disturbances. Disturbances are measured by triggering on an abnormality in the voltage or the current. Transient voltages may be detected when the peak magnitude exceeds a specified threshold. RMS voltage variations (e.g. sags or interruptions) may be detected when the RMS variation exceeds a specified level.

2. Steady State Variations. These include normal RMS voltage variations and harmonic distortion. These variations must be measured by sampling the voltage and/or current over time. The information is best presented as a trend of the quantity (e.g. voltage distortion) over time and then analyzed using statistical methods (e.g. average distortion level, 95% probability of not being exceeded).

In the past, measurement equipment has been designed to handle either the disturbances (e.g. disturbance analyzers) or steady state variations (e.g. voltage recorders, harmonics monitors). With advances in processing capability, new instruments have become available that can characterize the full range of power quality variations. The new challenge involves characterizing all the data in a convenient form so that it can be used to help identify and solve problems.

### **2.2.1. Steady State Voltage Characteristics**

There is no such thing as steady state on the power system. Loads are continually changing and the power system is continually adjusting to these changes. All of these changes and adjustments result in voltage variations that are referred to as long duration voltage variations. These can be undervoltages or overvoltages, depending on the specific circuit conditions. Characteristics of the steady state voltage are best expressed with long duration profiles and statistics. Important characteristics include the voltage amplitude and unbalance. Harmonic distortion is also a characteristic of the steady state voltage but this characteristic is treated separately because it does not involve variations in the fundamental frequency component of the voltage. Most end use equipment is not very sensitive to these voltage variations, as long as they are within reasonable limits.

### **2.2.2. Transients**

The term transients is normally used to refer to fast changes in the system voltage or current. Transients are disturbances, rather than steady state variations such as harmonic distortion or voltage unbalance. Disturbances can be measured by triggering on the abnormality involved. For transients, it could be the peak magnitude, the rate of rise, or just the change in the waveform from one cycle to the next. Transients can be divided into two sub-categories, impulsive transients and oscillatory transients, depending on

their characteristics. Transients are normally characterized by the actual waveform, although summary descriptors can also be developed (peak magnitude, primary frequency, rate-of rise, etc.). Figure 2-1 gives a capacitor switching transient waveform. This is one of the most important transients that is initiated on the utility supply system and can affect the operation of end user equipment. Transient problems are solved by controlling the transient at the source, changing the characteristics of the system affecting the transient or by protecting equipment so that it is not impacted. For instance, capacitor switching transients can be controlled at the source by closing the breaker contacts close to a voltage zero crossing. Magnification of the transient can be avoided by not using low voltage capacitors within the end user facilities. The actual equipment can be protected with filters or surge arresters.

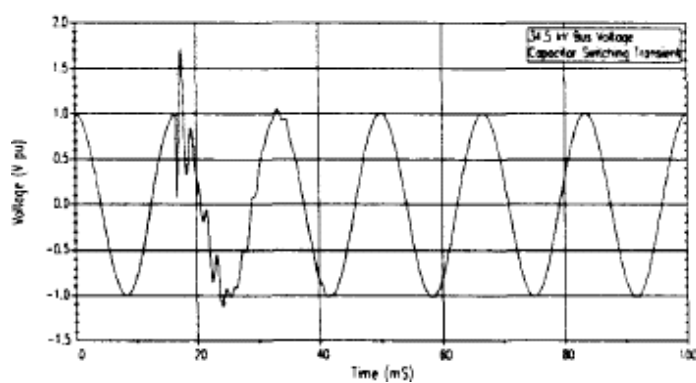


**Figure 2-1.** Disturbance due to a Capacitor switching.

### 2.2.3. Harmonic Distortion

Harmonic distortion of the voltage and current results from the operation of nonlinear loads and devices on the power system. The nonlinear loads that cause harmonics can often be represented as current sources of harmonics. The system voltage appears stiff to individual loads and the loads draw distorted current waveforms. Harmonic voltage distortion results from the interaction of these harmonic currents with the system impedance. The harmonic standard [4], has proposed two criteria for controlling harmonic levels on the power system. In the first case the end users must limit the harmonic currents injected onto the power system. In the second solution the power supplier will control the harmonic voltage distortion by making sure system resonant conditions do not cause excessive magnification of the harmonic levels. Harmonic distortion levels can be characterized by the complete harmonic spectrum with magnitudes and phase angles of each individual harmonic component. It is also common to use a single quantity, the *Total Harmonic Distortion*, as a measure of the magnitude of harmonic distortion. For currents, the distortion values must be referred to a constant base (e.g. the rated load current or demand current) rather than the fundamental component. This provides a constant reference while the fundamental can vary over a wide range. Harmonic distortion is a

characteristic of the steady state voltage and current. It is not a disturbance. Therefore, characterizing harmonic distortion levels is accomplished with profiles of the harmonic distortion over time (e.g. 24 hours) and statistics. Figure 2-2 illustrates some example current waveforms for different types of nonlinear loads [4].

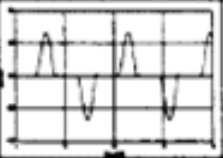
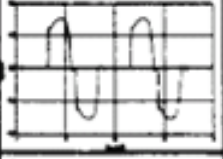
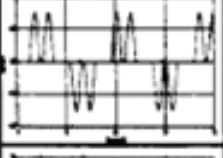
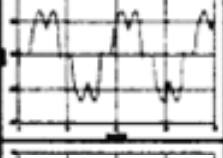
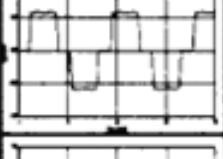
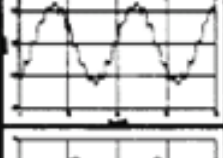
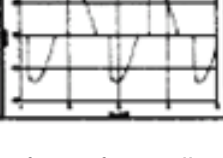
Type of load	Typical waveform	Current distortion
Single phase power supply		80% (high third)
Semiconverter		High 2nd, 3rd, 4th at partial loads
6 pulse converter, capacitive smoothing no series inductance		80%
6 pulse converter, capacitive smoothing with series inductance > 3%, or DC drive		40%
6 pulse converter, with large inductor for current smoothing		28%
12 pulse converter		15%
AC voltage regulator		Depends on firing angle

Figure 2-2. Current waveforms for nonlinear loads.

### 2.2.4. Short Duration Voltage Variations

Short duration voltage variations include variations in the fundamental frequency voltage that last less than one minute. These variations are best characterized by plots of the RMS voltage vs. time but it is often sufficient to describe them by a voltage magnitude and a duration that the voltage is outside of specified thresholds. It is usually not necessary to have detailed waveform plots since the RMS voltage magnitude is of

primary interest. The voltage variations can be a momentary low voltage (voltage sag), high voltage (voltage swell), or loss of voltage (interruption). Interruptions are the most severe in terms of their impacts on end users but voltage sags can be more important because they may occur much more frequently. A fault condition can cause a momentary voltage sag over a wide portion of the system even though no end users may experience an interruption. This is true for most transmission faults. Many end users have equipment that may be sensitive to these kinds of variations. Solving this problem on the utility system may be very expensive so manufacturers are developing ride through technologies with energy storage to handle these voltage variations on the end user side. A voltage dip is specified in terms of duration and retained voltage, usually expressed as the percentage of nominal RMS voltage remaining at the lowest point during the dip. A voltage dip means that the required energy is not being delivered to the load and this can have serious consequences depending on the type of load involved. Voltage sags - longer-term reductions in voltage - are usually caused by a deliberate reduction of voltage by the supplier to reduce the load at times of maximum demand or by an unusually weak supply in relation to the load. Motor drives, including variable speed drives, are particularly susceptible because the load still requires energy that is no longer available except from the inertia of the drive. In processes where several drives are involved, individual motor control units may sense the loss of voltage and shut down the drive at a different voltage level from its peers and at a different rate of deceleration resulting in complete loss of process control. Data processing and control equipment is also very sensitive to voltage dips and can suffer from data loss and extended downtime. There are two main causes of voltage dips: starting of large loads either on the affected site or by a consumer on the same circuit and faults on other branches of the network. When heavy loads are started, such as large drives, the starting current can be many times the normal running current. Since the supply and the cabling of the installation are dimensioned for normal running current the high initial current causes a voltage drop in both the supply network and the installation. The magnitude of the effect depends on how 'strong' the network is, that is, how low the impedance is at the point of common coupling (PCC) and on the impedance of the installation cabling. Dips caused by starting currents are characterized by being less deep and much longer than those caused by network faults - typically from one to several seconds or tens of seconds, rather than less than one second. The extent of a voltage dip at one site due to a fault in another part of the network depends on the topology of the network and the relative source impedances of the fault, load and generators at their common point of coupling. The duration of the dip depends on the time taken for the protective circuits to detect and isolate the fault and is usually of the order of a few hundred of milliseconds. Since faults

can be transitory, for example when caused by a tree branch falling onto a line, the fault can be cleared very soon after it has occurred. If the circuit were to be permanently disconnected by the protection equipment then all consumers on the circuit would experience a blackout until the line could be checked and reconnected. Autoreclosers can help to ease the situation, but also cause an increase in the number of dips. An autorecloser attempts to reconnect the circuit a short time (less than 1 second) after the protection equipment has operated. If the fault has cleared, the autoreclose will succeed and power is restored. Loads on that circuit experience a 100 % dip between disconnection and autoreclose while other loads see a smaller, shorter dip between the fault occurring and being isolated, as discussed above. If the fault has not cleared when the autorecloser reconnects, the protective equipment will operate again; the process can be repeated according to the program set for the particular autorecloser. Each time it reconnects the faulty line another dip results, so that other consumers can experience several dips in series. Utility performance in deregulated markets is partly - in some countries, such as UK, solely - judged on the average 'customer minutes lost', taking into account interruptions exceeding, typically, one minute. Minimizing this statistic has resulted in the widespread application of autoreclosers and an increase in the probability of dips. In other words, long term availability has been maximized but at the expense of quality.

Electronic equipment power supplies, such as those used in personal computers (PC) and programmable logic controllers (PLC) employ a reservoir capacitor to smooth out the peaks of the full wave rectified waveform, so they should be inherently resilient to short duration dips. The larger the capacitor, and the greater the difference between the stored capacitor voltage and the minimum required for the internal voltage converters to operate, the better the resilience will be. Designers will always try to reduce the size of the capacitor to a minimum to reduce size, weight and cost while ensuring that the charge stored is just sufficient at minimum voltage and maximum load. For good dip resilience a much larger capacitor is required, at least twice as large to enable the equipment to ride through one cycle, and 100 times as large if a one-second ride through was required. An alternative design strategy is to keep the minimum input voltage as low as possible to maximize the hold up time of the system. This is the approach taken, by default, in equipment designed to work over a wide range of voltage. For shallow dips, where there is considerable retained voltage, there are several established automatic voltage regulator technologies including electro-mechanical and electromagnetic devices. Because there is no need for stored energy, these devices can be used for long duration events such as under and over voltage. Where heavy loads or deep dips are concerned a Dynamic Voltage Restorer is used. This device is series coupled to the load and

generates the missing part of the supply; if the voltage dips to 70 %, the Restorer generates the missing 30 %. Voltage Restorers are normally expected to support the load for a short period and may use heavy-duty batteries, super capacitors or other forms of energy storage such as high-speed flywheels, hence they cannot be used to correct long term under and over voltage.

### **2.3. Power Quality Evaluation**

Systematic procedures for evaluating power quality concerns can be developed but they must include all levels of the system, from the transmission system to the end user facilities. Power quality problems show up as impacts within the end user facility but may involve interaction between all levels of the system. A consistent set of definitions for different types of power quality variations is the starting point for developing evaluation procedures. The definitions permit standardized measurements and evaluations across different systems. A data analysis system for power quality measurements should be able to process data from a variety of instruments and support a range of applications for processing data. With continuous power quality monitoring, it is very important to be able to summarize variations by means of time trends and statistics as well as characterize individual events. Many instruments and on-line monitoring equipment now include the capability to sample waveforms and perform FFT calculations. The capabilities of these instruments vary widely and the user must be careful that the accuracy and information obtained is adequate for the investigation. The following are some basic requirements for harmonic measurements used to investigate a problem:

- i. Capability to measure both voltage and current simultaneously so that harmonic power flow information can be obtained;
- ii. Capability to measure both magnitude and phase angle of each harmonic component;
- iii. Synchronization and a sampling rate matching the correct and accurate measurement of both harmonic components and transient phenomena;
- iv. Capability to characterize the statistical nature of harmonic distortion levels (harmonics levels change with changing load and/or system conditions).

Harmonic distortion is a continuous phenomena. It can be characterized at a point in time by the frequency spectrums of the voltages and currents. However, for proper representation, measurements over a period of time must be made and the statistical characteristics of the harmonic components and the total distortion determined.



### **2.3.1. Research and Standardization activity**

In the field of voltage quality, an intense research activity is conducted at international level; this work gives rise to very important pre-standardization documents, that are often taken as basis for the development of the international standards. In the following the most important working groups and standardization committees are reported, as well as their activity summarized.

*CIGRE/CIRED – Joint Working Group on Voltage Quality:* This Joint Working Group has carried out since many years research activity on the main aspects of voltage quality, i.e.: characterization of the various types of low frequency electromagnetic disturbances (harmonics, flicker, voltage dips and swells), criteria for their evaluation, measuring methods; assessment of criteria to establish adequate limits for these disturbances; mitigation methods, cost analysis for the various mitigation methods and/or for increasing the immunity of the sensible equipment. Recently some reorganization affected the activity of the group but two important items on the criteria for defining voltage quality held: characterization methods for assessing voltage quality; quality indices and measurement protocols. The final WG Report presents power quality data gathered from several different countries across a number of monitoring points over a number of years. The report provides guidance on the key factors that need to be considered when gathering and presenting data. In so doing the report considers the benefits of consistency but recognizes the inherent differences between different electrical systems and different power quality objectives. The report develops the case for a consistent set of power quality indices and objectives that can be seen as the outer envelope of performance for each power quality parameter. Relevant power quality indices are prerequisites for assessing site and system performance with respect to power quality. Such indices will eventually facilitate the task of system operators with their obligation to routinely report power quality performance. Some site indices have already been defined in standards, but others are still missing - in particular for high and extra-high voltage (HV-EHV) systems. Since system operators are at risk of being exposed to penalty payments for excursions in quality beyond the objective values it is important that the objectives are seen not only as achievable but also as being cost effective for all customers. This adds to the incentive for having well defined and recognized power quality indices. Optimizing the power quality performance of the electrical system is one of the roles of a system operator, the role of the regulator is to ensure that this is carried out in a cost-effective manner in that if customers expect power quality to be an intrinsic characteristic of the product they also want it at the lowest price. Recognizing that historically the electrical systems in different countries have been designed in different ways to cater for national/regional variations, such as different commercial or climatic

conditions, it is essential that any sets of internationally agreed power quality objectives also recognize these differences.

*IEEE Distribution Subcommittee - Working Group on Distribution Voltage Quality:* This Working Group carries out, mainly in USA, a research and development activity similar to that of the CIGRE/CIRED Working Group, with which it has a strict co-operation. The IEEE Subcommittee has prepared some important pre-standards, two of them appear particularly important:

- i. IEEE 1159 [2], which defines indices and criteria for the quality level of the electric energy;
- ii. IEEE 519 [4], regarding the criteria for checking the harmonics content.

Both the standards refer to a third document, the IEEE 1459 [3]. It lists the mathematical expressions that were used in the past, as well as new expressions, and explains the features of the new definitions.

The program of future work includes mainly the revision and possible extension of the above documents.

*EURELECTRIC/UNIPED and UIE Experts Groups:* In the field of voltage quality important pre-standardization activities are also conducted within EURELECTRIC (Union of the Electricity Industry) / UNIPED (International Union of Producers and Distributors of Electric Energy) and UIE (International Union for the Application of the Electricity). With reference to UNIPED, the activity has been carried out by the Expert Group "Characteristics of the product electricity and electromagnetic compatibility" of the Specific Committee on Standardization. With reference to UIE, the activity is carried out by Working Group "Power Quality", which, at present, in cooperation with the above CIGRE/CIRED Working Group, is preparing a Guide about the various aspects of voltage quality: types of disturbances and relevant standards; voltage dips and short interruptions; voltage distortion; voltage unbalance; flicker; transient and temporary overvoltages.

The real standardization activity is carried out at the international level by IEC, at the European level by CENELEC, at the national level by CEI.

*IEC Subcommittee "Electromagnetic compatibility - Low frequency phenomena":* This IEC Subcommittee has prepared a series of standards which are of interest for the definition of voltage quality. They can be classified as follows:

- ✓ series IEC 61000-2-x: standards for the definition of the electromagnetic environments and of the low frequency compatibility levels [7];
- ✓ series IEC 61000-3-x: standards for the limitation of the low frequency disturbances produced by the equipment connected to the distribution network [9];

- ✓ standards [13] and [14]: standards relating to the instrumentation and to the measuring techniques for the flicker and the harmonics;
- ✓ standards [12]: standards relating to the immunity of equipment to low frequency conducted disturbances. Within the Subcommittee, a specific Working Group on voltage quality was set up to prepare a standard defining detailed specifications for the instrumentation and the measuring methodologies. The work led to [15], which specifies these measuring aspects for the various parameters characterizing voltage quality.

*CENELEC - TC 210 "Electromagnetic compatibility"*: its activity in the field of voltage quality essentially consists in the transposition into European standards of the IEC standards described in the previous clause.

*CENELEC – BTTF 68-6 "Physical characteristics of electrical energy"*: an ad-hoc Task Force of the Bureau Technique prepared, on the basis of a document available within UNIPED, the standard [1], published in its first edition in 1994: presently this is the most important technical reference in Europe for the regulation of voltage quality supplied in medium and low voltage public distribution networks. This standard has also been adopted in Italy by the Italian Electrotechnical Committee as CEI 110-22. The standard EN 50160 was not specifically developed in relation to the European Directive 96/92/EC regarding the liberalization of the electric energy market, but it was conceived as a voluntary technical standard for the definition of voltage quality at the terminals of the energy supply to the medium and low voltage users, as a consequence of the European Directive 85/374/EEC, which considers the electrical energy as a product. The problem of voltage quality for the high voltage users and for the other points of energy exchange is outside the scope of EN 50160. Considering the particular importance of this standard, its content is reported in the following section.

### **2.3.2. Basic definitions of voltage parameters**

In standard [1] several voltage parameters are defined. In the following the most important ones are reported:

*Supply voltage* – the RMS value of the voltage at a given moment at the point of common coupling, measured over a given time interval.

*Nominal voltage of the system* ( $U_n$ ) – the voltage by which a system is designated or identified and to which certain operating characteristics are referred.

*Declared supply voltage* ( $U_c$ ) – is normally the nominal voltage  $U_n$  of the system. If, by agreement between the supplier and the user, a voltage different from the nominal voltage is applied to the terminal, then this voltage is the declared supply voltage  $U_c$ .

## 2. POWER QUALITY IN ELECTRICAL SYSTEMS

---

*Normal operating condition* – the condition of meeting load demand, system switching and clearing faults by automatic system protection in the absence of exceptional conditions due to external influences or major events.

*Voltage variation* – is an increase or decrease of voltage, due to variation of the total load of the distribution system or a part of it.

*Flicker* – impression of unsteadiness of visual sensation induced by a light stimulus, the luminance or spectral distribution of which fluctuates with time.

*Flicker severity* – intensity of flicker annoyance defined by the UIE-IEC flicker measuring method and evaluated by the following quantities: Short term severity ( $P_{st}$ ) measured over a period of ten minutes; Long term severity ( $P_{lt}$ ) calculated from a sequence of 12  $P_{st}$  – values over a two-hour interval.

*Supply voltage dip* – a sudden reduction of the supply voltage to a value between 90% and 1% of the declared voltage  $U_c$ , followed by a voltage recovery after a short period of time. Conventionally the duration of a voltage dip is between 10 ms and 1 min. The depth of a voltage dip is defined as the difference between the minimum RMS voltage during the voltage dip and the declared voltage. Voltage changes which do not reduce the supply voltage to less than 90% of the declared voltage  $U_c$  are not considered to be dips.

*Supply interruption* – is a condition in which the voltage at the supply terminals is lower than 1% of the declared voltage  $U_c$ . A supply interruption is classified as: prearranged in order to allow the execution of scheduled works on the distribution system, when consumers are informed in advance, or accidental, caused by permanent (a long interruption) or transient (a short interruption) faults, mostly related to external events, equipment failures or interference.

*Temporary power-frequency overvoltages* – have relatively long duration, usually of a few power frequency periods, and originate mainly from switching operations or faults, e.g. sudden load reduction, or disconnection of short circuits.

*Transient overvoltages* – are oscillatory or non-oscillatory, highly damped, short overvoltages with a duration of a few milliseconds or less, originating from lightning or some switching operations, for example at switch-off of an inductive current.

*Harmonic voltage* – a sinusoidal voltage with a frequency equal to an integer multiple of the fundamental frequency of the supply voltage. Harmonic voltages can be evaluated: individually by their relative amplitude  $U_h$  related to the fundamental voltage  $U_1$ , where  $h$  is the order of the harmonic Voltage Characteristics of Public Distribution Systems; globally, usually by the total harmonic distortion factor THD.

*Interharmonic voltage* – is a sinusoidal voltage with frequency between the harmonics, i.e. the frequency is not an integer multiple of the fundamental.

*Voltage unbalance* – is a condition where the RMS value of the phase voltages or the phase angles between consecutive phases in a three-phase system are not equal.

The standard [1] considers two groups of parameters characterizing voltage quality; for the first group limit values are indicated, whereas for the second only indicative values. Frequency, amplitude of the voltage (slow variations), rapid variations of the voltage, flicker (voltage fluctuations), harmonic distortions, interharmonics, three phase voltage unbalance and level of

communication signals injected on the network, are all parameters belonging to the first group. The second group includes the following other parameters: voltage dips and swells; short and long interruptions; transient and temporary overvoltages.

The standard does not contain detailed information on the instrumentation and on the measuring techniques to be adopted to assess the conformity of voltage quality. However, it gives general suggestions for the various parameters to be measured on the criteria for choosing the value (average value, RMS value, peak value, etc) that characterizes the parameter to be measured. Even the statistical method of evaluation is suggested, as far as the indication of the confidence level that a certain value is not exceeded (e.g.: 95%, 99%, 100%), the time interval necessary to obtain a single measurement (10 ms, 3 s, 10 s, 10 min.) and the observation period (one day, one week, one year).

It does not apply under abnormal operating conditions, such as:

- ✓ conditions arising as a result of a fault;
- ✓ in case of failure of a customer's installation or equipment to comply with the relevant standards or with the technical requirements for the connection of loads;
- ✓ in the event of the failure of a generator installation to comply with relevant standards or with the technical requirements for interconnection with an electricity distribution system;
- ✓ in exceptional situations outside the electricity supplier's control, in particular: exceptional weather conditions and other natural disasters, third party interference, actions of public authorities, industrial action (subject to legal requirements), power shortages resulting from external events.

Actually requirements are not particularly rigorous for the supplier. In fact the numerous situations in which the standard does not apply can excuse the majority of outages and voltage disturbance events that occur in practice. Thus, many suppliers interpret the requirements of EN 50160 as principally informative and claim no responsibility when the limits are exceeded. On the other hand, the consumer's point of view is usually totally different –regarding the limits given as requirements that must be guaranteed by the supplier. However, as mentioned before, for many consumers, even fulfilling the requirements of [1] does not assure a satisfactory level of PQ. In such cases the level of PQ required must be defined in a separate agreement between supplier and consumer.

### **2.3.3. Overview of power quality indices**

#### **Harmonic Components**

Obtaining harmonic indices consists of providing the spectrum of voltage or current over a given window of time; a site index from the spectra over a given period; and eventually a system index from the single site indices. Various methods for obtaining the spectrum

are discussed in the technical literature, but the method almost exclusively used in power quality monitoring is the Fourier transform. A number of international standard documents define the measurement process, including [13] and [15].

The method proceeds as follows:

- obtain the spectrum over a 10-cycle (50 Hz systems) or 12-cycle (60 Hz systems) window. The window shall be synchronized to the actual frequency during the measurement;
- the spectra (RMS) are combined to a spectrum over a 3-second interval (150 cycles for 50 Hz systems and 180 cycles for 60 Hz systems) and the so obtained values are referred to as "very short time" indices ( $U_{h,vs}$ );
- the 3-second values are combined to a 10-minute value and referred to as "short time" indices ( $U_{h,sh}$ );
- 3-second and 10-minute values are evaluated over a one-day or a one-week period depending on the index. The 95%, 99% or maximum values of the distributions are used as site-indices.

Other publications propose more specific indices such as:

- Technical report [11]:
  - The greatest 95 % probability daily value of  $U_{h,vs}$  (RMS value of individual harmonic components over "very short" 3 s periods);
  - The maximum weekly value of  $U_{h,sh}$  (RMS value of individual harmonics over "short" 10 min periods);
  - The maximum weekly value of  $U_{h,vs}$ . For measurements it refers to [13]. The minimum measurement period should be one week.
- Standard [15] also refers to [13] for measurements, more specifically to class 1, 10/12-cycle gapless harmonic sub-group measurement. The standard does not specify indices, but various indices are given as guidelines for contractual applications
  - The number, or percentage, of values during the interval that exceed contractual values might be counted;
  - The worst-case values might be compared to contractual values (the measurement interval might be different for this possibility, for example one year);
  - One or more 95 % (or other percentage) probability weekly values for 10-minute values, 95 % (or other percentage) probability daily values for 3-sec time interval values, expressed in percent, might be compared to contractual values.

A minimum assessment period of one week is recommended for 10-min values, and daily assessment of 3-sec values for at least one week. Standard [1], stipulates that during each period of one week, the percentile 95% of the 10- min mean RMS value ( $U_{h,sh}$ ) of each individual harmonic voltage is the quality index to be compared to the relevant

voltage characteristic. Other regional or national standards and guidelines also recommend indices that are often similar to those mentioned above.

### **Flicker**

The flickermeter algorithm as defined in [14] results in:

- a 10-minute “short-term flicker severity -  $P_{st}$ ”. This value is obtained from a statistical analysis of the “instantaneous flicker value” in a way which models incandescent lamps and our observation of light intensity variations.
- From the 10-minute value, a 2-hour “long-term flicker severity -  $P_{lt}$ ” is calculated.

Indices of flicker severity ( $P_{st}$  and  $P_{lt}$ ) are expressed in per unit of the irritability threshold of flicker, that is the level of flicker considered irritable by a significant portion of the people involved in the tests. Evaluation techniques might be agreed between parties: the number or percentage of values during the interval that exceed contractual values might be counted, as well as 99 % probability weekly values for  $P_{st}$ , or 95 % probability weekly value for  $P_{lt}$ , might be compared to contractual values.

### **Unbalance**

Only the fundamental components shall be used: all harmonic components should be eliminated by using DFT algorithm. The processing is defined similar as the above harmonic indices: from 10-cycle (50 Hz) and 12-cycle (60 Hz), to 3-second intervals, to 10-minute intervals. For unbalance also 2-hour values (obtained by combining 10-minute values) are used. The whole measurement and evaluation procedure is defined in detail in [15]. This standard suggests that 10-min and/or 2-hr values be assessed as follows:

- i. The number of values during the measurement interval that exceed contractual values might be counted;
- ii. the worst-case values might be compared to contractual values (the measurement interval might be different for this possibility, for example one year);
- iii. one or more 95 % (or other percentage) probability weekly values, NPS expressed as a percentage of PPS, might be compared to contractual values.

In standard EN 50160 the unbalance index is the 95 % of the 10-min mean RMS values of the negative phase sequence component of the supply voltage to be assessed during each period of one week.

The voltage limits set in ANSI Standard C84.1 at the point of use are at  $\pm 10\%$ , derating motor capacity at levels of unbalance greater than 1% and not exceeding 5%. The derating is based on the thermal effects on motors, and are therefore presumed to be related to long-time measurements rather than short-time measurements. The measurement specified is the difference between the average of the three phase magnitudes and the voltage that differs the most from that average, divided by the average.

### **Voltage Dips**

The first international definition and measurement method for the most common characterization of voltage dips in terms of magnitude and duration is provided in [15]. For the measurement of dips, such standard states that “the basic measurement of a voltage dip and swell shall be the value of the RMS voltage measured over one cycle and refreshed each half cycle”. From the RMS voltage as a function of time two basic characteristics can be determined:

- retained voltage or the dip depth;
- duration.

A voltage dip is characterized by a pair of data, either retained voltage and duration or depth and duration: the retained voltage is the lowest value measured on any channel during the dip; the depth is the difference between the reference voltage and the retained voltage expressed in % of the reference voltage; the duration of a voltage dip is the time difference between the beginning and the end of the voltage dip.

The choice of a dip threshold is essential for determining the duration of the event. This choice of threshold is also important for counting events, as events are only counted as voltage dips when the RMS voltage drops below the threshold. Dip threshold can be a percentage of either nominal or declared voltage, or a percentage of the sliding voltage reference, which takes into account the actual voltage level prior to the occurrence of a dip. The user shall declare the reference voltage in use.

Voltage dip envelopes may not be rectangular hence, for a given voltage dip, the measured duration depends on the selected dip-threshold value. The shape of the envelope may be assessed using several dip thresholds set within the range of voltage dip and voltage interruption threshold detection. A number of other characteristics for voltage dips are mentioned in an annex to [15] including phase angle shift, point-on-wave, three-phase unbalance, missing voltage and distortion during the dip. The use of additional characteristics and indices may give additional information on the origin of the event, on the system and on the effect of the dip on equipment. Even though several of these terms are used in the power-quality literature there is no consistent set of definitions.

Document [8] also refers to [15] for measurement, but introduces a number of additional recommendations for calculating voltage-dip indices. Recommended values are 90% and 91% for dip-start threshold and dip-end threshold, respectively, and 10% for the interruption threshold. Dips involving more than one phase should be designated as a single event if they overlap in time. The most commonly-referred to index is the System Average RMS variation Frequency Index or SARFI.



The term “RMS variation” is used in US literature to indicate all events in which the RMS voltage deviates significantly (typically seen as more than 10%) from its nominal value. This includes voltage dips, voltage swells and long interruptions.

The SARFI<sub>X</sub> index (where X is a number between 0 and 100%) gives the number of events per year with a duration between 0,5 cycle and 1 minute and a retained voltage less than X%. Thus SARFI<sub>70</sub> gives the number of events with retained voltage less than 70%. Strictly speaking, SARFI values are obtained as a weighted average over all monitor locations within a supply network or within part of the supply network. However the term is also used to refer to the event frequency at one location. By using the weighting factors, more weight can be given to location with more – or more important – load. The weighting factors are in most cases taken to be equal for all locations.

Indices used for transmission interruption reporting differ significantly from utility to utility.

The indices used can however be divided into the following categories:

- Number of events: actual number of events and the average number of events over the reporting period, i.e. the frequency of events;
- Duration of events: average total duration of events over the reporting period and average time to restore supply per interruption at each supply point. The availability of the supply is the converse of the duration and it gives an indication of the relative risk of interruptions;
- Severity of events: severity of the interruption events over the reporting period (i.e. the size of load affected) and indices estimating the cost impact per event.

### **2.3.4. Standard Measurement methods of PQ parameters**

#### **Requirements of EN 50160**

The correct operation of electrical equipment requires a supply voltage that is as close as possible to the rated voltage. Even relatively small deviations from the rated value can cause operation at reduced efficiency, or higher power consumption with additional losses and shorter service life of the equipment. Sometimes prolonged deviations can cause operation of protection devices, resulting in outages. Of course, the correct operation of equipment also depends on many other factors, such as environmental conditions and proper selection and installation. Investigation of the independent influence of each supply voltage parameter on equipment operation is easily performed, but when parameters vary simultaneously the situation is much more complex. In some cases, after detailed analysis of the effects of each of the different voltage parameters, results can be superimposed in order to estimate the total influence of many parameters. The increased concern for power quality has resulted in significant advances in monitoring equipment that can be used to characterize disturbances and power quality

variations. In particular, measurement and testing of supply voltage quality according to EN 50160 requires specialized apparatus and measuring methods monitoring, continuously over 7 days, the following parameters:

- ✓ voltage in three phases
- ✓ frequency
- ✓ total harmonic distortion factor  $THD_U$
- ✓ voltage unbalance factor, which is a multiple of positive and negative sequence voltage components
- ✓ fast and slow voltage variations, which are defined as short term ( $P_{st}$ ) and long term ( $P_{lt}$ ) flicker severity factors.

This arrangement also enables measurement of voltage dips and outages, its frequency and duration.

The measured parameters are processed and recorded as 10 minute time-segments (1008 segments over 7 days). For each segment the mean value of the measured parameter is calculated. After the 7-day recording period a so-called “ordered diagram” is produced, which shows the sum of the duration of a given distortion level in the observed time period. (for frequency measurement, the duration of each single segment is 10 seconds).

### **Requirements of IEC 61000-4 series**

Methods for measurement and interpretation of results for power quality parameters in 50/60 Hz a.c. power supply systems are defined in [15]. Measurement methods are described for each relevant type of parameter in terms that will make it possible to obtain reliable, repeatable and comparable results regardless of the compliant instrument being used and regardless of its environmental conditions. This standard addresses methods for measurements carried out at the monitored point of the system.

Measurement of parameters covered by this standard is limited to those phenomena that can be conducted in a power system. These include the voltage and/or current parameters, as appropriate. The power quality parameters considered in this standard are power frequency, magnitude of the supply voltage, flicker, supply voltage dips and swells, voltage interruptions, transient voltages, supply voltage unbalance, voltage and current harmonics and interharmonics, mains signalling on the supply voltage and rapid voltage changes. Depending on the purpose of the measurement, all or a subset of the phenomena on this list may be measured. The effects of transducers being inserted between the power system and the instrument are acknowledged but not addressed in detail in this standard. Precautions on installing monitors on live circuits are addressed.

Measurements can be performed on single-phase or polyphase supply systems. Depending on the context, it may be necessary to measure voltages between phase

conductors and neutral (line-to-neutral) or between phase conductors (line-to-line) or between neutral and earth. The basic measurement time interval for parameter magnitudes (supply voltage, harmonics, interharmonics and unbalance) shall be a 10-cycle time interval for 50 Hz power system or 12-cycle time interval for 60 Hz power system. Measurement time intervals are aggregated over 3 different time intervals. The aggregation time intervals are: 3-s interval (150 cycles for 50 Hz nominal or 180 cycles for 60 Hz nominal), 10-min interval, 2-h interval.

Aggregations are performed by using the square root of the arithmetic mean of the squared input values. Three categories of aggregation are necessary:

- i. Cycle aggregation - The data for the 150/180-cycle time interval shall be aggregated from fifteen 10/12-cycle time intervals. This time interval is not a "time clock" interval; it is based on the frequency characteristic.
- ii. From cycle to time-clock aggregation: The 10-min value shall be tagged with the absolute time. The time tag is the time at the end of the 10-min aggregation. If the last 10/12-cycle value in a 10-min aggregation period overlaps in time with the absolute 10-min clock boundary, that 10/12-cycle value is included in the aggregation for this 10-min interval. On commencement of the measurement, the 10/12-cycle measurement shall be started at the boundary of the absolute 10-min clock, and shall be re-synchronized at every subsequent 10-min boundary.
- iii. Time-clock aggregation: The data for the "2-h interval" shall be aggregated from twelve 10-min intervals.

During a dip, swell, or interruption, the measurement algorithm for other parameters (for example, frequency measurement) might produce an unreliable value. The flagging concept therefore avoids counting a single event more than once in different parameters (for example, counting a single dip as both a dip and a frequency variation) and indicates that an aggregated value might be unreliable. Flagging is only triggered by dips, swells, and interruptions. The detection of dips and swells is dependent on the threshold selected by the user, and this selection will influence which data are "flagged".

**Table 2-1.** Standard measurement methods of the voltage quality parameters.

Parameter	Supply voltage characteristics according to EN 50160	Low voltage characteristics according to EMC standard EN 61000	
		EN 61000-2-2	Other parts
Power frequency	LV, MV: mean value of fundamental measured over 10 s $\pm 1\%$ (49.5 - 50.5 Hz) for 99.5% of week -6%/+4% (47- 52 Hz) for 100% of week	2%	
Voltage magnitude variations	LV, MV: $\pm 10\%$ for 95% of week. mean 10 minutes rms values		$\pm 10\%$ applied for 15 minutes
Rapid voltage changes	LV: 5% normal 10% infrequently $P_{It} \leq 1$ for 95% of week  MV: 4% normal 6% infrequently $P_{It} \leq 1$ for 95% of week	3% normal 8% infrequently $P_{st} < 1.0$ $P_{It} < 0.8$	3% normal 4% maximum $P_{st} < 1.0$ $P_{It} < 0.65$ (EN 61000-3-3) 3% (IEC 61000-2-12)
Supply voltage dips	Majority: duration <1s, depth <60%. Locally limited dips caused by load switching on: LV: 10 - 50%, MV: 10 - 15%	urban: 1 - 4 months	up to 30% for 10 ms up to 60% for 100 ms (EN 61000-6-1, 6-2) up to 60% for 1000 ms (EN 61000-6-2)
Short interruptions of supply voltage	LV, MV: (up to 3 minutes) few tens - few hundreds/year Duration 70% of them < 1 s		95% reduction for 5 s (EN 61000-6-1, 6-2)
Long interruption of supply voltage	LV, MV: (longer than 3 minutes) <10 - 50/year		
Temporary, power frequency overvoltages	LV: <1.5 kV rms  MV: $1.7 U_c$ (solid or impedance earth) $2.0 U_c$ (unearthed or resonant earth)		
Transient overvoltages	LV: generally < 6kV, occasionally higher; rise time: ms - $\mu$ s.  MV: not defined		$\pm 2$ kV, line-to-earth $\pm 1$ kV, line-to-line $1.2/50(8/20)$ Tr/Th $\mu$ s (EN 61000-6-1, 6-2)
Supply voltage unbalance	LV, MV: up to 2% for 95% of week, mean 10 minutes rms values, up to 3% in some locations	2%	2% (IEC 61000-2-12)
Harmonic voltage	LV, MV	6%-5 <sup>th</sup> , 5%-7 <sup>th</sup> , 3.5%-11 <sup>th</sup> , 3%-13 <sup>th</sup> , THD <8%	5% 3 <sup>rd</sup> , 6% 5 <sup>th</sup> , 5% 7 <sup>th</sup> , 1.5% 9 <sup>th</sup> , 3.5% 11 <sup>th</sup> , 3% 13 <sup>th</sup> , 0.3% 15 <sup>th</sup> , 2% 17 <sup>th</sup> (EN 61000-3-2)
Interharmonic voltage	LV, MV: under consideration	0.2%	

### Power frequency

The frequency reading shall be obtained every 10-s. As power frequency may not be exactly 50 Hz or 60 Hz within the 10-s time clock interval, the number of cycles may not be an integer number. The fundamental frequency output is the ratio of the number of

integral cycles counted during the 10-s time clock interval, divided by the cumulative duration of the integer cycles. Before each assessment, harmonics and interharmonics shall be attenuated to minimize the effects of multiple zero crossings.

The measurement time intervals shall be non-overlapping. Individual cycles that overlap the 10-s time clock are discarded. Each 10-s interval shall begin on an absolute 10-s time clock,  $\pm 20$  ms for 50 Hz or  $\pm 16,7$  ms for 60 Hz.

#### **Magnitude of the supply voltage**

The measurement shall be the RMS value of the voltage magnitude over a 10-cycle time interval for 50 Hz power system or 12-cycle time interval for 60 Hz power system. Every 10/12-cycle interval shall be contiguous with, and not overlap, adjacent 10/12-cycle intervals.

#### **Classes of measurement performance**

For each parameter measured, two classes of measurement performance are defined.

##### *– Class A performance*

This class of performance is used where accurate measurements are necessary, for example, for contractual applications, verifying compliance with standards, resolving disputes, etc. Any measurements of a parameter carried out with two different instruments complying with the requirements of class A, when measuring the same signals, will produce matching results within the specified uncertainty. To ensure that matching results are produced, class A performance instrument requires a bandwidth characteristic and a sampling rate sufficient for the specified uncertainty of each parameter.

##### *– Class B performance*

This class of performance may be used for statistical surveys, trouble-shooting applications, and other applications where low uncertainty is not required.

For each performance class the range of influencing factors that shall be complied with is specified in [15]. Users shall select the class of measurement performance taking account of the situation of each application case. A measurement instrument may have different performance classes for different parameters. The instrument manufacturer should declare influence quantities which are not expressly given and which may degrade performance of the instrument.

#### **Voltage Harmonics**

Table 2-2: provides a summary comparison of harmonic indices between various standards and guidelines. It shows that in most cases the reference standard to perform harmonic measurements is [13]. This part of IEC 61000 is applicable to instrumentation intended for measuring spectral components in the frequency range up to 9 kHz which are superimposed on the fundamental of the power supply systems at 50 Hz and 60 Hz.

For practical considerations, this standard distinguishes between harmonics, interharmonics and other components above the harmonic frequency range, up to 9 kHz. This standard defines the measurement instrumentation intended for testing individual items of equipment in accordance with emission limits given in certain standards (for example, harmonic current limits as given in [10]) as well as for the measurement of harmonic currents and voltages in actual supply systems. Instrumentation for measurements above the harmonic frequency range, up to 9 kHz is tentatively defined. Practically, the most common index for harmonic voltage is the so-called short time or 10-min value ( $U_{h,sh}$ ). It is used mainly for voltage characteristics and the level of harmonics to be compared with the objectives is usually the value corresponding to 95% probability of weekly statistics.

Instruments for the harmonic and interharmonic emission measurement or for measurements above the harmonic frequency range up to 9 kHz are considered in the IEC standard. Strictly speaking, harmonic measurements can be performed only on a stationary signal; fluctuating signals cannot be described correctly by their harmonics only. However, in order to obtain results that are inter-comparable, a simplified and reproducible approach is given for fluctuating signals. Two classes of accuracy (I and II) are considered, to permit the use of simple and low-cost instruments, consistent with the requirements of the application. For emission tests, the upper class I is required if the emissions are near to the limit values.

New designs of instrument are likely to use the discrete Fourier transform (DFT), normally using a fast algorithm called fast Fourier transform (FFT). Therefore the standard considers only this architecture but does not exclude other analysis principles. The main instrument for harmonic frequency measurements comprises:

- input circuits with anti-aliasing filter;
- A/D-converter (including sample-and-hold unit);
- synchronization and window-shaping unit;
- DFT-processor providing the Fourier coefficients  $a_m$  and  $b_m$ .

The instrument is complemented by the special parts devoted to current assessment and/or voltage assessment. For full compliance with this standard, the window width shall be 10 (50 Hz systems) or 12 (60 Hz systems) periods with rectangular weighting. Hanning weighting is allowed only in the case of loss of synchronization. This loss of synchronization shall be indicated on the instrument display and the data so acquired shall be flagged. The time window shall be synchronized with each group of 10 or 12 cycles according to the power system frequency of 50 Hz or 60 Hz. The time between the leading edge of the first sampling pulse and the leading edge of the  $(M+1)^{th}$  sampling

**Table 2-2.** Summary comparison of harmonics indices between different standards and reference documents.

Harmonic voltage indices	Standard /document	Status	Purpose	Very short time indices	Short time indices	Other indices	Period for statistical assessment	Measurement method
International standard or guidelines	IEC 61000-3-6	Technical report type	Indicative planning levels for emission limits	$U_{h,vs}$ 95% daily	$U_{h,s}$ max. weekly	$U_{h,vs}$ max. weekly	One week minimum	IEC 61000-4-7
	IEC 61000-4-30	International Std.	Power quality measurement methods	$U_{h,vs}$ X% as agreed	$U_{h,s}$ X% as agreed		At least one week or more	IEC 61000-4-7
Regional or national standards and guidelines	EN 50160	European Std.	Supply voltage characteristics for public networks		$U_{h,s} +$ THD 95% weekly		One week	IEC 61000-4-7
	ANSI/IEEE 519	ANSI std. recommended practice	Emission limits and system design methods			95% (no definite indices)	Undefined	No specific method
	NRS 048-2	South African Std.	Minimum Std. used by the regulator		$U_{h,s} +$ THD 95% weekly		One week min.	Specified method
	EDF Emeraude Contract	(France) PQ contract	Supply voltage characteristic		$U_{h,s} +$ THD max		At least one week or more	IEC 61000-4-7
	ER G5/4	UK National Std.	Planning levels for controlling emissions			$U_{h1 \min} +$ THD 95% weekly	One week	Specified method
	H. Q. Voltage Characteristics	Voluntary (Quebec)	Supply voltage characteristic		$U_{h,s} +$ THD 95% weekly		One week	IEC 61000-4-7

pulse (where  $M$  is the number of samples) shall be equal to the duration of the specified number of cycles of the power system, with a maximum permissible error of  $\pm 0,03\%$ .

Instruments including a phase-locked loop or other synchronization means shall meet the requirements for accuracy and synchronization for measuring at any signal frequency within a range of at least  $\pm 5\%$  of the nominal system frequency. However, for instruments having integrated supply sources, so that the source and measurement systems are inherently synchronized, the requirement for a working input frequency range does not apply, provided the requirements for synchronization and frequency accuracy are met.

The output shall provide the individual coefficients  $a_m$  and  $b_m$  of the DFT, for the current or voltage, i.e. the value of each frequency component calculated. A further output, not necessarily from the DFT, shall provide the active power  $P$  evaluated over the same time window used for the harmonics. For the harmonic emission measurements according to [10], this power shall not include the d.c. component.

**Flicker**

The minimum measurement period should be one week (see [14]). For flicker, indices should be: 1.  $P_{st}$  99% weekly; 2.  $P_{lt}$  99% weekly. Standard [15] also refers to standard [14] for flicker measurement. Voltage dips, swells, and interruptions shall cause  $P_{st}$  and  $P_{lt}$

**Table 2-3.** summary comparison of flicker indices between different standards and reference documents

Flicker indices	Standard /document	Status	Purpose	Short time indices	Long time indices	Period for statistical assessment	Measurement method
International standard or guidelines	IEC 61000-3-7	Technical report type	Indicative planning levels for emission limits	$P_{st}$ 99% weekly	$P_{lt}$ 99% weekly	One week minimum	IEC 61000-4-15
	IEC 61000-4-30	International Std.	Power quality measurement methods	$P_{st}$ 99% weekly or X% as agreed	$P_{lt}$ 95% weekly or X% as agreed	At least one week or more as agreed	IEC 61000-4-15
Regional/national standards and guidelines	EN 50160	European Std.	Supply voltage characteristics for public networks		$P_{lt}$ 95% weekly	One week	IEC 61000-4-15
	NRS 048-2	South African Std.	Minimum Std. used by the regulator		$P_{st}$ 95% weekly	One week min.	IEC 61000-4-15
	EDF Emeraude Contract – A2	(France) PQ contract	Supply voltage characteristic		$P_{lt}$ no further specification	At least one week or more	IEC 61000-4-15
	ER P28	UK National Std.	Planning levels for controlling emissions	$P_{st}$ no further specification	$P_{lt}$ no further specification	Sufficient to capture full operating cycle of load	IEC 868
	H. Q. Voltage Characteristics	Voluntary (Quebec)	Supply voltage characteristic		$P_{lt}$ 95% weekly	One week	IEC 61000-4-15

output values to be flagged so that they can later be removed from statistics.  $P_{st}$  or  $P_{lt}$  might be considered. The minimum assessment period should be one week.

The minimum measurement period should be one week (see [14]). For flicker, indices should be: 1.  $P_{st}$  99% weekly; 2.  $P_{lt}$  99% weekly. Standard [15] also refers to standard [14] for flicker measurement. Voltage dips, swells, and interruptions shall cause  $P_{st}$  and  $P_{lt}$

Table 2-3 provides a summary comparison of flicker indices between various standards and guidelines. The most common reference for flicker measurement is basically standard [14]. The 95% or 99% weekly values of  $P_{st}$  or  $P_{lt}$  indices are mostly in use. Considering that  $P_{lt}$  and  $P_{st}$  values are often correlated by a definite or quasi-constant factor related to the characteristics of the disturbing process, it may be questioned whether it is redundant specifying both indices.

### Unbalance

Table 2-4 summarises the indices relevant to negative sequence voltage unbalance factor ( $U_{neg}$ ). 10-min values are most commonly in use. Although different equations may be used for calculating voltage unbalance factor, results should be similar for a given integration time provided they consider negative sequence voltage.

### Voltage dips

Various methods for reporting dips or sags have been proposed in literature. They can be classified in two categories: methods to characterize site or system performance as such, and methods most suitable to estimate the compatibility between equipment and supply.

Magnitude-duration table: Site performance as well as system performance are often described in the form of a voltage-dip table. Different table formats are discussed in [5]



but only the so-called density table is commonly used. The columns of the table represent ranges of voltage-dip duration; the rows represent ranges of retained voltage. The choice

**Table 2-4.** summary comparison of flicker indices between different standards and reference documents.

Voltage unbalance indices	Standard /document	Status	Purpose	Very short time indices	Short time indices	Long time indices	Period for statistical assessment
International standard or guidelines	IEC 61000-4-30	International Std.	Power quality measurement methods		$U_{neg,s}$ 95% weekly or as agreed	$U_{neg,l}$ 95% weekly or as agreed	One week minimum
	Cigré 1992 paper 36-203	Cigré 36.05 work	Assessing voltage quality in relation to harmonics, flicker and unbalance	$U_{neg,vs}$ 95% daily	$U_{neg,s}$ max. weekly		A few days including a week end
Regional or national standards and guidelines	EN 50160	European Std.	Supply voltage characteristics for public networks		$U_{neg,s}$ 95% weekly		One week
	NRS 048-2	South African Std.	Minimum Std. used by the regulator		$U_{neg,s}$ 95% daily		One week min.
	EDF Emeraude Contract – A2	(France) PQ contract	Supply voltage characteristic		$U_{neg,s}$ no further specification		At least one week or more
	ER P29	UK National Std.	Planning levels for controlling emissions		Max. of negative sequence measured over 1 minute		Sufficient to represent effect on rotating plant
	H. Q. Voltage Characteristics	Voluntary (Quebec)	Supply voltage characteristic			$U_{neg,l}$ 95% weekly	One week

of the magnitude and duration ranges for voltage-dip tables is a point of discussion. Different publications use different values.

*Voltage-sag coordination chart:* A method for reporting site information from event magnitude and duration is described in [5] and [6]. The method results in the so-called “voltage sag coordination chart”. An example of such a chart is shown in Figure 2-3. This figure is the result of monitoring from 6 years at 20 HV-sites. The chart, as defined in these standards, contains the performance of the supply at a given site, and the voltage tolerance of one or more devices. For the purpose of this document only the supply performance part of the chart is of relevance. The chart gives the number of events per year (sags and interruptions) as a function of the severity of the event. For the example shown here there is on average 1 event per year dropping the voltage below 50% for 100 ms or longer. There is also on average 1 event per year more severe than 80%, 80 ms and on average 0.1 event per year below 70% for longer than 500 ms.

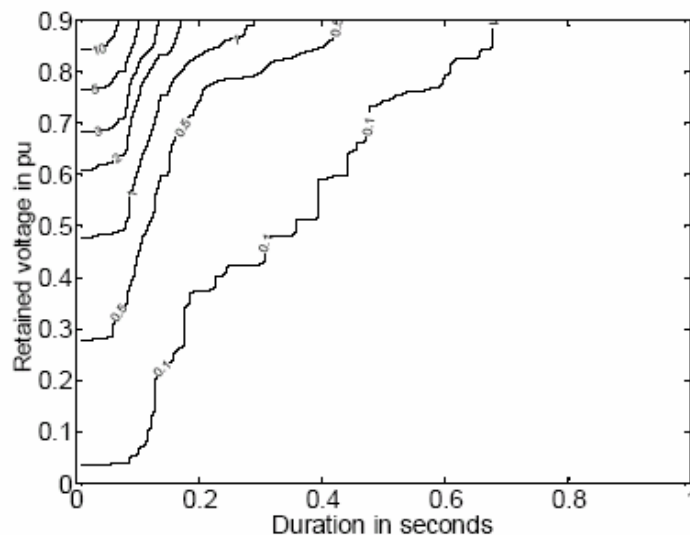


Figure 2-3. Voltage-sag coordination chart

### 2.3.5. Non conventional parameters for PQ measurement

Recently, the worldwide research activity in the field of both electrical systems and electric and electronic measurements has been focused on the detection and localization of the sources of disturbance within a network. The solution to this issue is getting more and more important in the management of electric systems because the location of a disturbing device can be strictly related to the economical and contractual aspects between utility and customers.

Reliable results of power quality monitoring systems depend on the correctness of the theoretical model of the electric network and of the installed devices. First of all, the sinusoidal balanced steady-state condition can be assumed no longer for modelling the whole electrical system, even though the 50 Hz steady state is considered as usual working condition for designing the devices and for the most popular simulation and measurement techniques. Considering for example the electric lines model: the simple 4-pole tap parameters model used correctly for a 50 Hz short electric line (220 kV, 100 km), has to be switched to a more complicated frequency-dependent model if the signal has a 2500 Hz frequency. The equivalent line length in this case is 5000 km. Hence, the model of the system has to be adapted in function of the type of disturbance under test.

When the presence and the main characteristics of a disturbance affecting the network are known, its propagation along the lines and loads has to be analyzed. In doing this, the main issue is the mathematical representation of the interaction between the device generating the disturbance and the system affected by its effects. Unfortunately, in most cases the direct method is not correct: it would consist in analyzing the disturbance contribution of the load under test by itself and then injecting the disturbance into the system to check its behaviour without the considered load be installed. The interactions

have no significant effect on the measurement instrumentation, but can affect the measurement procedure and/or the results interpretation.

The scientific literature proposes techniques based on different operating principles. No one of them, anyway, has been approved yet by the entire scientific community and by the governments, in fact each proposed approach can register and show some critical aspects of the network under test but can be misleading about other aspects. Some surveys or evaluations about the location methods proposed in case of periodic disturbances are reported in [17-24]. Instead of describing the theory standing beside each approach, it may be worthy to underline their common characteristic: most of the methods locating a source of disturbance in a network depend strongly on the measurement system chosen to implement it. For example, let's consider the techniques based on the evaluation of the sign of the harmonics active power contribution; the source of harmonic disturbances is assumed to be the load if the harmonic active power is negative, otherwise it is assumed to be the electric system if the harmonic active power is positive. The approach is suggested by the standard [13] aiming at recognizing the load responsible for the distortion affecting the line voltages, hence it is implemented in numerous commercial instruments designed for Power Quality monitoring, even if the scientific community showed the technique to be weak, mainly due to the fact that a load can be classified as polluting or polluted depending on the operation of all the other loads connected to the same power network.

Anyway, the method based on the sign of harmonic power components, compensated in its wrong aspects, is the most popular for the location of periodic disturbance sources. Hence, attention must be focused on the metrological characteristics of instrumentation used for the application of the method. In particular, the conditioning block, i.e. voltage and current transducers, must be carefully chosen in order to avoid that their phase error, by varying with frequency, leads to wrong evaluation of the harmonic components flow. On the basis of the sign of the harmonic active powers displayed by the instrument the operator would then mistake in assessing responsibilities for the voltage power quality degradation.

Often research groups present methods for the location of the source of disturbances based on distributed measurement systems; the analysis of data simultaneously captured in numerous points of the monitored network gives much more information on the system conditions. By the metrological point of view, distributed measurements introduce new uncertainty sources respect to spot measurements, such as lack of synchronization and data transmission delay.

### **2.4. *European Scenario: standards, guides and PQ level***

There is a worldwide trend of countries reforming their power sectors: liberalization and privatization have been introduced and a new approach is taken to the regulation of the remaining network monopolies. Generally, the main objectives of power sector reform have been to improve efficiency and quality levels. Regulators are assigned the task to attain objectives that are beneficial for society, and these typically include the promotion of high economic efficiency and adequate levels of quality.

Reliability is the most important quality feature in electricity distribution, in fact it is considered the core value of electricity service provision. Any service interruption temporarily ceases the provision of electricity therewith directly affects consumers. Network reliability means the continuous availability of electricity for the consumer. It is characterized by the number of outages for a customer and the duration of these outages. To most customers, it represents the most visible and sensible issue concerning the quality of supply. Therefore many regulators prioritize network reliability when starting regulating quality of supply. The situation of distribution and transmission networks is very different, as the first ones are characterized with many outages with relatively long duration and affecting a limited number of customers, whereas the latter ones are affected by rare outages, usually short in duration but involving many customers. The most interruptions are caused in the low voltage (LV) grid, followed by medium voltage (MV) grids. A survey by the Italian regulator in 1998 showed that within Italy the MV grids are responsible for 85% of the total minute lost, followed by the LV grid (12%) and the HV grids (3%).

As mentioned above, while EN 50160 gives general limits for public supply networks, various European countries have additional rules governing supply conditions. Many of these national regulations cover areas not included in EN 50160, such as the maximum permissible harmonic load to be connected to the PCC.

The German national standard VDE 0100 states that the voltage parameters defined in DIN EN 50160 reflect extreme situations in the network and are not representative of typical conditions. In planning networks the recommendations of VDE 0100 should be followed: it gives maximum values (per unit) for phase-angle controlled resistive loads (1700 VA single-phase, 3300 VA two-phase and 5000 VA balanced three-phase) and for uncontrolled rectifier loads with capacitive smoothing (300 VA single phase, 600 VA two-phase and 1000 VA balanced three-phase). The equipment standard VDE 0838 (EN 60555) is also quoted.

In Poland, the rules of electrical energy distribution established by the government give the fundamental parameters of the supply voltage and do not refer to EN 50160.

Additionally, consumers are divided into six groups, for which separate, permissible total annual outage times are defined. The document also deals in detail with various economic aspects of the energy market, principles of settlement between network and distribution companies etc.

In Italy there is an important document dealing with the continuity of supplied energy [16]. The Italian Regulatory Authority for Electricity and Gas (AEEG) has in fact set out a uniform system of service continuity indicators and has put in place a system of incentives and penalties in order to progressively bring continuity levels up to meet European standards. The Authority has divided the national territory into 230 geographical zones, sub-divided by areas of population density and has set improvement targets for each area on the basis of the previous year's performance. Utilities that succeed in improving by more than the required rate can recover the higher costs sustained. Conversely, companies have to pay a penalty if they fail to meet the improvement target. Interruptions due to third parties are not included in the calculation. The overall performance target is to bring continuity levels up to national benchmark levels based on European standards: 30 minutes of interruptions overall per user per year in large cities (high density); 45 minutes in medium-sized towns (medium density); and 60 minutes in rural areas (low density). Other countries have similar regimes imposed by the regulatory authorities.

The UK has a number of documents making up the distribution code. One of the most important is G5/4, discussed elsewhere in this Guide, which regulates the connection of harmonic loads to the point of common coupling. Measures to encourage the improvement of continuity are the responsibility of the Office of Gas and Electricity Markets (OFGEM).

Most European countries are collecting data on SAIFI (System Average Interruption Frequency Index) and SAIDI (System Average Interruption Duration Index): in their formulas the number of customers is used as a basis for weighting, but Austria, France and Spain are using the installed capacity (in MVA) for the same purpose, that is more consistent as weighting factor because it corresponds to the actual electric power that can be absorbed in each node. In MV networks the difference of customer size is reflected in this case, and for operators it is easier to count capacity than the number of clients. For distribution networks, SAIDI and SAIFI indicators are used by regulators in Great Britain, Hungary, Italy, Norway, Czech Republic, Greece, Portugal, France, Lithuania, Sweden, Estonia, Ireland, Germany and the Netherlands. Although different countries are using slightly different definitions, in Europe SAIFI and SAIDI are well accepted. For transmission networks only a few European countries are collecting the same indices (Czech Republic, France, Portugal, Norway and Italy). Actually regulators

prefer energy related indicators for monitoring reliability in this case, because they generally only have a few customers who are connected directly to their networks.

For interruptions with duration shorter than three minutes the MAIFI (Momentary Average Interruption Frequency Index) is used. For a customer, short interruptions are especially unpleasant in case of working with computers, as even an interruption of several seconds can lead to high costs. Among regulators, monitoring short interruptions is increasing, but still this phenomenon is registered by a limited number of countries, i.e. Finland, France, Hungary, Great Britain and Italy, some of them on both transmission and distribution networks. Probably the main reason for this is that for distribution companies it is not easy to measure short interruptions because they don't need human intervention. Actually, interruptions longer than 3 minutes can be reported manually as number of outages, whereas for short interruptions automatic monitoring equipment should be installed.

By comparing the data on SAIFI of the countries within Europe to establish their reliability performance, it shows that countries like Portugal and Finland have higher SAIFI functions than the other countries. Anyway countries like UK, Ireland and Netherlands have a higher average duration per outage. Based on the SAIDI, the Netherlands has the highest reliability and Portugal the lowest one. Although the SAIFI is different between UK and Italy, the reliability based on the SAIDI is equal for both of them.

In most countries outages caused by faults in other networks are considered as being caused outside of area of responsibility of the network operator. Because of its nature, the so-called Force Majeure is more difficult to assess, but should not be blamed to the operator. On the other hand, not including such exceptional and severe circumstances in quality regulation could lead to serious debts or even bankrupt of the network operator. Therefore, these events could be better monitored separately.

Outages caused by third parties, i.e. externally caused outages, and internally caused outages are not always easy to distinguish. Moreover, externally caused outages could be influenced by the network operator into some extent. For example, the operator could protect his system better to external faults or could provide better information to parties that potentially hurt the system. Moreover, the duration of the outage can be influenced largely by the network operator because he is restoring power supply.

Climate and weather influence the quality of supply, especially in case of overhead networks. The climate is a factor that could not be changed by the network operator, however he is the only party who is able to optimize expenditure and the final quality. Traditionally, the trade-off between quality of supply and network cost is different for rural area and urban areas. This results in more meshed underground networks in urban areas, and hence to a better quality of supply. In quality of supply regulation often urban and

rural networks are treated differently. Some European countries collect SAIDI and SAIFI data separately for different customer densities as well. Italy and Lithuania use the number of inhabitants of municipalities as the characteristic for classification, whereas Spain, Portugal and Latvia use a classification based on customers instead of inhabitants. Within the UK each company has to report about their availability. Advanced quality regulation should take into account both the energy consumed by the customer and the vulnerability of the customer. Of course, this could not be done for every individual customer connected to the distribution network, however a compromise should be create customer groups and collect quality data separately for different groups. Optimal quality is achieved if the additional costs to provide higher quality are equal to the resulting decrease in interruption costs experienced by the consumers. If quality is higher than the optimum, there is a welfare loss as consumers would be provided a level of quality where the additional costs of providing this high quality exceed the associated reduction in interruption costs. Conversely, if quality is below the optimum, there is also a reduction in interruption costs.

The cost of an interruption is driven by a number of factors, first of all its duration. For the industrial sector it has been found that the cost per hour of interruption decrease with duration, suggesting that there is a large initial fixed cost component and a variable component that decreases with duration.

Another factor influencing the cost of an interruption is the reliability level at which the customer is being supplied. Generally, the higher the reliability level the more severe the impact of an interruption will be. As the frequency of interruptions increases, consumers can make a better trade-off between expected interruption costs and the adaptive response costs thus minimizing total interruption costs. Interruption costs vary also with the time of the year, day of the week and time of the day.

The regulatory cap control framework provides companies with strong incentives to avoid over-investments, reduce costs and to improve efficiency. This may have strong implications on the short- and long-term reliability of the system. Therefore, regulators will need to accompany price regulation to protect customers against a decrease in quality and performance standards below certain limits. The introduction of the quality of supply regulation is in line with the main task of a regulator, the protection of customers from monopoly power of the network operators. In doing so, quality regulation helps to overcome incentives to reduce quality that are provided within the system of cap regulation. Thus, quality regulation is a necessary component of price regulation to balance the incentives to cut cost in order to provide the amount of quality the customers expect and are willing to pay for. Even though the quality reduction may cause additional cost for network users, the monopoly network operator may still find it more profitable to

cut costs at the expense of quality. The quality of supply is just as important as prices to customers. If standard services fall but prices remain the same, consumers are effectively suffering from an increase in prices. Another benefit of quality regulation is that it provides better guidance to the regulated companies in developing and implementing their quality policy. Even if providing high quality is important to the network service providers, this does not answer the question of how high this quality should actually be.

### **2.4.1. Reliability regulation**

Reliability is a measure for the ability of the network to continuously meet the demand from customers [25]. For its regulation three methods can be distinguished:

- a) Performance publication – indirect method;
- b) Standards;
- c) Incentive schemes.

a) performance publication is widely used by regulators. The regulator requires the companies to disclose information about trends in its quality performance to the public. Overviews of the company's quality performance are then provided, for example, in the company's annual reports, in dedicated regulatory publication or on the company's website. Additionally, the regulator can oblige the regulated service provider to take into consideration the views of customer representation groups or include customers in the advisory or supervisory boards. Performance publication is relatively simple to implement and requires limited regulatory involvement. The basic idea is to expose the company to public scrutiny by providing customers with information about the company's performance. The assumption is that the company would then be inclined to match its quality to customer demand because of its reputation.

b) standards put a floor to the performance level of the company. Violation of the standard can lead to a fine or tariff rebate. Examples of such standards are customer minutes lost, percentage of customers with outage, or some aggregated quality index. In regulation there is a distinction between overall standards and guaranteed standards. Overall ones are levels of performance set by the regulator and companies must do their utmost to comply with them. They are not measured with respect to performance for individual customers. Guaranteed ones are levels of performance which must be achieved in each individual delivery of a specified service. Customers who fail to receive the required level of service under a guaranteed standard may be entitled to receive a penalty payment.

Standards can be defined per region or zone. In this case, the standard is called a zonal standard. Usually, zones with higher customer density, such as urban areas, have a higher standard to reflect the higher costs involved in supplying customers living in rural and less densely populated zones. Consequently, the minimum standard for urban zones

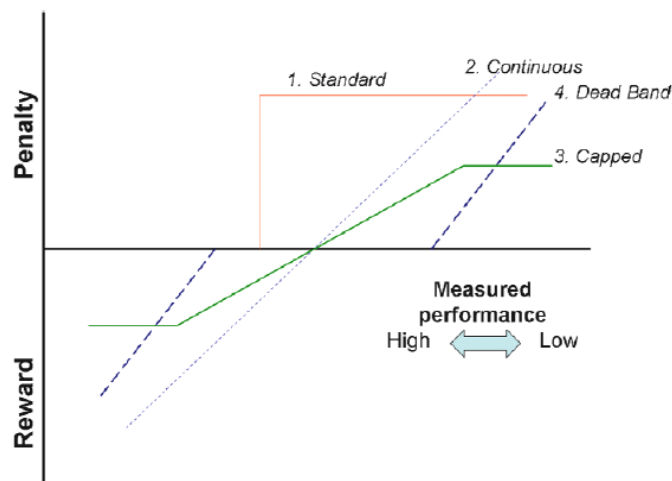


would be set higher than for rural ones. Within the regulatory practice standards tend more and more to be set as guaranteed standards since they are easier to measure and to document. Guaranteed standards intend to protect the single customer and do not incentive the average performance of the regulated network operator. Standards are used to set limits for commercial quality and reliability.

The main problem of a standard is that it imposes a discrete and not continuous relationship between quality and price. The company either pays a fine or it does not, depending on whether it violates the set standard: there is nothing in between. The question is at what level the standard should be set, and what the level of the fine should be. These two need to be low enough to be defensible and high enough to be effective. If they are set too high the standard may severely punish the company for not meeting unrealistic targets. If the standard is set too low, quality degradation may occur.

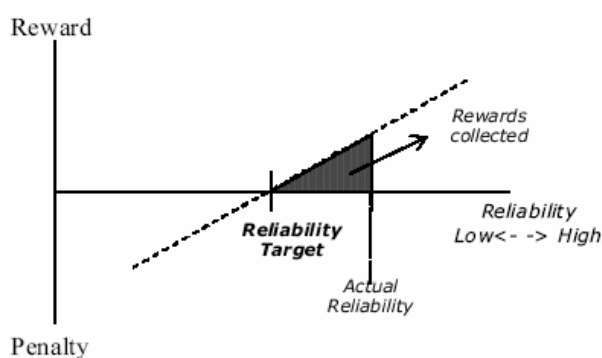
Quality incentive schemes can be considered as an extension of a standard. Alternatively, a standard can be considered as a special case of quality incentive scheme. The price and quality are closely related and the company's performance is compared to some quality target: deviations result in either a penalty or a reward there are many variations of quality incentive schemes. Price and quality can be mapped continuously, in a discrete way, or a combination of these; the level of the penalty can be capped, dead bands can be applied.

Figure 2-4 shows some examples, where the x-axis represents the measured quality level, the y-axis the penalty or reward.



**Figure 2-4.** Penalties/Rewards in function of quality.

Quality incentive schemes can be used for all kind of quality indicators. The measured performance can be expressed for example in terms of SAIDI or SAIFI. The Dutch regulator has introduced a quality incentive scheme that refers to these indices. Figure 2-5 reports the Dutch incentive scheme.



**Figure 2-5.** Quality incentives scheme for SAIDI and SAIFI.

Beside the three methods of quality regulation that are normally applied together regulatory practice is facing more and more tendency towards so-called integrated price-quality regulation. It solves the trade off between cost and quality by explicitly considering quality as a cost component within the benchmarking since it can be assumed that higher quality leads to higher cost and vice versa. By doing so, quality is taken into account while comparing the efficiency of the network operators within the analysis of data with a method to compare firms using multiple input and output factors.

Up to this point only short time measurement and short time implications of price regulation on reliability have been considered. Anyway, given the long term nature of investment decisions and the effects of a continuous maintenance, short term decisions on quality have a deep impact on future cost and quality that cannot be under control just with short time measurements. Long term analysis and assessment of reliability is becoming more and more important. Regulators should be aware of the interaction between short term incentives and long term consequences of their decision and use of additional tools to evaluate them. Long time reliability control should be in line with the general regulatory approach. It comes clear that cap regulation provides strong incentives to reduce cost more than obliged by the regulator in order to realize efficiency gains, leading to an overall decrease in quality of supply and quality restriction for certain customer groups. Quality regulation is important as a part of incentive regulation in order to ensure appropriate solutions for the cost-quality trade off respecting the customers demand for reliability.

By applying the above three methods the cost-quality trade off is not immediately solved. Hence, regulators introduce integrated price-quality regulation that considers the quality provided in the efficiency analysis. Moreover, the long-term aspects of quality become more and more a challenge for regulators to implement a balanced system that ensures the consistency of short time efficiency incentives and long term reliability.

### **2.4.2. Voltage quality regulation**

In many countries voltage quality is regulated to some extent, often using industrial standards or accepted practice to provide indicative levels of relevant performance. The main difference in voltage quality and network reliability is that until a certain voltage quality level the customer is not affected by a not perfect performance, whereas the same customer is affected by any interruption of the power supply. The customer does not have interest in improving the voltage quality as long as it stands within certain limits, while the customer has interest in avoiding all interruptions in the power supply.

In most European countries the voltage quality is not an issue for a large majority of the customers in distribution networks. This means that these customers will basically not benefit from improvements in the voltage quality. However, as connected equipment is not working due to the lack of voltage quality, improvement of the quality has a value to the customer. Because some equipment is more vulnerable to lack of technical quality than other equipment, some clients will value this quality increase differently. Therefore, it is hard to assess the value of technical quality and its individual dimensions than the value of prevented interruptions. This is the second main difference between voltage quality and network reliability.

A third difference is the cause of the lack of quality. While power interruptions for the customer are mainly caused in the electricity network or the connection of the customer, voltage quality is largely influenced by other customers. Harmonic distortion is caused by electronic equipment connected to the network and voltage dips could be caused by short circuits in the network or by welding apparatus. Hence the network operator should not pay for every single decrease of voltage quality, but it should be able to keep the voltage quality at least on acceptable levels by applying maximum disturbance levels and checking customers on keeping them. In most countries minimum standards are defined for voltage quality. This way if a minimum level of quality is met, the customer is not interested in a better quality, anyway the network operator is responsible for meeting a minimum of quality in his system. Since there is a large difference regarding the influence of lack of quality for different type of customers, some customers need higher quality than the minimum standard levels. In most cases, this is regulated by connection contracts. Dutch network operators are investigating a transparent classification system for the delivered voltage quality on the point of common coupling. Actually, the minimum standards are usually based on an international accepted standards, as the European EN 50160 “the characteristic of the supply voltage concerning: frequency, magnitude, waveform and symmetry of the phases”. Mostly these minimum standards for voltage quality are included in the grid code or the distribution code. Although EN 50160 gives indicative values for many of the phenomena, it is only applicable to voltage levels up to

35 kV. For higher voltage levels no standard exists; in the Netherland, Italy and Portugal some criteria from EN 50160 are extended to voltage levels up to 50 kV or higher.

In some countries, voltage quality standards introduced by regulators differ from the limits prescribed by EN 50160; in an increasing number of EU countries the EN reference levels are not found to be satisfactory both by regulators and customers. The CEER Benchmarking report and the Cigré workgroup on PQ both highly recommend that EN 50160 should be revised, taking into account both the actual levels of voltage quality in European transmission and distribution networks, the evaluation of customer's needs. Like network reliability, the voltage quality in distribution networks is influenced as well by the voltage quality in the interconnected transmission and distribution networks. A difference however is that where interruptions in the power supply could be related to a cause in a network, voltage quality is the result of many different causes which are changed during transmission and transformation. Thus, it is hard to identify the network owner who should be responsible for the level of power quality.

### 2.4.3. Monitoring the voltage quality within EU

A good knowledge of the real situation is a preliminary step towards any kind of regulatory intervention. Therefore, a growing number of European countries have monitoring systems installed or plan to install them in the near future, as shown in Table 2-5. Monitoring systems within a number of EU countries are based on a sampling either of transmission-distribution interface points or customer connection points.

**Table 2-5.** Monitoring system in European Countries.

VOLTAGE QUALITY MONITORING SYSTEM	Countries
Monitoring at both transmission and distribution levels	Italy, Norway, Portugal, Slovenia, the Netherlands
Monitoring only at transmission level	Czech republic
Monitoring only at distribution level	Hungary
Proposal stage	Spain and Sweden

In Norway a monitoring system has been applied for several years. From 2006 mandatory voltage quality monitoring started: each network company is obliged to monitor quality parameters continuously in different characteristic parts of its power system.

In Hungary the regulator owns 400 voltage quality recorders that are installed each semester in one of the six distribution companies, at low voltage only. The regulator chooses the network points randomly, in a way that does not depend on previous events or complains.

In Portugal there are 61 points monitored on the transmission grid (40 for 4 weeks and the rest all year long); in distribution system, all 423 substations in MV and 1270 power transformation stations in LV have been monitored for 3 years.

In Slovenia distribution and transmission companies are obliged to measure voltage quality parameters; monitoring is implemented in high voltage covering all the substations and about 10% of MV systems.

In Italy at the end of 2004 the regulator asked the transmission company to install about one hundred voltage quality recorders; as for distribution, a voltage quality monitoring system of 400 points is working in about 10% of MV bus-bars in HV/MV transformers.

In Spain the distribution companies and the regulator have been working on a procedure for controlling and measuring voltage quality; 10% of the busbars in MV of each province is involved.

In Czech Republic a monitoring systems is going to be installed at the interconnection points between transmission and distribution networks.

In the Netherlands the grid operators measure at 150 points (50 points at HV, 50 points at MV and 50 points at LV) the quality for one week each. Every year these points are selected randomly in such a way that does not depend on previous events or complains. The measuring devices are owned by the federation of energy companies in the Netherlands. With a limited number of measuring equipment 150 network points can be monitored. The grid operators started in 2005 with measuring the voltage dips at 20 EHV stations and 20 HV stations for a period of one year.

Although these monitoring systems within several countries are different from each other in many respects, a common point is that at least voltage magnitude, dips and harmonic distortion of the voltage waveform are monitored. The number and location of voltage recorders is quite different from one country to another.

As for individual voltage quality measurements, one case deserves special attention. In France the main distribution companies offer their customers customized contracts with assigned power quality levels. If the customer claims for better contractual levels than normal ones, he can ask the operator for customized contractual levels in is contract, paying an extra charge. Customers having customized contracts must be monitored by a recorder installed and owned by the customers themselves or by the operator. In distribution networks about 16% of MV customers have a power quality recorder, whereas in the transmission networks the monitoring involves about 12% of EHV and HV customers.

In comparison to regulation of reliability, the regulation of voltage quality is less advanced. Where some European countries are using complex and highly effective regulations (e.g.

incentive regulation) for reliability, for regulation of voltage quality most regulators rely on indirect measurements or minimum standards at most.

As definitions and procedures are in place, the reliability measurement is quite immediate, no special measurement equipment needs to be installed to collect duration of the power interruption and the number of affected customers, or the total amount of interrupted power. This is different for most dimensions of voltage quality, which need to be measured with specialized measurement devices. An important issue is that the voltage quality is different for every connection point in the network. Because it is not feasible to measure everywhere, statistical techniques are needed to report on average voltage quality of individual sensitive customers. In contradiction to this, reliability can be measured by just sorting out and summing all individual outage statistics. One more difference between reliability and power quality is the cause of their lack. For interruptions in most cases the cause could be found in one or more events in the public electricity network, whereas voltage quality is influenced by both conditions in the public electricity network and at the client site. Steel manufacturers are well known producers of voltage dips that are “exported” from their plants to the network, influencing the voltage quality of other clients. Although the network operator should be responsible for the voltage quality in its network, this aspect makes the voltage quality regulation a more complex issue.

In a number of EU countries (Italy, Norway, Portugal, Slovenia, Czech Republic, Hungary and the Netherlands) voltage quality monitoring systems are installed or currently under commissioning. Most countries apply recorders on both transmission and distribution, while Hungary, e.g., is interested in quality only of low voltage. Anyway, in most countries there is no systematic monitoring system for voltage quality, but a clear trend shows that the number of countries with monitoring systems is increasing.

For the measurement of system quality, in Norway, Hungary, Portugal, Slovenia, Netherlands, Italy and Spain a measurement program is or is planned to be installed. The program statistically determines parameters that provide general picture of voltage quality of the system by using a large set of voltage quality meters. For example, in Hungary 400 devices are installed in the low voltage network, for one semester at each place. In Portugal 1270 low voltage substations 423 medium voltage substations and 61 points in the transmission grid are monitored. Although measurement schemes are installed more and more, results of voltage quality are not yet easily accessible for the average client.

#### **2.4.4. Minimum standards**

Since voltage quality is an individual indicator, in almost all European countries a set of minimum standards are introduced to define the minimum voltage quality for individual connection points to be delivered by the network operator. Many EU countries apply EN 50160 as the minimum standard for voltage quality even if this standard is recognized to

be not perfect. One important disadvantage is that EN 50160 is valid only for voltage levels up to 35 kV, but in many countries the same or similar levels for higher voltage networks are used. Moreover, EN 50160 only provides mandatory standards for a limited number of Power Quality indicators, while for others only indicative values are provided. In addition to this, many standards are defined for 95% of the time, leaving out the rest of the time. Finally, sometimes EN 50160 is considered to be too weak.

Although EN 50160 is very common for European Regulators, a number of them is adapting their minimum standards on voltage quality so that the relevant disadvantages are overcome. E.g. Norway has adapted voltage quality standards on supply voltage variations, flicker severity, rapid voltage changes, voltage unbalance and harmonic distortion. The Norwegian standards are now made better compatible to immunity levels of equipment. Also France, the Netherlands and Portugal have adapted some of the EN 50160 standards. Currently several institutions such as Cigré and Cired are discussing improvements to the standard EN 50160.

If one issue is having sensible standards, another one is how to deal with voltage quality that does not meet the minimum standards. A large number of countries (Austria, Belgium, Czech Republic, Estonia, France, Latvia, Norway and Poland) distribution network operators have the obligation to verify voltage quality complaints of individual customers. Generally, this is done on customer's expenses, but sometimes customers only pay if the voltage quality meets the standards. Usually, not meeting the voltage quality standards does not lead to penalties and only leads to the obligation for the network operator to improve quality in order to fulfill the minimum standards.

Some countries have installed a complaint procedure, which includes a maximum response time for the network operators on power quality complaints of the customer. Sometimes a penalty payment is needed if the network operator exceeds this set time. In the U.K. in case of voltage complaint by a customer, the distribution network operator must visit the customer within 7 working days or send a substantive reply within 5 days. If the operator fails meeting this standard, the customer is provided with a payment of £ 20. similar complaint procedures exist in Norway, Hungary, Ireland, Italy, Latvia, Portugal and Slovenia. Penalties applied in these countries range from 8 Euro for 7 working days in Hungary (in case of domestic customers) to 75 Euro for 15 working days in Portugal (Medium and High voltage customers).

Hungary and Ireland apply also a standard for the correction of voltage quality problems. In the first country the operators need to pay a penalty of 20 to 120 Euro (depending on the size of the customer) if voltage complaints are not compensated within 12 months. In the second country a payment of 50 Euro is needed after three months.

### 2.4.5. Incentive schemes

Unlike power quality regulation with regard to reliability, currently no regulators are applying incentive regulation for voltage quality. However, some countries are applying so-called “power quality contracts”, i.e. individual contracts between network operator and customer agree on voltage quality standards which are different from the usual standard. In France network operators usually offer all customers such contracts, which could be customized to the desired quality level. The payment is related to the work that has to be done by the operator in order to meet these standards. While this contract is pretty popular for reliability (for which 1000 over 100,000 MV customers have a contract) only 92 customers have a contract with customized contractual levels on voltage quality. Because of different reasons, incentive regulation schemes are not yet in place for quality regulation. Since interruptions are considered to be more important by the majority of customers, regulators started with incentive regulation for reliability. On the other hand, some investigations show that costs of lack of quality are significant, e.g. Norwegian investigation shows that customers costs associated with short interruptions and voltage dips in Norway are similar to the customers costs related to long interruptions. However, some issues need to be addressed before being able to implement incentive regulation. Main issues are:

- ✓ Measurement of short interruptions and long and deep voltage dips;
- ✓ Determining customers costs in case of short interruptions and long and deep voltage dips.

**Table 2-6.** Methods for quality regulation in Europe.

Method	APPLIED FOR VOLTAGE QUALITY	Objective
Indirect	Monitoring voltage quality by large measurement programs	Monitor long term development
Standards	Individual guaranteed standards based on EN 50160	Protection of individual customer groups
	Quality contracts	Meeting voltage quality requirements of individual customers
Incentive scheme	Not applied	Ensuring an average voltage quality level

Table 2-6 provides a high-level overview of the methods used for quality regulation in Europe, categorized in indirect methods, minimum standards and incentive regulation. In some countries large voltage quality monitoring systems are installed. Using results relevant to more than one year the long term developments of voltage quality of the system could be monitored.

Since equipment at the customers will get more sensitive for lack of voltage quality it can be expected that the regulators will extend regulation on voltage quality. A better insight



in costs at customers due to lack of voltage quality, characteristic of regulation, individually for the different parameters of voltage quality could be helpful for them. It is important to consider all voltage quality parameters individually, e.g. regulating on voltage dips will be different from regulating on harmonics.

### References

- [1] EN 50160, "*Voltage characteristics of electricity supplied by public distribution systems*", CENELEC, Bruxelles (Belgium), 1999;
- [2] IEEE std 1159-1995, "*Recommended practice for monitoring electric power quality*", The IEEE, Piscataway (USA), Nov. 1995;
- [3] IEEE Trial-Use Std 1459-2000, "*Definitions for the measurements of electric power quantities under sinusoidal, nonsinusoidal, balanced or unbalanced conditions*", The IEEE, New York (USA), June 2000;
- [4] IEEE Trial-Use Std 519-1992, "*Recommended Practices and Requirements for Harmonic Control in Electrical Power Systems*" The IEEE, Piscataway (USA), June 1992;
- [5] IEEE Std 493-2007, "*IEEE Recommended Practice for the Design of Reliable Industrial and Commercial Power Systems*", The IEEE, Piscataway (USA), 2007;
- [6] IEEE Std 1346-1998, "*Recommended Practice for Evaluating Electric Power System Compatibility with Electronic Process Equipment*", The IEEE, Piscataway (USA), May 1998;
- [7] IEC 61000-2-X, "*Electromagnetic compatibility (EMC): Environment*", 2002;
- [8] IEC 61000-2-8, "*Electromagnetic compatibility (EMC): Environment – Voltage dip and short interruption on public electric power supply system with statistical measurements results*";
- [9] IEC 61000-3-X , "*Electromagnetic compatibility (EMC): Limits*";
- [10] IEC 61000-3-2, "*Electromagnetic compatibility (EMC): Limits for harmonic current emissions (equipment input current  $\leq 16$  A per phase)*";
- [11] IEC 61000-3-6, "*Electromagnetic compatibility (EMC) – Part 3:Limits – Assessment of emission limits for distorting load in MV and HV power systems*";
- [12] IEC 61000-4-X, "*Electromagnetic compatibility (EMC): Testing and Measurements techniques*", 2002;
- [13] IEC 61000-4-7, "*Electromagnetic compatibility (EMC) – Part 4-7: Test and Measurements techniques – General guide on harmonics and inter-harmonics measurements and instrumentation for power supply systems and equipment connected thereto*";
- [14] IEC 61000-4-15, "*Electromagnetic compatibility (EMC) – Part 4-15: Test and Measurements techniques – Flickermeter – Functional and design specifications*";
- [15] IEC 61000-4-30, "*Electromagnetic compatibility (EMC) – Part 4-30: Test and Measurements techniques – Power quality measurements methods*";
- [16] Autorità per l'Energia Elettrica e il Gas: "*Testo integrato delle disposizioni dell'Autorità in materia di qualità dei servizi di distribuzione, misura e vendita dell'energia elettrica*", Delibera 30 gennaio 2004, n.4/04;
- [17] E. J. Davis, A. E. Emanuel, D. J. Pileggi, "*Evaluation of single-point Measurements Method for Harmonic Pollution Cost Allocation*", IEEE Trans. on Power Delivery, vol. 15, n. 1, 2000, pp. 14-18;
- [18] P. J. Rens, P. H. Swart, "*On Techniques for the Localization of Multiple Distortion Sources in three-phase Networks: Time Domain Verification*", ETEP, Vol. 11, No 5, 2001, pp. 317-332;
- [19] C. Muscas, "*Assessment of Electric Power Quality: Indices for Identifying Disturbing Loads*", ETEP, Vol. 8, No. 4, 1998, pp. 287-292;

- [20] L. Cristaldi, A. Ferrero, S. Salicone, "*A distributed Measurement System for Electric Power Quality Measurement*", IEEE Trans. on Instr. and Meas., Vol. 51, No. 4, 2002, pp. 19-23;
- [21] D. Castaldo, A. Testa, A. Ferrero, S. Salicone, "*An Index for Assessing the Responsibility for Injecting Periodic Disturbances*", L'energia elettrica, vol. 81, 2004, "Ricerche";
- [22] A. Ferrero, R. Sasdelli, "*Revenue and Harmonics: a Discussion about New Quality Oriented Measurement Methods*", Proc. Of the 9<sup>th</sup> intern. Conference on metering and tariffs for energy supply, Publication 462, Birmingham, UK, 1999, pp. 46-50;
- [23] R. Sasdelli, C. Muscas, L. Peretto, "*A VI-based measurement system for sharing the customer and supply responsibility for harmonic distortion*", IEEE Trans. on Instr. And Meas., 1998, Vol. 47, No. 5, pp. 1335-1340;
- [24] C. Muscas, L. Peretto, S. Sulis, R. Tinarelli, "*Implementation of multi-point Measurement Techniques for PQ Monitoring*", Proc. Of the 21st IEEE IMTC/04, Como(Italy), 2004, vol. 3, pp. 1626-1631;
- [25] K. Keller, B.F.C Franken, "*Quality of Supply and Market Regulation; survey within Europe*", KEMA Consulting by order of the European Copper Institute, Arnhem, The Netherlands, December 2006.



### 3. Electromagnetic transients in power distribution networks.

#### Glossary

The definitions reported in the following have been developed and then harmonized by several standards-writing organizations.

*surge protective device (SPD)* - A device that is intended to limit transient overvoltages and divert surge currents. It contains at least one nonlinear component.

*surge reference equalizer* - A surge-protective device used for connecting equipment to external systems whereby all conductors connected to the protected load are routed, physically and electrically, through a single enclosure with a shared reference point between the input and output ports of each system. Sharing the references can be accomplished either by a direct bond or through a suitable device maintaining isolation during normal conditions but an effective bonding by means of a surge-protective device during the occurrence of a surge in one or both systems.

*back flashover (lightning)* - A flashover of insulation resulting from a lightning stroke to part of a network or electrical installation that is normally at ground potential.

*blind spot* - A limited range within the total domain of application of a device, generally at values inferior to the maximum rating. Operation of the equipment or the protective device itself might fail in that limited range despite the device's demonstration of satisfactory performance at maximum ratings.

*direct stroke* - A stroke impacting the structure of interest or the soil (or objects) within a few metres from the structure of interest.

*energy deposition* - The time integral of the power dissipated in a clamping-type surge protective device during a current surge of a specified waveform.

*failure mode* - The process and consequences of device failure.

*facility* - Something (as a hospital, machinery) that is built, constructed, installed or established to perform some particular function or to serve or facilitate some particular end.

*follow current* - Current supplied by the electrical power system and flowing through the SPD after a discharge current impulse and significantly different from the continuous operating current.

*leakage current* - Any current, including capacity coupled currents, that can be conveyed from accessible parts of a product to ground or to other accessible parts of the product.

*lightning protection system (LPS)* – The complete system used to protect a space against the effects of lightning. It consists of both external and internal lightning protection systems. In particular cases, an LPS might consist of an external LPS or an internal LPS only.

*lightning flash to earth* - An electrical discharge of atmospheric origin between cloud and earth consisting of one or more strokes.

*lightning stroke* - A single electrical discharge in a lightning flash to earth.

*mains* - The a.c. power source available at the point of use in a facility. It consists of the set of electrical conductors (referred to by terms including „service entrance”, „feeder”, or „branch circuit”) for delivering power to connected loads at the utilization voltage level.

*measured limiting voltage* - The maximum magnitude of voltage that appears across the terminals of the SPD during the application of an impulse of specified wave-shape and amplitude.

*nearby strike* - A strike occurring in the vicinity of the structure of interest.

*open-circuit voltage* (OCV) - The voltage available from the test set up (surge generator, coupling circuit, back filter, connecting leads) at the terminals where the SPD under test will be connected.

*point of strike* - The point where a lightning stroke contacts the earth, a structure, or an LPS.

*pulse life* - The number of surges of specified voltage, current amplitudes, and wave-shapes that may be applied to a device without causing degradation beyond specified limits. The pulse life applies to a device connected to an a.c. line of specified characteristics and for pulses sufficiently spaced in time to preclude the effects of cumulative heating.

*short-circuit current* (SCC) - The current which the test setup (surge generator, coupling circuit, back filter, connecting leads) can deliver at the terminals where the SPD under test will be connected, with the SPD replaced by bonding the two lead terminals.

*standby current* - The current flowing in any specific conductor when the SPD is connected as intended to the energized power system at the rated frequency with no connected load.

*surge response voltage* - The voltage profile appearing at the output terminals of a protective device and applied to downstream loads, during and after a specified impinging surge, until normal stable conditions are reached.

*swell* - A momentary increase in the power frequency voltage delivered by the mains, outside of the normal tolerances, with a duration of more than one cycle and less than a few seconds.

*temporary overvoltage* - An oscillatory overvoltage (at power frequency) at a given location, of relatively long duration and which is not damped or weakly damped. Temporary overvoltages usually originate from switching operations or faults (e.g.; sudden load rejection, single-phase faults) or from non-linear phenomena (ferro-resonance effects, harmonics).

*thermal runaway* - An operational condition when the sustained power loss of an SPD exceeds the dissipation capability of the housing and connections, leading to a cumulative increase in the temperature of the internal elements culminating in failure.

*two-port SPD* - An SPD with two sets of terminals, input and output. A specific series impedance is inserted between these terminals. The measured limiting voltage might be higher at the input terminals than at the output terminals. Therefore, equipment to be protected must be connected to the output terminals.

*voltage-limiting type SPD* - An SPD that has a high impedance when no surge is present, but will reduce it continuously with increased surge current and voltage. Common examples of components used as nonlinear devices are: varistor and suppressor diodes. These SPDs are sometimes called 'clamping type'.

*voltage-switching type SPD* - An SPD that has a high impedance when no surge is present, but can have a sudden change in impedance to a low value in response to a voltage surge. Common examples of components used as nonlinear devices are: spark-gaps, gas tubes, thyristors and triacs. These SPDs are sometimes called „crowbar type”.

### 3.1. Transients

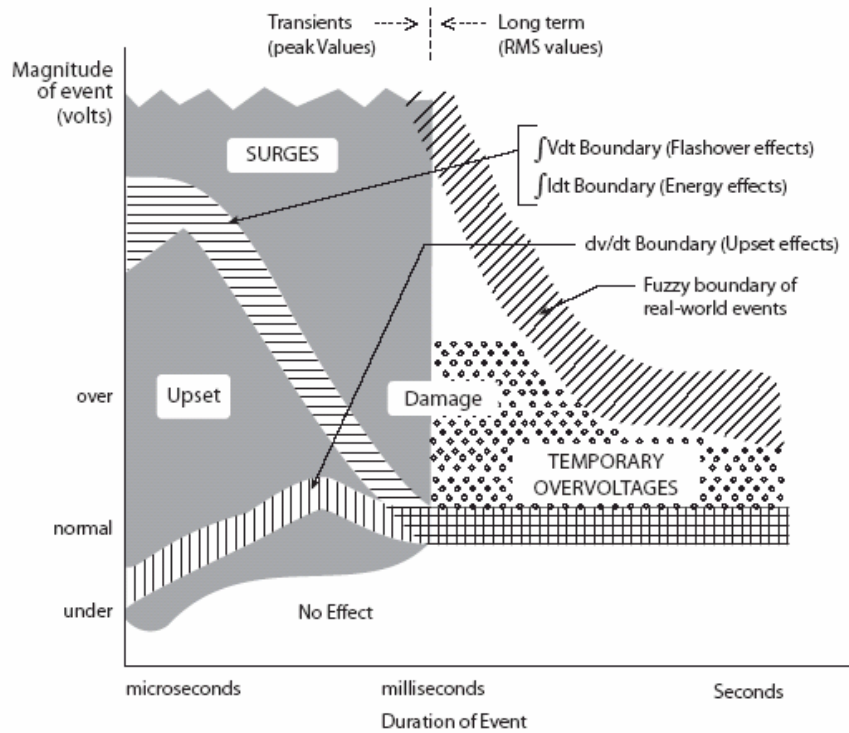


**Figure 3-1.** Voltage variations represented according to their duration, magnitude and effect on the power system

Transient overvoltages and currents, globally referred to as surges, occur in power systems as the result of several types of events or mechanisms, and can be classified in four categories:

#### 1. Lightning surges;

They are the result of direct strokes to the power or communications systems, or surges caused by lightning striking structures (with or without lightning-protection system) or the soil. Lightning surges can impact a facility by impinging upon the service entrance as they propagate along the conductors, having originated from one of three phenomena: a direct stroke to the lines; a resistively-coupled surge from a nearby strike; a voltage induced in the loops formed by line conductors and earth.

Lightning surges can also impact a facility as they are coupled directly into the facility wiring system, without having been brought to the service entrance, as described above. Several mechanisms are involved in this process: the earth-seeking, fast-changing current of a direct stroke to the facility - either to its intended lightning protection system (LPS) or to other structures (roof mounted equipment in particular) - will induce transient voltages in the facility circuits; the slower portion of the lightning current will couple transient voltages into the facility wiring through common impedances; the earth-seeking current

flowing in the facility wiring will divide among the paths available for dispersion, i.e. earthing electrode(s) of the facility, and any utility metallic path entering the facility.

#### 2. Switching surges;

Switching surges are the result of intentional actions on the power system, such as load or capacitor switching in the transmission or distribution systems by the utility, or in the low-voltage system by end-user operations. They can also be the result of unintentional events such as power system faults and their elimination. Transients associated with switching surges include both high-frequency transients and low-frequency transients.

High-frequency transients are generally associated with natural oscillations of the circuit elements in response to the stimulus of a change of state in the circuit. They involve relatively small stray capacitances and inherent inductances, hence their high frequency, and relatively low energy-delivery capability in a direct impact to the power port of equipment. On the other hand, the high frequency has the potential of coupling interference, rather than cause damage. In particular, fast switching currents in the power system can induce interfering voltages into control circuitry in the facility. This scenario might appear outside of the scope of „power quality” but should still be considered because its effects might mimic a power quality problem impinging the power port of equipment.

Low-frequency transients are primarily associated with the switching of capacitor banks. These banks can be a part of the utility system or of the facility. In general, they involve kVAr or MVA<sub>r</sub>, and therefore have considerable energy-delivery capability into an SPD that would attempt to divert them, or into the intermediate d.c. links of electronic power-conditioning equipment. Because of their low frequency, they can propagate a considerable distance from the point of origin because the wiring inductance does not have the mitigation effect available for the higher-frequency transients. Therefore, these capacitor-switching transients merit particular attention.

#### 3. Temporary overvoltages;

They occur in power systems as the result of a wide range of system conditions, both normal operation and abnormal conditions. These overvoltages merit attention because they not only cannot be mitigated by SPDs - the normal response of a designer confronted with „transients” - but also represent a significant threat to the survival of SPDs. For this reason,



while common wisdom might be that their power-frequency nature places them outside the scope of „transients”, reliable application of SPDs demands that they be taken into consideration.

4. System-interaction surges.

Transient overvoltages can occur between different systems, such as power and communications, during the flow of surge currents in one of the systems. These interactions might be deemed outside of the scope of Power Quality at the power port of equipment, but their effect can give the appearance of a „power quality problem”, and therefore they merit recognition if a solution is to be found. A system-interaction overvoltage is particularly important for equipment that is connected to both the power system and some form of communications systems, which is increasingly the case of industrial equipment. Because the two systems can be managed by different individuals or organizations, even though installed in the same facility, the earthing practices applied by these separate groups are often uncoordinated at best and counter-productive at worst.

Broadly speaking, the transients can be classified into two categories – impulsive and oscillatory. These terms reflect the waveshape of a voltage or current transient. Standard IEEE 1159 [1] takes into account also the frequency content of the event associated with its rising front rate and its duration. Table 3-1 reports such classification.

**Table 3-1.** Voltage transient phenomena.

Categories	Typical spectral content	Typical duration	Typical voltage magnitude
<b>Transients</b>			
<b>Impulsive</b>			
Nanosecond	5 ns rise	< 50 ns	
Microsecond	1 µs rise	50 ns – 1 ms	
Millisecond	0.1 ms rise	> 1 ms	
<b>Oscillatory</b>			
Low frequency	< 5 kHz	0.3 – 50 ms	0 - 4 pu
Medium frequency	5 – 500 kHz	20 µs	0 - 8 pu
High frequency	0.5 – 5 MHz	5 µs	0 - 4 pu

**3.1.1. Lightning**

The significant lightning parameters include waveforms, amplitudes, and frequency of occurrence. The literature contains data obtained by measurements as well as data produced by computations. Three types of coupling mechanisms can produce overvoltages in low-voltage systems. While this discussion makes reference to „overvoltages”, consideration of the current associated with the overvoltage, or the

current initially causing the overvoltage, is an important aspect of the subject. In the case of a direct stroke to the electrical system, the immediate threat is the flow of lightning current through the earthing impedances, resulting in overvoltages. The effective impedance of the lightning channel is high (a few thousand ohms). Accordingly the lightning current can practically be considered an ideal current source. In case of a near flash, the immediate threat is the voltage induced in circuit loops, which in turn can produce surge currents. In the case of a far flash, the threat is limited to induced voltages. Therefore, the response of an electrical system to the lightning event is an important consideration in assessing the threat. For a given flash, the severity of the overvoltage appearing at the end-user facility reflects the characteristics of the coupling path, such as distance and nature of the system between the point of flash and the end-user facility, earthing practices and earth connection impedance, presence of SPDs along the path, and branching out of the distribution system. All of these factors vary over a wide range according to the general practice of the utility as well as local configurations.

The world-wide annual frequency of thunderstorm days is shown in Figure 3-2. Long used for risk assessment, this information is now being superseded by maps of flash density for regions where a lightning detection system is in operation. Flash density maps provide more accurate information than the traditional „thunderstorm day”, and they are expected to supersede the thunderstorm maps as they become available.

Lightning surges in electrical systems can in general be classified according to their origin as follows: Current surges due to direct flashes to overhead lines, including back flashover events; Induced overvoltages on overhead lines due to flashes at some distance, and the resulting surge currents; Overvoltages caused by resistive, inductive, and capacitive coupling from systems carrying lightning currents, and the resulting surge currents. In the following paragraphs, these classes of overvoltages are briefly described.

#### **3.1.2. Direct flashes to overhead lines**

The effective impedance of the lightning channel is high and the lightning current can practically be considered as an ideal current source. The resulting overvoltages are therefore determined by the effective impedance that is seen by the lightning current. For a flash to an overhead line conductor, the impedance in the first moments is determined by the characteristic surge impedance of the line. Given the typical values of characteristic impedances, ranging from tens of ohms to 400 ohms, very high overvoltages occur that can be expected to cause flashover to earth long before the service entrance of a building becomes involved. Therefore, the lightning surge appearing at service entrances, while reflecting the severity of the lightning stroke and its distance, bears no resemblance to the actual lightning current.

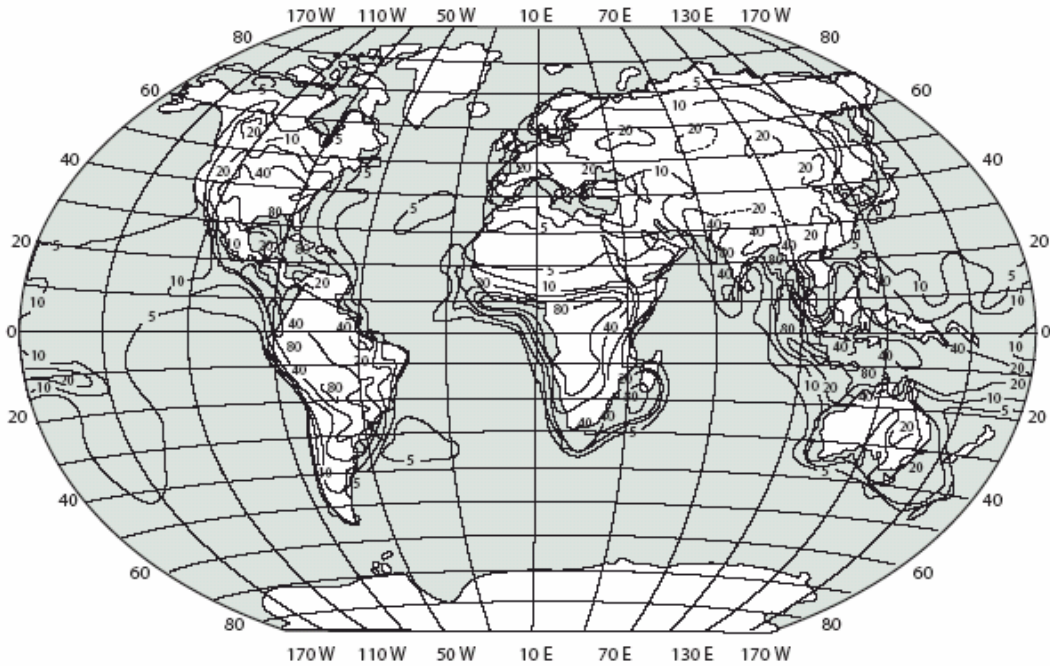


Figure 3-2. Example of world-wide annual frequency of thunderstorm days.

### 3.1.3. Induced overvoltages on overhead lines

Due to the changes in electromagnetic field caused by a lightning flash, surges are induced in overhead lines of all kinds, also at considerable distance from the flash. The voltages have essentially the same value for all conductors because the phase separation is small compared to the distance to the flash. For instance, in a high-voltage line with 10-m conductor height for a lightning current of 30 kA, the induced voltage is in the order of 100 kV for a flash at 100-m distance. For a low-voltage line with a height of 5 m, a current of 100 kA will induce a voltage of about 2 kV even at a distance of 10 km. However the induced voltage does not necessarily appear at the service entrance: the high levels will provoke flashover to earth or operation of a surge arrester, so that the surges appearing at the service entrances are more likely to be in the range of only a few kilovolts. As noted before, these surges involve significant overvoltages but relatively small current levels, in contrast with surges resulting from direct strikes where the current-source like phenomenon results in current surges that reflect the dispersion of the original stroke current among the earth paths.

### 3.1.4. Overvoltages caused by coupling with other systems

A lightning flash to earth or to a part of a system normally at ground potential can result in an earth potential of high value at the point of strike and in the vicinity. This phenomenon causes overvoltages in electrical systems using this point of earth as reference. At first, the potential of the earth electrode is determined by the local impedance that, for instance, might be 10 ohms: a high voltage is produced between the earthing system and electrical

installations inside the building, with a high probability of causing either insulation breakdown or operation of SPDs. Following such events, current impulses can flow into the various systems, mainly determined by their impedance to earth. In this way overvoltages are produced in the power supply system as well as in other connected services (telecommunication, data and signalling systems, etc.), but also transferred to other buildings, structures, and installations. For instance, all power installations supplied from the same distribution transformer as the one struck by lightning can be affected. Due to the high electromagnetic fields caused by the lightning current, inductive and capacitive coupling to electrical systems that are close to a lightning path can also cause over-voltages on electronic and data systems, causing failures and malfunctions.

#### **3.1.5. Lightning surges transferred from MV systems**

Because their structures are longer and higher than other structures located in their vicinity (houses, trees), MV overhead lines are in general more exposed to lightning than LV lines. The propagation of the surge through the MV system and the transfer rate to the LV system depend on the physical construction of the system. Some important differences can exist between the designs used in different countries. The lightning surges in MV systems are caused by direct flashes or induced by nearby flashes. In addition, back-flashovers can occur from flashes striking earth wires or extraneous metal parts of structures or equipment, or striking the earth close to a line structure.

#### **3.1.6. Surge magnitude and propagation in MV systems**

The surge propagation depends on the MV system structure and, in particular, on the surge-protective devices installed. High-level lightning surges are in general attenuated quickly during their propagation on the line by losses and flashover across the line insulators. In practice, after a few line spans, the magnitude of an overvoltage is reduced to the insulation levels of the line insulators. With the exception of direct strokes next to the MV/LV transformer, it can be assumed that overvoltages in an MV system are limited by the insulation level of the line insulators. In a 20 kV system; this is about 150 kV to 180 kV. For wood-pole lines without earthed cross-arms, however, much higher surges can occur. A second limitation of the surge level is provided by the surge-protective devices located usually at the primary side of the MV/LV transformer, or at the entrance of an underground network. These protection devices might be ZnO or SiC surge arresters or air gaps. The residual overvoltage (in the range of 70 kV for a 20 kV system, for instance) depends on the rated value and earthing impedance of the protection devices. When air gaps are used, one can expect the lightning surge to be followed by a power frequency follow current that can generate a temporary overvoltage.

### 3.1.7. Surge transfer to the LV system

The overvoltage surges generated in the MV system by lightning are transferred to the LV distribution system by capacitive and magnetic coupling through the MV/LV transformer or by earth coupling. The transferred surge magnitude depends on many parameters, such as LV earthing system (TT; TN, IT), LV load, LV surge-protective devices, coupling conditions between MV and LV earthing, transformer design. In case of a direct lightning flash to the MV line, the surge arrester operation or an insulator spark-over diverts the surge current through the earthing system and can produce a resistive earth coupling between the MV and LV systems. An overvoltage is transferred to the LV system (as shown in the typical case of Figure 3-3). Depending on the earthing impedance values, this earth coupling overvoltage can be much higher than the capacitive coupling through the transformer. In a TN system, if the neutral is also earthed at the customer installation, smaller overvoltages will occur. It should also be noted that this kind of resistive coupling can be avoided by using a separate earthing system for the LV part of the transformer.

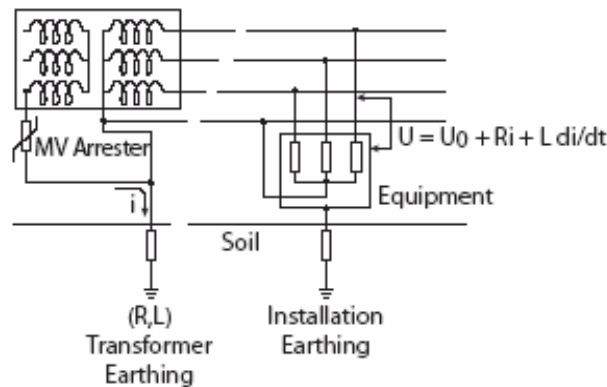


**Figure 3-3.** case of overvoltage in the LV plant due to the coupling of the earthing with the MV one.

A typical value of the overvoltage transmitted by capacitive and electromagnetic coupling to the secondary of the MV/LV transformer side is 2% of the MV phase-to-earth voltage between phase and neutral conductors and 8% between phase conductor and earth. In some particular situations, this MV/LV transfer rate can be higher. Induced lightning surges on the MV system produce much less surge current (usually less than 1 kA) than direct flashes, and the overvoltages are practically transferred to the LV system only by capacitive coupling and do not exceed a few kV. In such cases, the overvoltage induced directly in the LV system is in general higher than the one transferred from the MV side.

### 3.2. Transmission Lines

The Electro-Magnetic Transient Program, EMTP, is the environment in which the propagation of transient disturbances along the lines of a distribution network can be simulated and analyzed. The waveform of the voltages and currents at any point of the power system are obtained as analytical solution of the system of equations corresponding to the combination of the equivalent model of the lines and the boundary conditions imposed to the network. In EMTP environment the three-phase lines can be modelled by means of a constant-parameter line model, also known as the Dommel line model. In this case the distributed parameters of the line R, L, and C are assumed to be constant. In particular, they should be calculated for a frequency value representative of the range of interest. The model considers L and C to be distributed ("ideal line"), whereas R to be lumped at three places (line ends and line middle). One more difference respect to the theoretical line model (reported in Figure 3-4) consists in neglecting the conductance G. The frequency dependence of the line parameters is an important factor for the accurate simulation of waveform and peak values. However, the cp-line model is very robust and simple and provides a good alternative for a first approximation analysis and for the modelling of secondary lines.

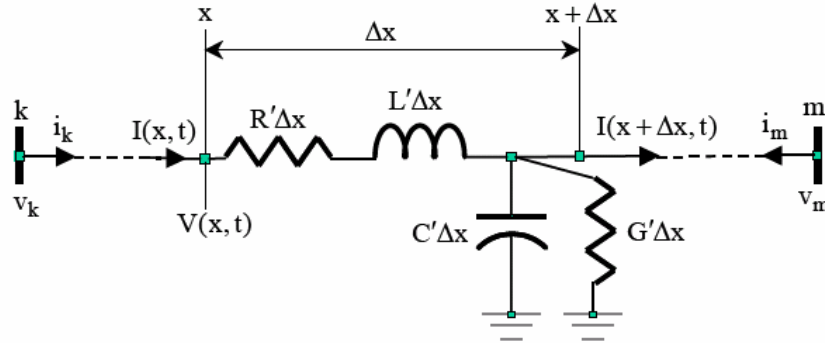


Figure 3-4. Distributed parameters line model.

The basic frequency domain equations of the single phase distributed parameter line shown in Figure 3-4, where the current and voltage values are reported in terms of phasors, are:

$$\frac{dV(x, t)}{dx} = -R' I(x, t) - L' \frac{dI(x, t)}{dt} \quad (3.1)$$

$$\frac{dI(x, t)}{dx} = -G' V(x, t) - C' \frac{dV(x, t)}{dt} \quad (3.2)$$

The primed variables are given in per line length. When Laplace transformation is used:

$$\frac{dV(x, s)}{dx} = -Z' I(x, s) \quad (3.3)$$

$$\frac{dI(x, s)}{dx} = -Y'V(x, s) \quad (3.4)$$

where:

$$Z' = R' + sL'$$

$$Y' = G' + sC'$$

Differentiation of equation (3.3) and (3.4) results into:

$$\frac{d^2V(x, s)}{dx^2} = \gamma^2V(x, s) \quad (3.5)$$

$$\frac{d^2I(x, s)}{dx^2} = \gamma^2I(x, s) \quad (3.6)$$

with:

$$\gamma = \sqrt{(R' + sL')(G' + sC')} = \alpha + j\beta \quad (3.7)$$

where  $\alpha$  is the attenuation constant and  $\beta$  is the phase constant.

The general solution of equations (3.5) and (3.6) is given by:

$$V(x, s) = V^+ e^{-\gamma x} + V^- e^{\gamma x} \quad (3.8)$$

$$I(x, s) = \frac{1}{Z_c} [V^+ e^{-\gamma x} - V^- e^{\gamma x}] \quad (3.9)$$

$$Z_c = \sqrt{\frac{R' + sL'}{G' + sC'}} = \hat{Z}_c \angle \theta_{Z_c} \quad (3.10)$$

$Z_c$  is the characteristic impedance of the line.

Substituting equation (3.7) into equation (3.8) and assuming that  $V^-$  and  $V^+$  are phasors gives:

$$V(x, s) = V^+ e^{j\theta} e^{-\alpha x} e^{-j\beta x} + V^- e^{-j\theta} e^{+\alpha x} e^{j\beta x} \quad (3.11)$$

The time-domain steady-state expression of this equation is:

$$V(x, t) = V^+ e^{-\alpha x} \cos(\omega t - \beta x + \theta^+) + V^- e^{+\alpha x} \cos(\omega t + \beta x + \theta^-) \quad (3.12)$$

Equation (3.12) can be modified and reused with equation (3.10) to convert equation (3.9) into time-domain steady-state:

$$I(x, t) = \frac{V^+}{Z_c} e^{-\alpha x} \cos(\omega t - \beta x + \theta^+ - \theta_{Z_c}) + \frac{V^-}{Z_c} e^{+\alpha x} \cos(\omega t + \beta x + \theta^- - \theta_{Z_c}) \quad (3.13)$$

The term  $e^{-\alpha x}$  is the attenuation of amplitudes of the waves. These expressions are the sums of forward travelling waves (+) and backward travelling waves (-).

A generic time-domain representation is written as:

$$V(x, t) = V^+(x - vt) + V^-(x + vt) \quad (3.14)$$

$$I(x, t) = I^+(x - vt) + I^-(x + vt) \quad (3.15)$$

with wave velocity:  $v = \frac{\omega}{\beta}$ .

The forward and backward travelling wave concept is interpreted using the illustration in Figure 3-5 for the waveform  $V^+(x-vt)$ . The travelling wave is first shown at  $t = 0$  where at  $x = a$  it has a value of  $V^+(a)$ . At any subsequent time  $t_x$  it has the same value at  $x = a + vt_x$  (distortion is neglected) as it formerly had at  $x=a$ . It means that the voltage distribution has moved in the direction of positive  $x$ .

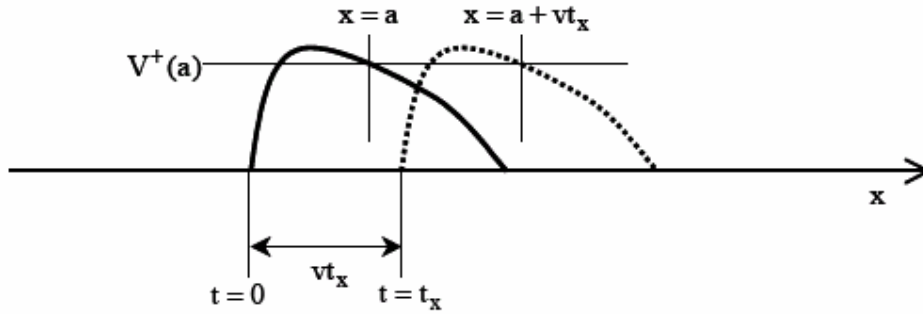


**Figure 3-5.** The forward travelling wave at  $t = 0$  and  $t = t_x$ .

A similar explanation is used for  $V^-$  which is travelling in the negative  $x$  direction.

In a lossless line the voltage and current waveforms feature the same shape and their amplitude depends on the characteristic impedance of the line; they travel along the line without being affected by distortion. Moreover, current and voltage waves have the same polarity if they travel in the positive  $x$  direction, whereas they have opposite sign if they are travelling in the negative  $x$  direction.

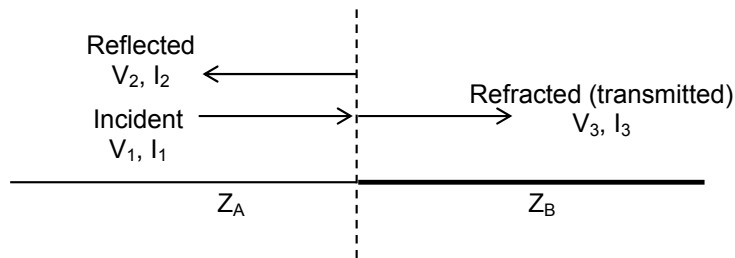


**Figure 3-6.** Propagation of voltage and current signals through a discontinuity point.

By referring to Figure 3-6 the reflection and refraction coefficients associated to any discontinuity section of the electric line can be computed.  $Z_A$  and  $Z_B$  are the characteristic impedances of the line portions before and after the junction, respectively. The equations given by the continuity condition in correspondence of the junction in Figure 3-6 are:

$$V_1 + V_2 = V_3 \qquad I_1 + I_2 = I_3$$

But also the relationships between voltages and currents determined by the line impedance hold:



$$I_1 = \frac{V_1}{Z_A}; \quad I_2 = \frac{V_2}{Z_A}; \quad I_3 = \frac{V_3}{Z_B}$$

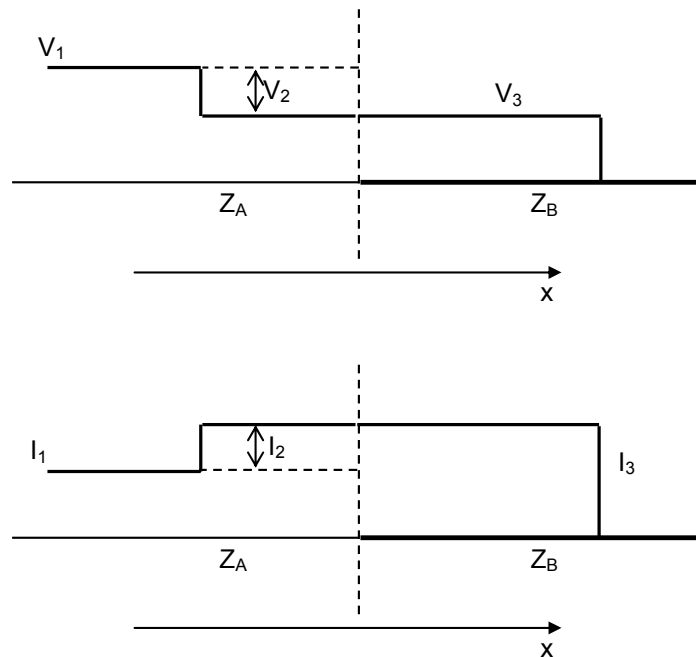
Hence the reflected and refracted values are:

$$V_2 = \frac{Z_B - Z_A}{Z_A + Z_B} \cdot V_1 = \Gamma_\alpha \quad (3.16)$$

$$V_3 = \frac{2 \cdot Z_B}{Z_A + Z_B} \cdot V_1 = \Gamma_\beta \quad (3.17)$$

$\Gamma_\alpha$  is the reflection coefficient and  $\Gamma_\beta$  the refraction one of the junction between the two line parts.

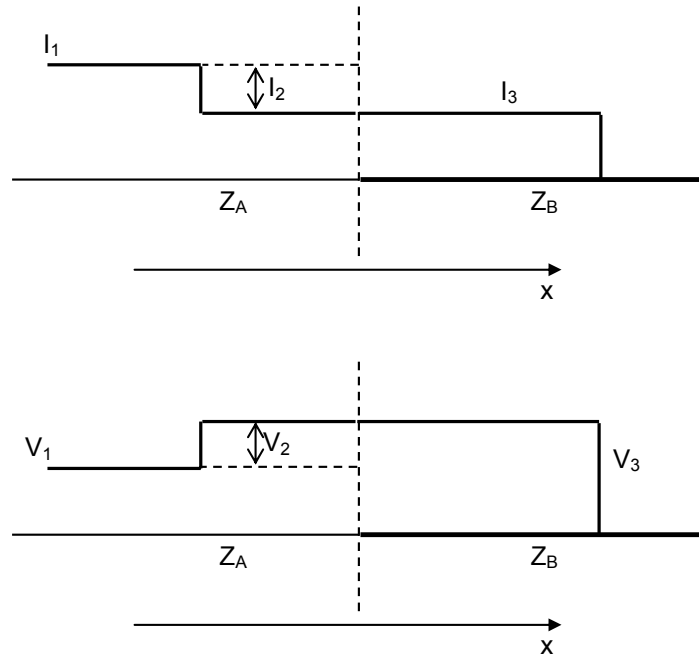
In case of  $Z_B < Z_A$ , as when overhead lines are connected to cables, the reflected voltage waveform is negative whereas the reflected current waveform is positive (see Figure 3-7).



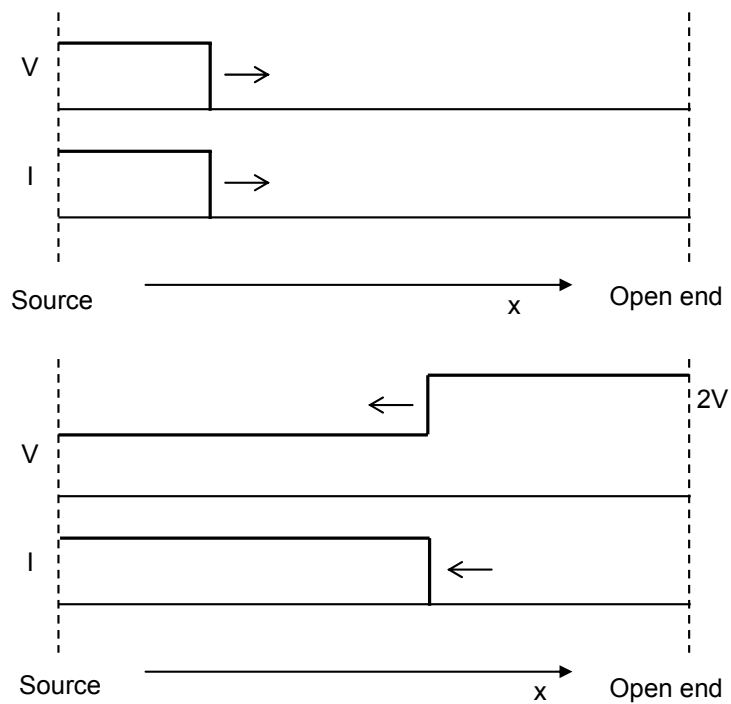
**Figure 3-7.** Discontinuity point in the case of  $Z_B < Z_A$ .

In case of  $Z_B > Z_A$  the reflection coefficient is positive, and the sign of the reflected waveforms is opposite respect to the previous case (see Figure 3-8.).

In the boundary condition of infinite  $Z_B$ , i.e. when the line is open at one end,  $\Gamma_\alpha$  is equal to 1 and  $\Gamma_\beta$  is 2. By considering the propagation of the signals along the line fed at the other end by an ideal source ( $Z_s = 0$ ), as time goes by a sequence of shots can be obtained, as reported in Figure 3-9.



**Figure 3-8.** Discontinuity point in the case of  $Z_B > Z_A$ .



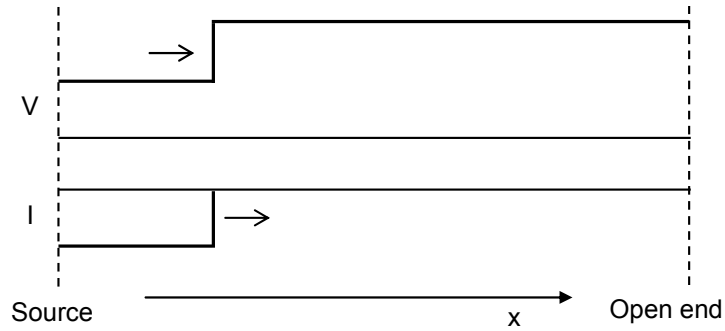


**Figure 3-9.** Propagation of current and voltage signals on a lossless open-ended line.

In practice, if  $T$  is the propagation time of the waves from one end of the line to the other end, the value of the voltage at the open end and the value of the current fed by the source are the ones represented in function of time in Figure 3-10 and Figure 3-11.

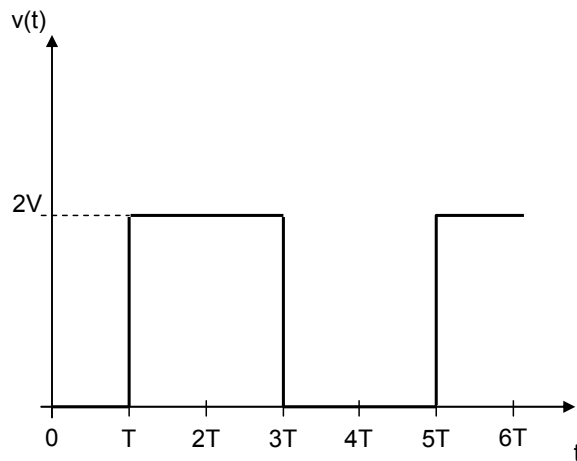


**Figure 3-10.** Voltage waveform registered at the open end of the line.

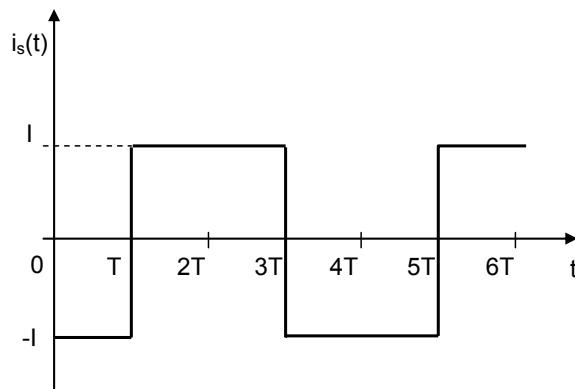


**Figure 3-11.** Current waveform generated by the source feeding the open ended line.

In the opposite condition, i.e. in case of short circuit at one end of the line,  $Z_B$  is assumed zero, so the propagation coefficients relevant to that end are:  $\Gamma_\alpha = -1, \Gamma_\beta = 0$ .

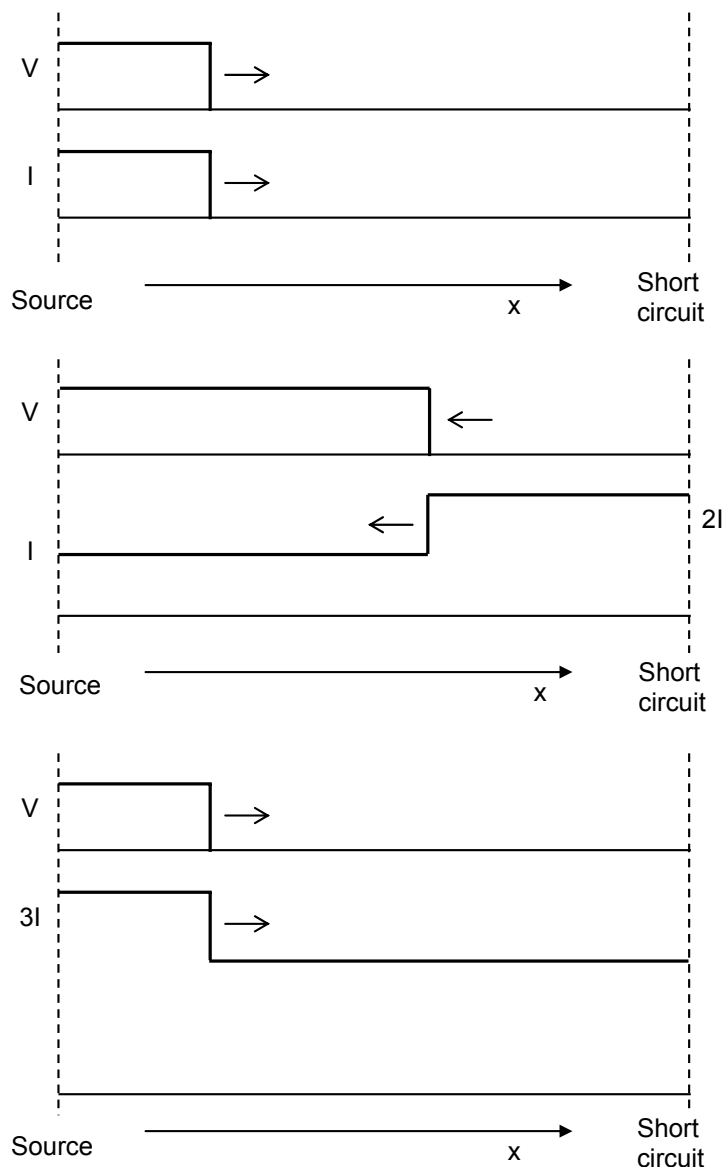


**Figure 3-12.** Propagation of current and voltage signals on a lossless short-circuited line.

In practice, if  $T$  is the time spent by the waves for propagating along the total line length, the currents at the source end and at the short-circuit point have the pattern represented in Figure 3-13 and Figure 3-14 respectively.

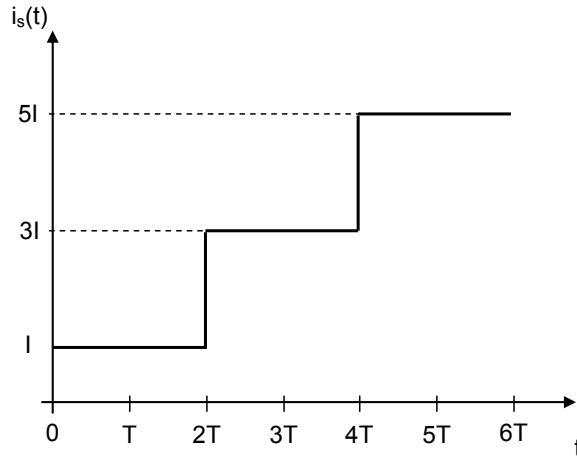


**Figure 3-13.** Current waveform at the source side of the short-circuited line.

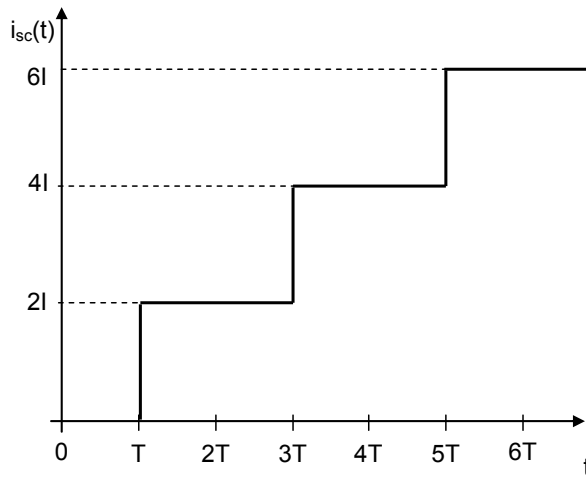


**Figure 3-14.** Current waveform at the short-circuit end of the line.

The ideal operating condition for a network is to have all the lines matched, that means having the same value of equivalent impedance at both sides of any discontinuity point. Such a condition is achieved by the presence of suitable adaptive resistance  $R_m$  at the end of the line, so that  $R_m = Z_A$ . In this way  $Z_A = Z_B = R_m$  and the line has the same behaviour of an equivalent infinitely long line, in fact no reflected wave can occur and the transmitted wave is identical to the incident one (see Figure 3-15).

In the case of a real transmission line, losses have to be taken into account; the main sources of energy loss are the non-zero resistance of conductors, the Corona effect and the leakage currents along insulators. The effects of leakage and of longitudinal resistance are the exponential fall of the waveform front of voltage and current respectively.

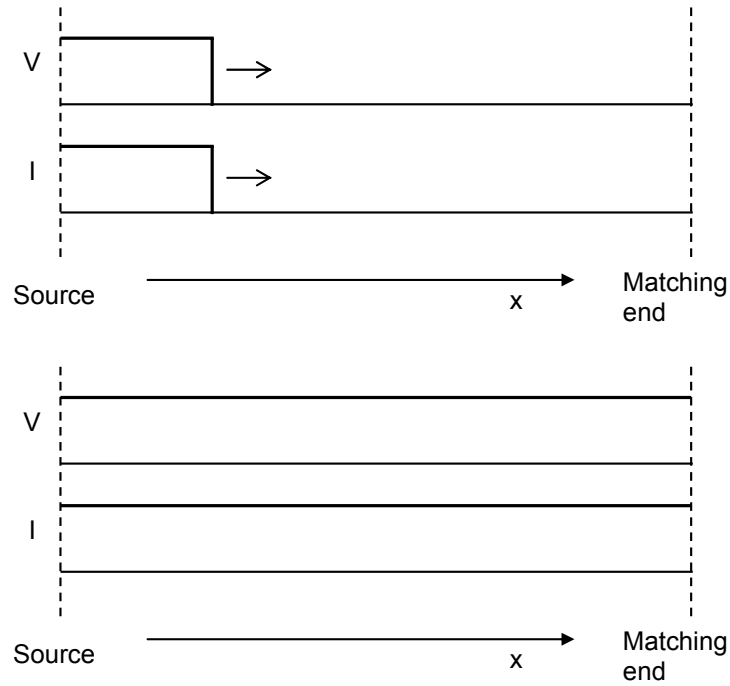


**Figure 3-15.** Propagation of current and voltage signals along a matched line.

In correspondence of the waveform front, anyway, the relationship between voltage and current still holds:

$$V = V_0 e^{-\frac{G}{C}t} \quad (3.18)$$

$$I = I_0 e^{-\frac{R}{L}t} \quad (3.19)$$

$$V = Z_s \cdot I \quad (3.20)$$

The system of the three above equations leads to the condition for a non-distorting lossy

$$\text{line: } \frac{R}{L} = \frac{G}{C} \quad (3.21)$$

The energy dissipated on the characteristic impedance  $Z_B$  of a line can be considered as the energy transferred from line A to line B. the energy portion not transferred to the B-line gives rise to a reflected wave. By the source-end perspective, the line behaviour is the one of a pure resistance only if the line is matched, but in general for the time interval  $0 < t < 2T$ .

$$\frac{R}{L} = \frac{G}{C} = Z_s^2 \Rightarrow I^2 R = V^2 G \quad (3.22)$$

In a non-distorting line the energy can be thought as shared in equal parts between the electric and magnetic field, moreover the same portion of energy is dissipated by resistive losses and leakage.

In case of multi-conductor lines the propagation of electric signals depends also on the coupling between conductors. For the sake of simplicity let us consider two conductors and the ground, configured as reported in Figure 3-16.

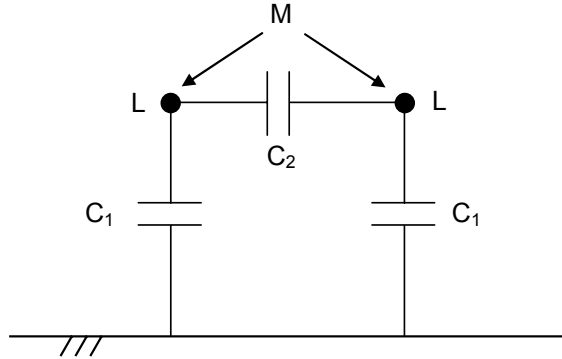


**Figure 3-16.** Two conductors line - representation of its equivalent coupling parameters.

$$-\frac{dV_1}{dx} = L \frac{dI_1}{dt} + M \frac{dI_2}{dt} \quad (3.23)$$

$$-\frac{dI_1}{dx} = C_1 \frac{dV_1}{dt} + C_2 \frac{d(V_1 - V_2)}{dt} \quad (3.24)$$

The system of equations above leads to the following expression:

$$(a^2 - b^2) \frac{d^4 V_1}{dt^4} - 2a \frac{d^4 V_1}{dt^2 dx^2} + \frac{d^4 V_1}{dx^4} = 0 \quad (3.25)$$

where:

$$a = L \cdot (C_1 + C_2) - MC_2$$

$$b = M \cdot (C_1 + C_2) - LC_2$$

The solutions of equation (3.25) have the following expression:

$$V_1 = f_1(x + vt) \quad (3.26)$$

$$V_2 = f_2(x + vt)$$

where obviously  $v$  is a velocity. It can be shown that couple of travelling waves propagate along the line at different speeds:

$$v_\alpha = \pm \frac{1}{\sqrt{a-b}}$$

$$v_0 = \pm \frac{1}{\sqrt{a+b}}$$

It can be said that there are two different propagation modes:

- i. conductor – conductor;
- ii. conductor – ground.

In general, if the line consists in N conductors at a certain height above the ground, N propagation modes exist. In the case of two conductors, i.e. N=2, if the ground is a perfect conductor ( $\rho=0$ )  $b$  is null, hence the propagation speed is unique. If the ground is not a perfect conductor, on each line conductor waves travelling at different speeds are present; finally, the resulting waveform is distorted. Such resulting voltages and currents are just the phase signals.

### 3.2.1. Travelling Waves

When a fault occurs along a transmission line, the voltage and current transients will travel towards the line terminals. These transients will continue to bounce back and forth between the fault point and the two terminals of the faulted line until the post-fault steady state is reached. Evolution of the terminal bus transients can be constructed by using the *Lattice Diagram* method.

Let us consider a single-phase lossless transmission line of length  $l$ , connected between buses A and B, with characteristic impedance  $Z_c$  and traveling wave velocity  $v$ . If a fault occurs at a distance  $x$  from bus A, this will appear as an abrupt injection at the fault point. This injection will travel like a surge along the line in both directions between the fault point and the two terminal buses until the post fault steady state is reached.

A lattice diagram illustrating the reflection and refraction of traveling waves initiated by the fault transients is shown in Figure 3-17. On the left side of the figure, a line connecting buses A and B is vertically drawn. A phase to ground fault is assumed to occur at point F,  $x$  miles from bus A. The horizontal axis developing from point F, corresponds to the time reference. The arrows shown below the lattice diagram indicate the arrival times of various waves reflected from the fault as well as bus B. The travel times from the fault to bus A, and from the fault to bus B are designated by  $T_1$  and  $T_2$  respectively. Given the traveling wave velocity  $v$ ,  $T_1$  and  $T_2$  will be given by:

$$T_1 = \frac{x}{v} \tag{3.27}$$

$$T_2 = \frac{l-x}{v} \tag{3.28}$$

Construction of the Lattice Diagram becomes computationally difficult if the attenuation and distortion of the signals are taken into account as they travel along the line. This is the case of lossy as well as non matched line, as above explained. In fact the reflection and refraction coefficients in the discontinuity points depend on the characteristic impedance of the line and on the equivalent impedance of source and load busses. On the other hand, time-frequency analysis of the transient signals can be used to determine the propagation times of these transients between the fault point and the line terminals.



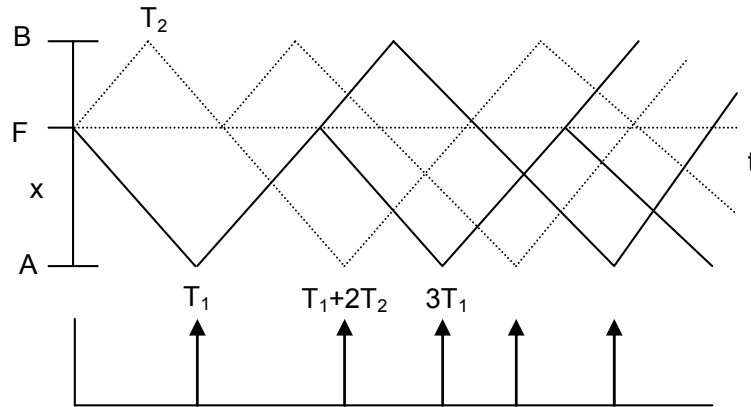


**Figure 3-17.** Lattice diagram for a fault at  $x$  miles from A.

In three-phase transmission lines, if losses are taken into account, there are three modes of propagation, therefore for the analysis of the traveling wave effect, phase values must be converted into modal values.

### 3.2.2. Modal Transformation

In three-phase systems the phase domain signals are first decomposed into their modal components by means of the modal transformation matrices:

$$S_{\text{mode}} = T \cdot S_{\text{phase}} \quad (3.29)$$

where  $S_{\text{mode}}$  and  $S_{\text{phase}}$  are the modal and phase signals (voltages or currents) vectors respectively.

The line currents transformation matrix  $T_i$  is the matrix that makes diagonal the product  $Y_{ph} \cdot Z_{ph}$  where  $Y_{ph}$  is the shunt admittance matrix in phase quantities and  $Z_{ph}$  is the series impedance matrix in phase quantities.

The resulting diagonalizing matrix, called  $T_i$ , determined by the eigenanalysis routines, is complex. To standardize the results,  $T_i$  is normalized by using the Euclidean Norm.

The voltages transformation matrix  $T_v$  (which diagonalizes the reverse product  $Z_{ph} \cdot Y_{ph}$ ) is not determined by the eigenanalysis routines, but calculated directly from the relationship  $T_v = T_i^{-t}$  (where the superscript means inverse transposed). The matrices  $Y_{ph} \cdot Z_{ph}$  and  $Z_{ph} \cdot Y_{ph}$  are not equal but have the same eigenvalues that, squared form the diagonal matrix  $[\gamma]^2$ . The elements  $\gamma_i$  of the matrix represent the propagation constant of mode  $i$ . They are complex numbers  $\gamma_i = \alpha_i + j\beta_i$  where  $\alpha_i$  is the attenuation constant and  $\beta_i$  is the phase constant of the mode  $i$ .

For a perfectly balanced line, the modal transformation matrices to relate modal and phase quantities do not change with frequency (constant transformation matrices) and can be chosen to be real (e.g. generalized Clarke). In particular, Clarke's transformation

is one of the commonly used modal transformations for fully transposed lines to decouple the phase domain signals into independent modal components. One advantage of Clarke's transformation is that, unlike the symmetrical component transformations, the corresponding transformation matrix is real. Clarke's transformation matrix, which relates the modal vectors  $V_{1,2,3}$  to the phase vectors  $V_{a,b,c}$  is given below:

$$\begin{bmatrix} V_1 \\ V_2 \\ V_3 \end{bmatrix} = \begin{bmatrix} 1 & 1 & 1 \\ 2 & -1 & -1 \\ 0 & \sqrt{3} & -\sqrt{3} \end{bmatrix} \begin{bmatrix} V_a \\ V_b \\ V_c \end{bmatrix} \quad (3.30)$$

If the studied line is untransposed, then an eigenvector based transformation matrix, which is frequency dependent, has to be used. This matrix should be computed at a frequency equal or close to the frequency of the initial fault transients.

For processing purpose of line models in time-domain real transformation matrices  $T_i$  and  $T_v$  can be used. To obtain approximate  $T_i$  and  $T_v$  matrices, the columns of  $T_i$  (complex) can be rotated to make the imaginary parts of its elements small and then retain only the real parts. In the case of the pi-exact model, the final form of the model is expressed in terms of self and mutual phase quantities, and there is no impediment in using exact complex transformation matrices at each frequency at which the model is produced. This model, however, is a one-frequency model, valid for steady-state solutions but not for transients simulations.

### 3.3. Time-frequency representation of signals

The analysis of non-periodic signals with continuous spectrum (as transient phenomena affecting power lines are) is carried out by using the wavelet transform, one of the most powerful tools for this kind of study.

The wavelet transform is based on the use of the time-frequency representations (TFR), which allow to estimate how the signal spectrum is modified vs. time. Instead of transforming a time-domain representation into a frequency-domain representation, like traditional operators (e.g. the Fourier transform), it uses a time-frequency correlated description. This way, it is easier to understand the time instant at which an event occurs.

Let us consider a generic signal  $x(t)$  expressed as a linear combination of  $N$  signals, whose generic term is denoted by  $x_k(t)$ :

$$x(t) = \sum_{k=1}^N a_k x_k(t) \quad (3.31)$$

Moreover, let us denote the time-frequency representation of  $x(t)$  by  $T_x(t, f)$ .

The TFRs are classified into linear and quadratic. As for the linear ones, the following relationship holds:

$$T_x(t, f) = \sum_{k=1}^N a_k T_{x_k}(t, f) \quad (3.32)$$

being  $T_{x_k}(t, f)$  the time-frequency representation of  $x_k(t)$ . The quadratic TFRs are characterized by a non-linear combination of the terms  $T_{x_k}(t, f)$ . For the sake of simplicity, but without loss of generality, for  $N = 2$  equation (3.32) turns into:

$$T_x(t, f) = a_1^2 T_{x_1}(t, f) + a_2^2 T_{x_2}(t, f) + a_1 a_2^* T_{x_1 x_2}(t, f) + a_1^* a_2 T_{x_2 x_1}(t, f) \quad (3.33)$$

where the asterisk refers to the complex conjugate and  $T_{x_1 x_2}(t, f)$ ,  $T_{x_2 x_1}(t, f)$  are cross terms due to the interference between spectral components.

The TFR of a signal, no matter whether it is linear or not, links a one-dimensional function of time (the signal  $x(t)$ ) into a bi-dimensional function of time and frequency  $T_x(t, f)$ . Hence, it can be represented by means of a 3-D surface, like that depicted in Figure 3-19. This surface is the result of the application of a linear TFR to signal  $x(t)$  plotted in Figure 3-18.

The Short Time Fourier Transform (STFT) and wavelet transforms are typical linear TFRs, whereas the Wigner-Ville Distribution (WD) is a typical quadratic TFR. By way of example, the main features of the STFT are briefly recalled in the following.

The STFT is a windowed Fourier transform. To apply it, the observation interval is divided into a given number of subintervals. Then, the STFT is computed, over each subinterval, according to the following equation:

$$X_{STFT}(t, f) = \int_{-\infty}^{\infty} x(\tau) \cdot w(t - \tau) \cdot e^{-j2\pi f\tau} d\tau \quad (3.34)$$

where  $w(t)$  is the windowing function, which defines the length of the subinterval and can be one of well-known (rectangular, Hanning, Hamming, ...) analysis functions, and  $X_{STFT}(t, f)$  is the result of the transform.

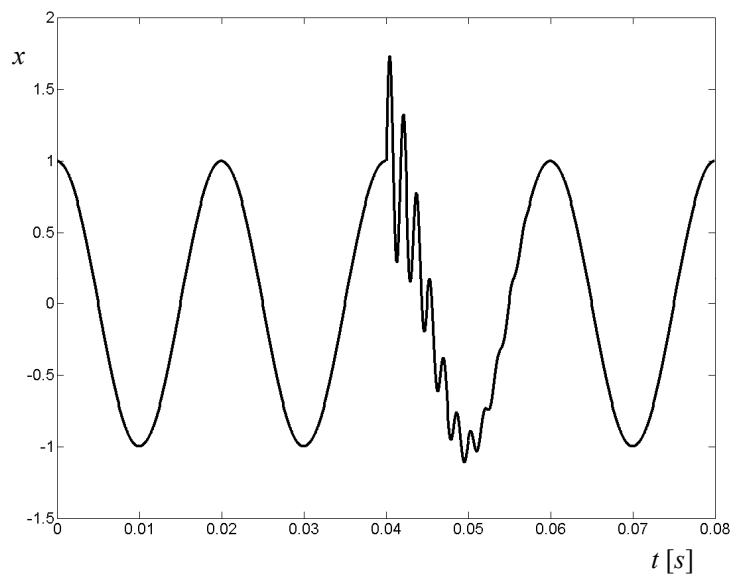


Figure 3-18. Aperiodic signal.

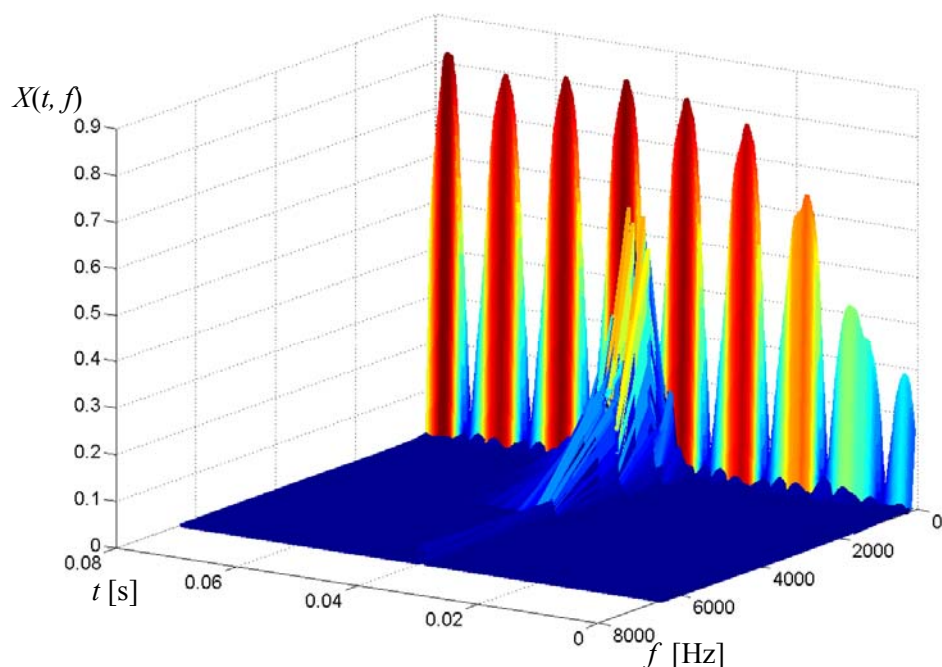


Figure 3-19. TFR of the signal  $x(t)$  shown in Figure 3-18.

The main drawback of the STFT is that the time-frequency resolution is constant and given by the duration of the window. However, it is essentially based on the well known Fourier transform and this fact makes it easy and fast to implement.

### 3.3.1. The wavelet transform

The wavelet transform is a TFR representation of a signal  $x(t)$ . This kind of representation is alternative to the traditional Fourier-based transform and the use of one rather than the other is strictly dependent on the characteristics of the signal to be analyzed. In practice, the wavelet transform becomes very useful when periodic signals with short non-periodic components superimposed have to be studied. In other words, the wavelet transform allows good frequency resolution at low frequencies and good time resolution at high frequencies. It means that it is possible to discriminate high frequency components very close to each other in time and low frequency components very close to each other in frequency. This property is particularly suitable for the study of the above kind of signals and, as it will be clarified soon, it is due to the nature of the functions which form the basis for the wavelet transform.

From an historical point of view, the first work where the main concept can be found was published at the beginning of the XX century [2], but it is in the '80s that the wavelet transform starts to become very popular, see e.g. [3 - 7], and applied in many fields, such as power quality (mainly for the characterization of electromagnetic transients), diagnostics, image processing, data compression, biomedicine, geophysics (by way of example, see [8 - 13]).

The Continuous Wavelet Transform (CWT)  $X(a,b)$  of a function  $x(t)$  is defined as follows:

$$X(a,b) = \frac{1}{\sqrt{|a|}} \int_{-\infty}^{+\infty} x(t) \cdot w\left(\frac{t-b}{a}\right) dt = \int_{-\infty}^{+\infty} x(t) \cdot w_{a,b}(t) dt \quad (3.35)$$

where  $w_{a,b}(t)$  is the wavelet derived from a function  $w(t)$ , which is referred to as mother wavelet, by changing the parameters  $a$  (scale) and  $b$  (time). The mother wavelet  $w(t)$  is usually referred to as  $w_{1,0}(t)$ . The factor  $1/\text{rad}(|a|)$  ensures that  $|w_{a,b}| = |w| = 1$ . Figure 3-20 shows the plot of the mother wavelet of Morlet.

The mother-wavelet frequency spectrum is similar to the one of a band-pass filter. Parameter  $a$  both varies and shifts the frequency bandwidth (narrow band at low frequency, wide band at high frequency). In the time domain, it corresponds to a dilatation or a contraction of  $w(t)$ . Parameter  $b$  simply operates a time translation of the mother wavelet. The so-obtained functions (wavelets) are the basis for the transform. In this way,  $x(t)$  is analyzed with different resolution in frequency and time, and is decomposed into sub-bands having bandwidth scaled by  $a$ .

A generic function must meet two simple conditions in order to be defined as mother wavelet:

- i. being well localized in time and
- ii. have zero mean.

However, further properties such as orthogonality and biorthogonality are, in practice, required, as explained in the following. Finally, it is worthwhile emphasizing that the wavelet transform of a signal  $x(t)$  is the inner product between the signal itself and the wavelet  $w_{a,b}(t)$ :

$$X(a,b) = x(t) \cdot w_{a,b}(t)$$

It means that the coefficients  $X(a,b)$  are indices of the similarity between  $x(t)$  and  $w_{a,b}(t)$ .

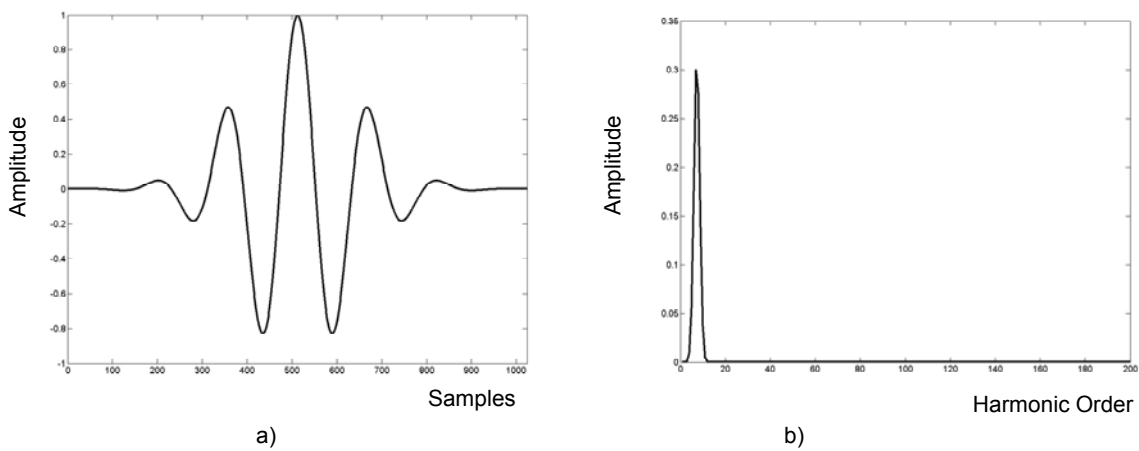


**Figure 3-20.** Mother wavelet of Morlet (a) and the relevant magnitude spectrum (b).

Hence, a function  $w(t)$  which is good for the analysis of a given signal, could not be as much useful for another one. The choice of the more fitting mother wavelet is still an issue when application of the analysis is concerned; studies are at present in progress aimed at developing suitable algorithm which automatically select the mother wavelet in function of the signal to be analyzed.

To better clarify this point, let us consider Figure 3-20 and Figure 3-21. Figure 3-20b depicts the magnitude spectrum of the wavelet of Morlet of Fig. 4.5 and Figure 3-20a, which is, as above mentioned, quite similar to the one of a band-pass filter.

By decreasing the value of  $a$ , a contraction in the time domain occurs, as shown in Figure 3-21a. Figure 3-21b shows the effects in the frequency domain: the spectrum is shifted to higher frequencies and the bandwidth is increased. By decreasing again the value of  $a$ , the function is some more contracted and the spectrum is some more shifted and increased. It is clear that, if  $a$  is increased, the behavior of the function is exactly reversed: dilatation in time vs. contraction and down-shifting in frequency.

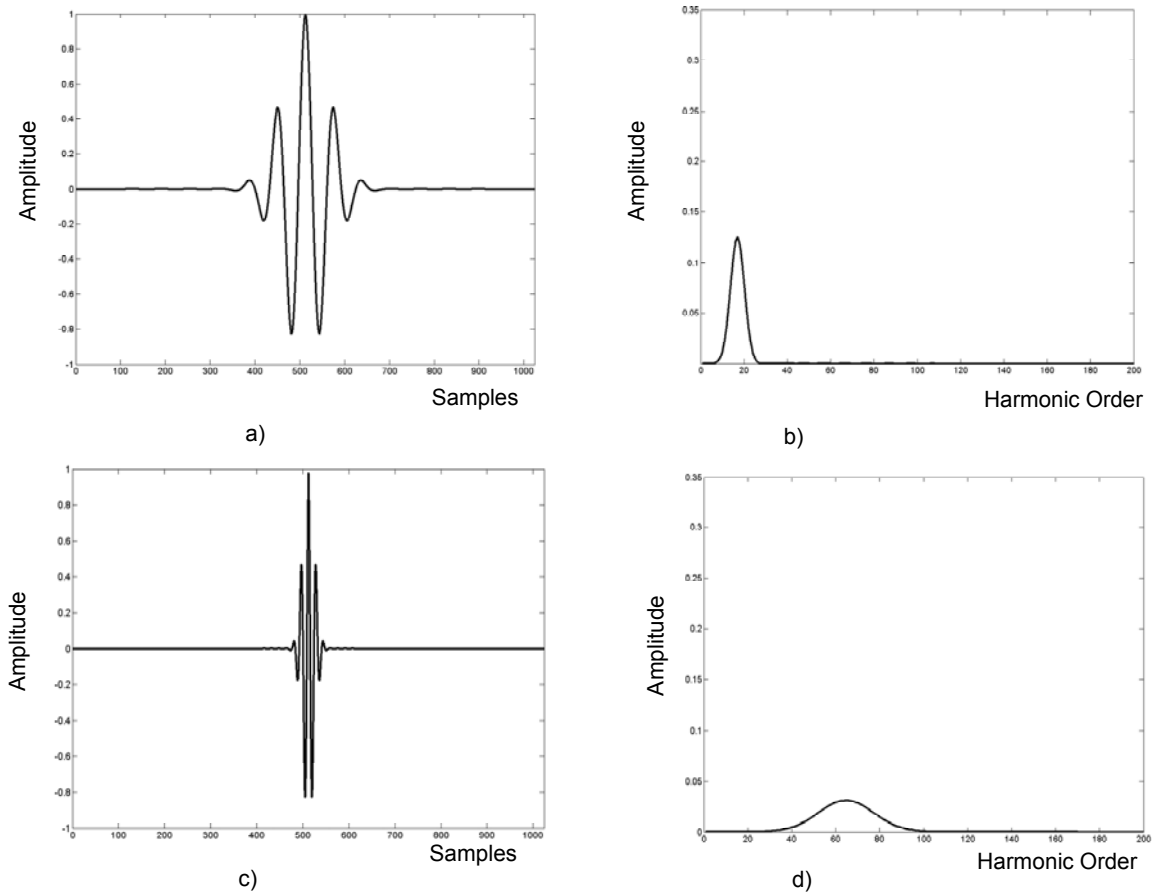


**Figure 3-21.** Wavelet obtained by contracting the mother wavelet of Morlet (a, c) and the relevant magnitude spectrum (b, d).

### 3.3.2. The discrete-time wavelet transform

The CWT defined by (3.35) cannot be used for practical applications because it cannot be implemented on DSP systems. The discrete-time wavelet transform (DTWT) is the digitally usable version of the CWT. It is defined by the following expression:

$$X_{m,i} \triangleq \frac{1}{\sqrt{a_0^m}} \sum_n x[n] \cdot w\left[\frac{i - na_0^m}{a_0^m}\right] \quad (3.36)$$

Where  $x[n]$  and  $w[\cdot]$  refer to the digitized input signal and the discrete counterpart of the mother wavelet, respectively. Parameters  $a$ ,  $b$  have been expressed by the following functions:

$$a = a_0^m, b = na = na_0^m,$$

where  $a_0$  and  $m$  are integer and  $m$  refers to the generic  $m$ -th frequency sub-band of the signal. Typically, it is chosen  $a = 2$ , thus allowing to analyze the signal in a high number of sub-band.

In order to present how the DTWT is usually implemented, let us discuss the following example taken from [14], in which DTWT is based on the Haar basis [2]. Let us consider

the following elements of  $x[n]$ :  $x[0]$ ,  $x[1]$ ,  $x[2]$ ,  $x[4]$ . The transform replaces these four numbers with other four numbers  $y[0]$ ,  $y[1]$ ,  $y[2]$ ,  $y[4]$  that are, due to the linearity, a linear combination of the formers. The following sums and differences are made:

$$y[0] = x[0] + x[1] \qquad y[2] = x[2] + x[3]$$

$$y[1] = x[0] - x[1] \qquad y[3] = x[2] - x[3]$$

If the values

$$x[0] = 1.2, \quad x[1] = 1.0, \quad x[2] = 1.0, \quad x[4] = -1.2$$

are considered, the following results hold:

$$y[0] = 2.2, \quad y[1] = 0.2, \quad y[2] = -2.2, \quad y[3] = 0.2.$$

It should be noted that the value of  $y[1]$  and  $y[3]$  can be considered negligible with respect to  $y[0]$  and  $y[2]$ . Hence, one can conclude that, in this new representation, only two terms are sufficient to represent this signal and compress it by cancelling  $y[1]$  and  $y[3]$ . Obviously, in such a case we are not able to perform a perfect reconstruction of  $x$ . Moreover, it should be underlined that  $y[0]$  and  $y[2]$  are obtained by summing consecutive input samples and, hence, they are a kind of moving “average” of the input signal. It means also that they are the result of a low-pass filter. As for  $y[1]$  and  $y[3]$ , they are gauged by the difference of consecutive input samples: hence, they are a kind of moving difference of  $x$ . This is the typical result of high-pass filter. In particular, this filter is the mirror of the above low-pass filter.

Summarizing, the application of the transform has allowed to divide the highest frequency components, which are referred to as details, from the lowest ones, which are referred to as approximations. Figure 3-22 depicts this situation.

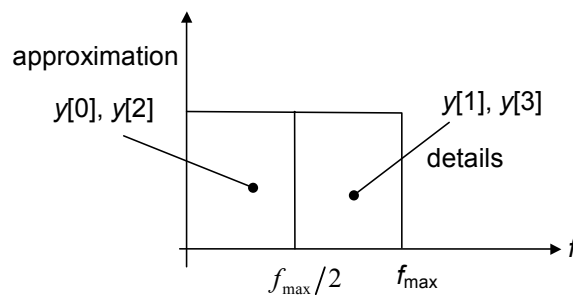


**Figure 3-22.** Details and approximation in the frequency domain.

a sampling frequency equal to  $f_s$  was assumed and hence  $f_{\max}$  is the Nyquist frequency  $f_s/2$ . If the transform is then applied to these approximations, other details and approximations will be gauged:

$$z[0] = y[0] + y[2] = 0 \qquad z[2] = y[0] - y[2] = 4.4$$

The term  $z[0]$  is the approximation (lower component) whereas  $z[2]$  is the detail (higher component). Figure 3-23 depicts this result.



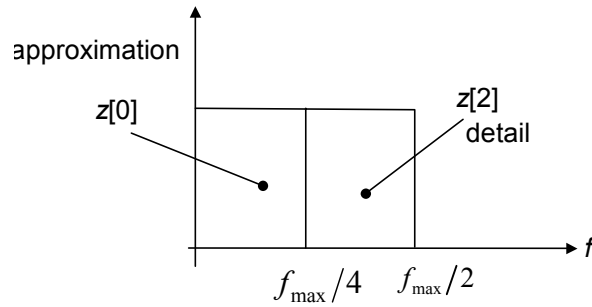


**Figure 3-23.** Details and approximation in the frequency domain after the iteration of the procedure.

Moreover it should be noted that the component  $z[2]$  does most of the work of the original four. Hence, a strong compression of the data can be obtained. The described procedure turns into a multi-resolution analysis. The meaning of this term becomes clear if Figure 3-24, which is gauged by combining Figure 3-22 and Figure 3-23, is observed.

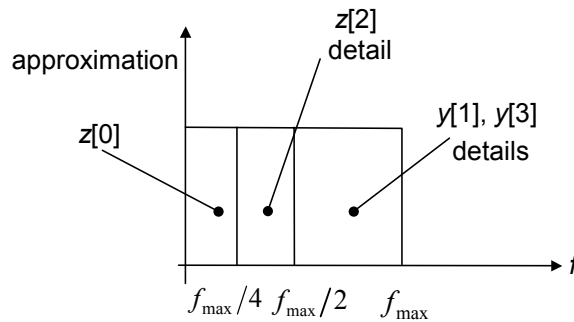


**Figure 3-24.** Sub-bands obtained by the iteration of the low-pass and high-pass filters.

As a result, the input signal has been analyzed by means of band-pass filters having bandwidth scaled by power of 2. By keeping in mind, as mentioned in the previous Section, that wavelets are essentially suitable band-pass filters, one can conclude that the DTWT can be implemented by following a procedure like this.

At the end of this example, two considerations must be pointed out: it is possible to implement the DTWT by means of a cascade of proper low-pass and high-pass filters (filter bank); the wavelet transform can be used also to compress data, since it represents the signal with many negligible terms.

### 3.3.3. Filter banks

A filter is a linear time-invariant operator which acts on an input vector  $x$  and produces an output vector  $y$  given by the convolution of  $x$  with a given vector  $h$  [14]. This vector contains filter coefficients  $h[0], h[1], \dots$ . It holds

$$y[n] = \sum_k h[k] \cdot x[n - k] \quad (3.37)$$

$h[0], h[1], \dots$  are the elements of the impulse response, obtained by applying a unity amplitude sample. In the frequency domain can be rewritten as:

$$Y(\omega) = H(\omega) \cdot X(\omega) \quad (3.38)$$

Where

$$X(\omega) = \sum_{n=-\infty}^{+\infty} x[n] \cdot e^{-j\pi\omega n} \quad (3.39)$$

$$H(\omega) = \sum_{n=-\infty}^{+\infty} h[n] \cdot e^{-j\pi\omega n} \quad (3.40)$$

A filter bank is a set of filters, which can be divided in analysis bank and synthesis bank, and has often two filters, low-pass and high-pass. The analysis banks split the input signal into frequency bands whereas the synthesis one allows the signal to be recombined. Figure 3-25 shows a typical two-channel filter bank.  $H_0$  and  $H_1$  are a low-pass and a high-pass filter, respectively, whereas  $F_0$  and  $F_1$  are the corresponding filters of the synthesis bank.

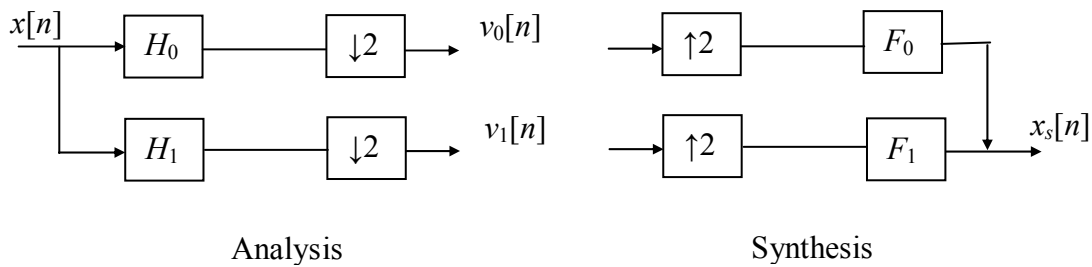


**Figure 3-25.** Analysis and synthesis block diagrams of a two-channel filter.

As for symbols  $\downarrow 2$  and  $\uparrow 2$ , they indicate a decimator and an expander by 2, respectively. The length of the output of the analysis bank is doubled, since both  $v_0$  and  $v_1$  have the same length as  $x$ . This information is redundant and hence it is possible to down-sample the outputs by removing, for example, the odd-numbered elements. This is a linear operation but it is not time-invariant. The filtering and decimation operations can be done with one matrix only where the down-sampling is performed by removing the odd-numbered rows of the filter matrix and hence, in the resultant matrix, which becomes rectangular, each row can be obtained from the previous one with a double-shifting.

As for the expander  $\uparrow 2$ , it performs an up-sampling by inserting zeros in odd-numbered elements. To do this with a matrix, zero rows have to be inserted. In other words, each column can be obtained from the previous one with a double-shifting.

When  $x_s[n]$  is equal to  $x[n]$ , with at the most a delay  $l$ , the filter bank performs a perfect reconstruction. The following two conditions have to be met for a perfect reconstruction:

$$F_0(z) H_0(z) + F_1(z) H_1(z) = 2z^{-l} \quad (3.41)$$

$$F_0(z) H_0(-z) + F_1(z) H_1(-z) = 0 \quad (3.42)$$

The first condition states that there is no distortion, whereas the second condition determines alias cancellation. Moreover, the latter one provides simple relationships between the filter coefficients (alternating signs):

$$F_0(z) = H_1(-z) \text{ and } F_1(z) = -H_0(-z) \quad (3.43)$$

A filter bank which performs perfect reconstruction is biorthogonal. It means that the filters of the synthesis bank are the inverse of filters of the analysis bank. Moreover, when the synthesis bank is the transpose of the analysis one, the filter bank is orthogonal. In such a case, a further condition on filter coefficients arises:

$$h_1[k] = (-1)^k h_0[N-k] \quad (3.44)$$

where  $N$  is an odd number denoting the number of taps. Hence, under orthogonal conditions, fixing the coefficients of the low-pass filter allows defining all filter banks by means of (3.43) and (3.44).

### 3.3.4. Wavelets and filter banks

As a conclusion of the above discussion, it should be clear that the DTWT can be implemented by means of the analysis filter bank, such as the one shown in Figure 3-26. called wavelet decomposition tree. In this picture,  $h$  and  $g$  are the impulse response of a suitable high-pass and of its dual low-pass filters, respectively. The number  $\gamma$  and the value of the coefficients of each filter are typical of a given mother wavelet.

These filters have three main characteristics:

- I. they are FIR filters;
- II. the sum of their coefficients is 1;
- III. their norm is 1.

The generic  $m$ -th stage of the filter bank, which performs a parallel filtering and a downsampling of the filters output, produces two output vectors  $y_m$  and  $\beta_m$ , which are referred to as detail coefficients and approximation coefficients, respectively.

Each vector  $\beta$  feeds the following stage. It coincides with the input sequence  $x[n]$  when the first stage is considered.

The detail vectors  $y_0, y_1, \dots, y_m, \dots$  represent the signal in the sub-bands  $0, 1, \dots, m, \dots$ , respectively.

Both vectors  $y_m$  and  $\beta_m$  relevant to the  $m$ -th sub-band can be expressed, as suggested in [14], by means of the following matrix form:

$$\begin{bmatrix} \beta_m[j] \\ y_m[j] \\ \beta_m[j+1] \\ y_m[j+1] \\ \vdots \\ \vdots \end{bmatrix} = \begin{bmatrix} \cdot & \cdot & \cdot & \cdot & \cdot & \cdot & \cdot & \cdot & \cdot & \cdot \\ \cdot & g[0] & g[1] & g[2] & \cdot & g[\gamma-1] & 0 & \cdot & \cdot & \cdot \\ \cdot & h[0] & h[1] & h[2] & \cdot & h[\gamma-1] & 0 & \cdot & \cdot & \cdot \\ \cdot & 0 & 0 & g[0] & g[1] & g[2] & \cdot & g[\gamma-1] & 0 & \cdot \\ \cdot & 0 & 0 & h[0] & h[1] & h[2] & \cdot & h[\gamma-1] & 0 & \cdot \\ \cdot & \cdot & \cdot & \cdot & \cdot & \cdot & \cdot & \cdot & \cdot & \cdot \\ \cdot & \cdot & \cdot & \cdot & \cdot & \cdot & \cdot & \cdot & \cdot & \cdot \end{bmatrix} \begin{bmatrix} \beta_{m-1}[j] \\ \beta_{m-1}[j+1] \\ \beta_{m-1}[j+2] \\ \beta_{m-1}[j+3] \\ \vdots \\ \vdots \end{bmatrix} \quad (3.45)$$

When the mother wavelet gives rise to orthogonal basis, also the matrices (and the filter bank) are orthogonal. The following relationship between taps holds:

$$g[n] = h[\gamma-n-1] \quad n = 0, 1, \dots, \gamma-1 \quad (3.46)$$

It must be noted that an ideal filter bank cuts the frequency band in half and hence there is no overlap between the sub-bands. But in practical applications actual filters with a finite number of coefficients are used and hence overlapping of sub-band arises. This causes a sharing of information between adjacent sub-bands, making hence less effective the filtering properties of such a transform.

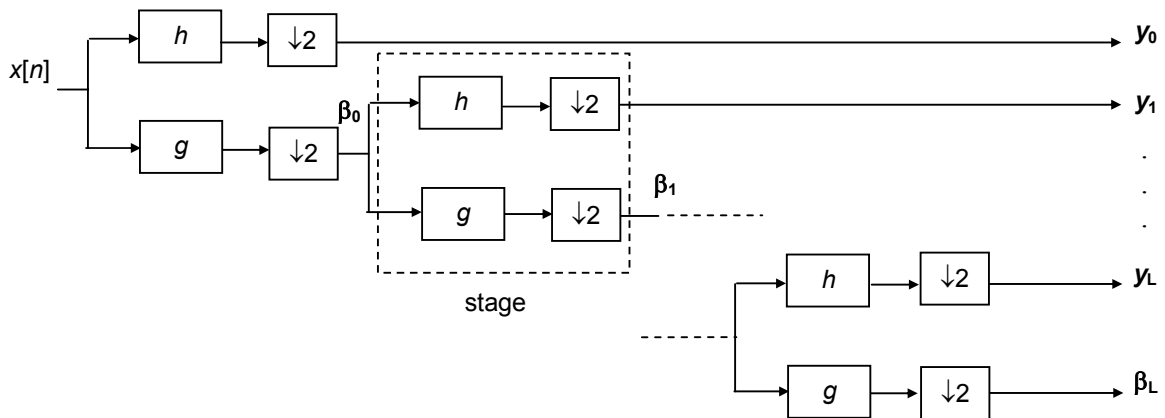


Figure 3-26. Filter bank for the DTWT implementation

Thanks to its interesting properties of multi-resolution analysis, which allows to get good frequency resolution at low frequencies and good time resolution at high frequencies, wavelets are widely applied in power quality, specially to the study of voltage transients. Hence, several papers relevant to this application can be found in the literature. Although it started to be used in image processing up to the last few years, it is only in 1993 that the wavelet transform is associated to power quality and in 1994 the first results are published where some voltage disturbances are analyzed by means of the CWT. It must be noted that different kinds of Daubechies mother-wavelet (with 4, 6, 8 and 10 coefficients) allows the most part of voltage transients to be correctly analyzed. In

particular, db4 (Daubechies with 4 coefficients) and db6 seem to be useful for “fast” transients, whereas db8 and db10 become more attractive in the presence of “slow” transients.

#### **3.4. Fault location methods for distribution networks**

Fault location is important for safe operating conditions of power systems. In transmission power systems the development of techniques for estimating the location of a fault along the lines has been considered an essential requirement for power companies. Despite somehow useful, little work has been done in the development of fault location techniques for distribution networks, until recent past; in this sense fault locators have been considered not essential on distribution systems. Nowadays, this issue has become one of the main subjects in distribution companies, as a consequence of the trend in regulation and pricing towards efficiency and power quality improvements.

Hence, the importance of accurate fault location in distribution networks is increased. Willis [15] presented a resume of some of the classical techniques that have been used through the years to locate cable faults in distribution systems. A general but useful reference is a report of the CIRED working group [16], where the problem of fault location is presented as one of the main issues in a fault management system. Tang, *et al.* [17] review the fault indicator applications both in transmission and distribution systems; principles, merits and demerits of fault location techniques are discussed.

In electrical distribution networks one of the main issues is the fault location for repair and inspection purposes, because fault management is essential to reduce outage times. It has not so much to do with protective relaying, since the protection scheme is an on-line application and the speed of operation is the main issue, whereas the fault location techniques are usually off-line applications in which accuracy aspects are the main concern. Fault location in distribution systems differs considerably from the approaches applied for transmission systems. In fact the significant differences in networks structure, dimensions and grounding principles must be considered when a fault location method is used in distributions systems. It must be pointed out that many of these characteristics have not been totally considered in the bibliography for example most of the fault location approaches for distribution systems are developed for solidly grounded systems, a little percentage of publications consider and apply successfully the method to a feeder with multilaterals, and, last but not least, very rare are the techniques that can be used in case of networks consisting in both overhead lines and cables.

Most of the fault location methods were developed for transmission systems and are not suitable for radial distribution networks. Traditionally, the short circuit faults in power distribution lines were located by trial and error method, i.e. by dividing the line into sections and trying to close the energizing circuit breaker: The approach takes a long time and stresses the equipment even more than the fault itself. A fault can thus be located in several "iterations", its main drawback is the time required to localize the

faulted section and the fault. Crew productivity can be improved through the use of faulted circuit indicators, i.e. single or multiphase devices designed to sense the fault current flowing through the power conductor(s) at the point where their sensors are installed and provide an indication of the event [18].

Nowadays considerable research efforts into development of new fault location techniques for distribution systems have been spent; the techniques can be classified under two main categories, reported in the diagram of Figure 3-27.

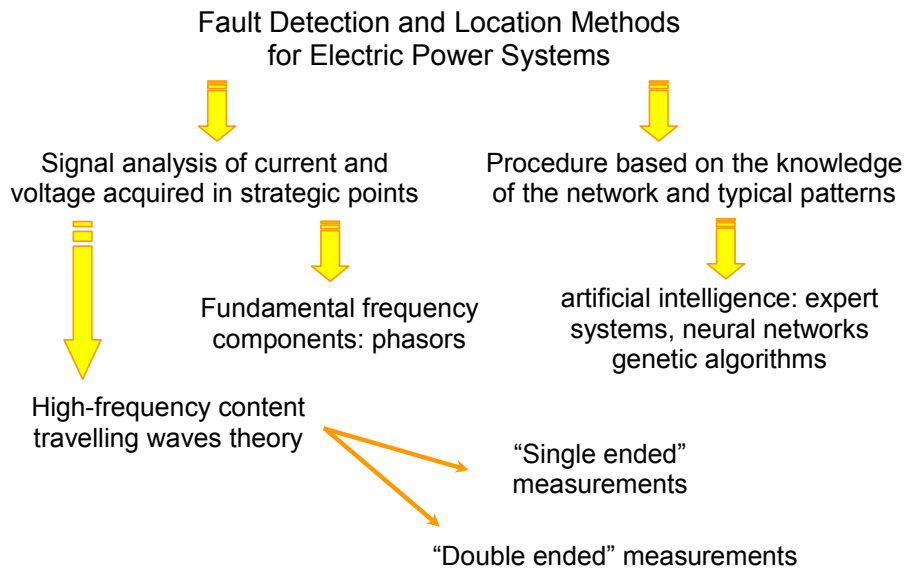


**Figure 3-27.** Different approaches present in scientific literature for fault location in distribution systems

In recent years signal analysis approaches increased a lot. In particular, with the rapid developments of microprocessor technology, research activities focused on the high frequency components of voltage and current signals. Fault location techniques using signal analysis are based on measurements of current and voltage. These techniques can be divided into two categories: methods analyzing the fundamental frequency components and methods analyzing the high frequency components. The latter methods can be further classified into two sub categories, according to the available measurements: so-called single ended or double ended methods.

Single ended techniques use only one terminal measurements, and are based most of the times on the information provided by digital fault recorders installed at the head of the feeder. the advantage showed by this approach is that communications are not needed. The double ended techniques give more reliable and accurate results, but communication channels have to be included in the measurement system. The fact that a feeder has many branches makes the location of each fault much more difficult, in fact the voltage and current signal analysis yields to obtain more than one fault point candidate within the network.

#### **3.4.1. Signal analysis of fundamental frequency components**

The fault location techniques based on fundamental frequency use the power frequency phasors to estimate the fault distance in distribution systems. Till now different algorithms for single-ended fault location methods have been proposed, where a trend towards impedance measurement techniques is shown. The value of the apparent impedance must be compensated at each fault occurrence of the contribution corresponding to the fault resistance, hence such methods have limited applications because they cannot provide the required accuracy in the location when system or fault conditions change.

In 1993, A. Girgis et al. [19] presented a single-ended fault location technique for rural distributions feeders based on phasors obtained with a recursive optimal estimation algorithm. The distance from the head of the feeder to the fault is then estimated on the basis of the apparent impedance computed by using updated values of voltages and currents. The approach [19] has then been considered as a reference point for the development of some later fault location methods, for example [20]. In this paper the authors increase accuracy of the fault location, provided there is no remote in fed. Upon the detection of a disturbance, phasor quantities of voltage and current are obtained by an estimation program; the variation in the magnitudes of the phasors is used as the criteria to classify the type of fault and identify the faulted phases. In particular, the relative change in the magnitude over the reference value of each phase current is computed and compared with a threshold value in order to detect the faulted phases. After the classification of the type of fault, a pair of voltage and current phasors is chosen to compute the relevant apparent power. The fault boundary conditions and the sequence network parameters are used to calculate the sequence components of that voltage and current, so that the equivalent apparent impedance is found. A compensating current is considered to be fed into the fault point to eliminate the fault resistance contribution to the apparent impedance. The obtained value of apparent impedance is used to estimate the distance from the fault location. In this approach, to overcome the lack of information about the fault resistance, it was assumed that the current contribution due to the fault is the change in the current magnitude from pre- to post-fault.

In 1997 R.K. Aggarwal, et al. [21] presented a single-ended fault location technique for overhead distribution systems, based on the concept of superimposed components of voltages and currents, defined as the difference between the total post-fault and pre-fault quantities. By using a specified model of the distribution system, voltage and current values of the superimposed components are computed so that a superimposed components circuit can be considered. In this equivalent circuit the position of the fault is systematically varied along a line in order to deduce the point giving the minimum value of superimposed current in the healthy phase(s). In this way the fault locator can be



highly insensitive to variations in local and remote source impedances, to the fault resistance and to the presence along the feeder of taps with variable loads.

In 2003, P.M. Van Oirsouw, et al. [22] reported the experience of the Dutch distribution company about a reactance based methodology for fault location. The system revealed to be able to locate two- and three-phase faults within the required accuracy of 100 meters and single phase faults within 1000 meters. 5 minutes after the fault occurrence the dispatch center could communicate to the emergency crew where the fault should be checked, hence the company could save around one hour to look manually for the fault.

#### **3.4.2. Signal analysis of high frequency components**

The use of non-power frequency components for power system analysis has been contemplated for a long time, especially in power system protection, but only in the last years has been significantly developed. Recently, travelling waves methods, almost used in the past for protection purposes in transmission lines, are back as an alternative approach for fault location. The theory behind these methods is based on the correlation between the forward and backward travelling waves along the line. These methods monitor the correlation coefficient between high frequency waveforms, which increases significantly in case of fault. The transient generated by the occurrence of a fault will get to the measurement point and then will be reflected back towards the fault point; the same happens at the fault position, finally the transient will arrive at the relay terminal as a highly correlated signal after a time delay equal to twice the travelling time of the transients from the relay to the fault location. This time interval can then be used to estimate the distance of the fault point from the relay terminal.

However, for distribution systems, the problem becomes more complex because the topology in radial grid involves many reflections. Unfortunately, it is well known that the travelling waves based method does not perform well for certain type of faults and/or system conditions. For example, faults very close to the measurement point as well as faults occurring close to a zero crossing of the steady-state voltage waveform.

One of the first reports on the use of high frequency components to determine fault location in distribution systems was proposed in 1992 by A.T. Johns [23]. The technique is quite robust respect to variations of the type of fault, of the value of fault resistance, of the source short-circuit level and to the point-on-wave of fault occurrence. The main drawback is that to obtain such performance the locators need to be installed at strategic and convenient regular intervals along the overhead distribution network.

In 1998, Z.Q.Bo presented the application of transient based fault location techniques to the distribution systems by utilizing GPS [24]. It relies on detecting high frequency signals generated by faults and overcomes the longstanding issue which restrict the use of travelling wave techniques: the identification of multiple reflections from the busbars and

the fault point. The fault location is performed by comparing the differences between instances in time for all locators in the system.

In [25], despite the complexity of distribution systems, the authors show that it may be possible to obtain accurate fault location even by applying standard and well known techniques developed for EHV networks. The fundamental idea presented in the paper is that the transient disturbance travels on every transmission line and gets to the substation busbars, generating again transmitted and reflected transients. While on the faulted line there will be both incident and reflected pulses, on all the other safe transmission lines only the transmitted transient should be found. Hence, by measuring the currents affected by the fault transient, the voltage on the lines is estimated considering only one propagating wave. Finally, to locate the fault, arrival time of each incident wave at the measurement point is identified by means of the cross correlation between reflected and incident waves.

The main drawback of the previous proposals is that they are based on a double-ended method and due to investment and installation costs these schemes are costly respect to the effects of faults in distribution systems.

A more attractive approach is a fault location method where current or voltage signals are measured at just one end of the line (single-ended), usually at the substation. In this case fault location relies on the analysis of the signals to detect the reflections between the measuring point and the fault. One of the main problems is the presence of multiple possible location of the fault for a given recording at the measurement point.

One of the first attempts in this line was proposed in 1999 by F. Magnago, et al. [26]: the analysis is performed using the transient signals recorded at the substation during the fault. The method identifies the faulted lateral, firstly estimating the distance from fault point according to the travelling wave information provided by the high frequency components of the event, secondly by using the special properties of wavelet transform coefficients to find the right position within all the faults that can occur along different laterals of the same main feeder, equally distant from the main substation. Then, the fault location along the identified lateral is computed on the basis of a simplified network model and on the steady-state phasors as in the methodology [19].

Unlike the correlation-based methods, where the forward and backward travelling wave components are computed and used for the cross-correlation, in the wavelet based approach the entire signal acquired at the relay position in the network is directly analyzed.

Transients along multiphase transmission lines can be analyzed by using the modal transformations, decoupling the traveling wave equations into independent equations for each mode. Voltage and current signals at the line terminals can be transformed into

modal components, and each mode can then be analyzed separately. First mode is usually referred to as ground mode, second mode is also known as aerial mode and can be found for any kind of fault.

The single-ended recording method turns into two different techniques depending on the fact that the fault is grounded or ungrounded. If the short circuit is a line-to-line or a three-phase one the fault is ungrounded, hence not significant reflections are caused by the remote-end bus during the transient. In such cases, the distance from fault to recorder can be easily computed on the basis of the time delay between consecutive peaks by using the wavelet transform coefficients at the first decomposition level. When the short circuit involves a connection to ground, the second approach is followed: signals can be affected by a significant reflections contribution due to the remote-end bus superposed to the ones coming from the fault location. Therefore, other levels of coefficients of the wavelet decomposition are analysed in order to confirm that the fault is grounded, then the first decomposition level is considered to understand in which half part of the line the fault can be found, and finally the right expression for the distance of the fault is chosen and applied.

In 1999, Z. Q. Bo et al. [27] takes into account the main issues in the state of the art relevant to fault location methods: on the one hand impedance based methods, being power-frequency based measurement methods, suffer from limitations due to the system conditions: fault path resistance, line loading, source parameters, and so on. On the other hand, travelling wave based methods exhibit shortcomings: the fault occurrence does not generate many travelling waves components when it corresponds to a phase angle near zero of the 50 Hz voltage component; faults close-up to the measurement station give rise to incident and reflected waves hard to be separately detected. Do not forget the limited bandwidth of the current and voltage transducers feeding the measurement system.

In order to overcome most of the above issues, the authors present a technique relying on the detection of the high frequency signals generated by the fault arc. These components don't vary with the point of the voltage waveform at which the fault occurs; moreover, multiple reflections from busbars and the fault point are not needed to be detected. The principle of the fault locator is the identification of the arrival sequence of the transient high-frequency voltage signals (1÷10 MHz) at the busbar where the locator is installed. The busbar impedance is dominated by capacitance effect, thus the reflected wave coming from the remote busbar should have opposite polarity respect to the one coming from the fault point: a distinction between reflection points is obtained. In this case the accuracy of the location is proportional to the sampling rate of the locator device.

Peak magnitudes of the signals are ignored, in favour of their polarity and arrival time detection.

In 2002 P.F. Gale, et al. [28] show that it is possible to locate a fault on a distribution feeder consisting of underground cables, overhead lines and tapped load, using measurement at a single location. The magnitude of the reflected and transmitted components depends on the variation of the equivalent impedance in discontinuity points of the power system. Identification of the desired signal is of crucial importance for the correct operation of the fault location method. A probable location of the fault is estimated by comparing the relative distance of each peak in the high frequency current signals to the known reflection points in the distribution feeder. The estimated fault location is then used within a transient power system simulator that models the actual network. The resulting simulated current waveforms are then cross-correlated against the signal captured on the real network: if the position of the fault is correctly estimated, high frequency components in the simulated waveform will be similar to that of the measured waveform, and thus the obtained cross-correlation value will be high positive. It must be noticed that in this approach the cross correlation is carried out not on the basis of the Bewley lattice diagram, very difficult to follow when the fault resistance is high and in general because of the multiple reflections travelling from remote ends of the laterals to the monitoring point. The time trees technique has been used for waveform prediction, which gives a good visual description of the way waveforms are generated at each end of the network, by considering the travelling path from the fault position towards the discontinuity points along the network.

Nucci et al. proposed in [29] a procedure based on the continuous wavelet transform for the analysis of voltage transients due to line faults. The analysis, carried out by applying the method for fault location in distribution networks, shows that there is correlation between some characteristic frequencies of the transformed signal and specific paths along the network covered by the travelling waves generated by the fault. The correlation provides useful information for the location of the faulted section by using the recorded transients at one or more busses. In this paper the continuous wavelet transform is used instead of the discrete wavelet one, so that a more detailed analysis of the spectrum energy of the voltage transient can be performed. The continuous wavelet transform can operate at any scale, and is also continuous in terms of shifting. The distinctive frequencies of propagation and reflections of the fault transient are detected. By knowing the network topology and the propagation speed of the signals, the location of the fault can be inferred.

### 3.4.3. Artificial neural networks techniques

Artificial intelligence techniques, such as expert system, neural network, fuzzy logic and genetic algorithm, have been employed to fault location in distributions systems. The use of artificial neural network does not require the formulation of the solution algorithm, because it should be able to employ implicit dependencies on various parameters in the training data. These techniques are based on the assumption that during the fault the voltage and current signals measured by the network units contain information about the location of the fault. The uniquely defined fault pattern can be recognized by the ad hoc designed neural network.

Initial attempts (1991) at the applications of expert system for fault location in distribution network can be found in H. Yuan-Yih, et al. [30], where an expert system is proposed to help the dispatchers to locate the faults in distribution systems, the effectiveness of the designed expert system is demonstrated on a distribution system within the service area of the Taipei City District Office of Taiwan Power Company.

In 1996, Jarventausta, et al. [31] proposed an expert system that combines information obtained from the network database and heuristic knowledge of operators aiming at obtaining potential fault locations. The electrical distance between the feeding connection and the fault point is determined by comparing the measured short circuit current and the type of fault with the calculated fault currents of each line section.

The information obtained from the remote control system is affected by various uncertainty contributions and may be wrong, partially misleading or not sufficient to the purpose.

A more interesting method than the conventional solutions for fault location in distribution system is the use of artificial neural network (ANN), since it does not require the explicit formulation of the solution algorithm, but is able to implicitly employ various dependencies in the training data. The technique is based on the assumption that during the fault, before it is cleared, the voltages and currents measured by the network units contain information about the location of the fault in the system. These measured quantities uniquely define a fault pattern (or signature) that can be recognized by a specially designed neural network. The challenge in ANN fault location technique is to be able to process the data for a given pattern and reliably extract the information about fault location. A comparison of ANN techniques for fault location was carried out in 1996 by J.A. Momoh [32]. The authors conclude that higher success rates are achievable using the back propagation method and the clustering method when compared with the counter propagation method.

Probabilistic methods are other approaches for fault location, for example, in 2000, S. Hanninen, et al. [33], proposed a probabilistic method based on the change of the neutral-voltage and zero-sequence currents.

Concluding the survey, it can be said that no technique features all the desirable features that lead to the accurate fault location in distribution systems. On the one hand traditional fault location techniques in which fundamental voltages and currents at line terminals are considered, are difficult to be applied in distribution lines with tapped loads. On the other hand, Travelling waves based fault locators are significantly more reliable if a double-ended method is used, when single-ended fault location should be cheaper and hence preferred in case of distribution systems.

Nowadays research interests and activity are actually trying to develop a novel fault location method, based on a central fault locator installed in the substation with only currents and voltages measurements available. To do this the signal-analysis based method and the knowledge-based method can be conveniently combined in order to develop hybrid systems that could overcome limitations of the single solutions. Hence, there is a technical challenge in research and development for the successful design and implementation of a practical fault location method for distribution systems.

### 3.5. *Distributed measurement system detecting transient disturbances and method to locate the transient source*

In the contribution [34] the electric and electronic measurement group of Bologna presented a distributed measurement system for power quality monitoring. In particular, the use of such a system was discussed in connection with a lightning location system aiming at investigating on the correlation between impulsive transients and their induction by strokes. On the basis of the same distributed measurement system a new function is proposed, i.e. the detection of transient events affecting the lines signals and the location of the source of disturbance within the monitored distribution network. The measurement system consists in a master-slave architecture, where all the slave units have the same time reference and can communicate information to the master unit.

The method for the real-time location of the fault or any other transient source relies on the measurement of the starting instant of the disturbance at given points of the network, hence it does not involve any signal analysis.

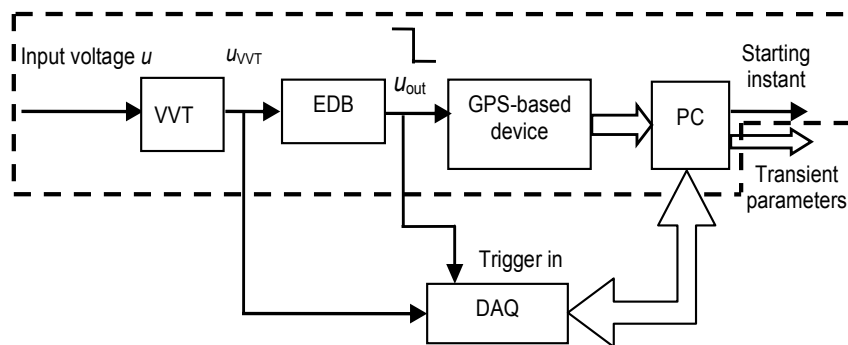


**Figure 3-28.** Block diagram of a slave unit channel.

Figure 3-28 is the block diagram of one of the three measurement channels of a remote unit (slave). The hardware included in the station will be described and metrologically characterized in chapter 5. As a transient distortion affects the input voltage, the system acquires both the starting instant and the waveform of each transient. The former information is then sent to the master unit which locates the source of the transient by processing the data received from all the slaves. The dashed box in Figure 3-28 contains the blocks performing the measurement of the transient starting instant. Only by way of example, in this case the three phase-signals chosen for the network monitoring are the line-to-ground voltages.

In each channel the voltage  $u(t)$  at the monitored point is conditioned by a Voltage-to-Voltage Transducer (VVT), whose output  $u_{VVT}$  feeds an Event Detection Block (EDB). The EDB output  $u_{out}$  is a logic signal that, as a transient occurs, triggers both a Data Acquisition board (DAQ) and a GPS-based device, which provides the relevant “time

stamp". The time stamp is determined with an uncertainty that propagates through the algorithm which the proposed measurement procedure relies on, and affects the estimate of the transient source location. In chapter 5 also the combined uncertainty affecting the location is estimated.

In the same way the measurement system can also locate the source of transient currents. In such a case, in Figure 3-28 the output of a suitable current-to-voltage transducer in place of  $u_{VVT}$  has to be considered.

### 3.5.1. Procedure to locate the source of a transient

The method requires that the characteristics of the considered network (topology, geometry of the lines, type of conductor and space between them) are known. Such a requirement is not a problem in practical implementations. Since the method relies on the travelling waves theory, reference propagation time intervals along the lines between two adjacent slaves must be determined. This can be done, for instance, by carrying out simulations in Electro Magnetic Transient Program (EMTP) environment, or by computing the propagation speed of signals on the basis of the theoretical model of the lines.

Slave units should be installed in each network terminal, in each node, and at points where the number of phases eventually varies. The procedure proposed for locating the source of transients relies on the obvious concept that the more distant is a slave from the source, the greater is the time stamp value it registers in correspondence of the disturbance arrival.

Let  $t_{mj}$  be the time stamp of the starting instant of the transient voltage measured by the generic  $m$ th slave ( $1 \leq m \leq M$ ) on the  $j$ th phase ( $j = a, b, c$  in the case of a three-phase network). Moreover,  $T_{nj\text{ref}}$  and  $T_{nj\text{meas}}$  denote respectively the reference and measured propagation time intervals on the  $j$ th phase of the  $n$ th line section ( $1 \leq n \leq M-1$ ). The two adjacent slaves at the ends of the considered line are separated by the distance  $D_{nj}$  that is the nominal length of the  $n$ th line section.

In ideal conditions, when the  $n$ th section is safe,  $T_{nj\text{meas}}$  should be identical to  $T_{nj\text{ref}}$ . Despite, due to the effects of the difference between study hypothesis and real conditions which lead to a non-perfect estimation of some parameters for all the operating conditions,  $T_{nj\text{meas}}$  can differ from the relevant  $T_{nj\text{ref}}$ . Anyway, the former parameter is always lower than the latter one when the source of the transient is located within the considered couple of points.

The algorithm running on the master unit processes the data simultaneously sent by the slaves, i.e. the timestamps. For each phase and each couple of adjacent points, the following quantity is determined:



$$\Delta_{nj} = \frac{T_{nj\text{ref}} - T_{nj\text{meas}}}{T_{nj\text{ref}}} \quad (3.47)$$

which ranges from 1 to 0 as the transient source moves from the midst of the  $n$ th line up to outside the line itself.

Then,  $(\Delta_{nj})_{\max}$  i.e. the maximum for  $\Delta_{nj}$  is found, to identify which phase and above all which line section is affected by the fault. Once the faulted line is detected,  $(\Delta_{nj})_{\max}$  allows also determining the distance  $d$  of the transient source from the nearest slave:

$$d = \frac{D_{nj}}{2} (\Delta_{nj})_{\max} \quad (3.48)$$

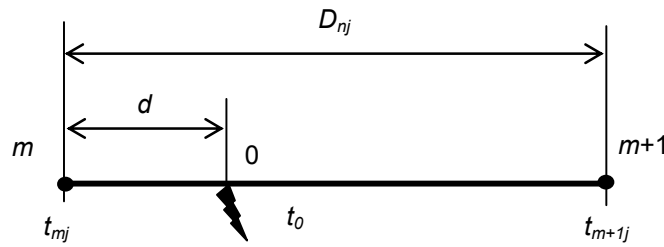


**Figure 3-29.**  $n$ th line, connecting node  $m$  to node  $m+1$ ,  $D_{nj}$  long

To explain the final expression used in the location algorithm, Figure 3-29 can be considered: the section between two generic adjacent slaves separated by the distance  $D_{nj}$ . Let us assume that the transient event starts in point 0 at time instant  $t=t_0$  and is detected by the slaves  $m$  and  $m+1$  at instants  $t_{mj}$  and  $t_{m+1j}$ , respectively. If  $T_{nj\text{ref}}$  is the propagation time interval relevant to the considered section, thus the reference propagation speed  $v_{nj\text{ref}}$  is:

$$v_{nj\text{ref}} = \frac{D_{nj}}{T_{nj\text{ref}}} \quad (3.49)$$

The distances of the transient source from the considered slaves can be expressed as follows:

$$d = v_{nj\text{ref}} \cdot (t_{mj} - t_0) \quad (3.50)$$

$$D_{nj} - d = v_{nj\text{ref}} \cdot (t_{m+1j} - t_0) \quad (3.51)$$

$d$  is the distance between the point 0 and the closest slave. By subtracting (3.51) to (3.50) we get:

$$2d - D_{nj} = \frac{D_{nj}}{T_{nj\text{ref}}} (t_{mj} - t_{m+1j}) \quad (3.52)$$

By denoting  $T_{nj\text{meas}} = (t_{mj} - t_{m+1j})$  and then substituting (3.47) in (3.52), the distance  $d$  is finally determined:

$$d = \frac{D_{nj}}{2} \left( \frac{T_{njref} - T_{njmeas}}{T_{njref}} \right) = \frac{D_{nj}}{2} (\Delta_{nj})_{\max} \quad (3.53)$$

Some consideration about the proposed approach can be drawn. The EMTP simulation campaign on both the distribution feeders that will be presented in the next Chapter proves that the method described above features very well the fault location in all the simulation cases, leading to low-biased results.

Such good performance of the procedure are mainly due to:

- a) the large number of measurement points;
- b) the sensitivity of EDB devices installed in the slave units, whose threshold value has a lower limit depending on the quality of voltage waveforms just to avoid fake detections in steady state conditions.

Despite, by the economical point of view, the method would have a weak appeal because of its relatively large capital and installation costs. As a matter of fact, in the configuration described above, the method requires a slave unit at the head and at the end of each line. The cost of each remote station is in the order of 6,000 €.

Aiming at decreasing the global cost of the distributed measurement system, the fault location algorithm running on the master unit is proposed to be modified so that the number of slave units is reduced of around 50%, in fact if  $M$  is the number of remote stations installed to monitor a distribution network, the different approach needs only  $(M/2 + 1)$  slaves.

### **3.6. *Fault location method integrating the distributed measurement system and wavelet analysis***

The alternative version of the fault location method relies on a proper integration between a distributed measurement system performing the procedure described in previous section and a signal processing technique based on the Wavelet transform. In particular, the number of remote units decreases because for each lateral line of the network single-ended measurements are used instead of double-ended ones. In this connection, for a typical radial distribution system, the slave units are placed at the head and at the end of the main power feeder and at the connections with laterals getting to the load busses. If the previous procedure were adopted for fault location on the whole distribution network, also remote stations installed in all the load busses (i.e. at the end of each lateral) were needed.

The lack of information on the propagation of the disturbance no longer available at the latter measurement points is compensated in the new method by the analysis of the voltage waveforms acquired in the nodes along the main feeder. In this connection, the Discrete Wavelet Transform (DWT), which is the digitally performed version of the Continuous Wavelet Transform, is implemented. The travelling-waves theory is exploited to estimate the position of a fault along the laterals. In practice, the sections of the main feeder are still monitored by the double-ended technique, whereas the lateral lines are monitored in a single-ended way.

To describe some details of the method let us refer to a typical distribution network monitored by the fault location system. The topology of the power system is shown in Figure 3-30. It consists in a 10-km long main feeder (lines L1, L2 and L5) and in two laterals: L4 (2-km long) and L3 (1-km long). In the system three-phase overhead lines are used. The radial distribution network is fed by a 150/20 kV substation G, where the transformer T is of the  $Y_g/d$  connection type. All the load busses are equivalent to three-phase balanced impedances. Each load is connected to the relevant lateral through a 20/0.4 kV transformer.

Four slave units of the distributed measurement system, denoted by S1, S2, S3 and S4, are placed in correspondence of the black bullets in Figure 3-30.

As any type of short circuit occurs in one of the lines, the transient waveforms and the relevant time stamps are acquired by the four slave stations and sent to the master unit, which detects the nearest slave to the fault position, updates the value of the propagation speed on the basis of the modal voltages computed for the selected node, and then obtains the value of delta for the sections L1, L2 and L5. The delta values are compared with a threshold, in order to check if the faulted line belongs to the main feeder and eventually identify the section affected by the fault. The value of delta greater than the

threshold allows to detect the faulted section of feeder, hence the master unit can implement (3.48) to compute the position of the transient source along that line.

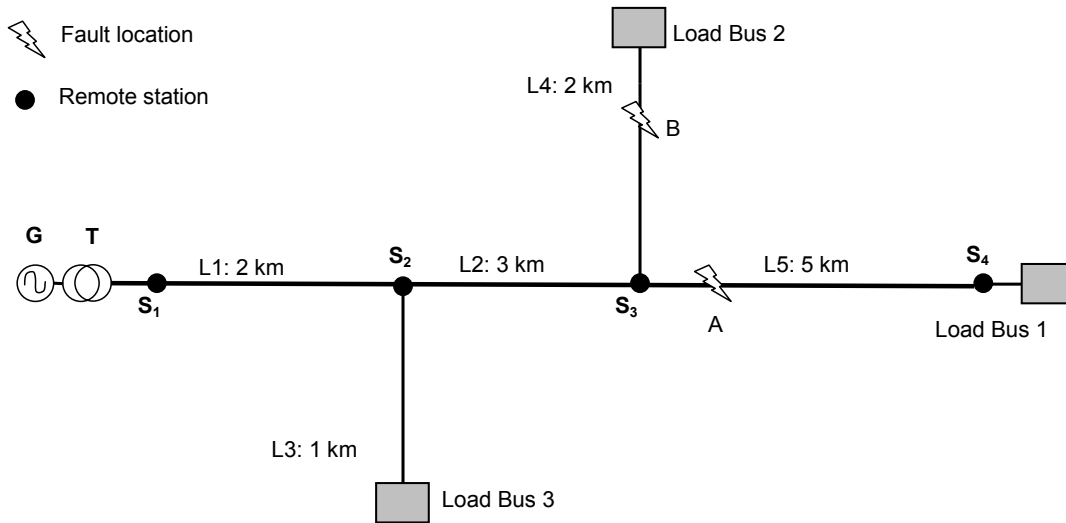


**Figure 3-30.** Distribution network (three phase overhead lines) monitored by the measurement system.

For example this would be the case of a short circuit in A in Figure 3-31.

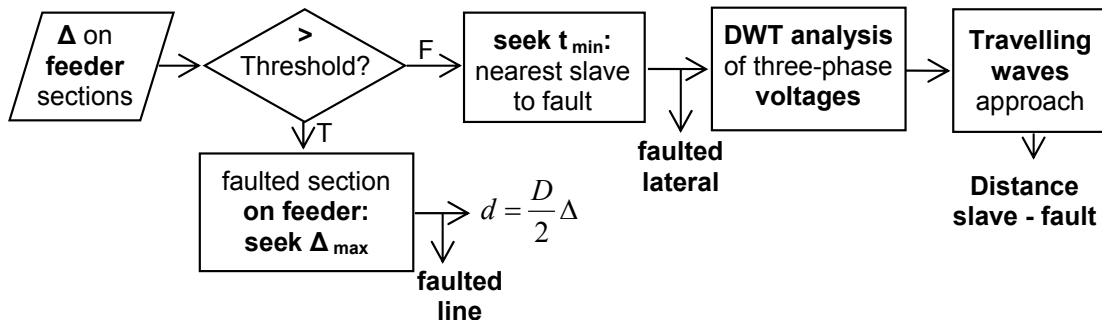


**Figure 3-31.** Block diagram of the integrated fault location method.

If the threshold is larger than the delta values relevant to all sections L1, L2, L5, the main feeder of the network is assumed to be not affected by faults, and thus the algorithm identifies the faulted line as the lateral whose head is monitored by the slave unit that recorded the minimum time stamp.

The distance of the fault point from the selected measurement unit is computed by analyzing the three phase voltage signals acquired at the head of the selected line by means of the DWT. This procedure would be applied to a fault occurring in point B in Figure 3-30.

As Mother wavelet the Daubechies 4 has been chosen, because of the high correlation degree between its pattern and the typical oscillations of the dumped transients developing in the network as the fault occurs. In order to choose the most useful mother

wavelet to the purpose, preliminary simulations tests have been carried out by considering a single three phase line fed by one end and loaded by the other end, affected by a short circuit to ground. The line voltages at the source point were analysed by applying the DWT based on different mother wavelets. The set of mother wavelet to be used was selected according to their waveshape compared to the oscillations of a transient disturbance. Also the value of the fault resistance was varied. At the end of such analysis the mother wavelet leading to the highest number of correct locations was adopted.

The equivalent sampling frequency of the distributed measurement system (10 MSA/s) leads to a frequency sub-band for the first DWT level of Details in the range [2.5, 5] MHz. The main spectrum content of transients generated by short circuits is known to be largely below 1 MHz, in fact the energy content associated to the first level of coefficients is always lower than other inferior frequency sub-bands. Despite, aiming at computing the distance of the transient source from the slave on the basis of the travelling waves theory, the detail coefficients of the first level of decomposition are analyzed, because high coefficients are found only when the voltage transient presents very fast rising and falling fronts, and thus a single spike can be identified.

The proposed strategy to detect when an event occurs is enforced by a huge number of experimental tests in which the details belonging to the 5 higher decomposition levels of the signals acquired at the head of a line were analyzed. Both the amplitude and the energy content of each details level were taken into account as information on which the position of the fault along the line could be estimated; the type of fault, its resistance as well as position were systematically varied in order to understand which decomposition level could give correct results in most cases. Finally, it should be reminded that the best time resolution is obtained at the first decomposition level.

By monitoring the coefficients sequence (and thus the oscillations belonging to the transient waveform) the algorithm:

- i) seeks the first pulse front (no matter if rising or falling) associated with the travelling wave propagating from the fault point to the head of the line;
- ii) selects a sequence of details starting with the first pulse whose length corresponds to the propagation time of the surge from the head to the end of the line and back;
- iii) in this time window seeks the second spike, assumed as the travelling wave reflected once from the measurement point to the fault, and then back from the fault position to the slave.

From a computational point of view, operations i) and iii) become easier if the squares of the details are used. Actually in doing this the information on the sign of each transient

surge is lost; by considering that it is due to the value of reflection and refraction coefficients at the fault and load points it could sound like losing useful data. Despite, the equivalent impedance of the fault and the power absorbed by the load bus at the occurrence of the fault itself cannot be known, hence no general relationship let further information on the fault condition be found by analyzing the surges sign.

A critical aspect of the analysis described for estimating the distance from the fault point to the measurement unit is that the order by which the surges get to the measurement point depends on the fault position along the monitored line: the concept can be easily shown referring for example to Figure 3-17. The oscillation registered in point A for  $t=3T_1$  due to the surge reflected by the fault point is the second event only if  $0 < x < 2l/3$ . For faults distant more than  $2l/3$  from point A the pulse ( $t = T_1 + 2T_2$ ) due to the surge reflected in B and refracted in F gets to point A before the above one.

The distance  $x$  is not known, obviously, and hence such condition can be misleading. Moreover, the equivalent resistance of the fault in F has a strong influence on the amplitude of the refracted surges respect to the reflected ones, but also the fault resistance cannot be known a priori. Trying to overcome this issue, the refraction coefficient of the fault point is estimated by checking the amplitude of the coefficients in correspondence of the time  $t = (3T_1 + 2T_2)$  in Figure 3-17, i.e. the time when the first surge seen in point A ( $t = T_1$ ) gets back there after travelling along the line till the reflection point B. If a significantly high coefficient is found the refraction coefficient of the fault point (and hence its resistance) is assumed to be high.

As the couple of time instants  $N_1T_s$  and  $N_2T_s$  ( $T_s = 1/f_s$ ) relevant to the above events are known, the distance  $d_1$  of the short circuit point from the head of the selected lateral is computed by means of the following relationship:

$$D_1 = T_s \cdot (N_2 - N_1) \cdot v_\alpha \quad (3.54)$$

where  $v_\alpha$  is the propagation speed relevant to the  $\alpha$  mode.

## References

- [1] IEEE std 1159-1995, "Recommended practice for monitoring electric power quality", The IEEE, Piscataway (USA), Nov. 1995;
- [2] A. Haar, "Zur theorie der orthogonalen funktionen-system", *Math. Ann.*, vol. 69, 1910, pp. 331-371.
- [3] A. Grossmann, J. Morlet, "Decomposition of Hardy functions into square integrable wavelet of constant shape", *SIAM J. Math. Anal.*, vol. 15, 1984, pp. 723-736.
- [4] I. Daubechies, "Orthonormal bases of compactly supported wavelets", *Comm. Pure & Appl. Math.*, vol. 41, 1988, pp. 909-996,.
- [5] S. G. Mallat, "A theory for multiresolution signal decomposition: the wavelet representation", *IEEE Trans. on Pattern Analysis and Machine Intelligence*, vol. 11, no. 7, 1989, pp. 674-693,.
- [6] C. Heil, D. Walnut, "Continuous and discrete wavelet transform", *SIAM Review*, vol. 31, 1989, pp. 628-666.
- [7] G. Strang, "Wavelets and dilation equations: a brief introduction", *SIAM Review*, vol. 31, 1989, pp. 614-627.
- [8] P. F. Ribeiro, "Wavelet transform: an advanced tool for analyzing non-stationary harmonic distortions in power system", *Proc. IEEE ICHPS VI*, Bologna, Italy, 1994, pp. 365-369.
- [9] W.B. Richardson Jr., "Applying wavelets to mammograms", *IEEE Engineering in Medicine and Biology Magazine*, vol. 14, n. 5, 1995, pp. 551-560.
- [10] S. G. Mallat, "Multifrequency channel decompositions of images and wavelet models", *IEEE Trans. on Acoustics, Speech, and Signal Processing*, vol. 37, n. 12, 1989, pp. 2091- 2110.
- [11] L. Angrisani, P. Daponte, M. D'Apuzzo, A. Testa, "A new wavelet transform based procedure for electrical power quality analysis", *Proc. ICHQP 96*, Las Vegas, USA, 1996, pp. 608-614.
- [12] L. Khadra, M. Matalgah, B. el-Asir, S. Mawagdeh, "The wavelet transform and its applications to phonocardiogram signal analysis.", *Med Inform*, vol. 16, n.3, 1991, pp. 271-277.
- [13] J. G. Teti, Jr., H. N. Kritikos, "SAR ocean image representation using wavelets", *IEEE Trans. on Geoscience and Remote Sensing*, vol. 30, n. 5, 1992, pp. 1089-1094.
- [14] G. Strang, T. Nguyen, "Wavelets and filter banks", *Wellesley-Cambridge Press*, Wellesley, USA, 1996.
- [15] O.L. Willis, "A review of fault locating techniques in medium-voltage power cable," in *Proc. 1991 Petroleum and Chemical Industry Conf.*, pp. 225-228.
- [16] Cired Report, "Fault Management in electrical distribution system," Tech. Rep. CIREC working group WG03, Dic. 1998.
- [17] Y. Tang, H.F. Wang, R.K. Aggarwal, and A.T. Johns, "Fault indicators in transmission and distribution systems," in *Proc. 2000 International Electric Utility Deregulation and Restructuring and Power Technologies Conf.*, pp. 238-243.
- [18] *IEEE guide for testing faulted circuit indicators*, IEEE Standard 495-1986, Apr. 1986.
- [19] A. A. Girgis, C.M. Fallon, and D.L. Lubkeman, "A fault location technique for rural distribution feeders," *IEEE Trans. Industry Applications*, vol. 29, pp. 1170-1175, Nov.-Dec. 1993

- [20] J. Zhu, D.L. Lubkeman, and A.A. Girgis, "Automated fault location and diagnosis on electric power distribution feeders," *IEEE Trans. Power Delivery*, vol. 12, pp. 801- 809, Apr 1997.
- [21] R.K. Aggarwal, Y. Aslan, and A.T. Johns, "New concept in fault location for overhead distribution systems using superimposed components," *Proc. Inst. Elect. Eng.- Gener. Transm. Distrib.*, vol. 144, pp. 309-316, May 1997.
- [22] P.M. Van Oirsouw and F. Provoost. "Fault localisation in an MV distribution network," in *Proc. 2003 CIRED 17th International Electricity Distribution Conf.*
- [23] M. El-Hami, L.L. Lai, D.J. Daruvala, and A.T. Johns, "A new traveling-wave based scheme for fault detection on overhead power distribution feeders," *IEEE Trans. Power Delivery*, vol. 7, pp. 1825-1833, Oct. 1992.
- [24] Z.Q. Bo, G. Weller, F. Jiang, and Q.X. Yang, "Application of GPS based fault location scheme for distribution system," in *Proc. 1998 POWERCON'98 International Power System Technology Conf.*, Beijing, China, 1998, vol. 1, pp. 53-57.
- [25] D. W. P Thomas, R. J. O. Carvalo, E. Pereira, "Fault Location in Distribution Systems based on Travelling Waves", *2003 IEEE PowerTech Conference*, Bologna, Italy, June 23-26.
- [26] F.H. Magnago and A. Abur, "A new fault location technique for radial distribution systems based on high frequency signals," in *Proc 1999 IEEE Power Engineering Society Summer Meeting Conf.*, Edmonton, Alta, Canada, 1999, vol. 1, pp. 426-431.
- [27] Z.Q. Bo, G. Weller, M. A. Redfern, "accurate fault location technique for distribution system using fault-generated high-frequency transient voltage signals", *IEE Proc. On Gener. Transm. Distrib.*, Vol. 146, No. 1, January 1999.
- [28] H. Hizam, P.A. Crossley, P.F. Gale, and G. Bryson, "Fault section identification and location on a distribution feeder using traveling waves," in *Proc. 2002 IEEE Power Engineering Society Summer Meeting*, vol. 3, pp. 1107- 1112.
- [29] A. Borghetti, S. Corsi, C.A. Nucci, M. Paolone, L. Peretto and R. Tinarelli: "On the use of continuous-wavelet transform for fault location in distribution power systems", *International Journal of Electrical Power & Energy Systems*, vol. 28, n. 9, November 2006, pp. 608-617;
- [30] H. Yuan-Yih, F.C. Lu, Y. Chien, J.P. Liu, J.T. Lin, P.H.S. Yu, and R.R.T. Kuo, "An expert system for locating distribution system faults," *IEEE Trans. Power Delivery*, vol. 6, pp. 366-372, Jan. 1991.
- [31] P. Jarventausta, P. Verho, M. Karenlampi, and J. Partanen, "AI-based methods in practical fault location of medium voltage distribution feeders," in *Proc. 1996 ISAP'96 International Intelligent Systems Applications to Power Systems Conf.*, pp. 164-169.
- [32] J. A. Momoh, L.G. Dias, and D.N. Laird, "An implementation of a hybrid intelligent tool for distribution system fault diagnosis," in *Proc. 1996 IEEE Transmission and Distribution Conf.*, pp.123-128.
- [33] S. Hänninen, M. Lehtonen, and U. Pulkkinen. "A probabilistic method for detection and location of very high resistive earth faults," *Electric Power Syst. Res.*, vol. 54, pp. 199-206, Jun. 2000.



[34] L. Peretto, P. Rinaldi, R. Sasdelli, R. Tinarelli, "A system for the measurement of the starting instant of impulsive transients", *Proc. of the IEEE IMTC/2004*, Como, Italy, May 2004, vol.2, pp.1394-1398.



## **4. Analysis of the performance featured by the fault location method based on distributed simultaneous measurements - simulations of distribution networks in EMTP-RV environment**

### **4.1. Implementation of an IEEE Std. test network affected by bolt faults**

IEEE proposed in [1] four models of network to be used by researchers involved in power quality analysis to compare the results of different investigation methodologies. Among these models, the IEEE 34-Node Test Feeder, shown in Figure 4-1, was chosen to test the performance of the location methodology for transient sources in distribution systems. Such an overhead network is characterized by a radial distribution of three-phase lines where a part of single-phase laterals can be found; the entire network is supplied by a substation transformer having the following specifications: 2500-kVA rated power, 345-kV/24.9-kV voltage ratio,  $\Delta$ -y grounded connection, per-unit equivalent impedance equal to: (0.01+j0.08). The three-phase short circuit power, on the 345-kV side, is 1800 MVA at an angle of 85 degrees.

Both spot and distributed “Y” connected loads having constant active and reactive power are installed in the network. In the document [1] the active and reactive nominal powers per phase are given for all the spot and distributed loads. Finally, an in-line autotransformer converting the feeder voltage from 24.9 kV to 4.16 kV is used to supply the terminal 890.

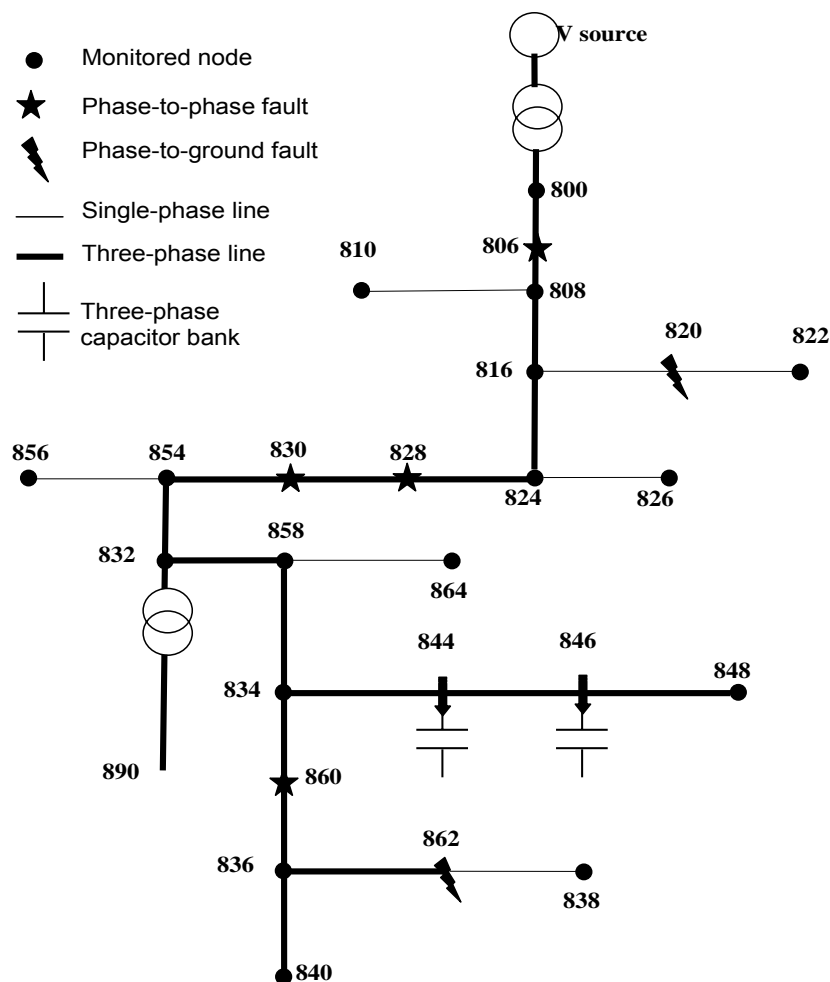
The network in Figure 4-1 has been implemented in EMTP environment and the transient voltages too.

Table 4-1 reports the values of  $D_{nj}$  and  $T_{njref}$  for the network in Figure 4-1. The values of  $T_{njref}$  have been determined by simulating the injection of a voltage pulse in point 800.

The proposed location procedure is based on the measurement of time instants; hence, the simulations have been performed in time domain. The initial conditions for each simulation run are given by the 50 Hz steady state obtained by EMTP as load-flow solution. In this way the entire duration of the simulation is useful to test the propagation of the disturbance since the fault occurs. The simulation time step has been set 10 ns to grant a time resolution sufficiently higher than the accuracy associated with the real employed instrumentation.

For the overhead lines of the network, the Constant Parameters Line Model has been adopted during simulations. Such a choice can sound contradictory respect to the lines theory shortly reported in Section 3.2, according to which an exhaustive model of the electric line should take into account the dependence on frequency of the equivalent

distributed parameters. Indeed, the characteristic impedance of the line would be influenced by the signal frequency content. Actually, the line characteristic in function of frequency is almost flat, and hence usually the operator assumes constant values for the model parameters. In doing this, each parameter value has to be chosen in correspondence of a frequency representative of the phenomenon to be simulated. In particular, for the approximation of the model with the CP lines, in the case of transients generated by faults the line parameters can be computed at 100 kHz, because the typical frequency bandwidth associated with the first oscillations belongs to the range 10 kHz – 500 kHz. In order to verify the correctness of neglecting the frequency dependence of the distributed parameters in the model, at first simulations have been run by considering the same condition and location of transient source in the network under test, and by loading in the former case the FD-line, in the latter case the CP-line model for all the sections. The results of the fault detection and location procedure were identical in the two cases.



**Figure 4-1** Diagram of the IEEE 34-node Test Feeder (not in scale)

It should be noted that the MV distribution networks used for tests, as well as actual radial networks, are characterized by quite short laterals, less than 10 km long. The dependence on frequency of the line model used during transient simulations could significantly affect the results for lines length much higher than a few km. Moreover, the

influence of the frequency content of the signals propagating along the lines could lead to differences in the values of reflection or refraction coefficients in the network nodes respect to the case of CP lines, and thus lead to a different transient pattern obtained as superposition of direct, reflected and refracted waves. Despite, the method proposed for the location of transient sources uses information on the propagation of the travelling waves strictly related to the first direct surge, and no analysis of the high frequency signal is carried out, hence it seems reasonable that the measured propagation times are not significantly influenced by the lines model. As a matter of fact, the network considered for tests is homogeneous, in the sense that the only parameter varying from one line section to any other one is length. This means that different values of the lines parameters turn into a different value of the propagation speed of travelling waves, but the order by which the slave units can detect the arrival of the disturbance remains the same.

**Table 4-1** lines length and reference transmission time intervals relevant to the Network represented in Figure 4-1

Slave Couples	$D_{n_a}$ [m]	$T_{n_{a,ref}}$ [ $\mu$ s]	$D_{n_b}$ [m]	$T_{n_{b,ref}}$ [ $\mu$ s]	$D_{n_c}$ [m]	$T_{n_{c,ref}}$ [ $\mu$ s]
800–808	11137	37.9	11137	37.9	11137	37.9
808–816	20589	70.4	20589	70.4	20589	70.4
816–824	3112	10.6	3112	10.6	3112	10.6
824–854	6644.6	22.6	6644.6	22.6	6644.6	22.6
854–832	11229	38.2	11229	38.2	11229	38.2
832–858	1493.5	5.1	1493.5	5.1	1493.5	5.1
858–834	1777	6.1	1777	6.0	1777	6.1
834–848	1767.8	6.0	1767.8	6.0	1767.8	6.0
834–836	1432.6	4.9	1432.6	4.9	1432.6	4.9
836–840	262.13	0.9	262.13	0.9	262.13	0.9
836–838	1566.7	5.3	-	-	-	-
808–810	-	-	1780	6.1	-	-
816–822	19385	66.0	-	-	-	-
824–826	-	-	923.54	3.1	-	-
854–856	-	-	7111	24.2	-	-
858–864	493.77	1.7	-	-	-	-

Different events giving rise to damped oscillatory transient voltages have been simulated:

- i. short circuits between two phases (in different points marked by stars in Figure 4-1);
- ii. phase-to-ground short circuits (in points marked by flashes);
- iii. insertion of three-phase capacitor banks in nodes marked by arrows (100-kVAR rated power in node 844 and 150-kVAR in node 846, respectively). In the cases i) and ii) the capacitor banks were disconnected.

No slave unit has been set in 890 because it is characterized by a different nominal voltage. In practical applications it should be monitored by another measurement system, given that it belongs to a different network.

The results have been obtained by processing in Matlab environment the voltage signals provided by EMTP simulations. In all the monitored points three-phase voltage probes have been installed. In this first tests set for the validation of the proposed method, Matlab has been used to simulate the operation of the whole measurement system in terms of both slave and master units, thus first determining the time stamps, then locating the transient source on the basis of time data.

At the end of each fault simulation carried out in EMTP-RV environment, the waveforms of the voltage signals acquired by the probes in the monitored points of the test network are imported in the Matlab Workspace. The following elaborating procedure is repeated for each one of the three phases:

- A function emulating the Event Detection Block is applied to the imported data so that the timestamps associated to the beginning of the transient disturbance are found for all the monitored points. The function implemented compares the difference between each sample and the previous one of the input waveform to a threshold value and gives as output the time reference corresponding to the first overcome of the threshold. The timestamps are saved into an array.
- Every section of line belonging to the network is associated to a couple of monitoring points corresponding to its ends: the minimum of the two timestamp is found. Then, the measured propagation time is computed as the difference between the two timestamps.
- On the basis of the nominal line length, also the reference propagation time is computed for each line section.
- The parameter delta is computed for all the lines, then the maximum delta is found.
- The line associated to the maximum delta is declared as faulted; its length and the minimum of the two timestamps at its ends are used to locate the fault.

To obtain the highest accuracy in the time reference and hence in the location of the fault, the absolute maximum value between the three relative  $(\Delta)_{\max}$  found for the phases is used to compute the distance  $d$ . Moreover, the phase conductor corresponding to the absolute maximum is for sure affected by the fault, because the beginning of the transient on this voltage occurs earlier than on the safe phases. Anyway, the electromagnetic coupling between the conductors of the three phases belonging to the same overhead line leads to find the same transient disturbance on all the line-to-ground voltages, so that no information can be given on the number of phases involved in the fault.

### 4.1.1. Experimental Results

#### 4.1.1.1. Line-to-line short circuit

An ideal switch, closed 1.5 ms after the simulation starting, has been employed to simulate a short circuit between two phases. The positions of the fault, along with the phases involved, have been changed during the different simulations. Figure 4-2 is the plot of the voltage signal at node 858 caused by a short circuit between phases *a* and *c* in 828.

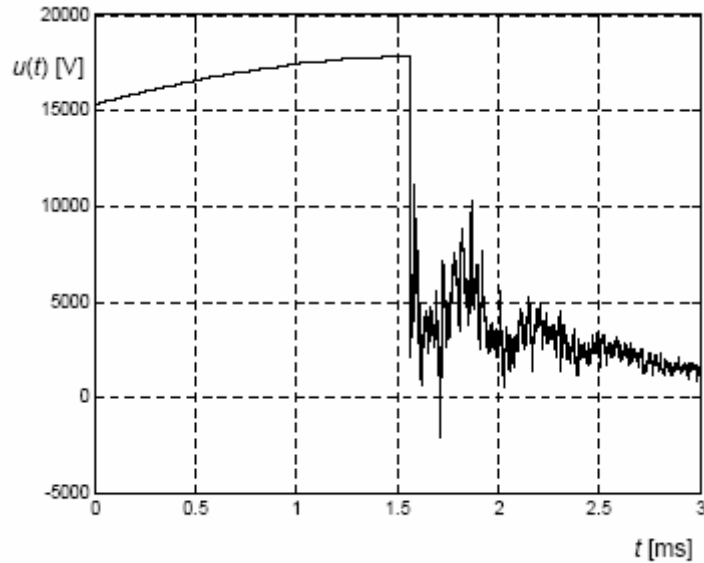


**Figure 4-2** Transient pattern registered in node 858 when the line-to-line short circuit occurs in point 828

By way of example, Table 4-2 reports the values of  $\Delta_{nj}$  estimated for all the portions of the network under test, in the case of two short-circuit locations. In both this table and the following ones, the values of  $(\Delta_{nj})_{max}$  are in bold characters. The line between the nodes 824 and 854 is correctly identified as faulted when the fault occurs in 828 between phases *a* and *c* (case #1). Moreover, the section 800-808 is correctly marked as faulted when the fault occurs in 806 between phases *a* and *b* (case #2). The values of *d* computed according to (3.48) are 257 m for case #1 and 1312 m for case #2. The actual distances are 257 m and 1314 m, respectively. The proposed procedure shows identical good performance when short-circuits are simulated between both phases *b-c* in 830 and *a-b* in 860, thus the results are not reported.

**Table 4-2**  $\Delta_{nj}$  estimated for all the portions of the network in the case of two short-circuit locations

Nodes couples	Fault in 828 ( <i>a-c</i> phases)			Fault in 806 ( <i>a-b</i> phases)		
	$\Delta_{na} (\cdot 10^{-2})$	$\Delta_{nb} (\cdot 10^{-2})$	$\Delta_{nc} (\cdot 10^{-2})$	$\Delta_{na} (\cdot 10^{-2})$	$\Delta_{nb} (\cdot 10^{-2})$	$\Delta_{nc} (\cdot 10^{-2})$
<b>800-808</b>	0.01	0.01	0.01	<b>24</b>	<b>24</b>	<b>24</b>
808-816	0	0	0	0	0	0
816-824	0	0	$9 \cdot 10^{-4}$	0	0	0.09
<b>824-854</b>	<b>7.7</b>	<b>7.7</b>	<b>7.7</b>	0.04	0.04	0
854-832	0	0.03	-0.03	0	0	-0.03
832-858	0	0	0	-0.2	0	0
858-834	0.2	0	0.3	0.2	0	0.2
834-848	0	0.2	-0.2	0	0	0
834-836	0.2	0.2	-0.2	0	0	0
836-840	0	0	0	0	0	0
836-838	-0.2	-	-	0	-	-
808-810	-	0	-	-	0	-
816-822	0	-	-	0	-	-
824-826	-	0	-	-	0	-
854-856	-	0.04	-	-	0	-
858-864	0	-	-	0	-	-

#### 4.1.1.2. Line-to-ground short circuit

An ideal switch closed 1.5 ms after the simulation starting, has been employed to simulate a phase-to-ground short circuit. The position of the fault has been changed in the simulations. Figure 4-3 shows the damped transient voltage caused in node 854, phase *a*, by the fault in 862.

Table 4-3 reports the values of  $\Delta_{nj}$  for the short circuits between phase *a* and ground in point 820 (case #3) and also between phase *a* and ground in 862 (case #4). The sections marked as faulted are correctly identified between slave units 816-822 and 836-838, respectively. As far as the distance of the fault from the nearest slave is concerned, the application of (3.48) provides 4188 m for case #3 and 85 m for case #4; these computed distances are equal to the actual ones.



**Table 4-3**  $\Delta_{nj}$  registered for the phase a-to-ground short circuits in points 820 (case #3) and 862 (case #4)

Nodes couples	Fault in 820 (a-gnd)			Fault in 862 (a-gnd)		
	$\Delta_{na} (\cdot 10^{-2})$	$\Delta_{nb} (\cdot 10^{-2})$	$\Delta_{nc} (\cdot 10^{-2})$	$\Delta_{na} (\cdot 10^{-2})$	$\Delta_{nb} (\cdot 10^{-2})$	$\Delta_{nc} (\cdot 10^{-2})$
800-808	0.01	0.01	0.01	-0.01	-0.01	-0.07
808-816	0	0	0	0	-0.01	0.04
816-824	0	0	0.09	-0.09	0	-0.03
824-854	0.04	0.04	0	-0.04	-0.04	-0.04
854-832	0	0	-0.03	0	0.02	-0.03
832-858	-0.2	0	0	0	0	0.1
858-834	0.2	0	0.2	0.2	0	0.3
834-848	0	0	-0.2	0	0.2	-0.3
834-836	0	0	0	0.4	0.4	0.2
836-840	0	0	0	0	0	-1
836-838	0	-	-	<b>11</b>	-	-
808-810	-	0	-	-	-	-
816-822	<b>43</b>	-	-	0	-	-
824-826	-	0	-	-	0	-
854-856	-	0	-	-	0	-
858-864	0	-	-	0	-	-

#### 4.1.1.3. Insertion of a capacitor bank

An ideal switch (closed 1.5 ms after the beginning of the simulation) has been used to connect each capacitor bank to the relevant node. Table 4-4 shows the values of  $\Delta_{nj}$  obtained as a consequence of the insertion of a three-phase balanced capacitor bank with reactive power equal to 300 KVAR in node 844 (case #5) and 450 kVAR in node 846 (case #6).

In both cases, the portion of network into which the sources of the transients are located is correctly identified as 834-848. The computed distances are: 499 m from node 834 (case #5) and 162 m from terminal 848 (case #6), whereas the actual ones are 497 m and 162 m, respectively.

The capacitor banks in points 844 and 846 have been assumed normally not connected on the basis of first tests. In fact, the fault location method is not reliable if a fault occurs in any point of the network when the capacitor banks are already connected in the relevant nodes. In such conditions the equivalent impedance of the line 834-848 is very much different with respect to the other overhead lines, and the capacitors represent a sort of short circuit for the high-frequency components of the signals due to the transient event.

In practice, even if the line 834-848 is safe, the measured propagation time obtained on the basis of the propagation of the transient from one end to the other differs from the reference propagation time of a quantity that is not comparable to the usual non-zero differences due to the intrinsic uncertainty contribution of the method. In this case the maximum value of delta cannot be associated any longer with the faulted line, but most of the times corresponds to the line where capacitor banks are connected. This issue does not seem to be solved by evaluating how much the presence of capacitors influences the propagation of the travelling waves, because their contribution is not constant, as well as the power of the banks in real operating conditions.

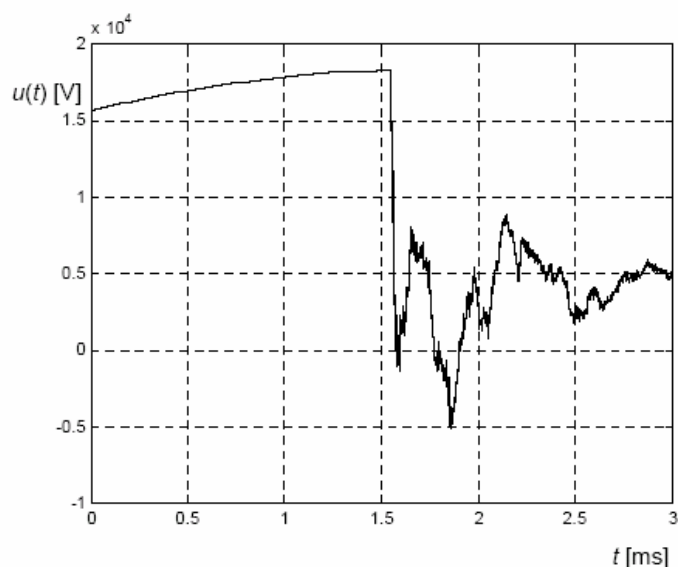


**Figure 4-3** Transient pattern registered in node 854 when the line-to-ground short circuit occurs in point 862

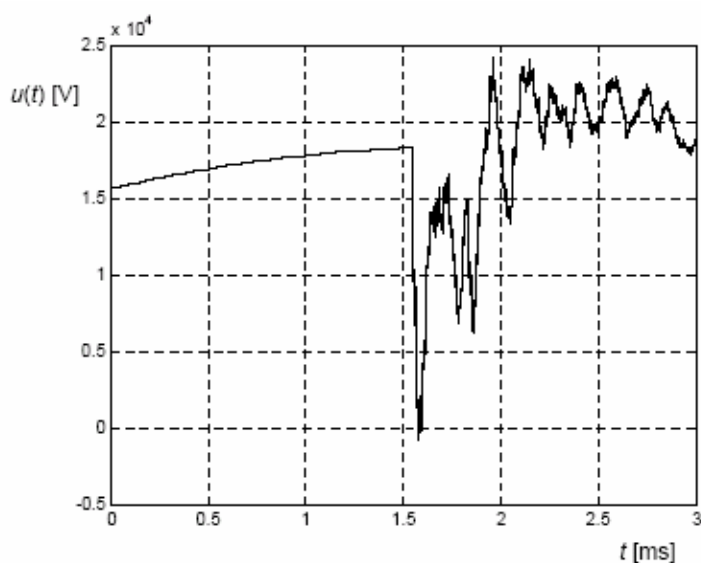


**Figure 4-4** Transient pattern registered in node 854 when the capacitor bank is connected in point 862

**Table 4-4**  $\Delta_{nj}$  registered for the connection of capacitors in points 844 (case #3) and 846 (case #4)

Nodes couples	Capacitor bank in 844			Capacitor bank in 846		
	$\Delta_{na} (\cdot 10^{-2})$	$\Delta_{nb} (\cdot 10^{-2})$	$\Delta_{nc} (\cdot 10^{-2})$	$\Delta_{na} (\cdot 10^{-2})$	$\Delta_{nb} (\cdot 10^{-2})$	$\Delta_{nc} (\cdot 10^{-2})$
800-808	-0.01	-0.01	-0.04	0.01	-0.01	-0.09
808-816	0	0	0.03	-0.01	0	0.03
816-824	0	-0.09	-0.09	0	-0.09	-0.09
824-854	0	0.04	0	0	0.04	0
854-832	0	0.03	-0.03	0	0.03	-0.03
832-858	0	0	0	0	0	0
858-834	0.2	0	0.5	0.2	0	0.5
834-848	<b>56</b>	<b>56</b>	<b>56</b>	<b>18</b>	<b>18</b>	<b>18</b>
834-836	0.4	0.4	0.2	0.4	0.4	0.2
836-840	0	0	-1	0	0	-1
836-838	0	-	-	0	0	-
808-810	-	0	-	-	0	-
816-822	-0.02	-	-	-0.01	-	-
824-826	-	0	-	-	0	-
854-856	-	0.04	-	-	0.04	-
858-864	0	-	-	0	-	-

In order to obtain correct results for the position of the fault within the test network, the number of slave stations should be increased and two more measurement points should be added to the system: just the nodes where capacitor banks are connected to the line. This is the simplest but even the most robust way to evaluate correctly how the transient propagates along the line 834-848, monitoring three separate sub-sections.

Some considerations can be drawn from the results presented in Tables 4-2, 4-3, 4-4. The proposed method correctly identifies the lateral or the section of line where the transient occurs and computes with good accuracy the distance between the source and the nearest slave. However, non-zero values of  $\Delta_{nj}$  are found also for non-faulted sections. This is reasonably due to the superposition of direct and reflected waves which, case by case, modify the voltage waveforms in the nodes. Therefore, errors may arise in the measurement of  $T_{nj\text{meas}}$  and, hence, in the relevant  $\Delta_{nj}$ . Since the effect of reflected and refracted waves depends on the transient source location, the hypothesis is strengthened by considering the number of zero values of  $\Delta_{nj}$ . The results relevant to cases #2 and #3, which refer to faults located close to point 800, feature the highest occurrence of zero values. Point 800, next to the HV/MV station, corresponds to the point where the pulse used to determine  $T_{nj\text{ref}}$  was injected. The effect of the reflected waves on  $T_{nj\text{ref}}$  and  $T_{nj\text{meas}}$  is therefore almost the same; hence, no appreciable difference between  $T_{nj\text{meas}}$  and  $T_{nj\text{ref}}$

is found. The impact of this error turns into a reduced sensitivity when computing the distance  $d$ . Indeed, when the transient source is located near a slave, the value of the relevant  $\Delta_{nj}$  could not be  $(\Delta_{nj})_{max}$ ; in such a case the method would not provide correct information. In Tables 4-2, 4-3 and 4-4 the largest incorrect value of  $\Delta_{nj}$  is in the order of  $10^{-2}$ , which corresponds to a resolution  $d_{min} = 0.5\% \cdot D_{nj}$ . It is worthwhile emphasizing that such resolution depends on the distance between the couple of slave units, whereas the uncertainty affecting the measurement of  $d$  is a constant value.

The longest section of the network (i.e. the one between point 808 and node 816) leads to  $d_{min} = 100$  m. This value is lower than the extended standard uncertainty affecting the fault location due to the only contribution of the GPS-device if a coverage factor equal to 3 is taken, which is 180 m.

In order to simulate actual situations, also the presence of noise affecting the signals of the power system voltage to be processed should be considered. Noise consists of any unwanted distortion of the power signal that cannot be classified as harmonic distortion or transient [2]. It has broadband spectral content lower than 200 kHz and may arise from the operation of power electronic devices, control circuits, arcing equipment, loads with solid state rectifiers and switching power supplies. The frequency range and magnitude level of noise depend on the source, which produces the noise and the system characteristics; a typical magnitude of noise is less than 1% of the voltage magnitude, [2]. Moreover, the voltage signals are also affected by white noise arising from the measurement hardware.

For the above reasons, white noise has been added to the system voltages and new simulations have been run for cases #1, #3, and #6. The noise has been filtered in order to cancel the components with frequency higher than 200 kHz; a noise amplitude close to 200 V peak to peak has been assumed. Of course, the voltage threshold value in the algorithm simulating the operation of the EDB has been increased.

In all the three cases the method correctly both identifies the power system portion where the source of the transient is located and determines the value of  $d$ . In particular, the simulation results for cases #1 and #3 are just the same as those obtained without noise superposed to the signal. As for case #3, values of  $d$  have been found that are slightly different from those achieved without noise as far as the different phases are considered; however, the difference is in the order of 1.2%. This leads to conclude that the measurement system performs very well even in the presence of noise.

The analysis of the experimental results allows to state that the approach performs very satisfactorily. Given that other factors usually affect the operation of a real network, simulations to test the performance of the proposed method in different conditions have been run.

## **4.2. Implementation of a distribution network operating in actual conditions – variation of fault parameters**

### **4.2.1. Improvements in the procedure**

Test results reported in former Section show that in case of phase-to-phase and phase-to-ground short circuits the previous version of the algorithm correctly detects the faulted line section and locates the fault point with good accuracy. However, during the above simulation tests some more information on the system and fault conditions came out by observing the obtained data set.

Aiming at improving the system performance in terms of both accuracy and reliability of results in general conditions, a couple of operations have been added to the procedure. First of all, the master unit seeks for the minimum time stamp value  $(t_{mj})_{min}$  before analyzing any data sent by the slaves.  $(t_{mj})_{min}$  identifies the slave nearest to the fault, so the location procedure can be applied only to a limited network area. The master selects the group of line sections having one common end in the node associated to the  $(t_{mj})_{min}$ . Simulation tests reported in the following showed that this simple operation strongly reduces both the computation time and above all the occurrence of wrong results. In fact, seeking for the  $(t_{mj})_{min}$  allows to detect which one of the phases is certainly affected by the fault. Despite, if grounded short circuits characterized by a high value of the fault resistance are considered, the dumped oscillations induced on the voltages are very small. The EDB installed in the slave units cannot detect the correct timestamp at the beginning of the transient voltage on each phase and this fact can turn into a wrong operation of the location procedure, often leading to different results on the three phases for a fixed position. In such cases the location of the fault is assumed as a correct result only if the three positions obtained by the data relevant to each single phase are coherent with each other.

Moreover, losses on actual electric conductors dump the oscillating distortion as it propagates farther and farther from the transient source, thus compromising the fault location system operation. Indeed, the amplitude of the transient can be lower than the threshold value of the EDB in slaves far from the disturbance source, hence some of them could not detect the event. The algorithm has been improved in order to tackle this issue: the faulted line is identified by comparing the values of delta no longer relevant to all the lines, but only to the lines included between a couple of slaves detecting the event. In practice the minimum number of timestamps needed for the location of the fault is two, and in such a case the two slaves detecting the event will be the ones monitoring the ends of the faulted line.

Finally, the three phase-signals registered by the slave unit nearest to the fault are considered: the transformation from phase to modal voltages is applied and the zero mode component is analyzed. In this way grounded faults can be distinguished from ungrounded ones on the basis of the magnitude of the zero-mode voltage, and a more correct value of the propagation speed can be assumed in both cases for  $v_{njref}$ . In fact, for grounded short circuits the mode relevant to the coupling with ground prevails, which is characterized by a slightly lower propagation speed of the travelling wave respect to the case of phase-to-phase faults. In Figure 4-5 the block diagram of the updated procedure is represented.

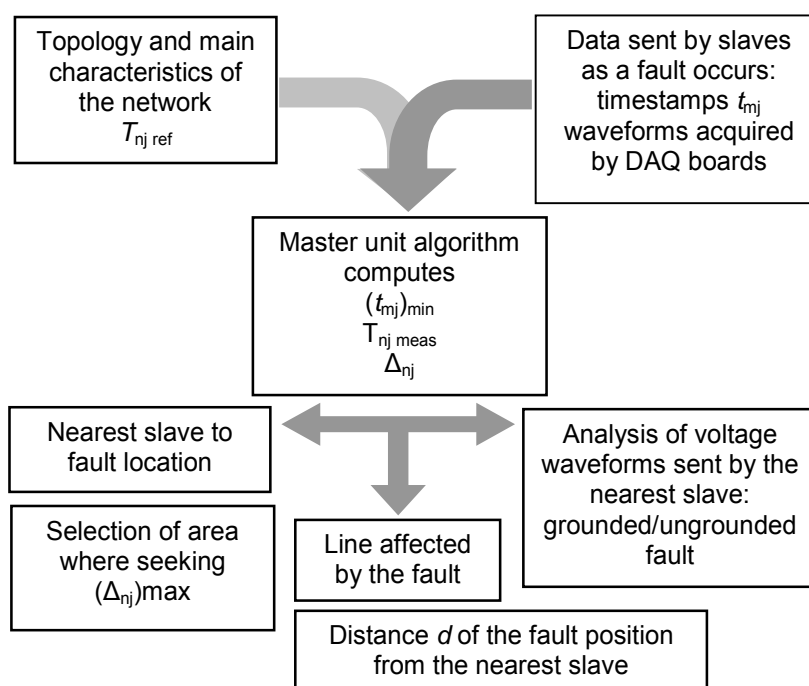


Figure 4-5 upgraded version of the procedure implemented by the master unit

#### 4.2.2. Test conditions: non ideal faults and network elements

In the above simulations of the MV network realistic fault parameters were not yet taken into account because faults were modelled as ideal short circuits. Actually, the amplitude of the transient generated by the fault depends on the values of several parameters at the occurrence of the event, i.e. the position of the fault point, the type of fault, the magnitude of the equivalent fault resistance  $R_f$  and the instantaneous voltage value between the faulted conductors. To show the strong influence of the latter couple of fault parameters on the magnitude of the event, Figure 4-6 can be considered. Three acquisitions of the line-to-ground voltages are reported, relevant to the same slave node and the same position of the phase *a*-to-ground short circuit, to underline the impact of  $R_f$  and  $V_f$  on the network.

Simulations have been run in EMTP-RV environment [3] to test the ability of the measurement system to detect and locate faults affecting a typical radial distribution network operating in real conditions. Most frequent kind of faults have been simulated: phase-to-ground, phase-to-phase short circuits and lightning events; all of them generate dumped oscillatory transients. Moreover, noise and harmonic distortion of the voltage have been considered to verify if such critical parameters could influence the detection method performance. As above explained, noise could lower the sensitivity of the measurement system leading to wrong information. In order to avoid fake event detections the threshold value of each EDB has been increased till 2% of the power system component of  $u_{VVT}$ .

$u'$  = voltage on the faulted phase when the short circuit occurs.

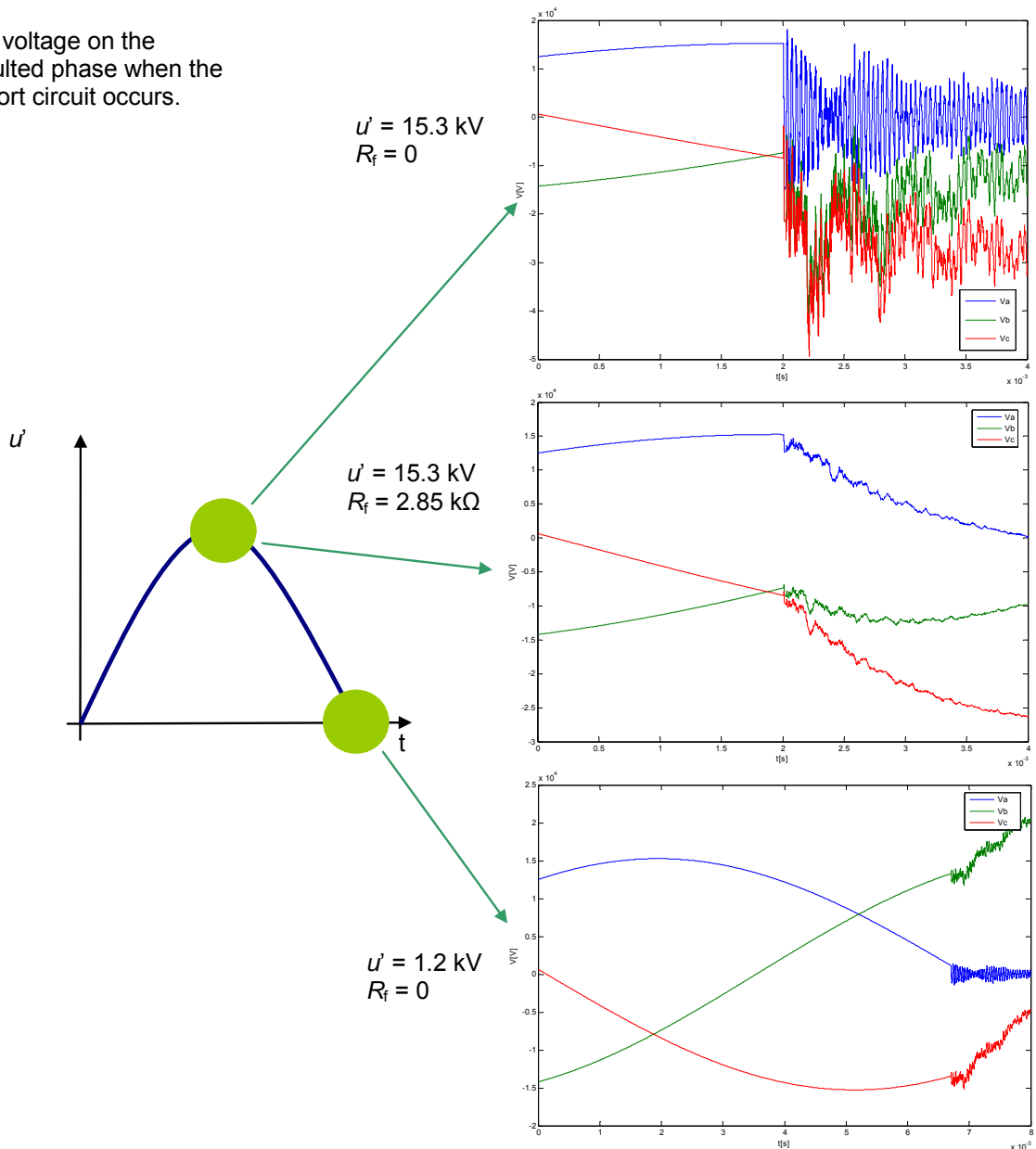


**Figure 4-6** patterns of the transient disturbances affecting line voltages in case of different line-to-ground short circuit conditions

The proposed method needs to know data relevant to the topology of the monitored network in order to feature correct location of the faults. In usual operating conditions a distribution network has not a constant and fixed topology, therefore simulations have been run taking into account manoeuvres that may occur in a real network. Variations of loads power, disconnection of lines or loads have been implemented to test whether configuration changes of the network can lead to wrong results. The measurement system has also been tested in the presence of more than one of the above parameters.

### 4.2.3. Models of Power distribution and Measurement Systems

In previous simulations, carried out to test the first version of the method, both the measurement chain representing the remote unit and the location procedure were implemented by using Matlab scripts. In this case most of the hardware installed in the slaves has been implemented in EMTP-RV environment, whereas MATLAB scripts have been used both to simulate the GPS station of each slave and to develop the location procedure. The algorithm is applied to the solutions provided by EMTP, i.e. set of voltage waveforms in the monitored points of the network under test along with the logic signals at the output of the relevant EDB. The analog devices of the slaves implemented in EMTP environment are reported in Figure 4-7: they allow a reliable performance analysis of the measurement system, in the sense that the equivalent circuits of the devices in the measurement chain model satisfactory the actual behaviour of the blocks. The input signal  $v_{MV}$  is conditioned by the block "loss" with nominal transformation ratio = 10,000 : 1, as the capacitive voltage divider installed in the measurement unit. The output signal of this block drives a controlled voltage source (cV1) to obtain the output of the transducer ( $v_{in}$ ). As the EDB is concerned, first of all two DC components  $v_{off+}$  and  $v_{off-}$ , equal magnitude but opposite sign, are superposed to the  $v_{in}$ , then the two obtained signals  $v_{in+}$  and  $v_{in-}$  are sent to two comparators. The signal  $v_f$  is the output of the low-pass filter  $R_1/C_1$  whose characteristics are clarified in the next chapter. The signal  $v_f$  is compared to the two full-bandwidth signals  $v_{in+}$  and  $v_{in-}$  by the two blocks "compare" which emulate the operational amplifiers used in the real EDB scheme configured as comparators. The logic signals at the output of the couple of comparators are conditioned in order to obtain the two TTL-compatible output signals  $v_{out+}$  and  $v_{out-}$ . The final output  $v_{out}$  is a TTL signal which changes its level (0 – 5 V) every time that one of the two  $v_{in}$  waveforms cross the  $v_f$  waveform.

The voltage source  $v_{point}$  placed in series to the controlled generator cV1 is used to superpose to the EDB input the white noise component.

The signal  $v_{out}$  coming from the EDB is imported in Matlab, where a function is written to simulate the GPS station. As a matter of fact, the GPS script reads a matrix reporting the EDB output in terms of two columns, one for the amplitude of each sample, the other one



for the corresponding sampling time; a change of the status level corresponds to the first non-zero value in the first column, thus the relevant time reference is registered by the program.

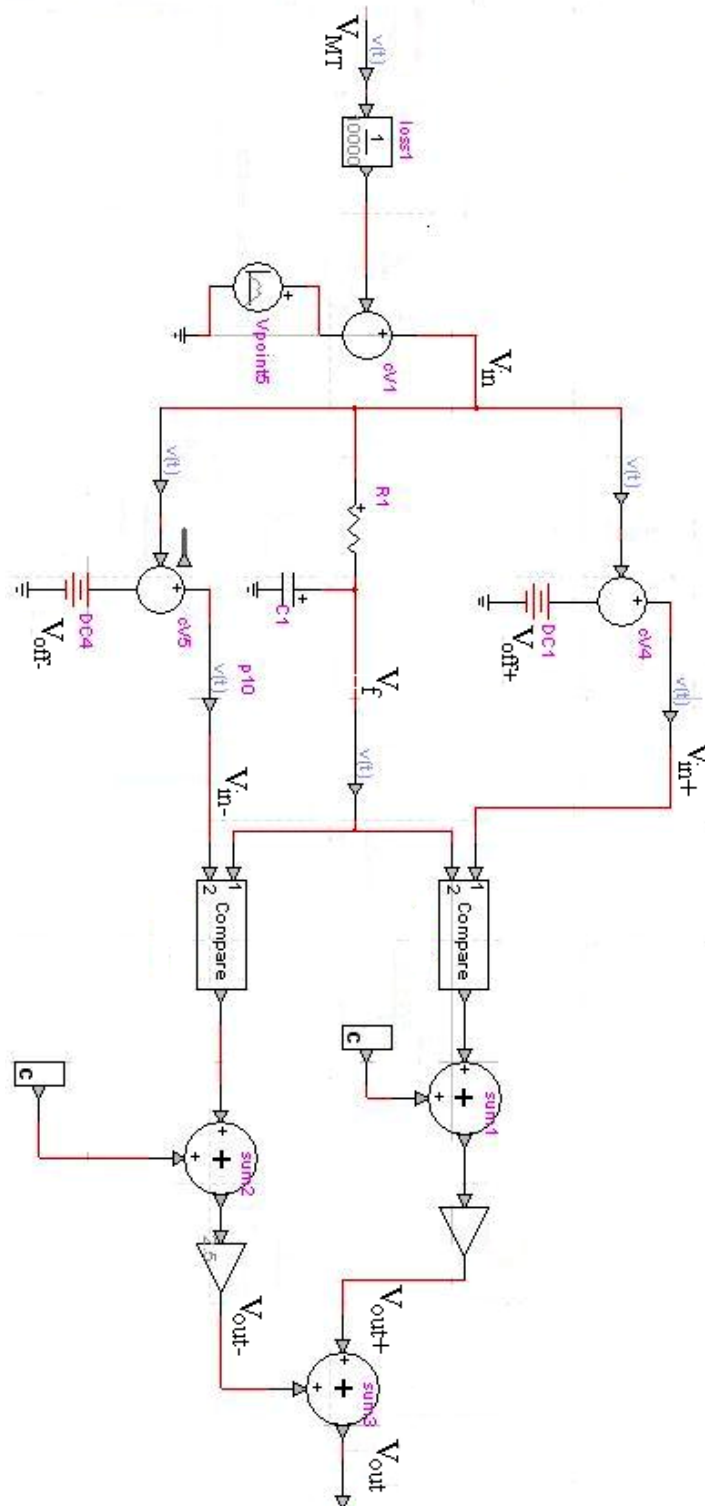


**Figure 4-7** Equivalent model of the EDB realized in EMTP environment

The analysis of the propagation of a transient disturbance caused by a fault starts from steady state conditions. Even for this network the EMTP simulation has been configured to determine the amplitude of the 50 Hz components of voltages and currents, and then

to take these data as initial conditions in the time-domain solution. The integration time has been set equal to 100 ns - nominal resolution of the distributed measurement system. Figure 4-8 is a map of the overhead distribution network under test, which features a typical radial topology consisting in a long main feeder (portions L1, L2, L3, L4) and in laterals connected with it getting to the load busses (lines L5, L6, L7, L8, L9). The three-phase power distribution network is fed by a 150/20 kV station; the source G represents the High Voltage line at its primary side and the transformer T nominal power and connection type are 10 MVA and  $Y_g/d$  respectively. Each load bus consists of a three phase balanced R-L impedance, connected to the relevant feeder through a 20/0.4 kV transformer  $D/y_g$  connected. As found in some literature, e.g. [4], relevant to fault location techniques, parasite capacitors must be considered in parallel to both sides of each MV/lv transformer simulating the behaviour of transformers when signals having frequency components of some hundreds of kHz are concerned. During simulations the power factor of all the loads was constant and assumed equal to 0.9, under the hypothesis that all the load busses were provided with an automatic capacitor bank compensating the phase shift between current and voltage at that point.

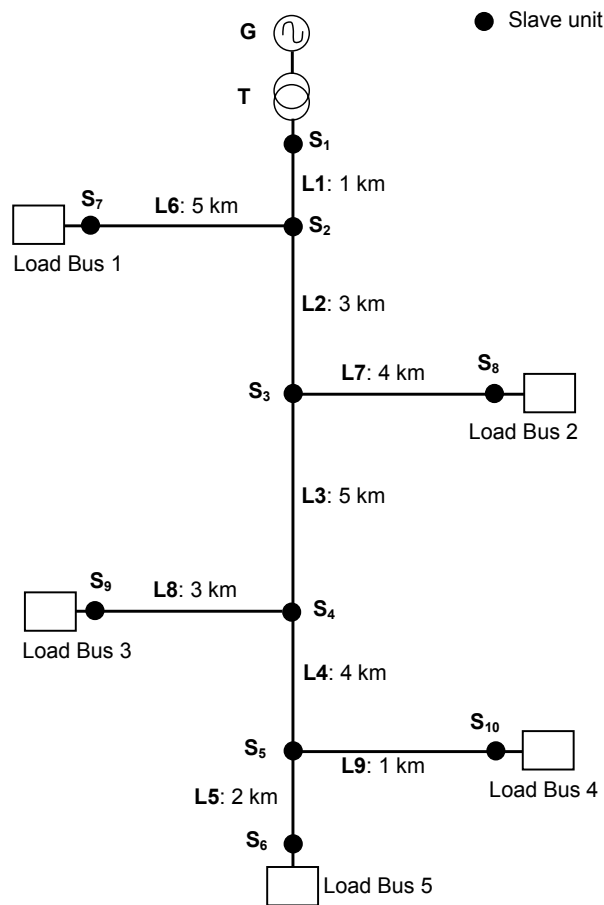


Figure 4-8 Distribution network under test (not in scale)

The EMTP Constant Parameter line model has been adopted for the network lines even in this case. For the first simulations continuously transposed three-phase lines have been considered, since the time domain solution of the transient propagation is easier under these conditions. Indeed, the symmetry between the conductors leads to only two equivalent propagation modes instead of three. Then, the simulations have been repeated without this configuration, since the Italian Medium Voltage system lines are not continuously transposed. The results obtained in both cases are similar, as shown in the following.

Figure 4-9 shows the three phase-to-ground voltage waveforms acquired by the slave S1 at the occurrence of a short circuit between phases *a* and *b* 2500 m far from the measurement point. The fault starts in correspondence of a line-to-line voltage  $v_{ab}$  of 26 kV (the maximum value) and its equivalent resistance is zero in the first case, equal to 9.5 k $\Omega$  in the second case. In the third graph the three phase voltages acquired by the same S1 slave are represented when the line-to-line fault has equivalent fault resistance 400  $\Omega$  and occurs when the  $v_{ab}$  is 1.66 kV. How different is the magnitude of the transient distortion in the three simulations can be appreciated. It should be noted that the considered faults feature extreme conditions as far as  $R_f$  and  $V_f$  are concerned.

Before going on with the report of results, it can be useful making clear the criteria adopted for the analysis of the performance of the proposed method by varying the above parameters and conditions. In every simulation campaign a given fault has been simulated on each line portion of the network under test. The configuration of the network is fixed, whereas the boundary levels of fault parameters are looked for, so that information on the limits of the system are available. To do this, the position of the fault and the number of conductors involved is fixed; for the first simulation the heaviest short circuit is considered, hence zero fault resistance and occurrence of the fault in correspondence of the maximum value of the voltage between faulted conductors. The location obtained in such conditions is assumed as reference for the following simulations. Then, by keeping constant all the other parameters, the fault resistance is increased and the fault location procedure is applied. The result obtained at the end of each simulation is considered correct only if the position is the same one given by the first case. Aiming at determining the boundary value of the fault resistance that allows a correct location,  $R_f$  is varied according to the bisection algorithm: the boundary value  $(R_f)_{max}$  is obtained at the end of iterations with different  $R_f$  values and corresponds to the condition:  $(R_f)_{max}$  leads to correct result,  $(R_f)_{max} + 100\Omega$  leads to wrong result. Once the  $(R_f)_{max}$  is found, the same simulations sequence is repeated for a lower value of voltage between faulted conductors. For the parameter  $V_f$  such a criteria for the variation leads to a minimum value, i.e. that value that give rise to a too low transient even if the  $R_f$  is null.

4. ANALYSIS OF THE PERFORMANCE FEATURED BY THE FAULT LOCATION METHOD  
SIMULATIONS OF DISTRIBUTION NETWORKS IN EMTF ENVIRONMENT

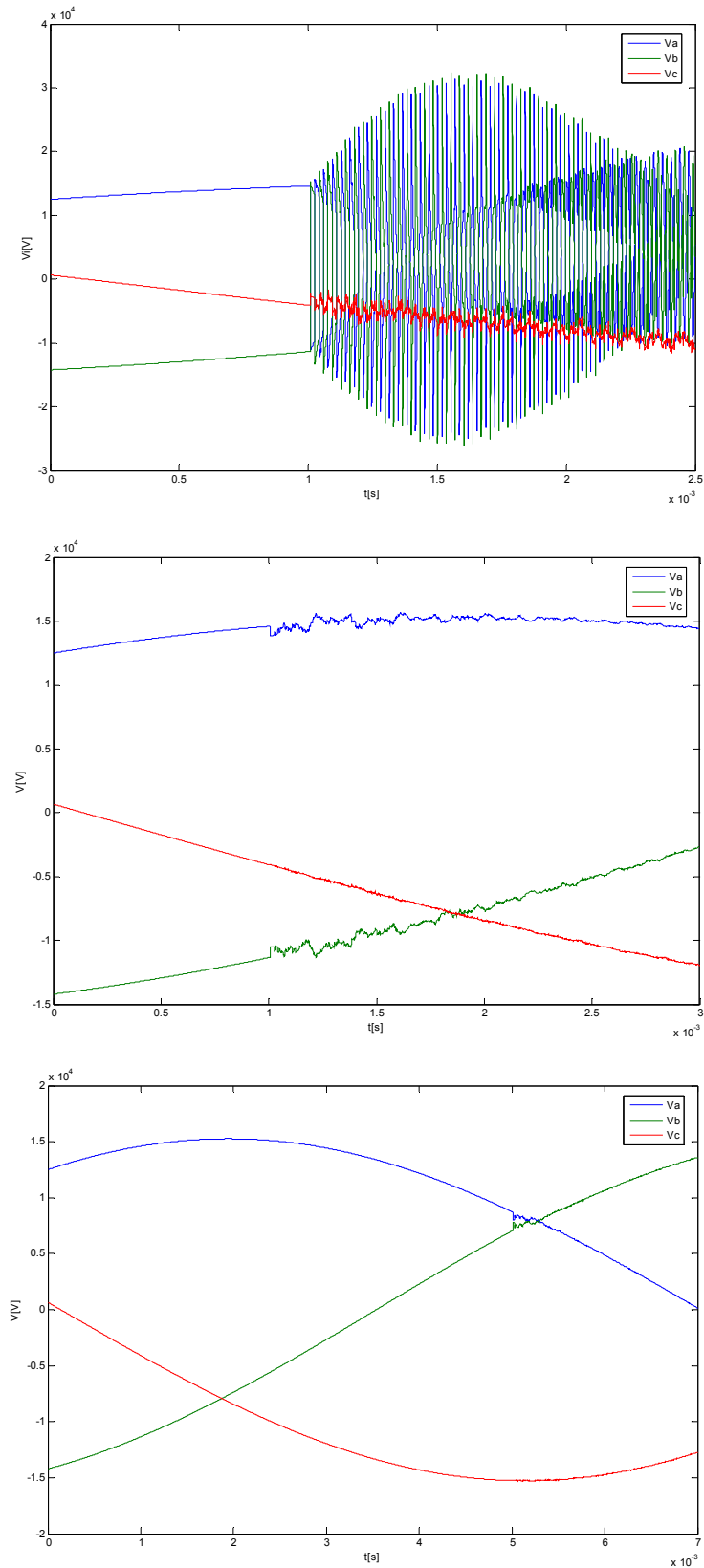
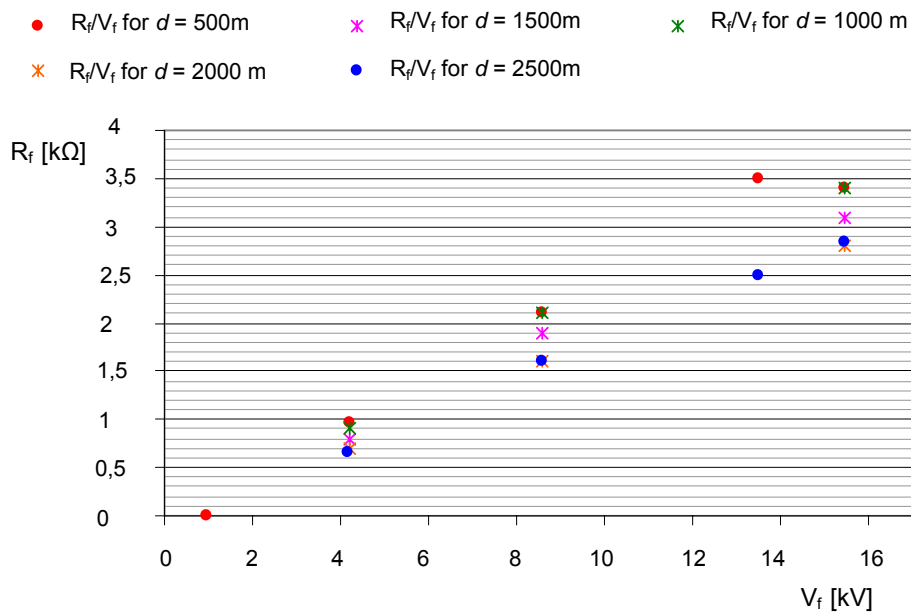


Figure 4-9 patterns of the transient disturbances affecting line voltages for different line-to-line fault conditions

#### 4.2.4. Simulations results

First of all, simulations have been run in which the short-circuit point was moved step by step along the faulted line (L1) from nearby one end to the midst, in order to determine the worst condition for the location in terms of distance from fault point to slave unit. In Figure 4-10 the relevant results are reported by using a characteristic  $R_f/V_f$  for the different positions of the fault along L1. When the fault occurs in the midst of the line it is correctly detected and located with the greatest difficulty. In order to reduce the number of simulations to be run for the performance analysis of the method, the worst condition is assumed for the different parameters, and thus during simulations the fault has been positioned always at the midst of each one of the nine lines.

In Figure 4-11 the results obtained for a line-to-ground fault on line L6 by implementing the previous version and the updated version of the location procedure are reported in terms of the same  $R_f/V_f$  chart. The usefulness of the improvements made in the latter one with respect to the algorithm developed in Section 3.4 is confirmed, in the sense that a much larger range of fault conditions can be correctly detected and located (red area plus blue area instead of blue area).



**Figure 4-10** Limit fault conditions allowing correct results for different values of the distance fault-slave

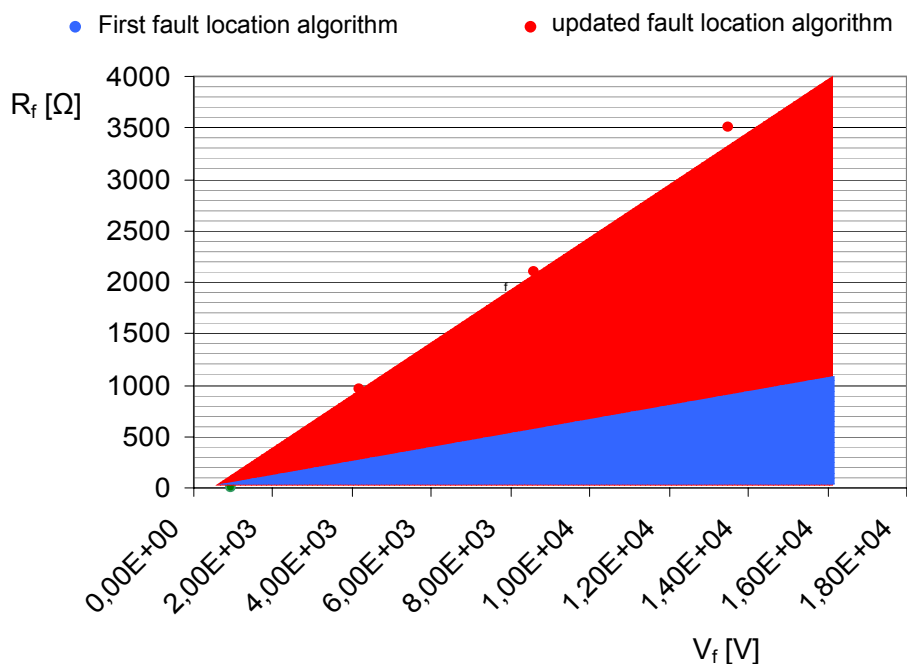


**Figure 4-11** Comparison of fault conditions leading to correct results when both versions of the location procedure are applied

The type of faults considered in the tests are phase-to-ground and phase-to-phase short-circuits and lightning strokes. They have been implemented at the midst of each line of the network under test. The types of faults chosen for the simulations have not to be considered as a limit for the validity of the final performance of the fault location method. In fact other fault cases than the considered ones would affect a higher number of conductors (three-phase short circuit, two phase-to-ground short circuit, etc.) and hence would be heavier for the power system. In this sense the chosen fault configurations are representative of the “worst conditions” for the distributed detection system, and the relevant performance limits of the proposed method can be considered reliable for every other fault occurrence.

#### 4.2.4.1. Direct lightning

Figure 4-12 reports the circuit used to model the lightning event in EMTP and the relevant current parameters. As far as lightning strokes are concerned, the induced transient voltage always has so great amplitude that the measurement system detects the beginning of the transient in all the slaves and the method gives correct results in all cases. Actually, in the simulated MV network there are no surge arresters installed in the nodes, and their effect on the path of the propagating transient is not taken into account. The presence of such devices, anyway, cannot turn into significant degradation of the method operation, since surge arresters at the ends of the line stroke by the direct lightning are designed to start working when the induced overvoltage reaches values 3 - 4 times the nominal voltage. For example, in Figure 4-13 [5] the characteristic of a surge

arrester with 8.5 kV rating (i.e. the line-to-ground voltage level for a three phase system with 15 kV nominal line-to-line voltage) is reported. The surge arrester starts conducting the lightning induced current when the relevant voltage gets to 30 kV. In any case the waveforms at the monitored points of the network will present a first fast rising front getting to the peak value for sure much higher than the EDB threshold.

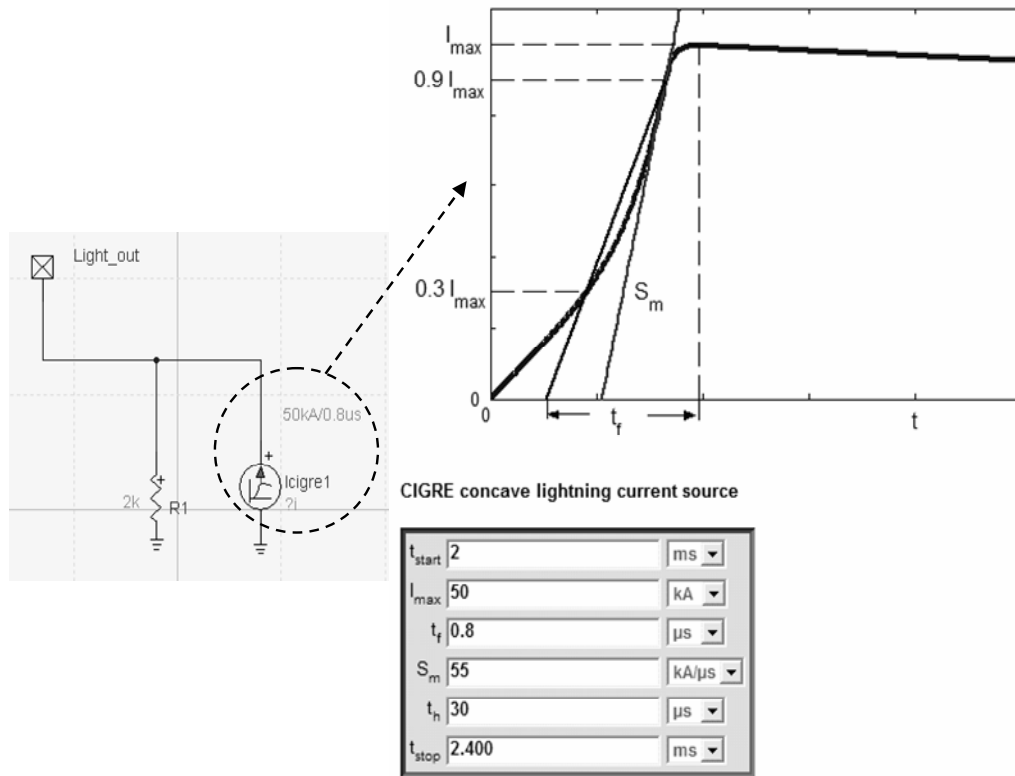


Figure 4-12 Model of the Lightning fault

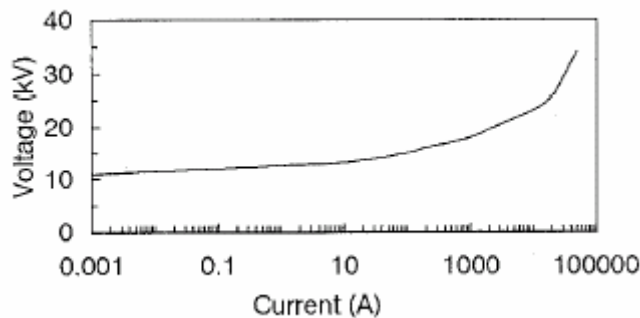


Figure 4-13 voltage-current characteristic of a surge arrester

#### 4.2.4.2. Phase to ground short circuit - Transposed lines

The maximum value of fault resistance ( $R_f$ ) for different magnitudes of the voltage  $u'$  in the case of phase-to-ground faults is reported in Figure 4-14. Each symbol in the plot refers to a set of results relevant to faults located at the midst of the same line. In particular, Figure 4-14 shows the performance of the proposed method when the lines are continuously transposed.

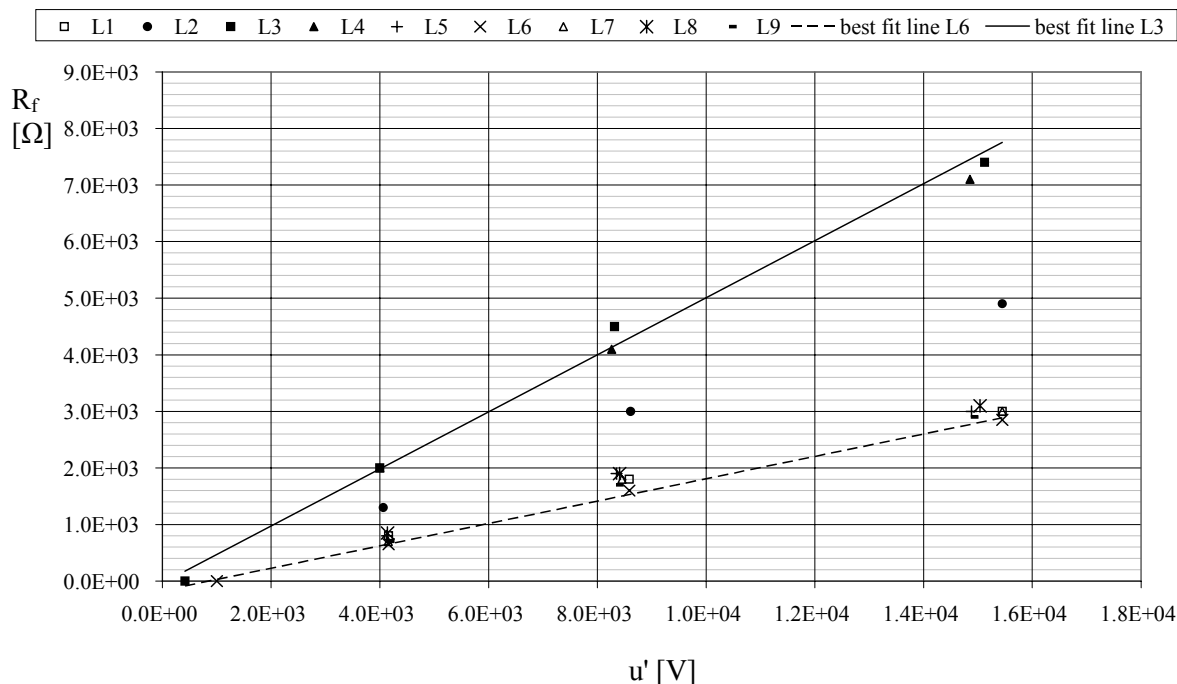


Figure 4.14 Grounded fault on transposed lines: maximum value of  $R_f$  for different  $u'$  values – limit fault conditions allowing correct results for faults positioned at the midst of each line

A main difference can be seen between the results obtained when the fault affects a line connected to a transformer (the laterals feeding the load busses and the portion connected to the HV/MV station) or a section connected only to other lines. When the fault affects the latter type of lines, the method performance is better in the sense that higher  $R_f$  values let the procedure compute a correct location. The presence of a transformer at one end of a line section seems to have a strong influence on the boundary fault conditions, indeed the points in the graph representing results obtained when the faulted line is a lateral are almost superposed. On the contrary the points relevant to the cases in which the fault is located along the feeder are not coincident. The influence of the length of the faulted section can be appreciated: the method performs better when the fault affects line L3 (5 km), then line L4 (4 km) and finally L2 (2 km).

Moreover, the efficiency of the proposed detection and location method has been checked by comparing the maxima values of  $R_f$  in Figure 4-14 to actual equivalent resistance values for the same type of fault. In 2000 the main Italian electricity utility carried out a measurement campaign on the values of fault resistance, whose report is represented in Figure 4-15. It can be easily seen that over 50% of grounded short circuits featured an  $R_f$  value lower than 10 Ω; about 90% of them had  $R_f < 1$  kΩ.

The simulation results have been compared to the cumulated frequency of real values of  $R_f$  for the same type of fault. In order to define the characteristics of a new automatic protection equipment to be installed in MV networks, in particular dealing with a threshold setting in case of grounded short circuits, the main Italian utility carried out a measurement campaign. In 2000, measurements aiming at obtaining the frequency



distribution of  $R_f$  values were made by analyzing the data registered by the protection equipments at the time of intervention. The results of such measurements (around 1000 acquisitions) are reported in Figure 4-15 in terms of frequency distribution and cumulated frequency as well.

**Table 4-5** Fault parameters relevant to the points reported in Figure 4-14

	L2	L3	L4	L6
$u'$ [V]	$R_g$ [ $\Omega$ ]	$R_g$ [ $\Omega$ ]	$R_g$ [ $\Omega$ ]	$R_g$ [ $\Omega$ ]
1,54E+04				2,85E+03
1,49E+04		7,40E+03		
1,47E+04			7,40E+03	
1,52E+04	8,40E+03			
8,77E+03				1,70E+03
4,44E+03				750
8,66E+03	5,40E+03			
4,34E+03	2,70E+03			
8,49E+03		4,70E+03		
4,28E+03		2,30E+03		
8,41E+03			4,70E+03	
4,28E+03			2,40E+03	

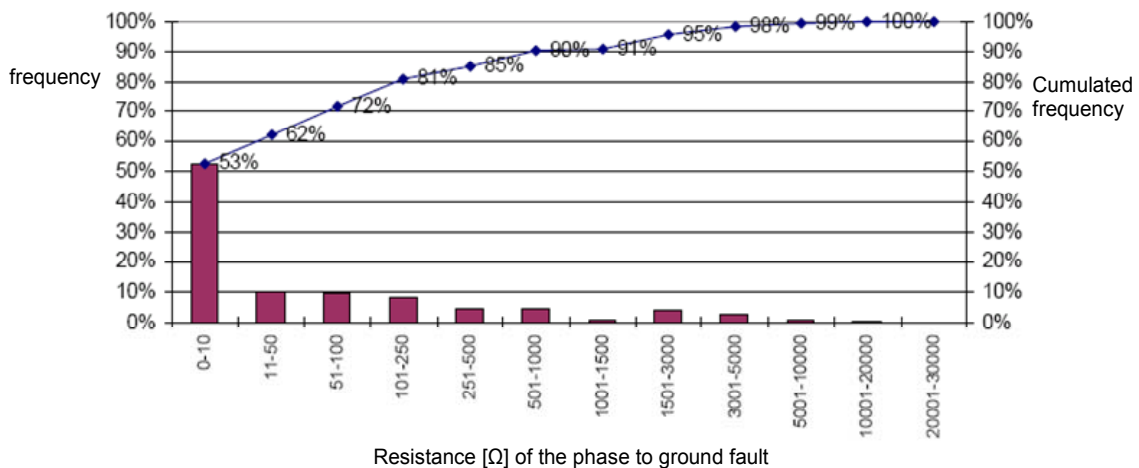
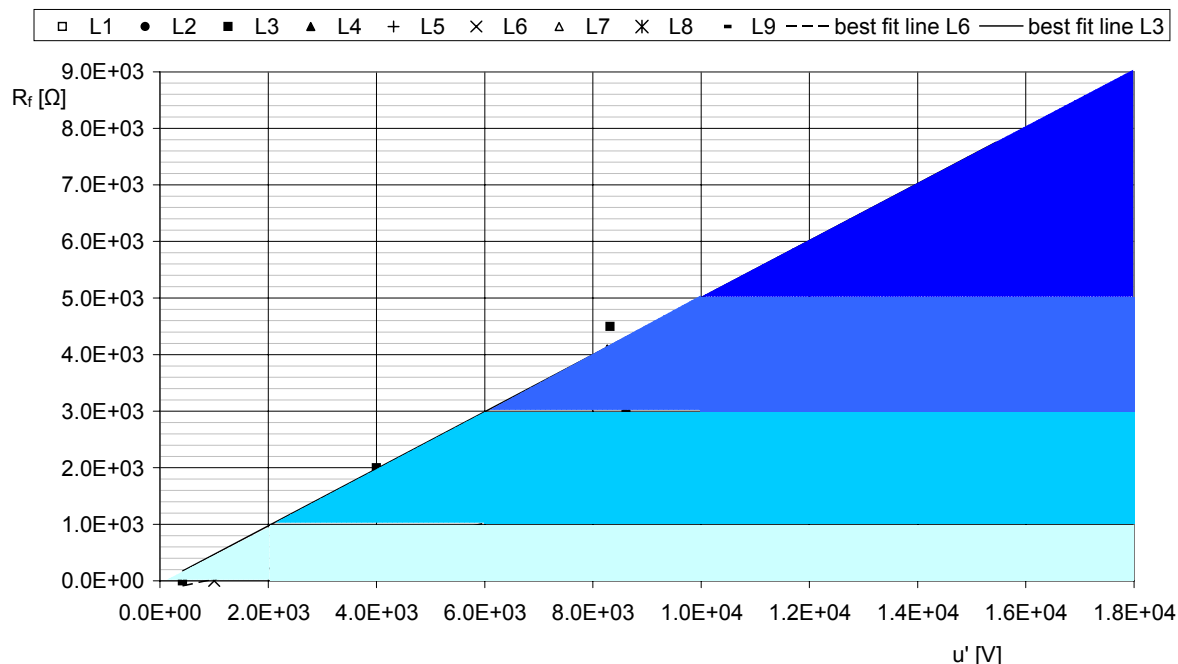


**Figure 4-15** measurement results of the Italian utility campaign on grounded faults

It should be noticed that the values reported in the histogram are not the actual fault resistances, but the equivalent ones seen by the protection equipment, whose value can depend on the protective settings of each device.

Figure 4-16 reports the percentage of phase-to-ground faults registered by the utility that could have been correctly detected and located by the proposed method. Each colour of

the area relevant to fault conditions leading to a correct location corresponds to a particular value of cumulated frequency of  $R_f$  in Figure 4-15. The comparison shows the high efficiency of the procedure in locating faults.



Cumulated frequency of  $R_f$  values of phase-to-ground faults obtained by a measurement campaign on electric power distribution systems; comparison with the best performance of the proposed method in terms of percentage of detected faults as  $R_f$  increases:

>98%; 98%; >91%; >85%.

**Figure 4-16** Comparison of real values of grounded-fault resistance registered in MV systems with the range of  $R_f$  values that allow the method to correctly locate the fault.

#### 4.2.4.3. Phase-to-ground short circuit - Untransposed lines

**Table 4-7** Fault parameters relevant to the points represented in Figure 4-17

	L2	L3	L4	L6
$u'$ [V]	$R_f$ [Ω]	$R_f$ [Ω]	$R_f$ [Ω]	$R_f$ [Ω]
1,54E+04				2,85E+03
1,49E+04		7,40E+03		
1,47E+04			7,40E+03	
1,52E+04	8,40E+03			
8,77E+03				1,70E+03
4,44E+03				750
8,66E+03	5,40E+03			
4,34E+03	2,70E+03			
8,49E+03		4,70E+03		
4,28E+03		2,30E+03		
8,41E+03			4,70E+03	
4,28E+03			2,40E+03	

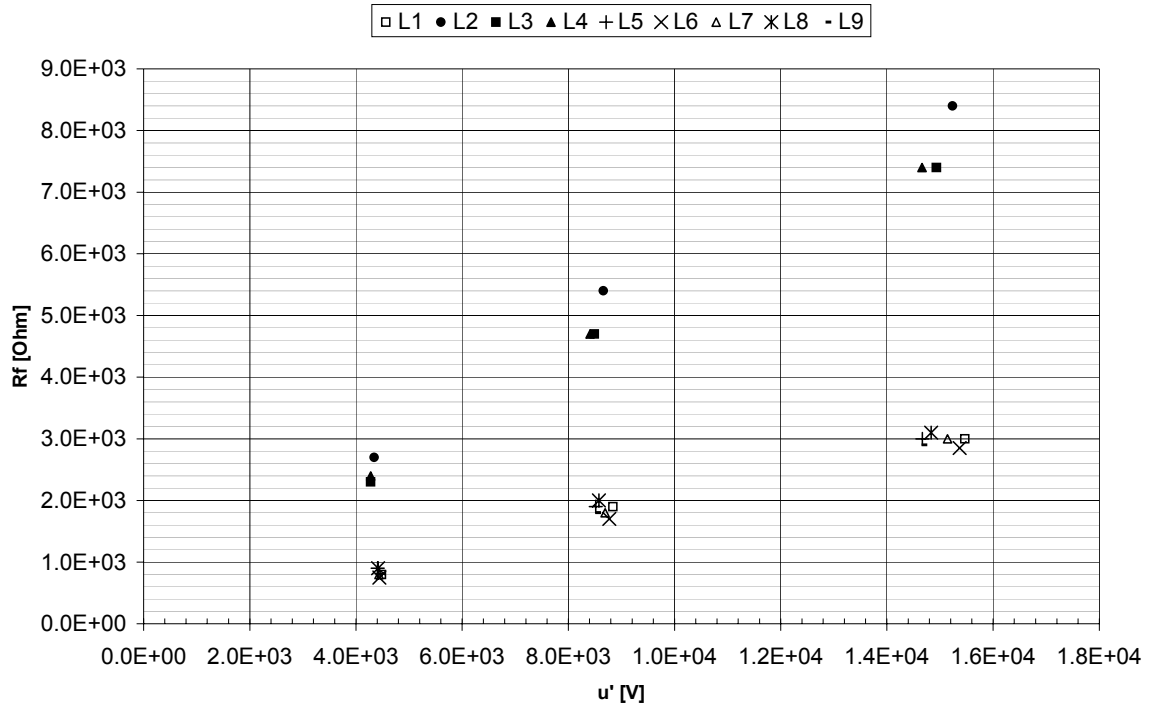


**Figure 4-17** line-to-ground fault on untransposed lines: maximum value of  $R_f$  for different  $u'$  values. Limit conditions allowing correct results for faults positioned at the midst of each line.

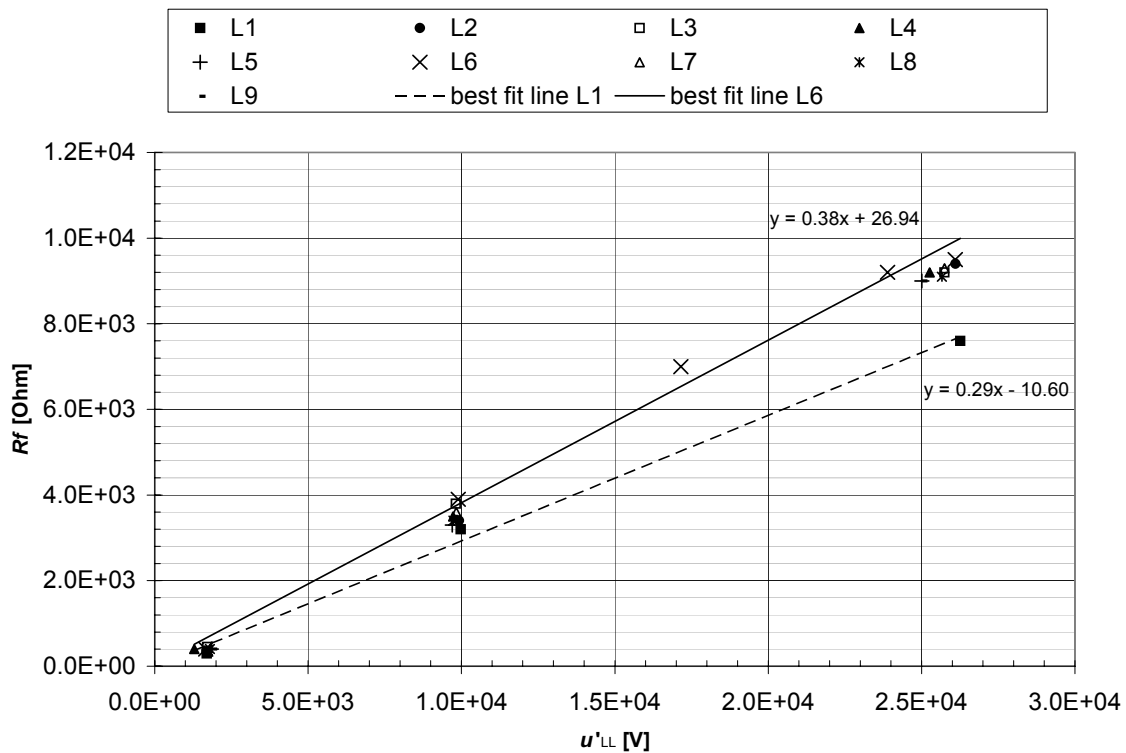


**Figure 4-18** line-to-line fault on untransposed lines: maximum value of  $R_f$  for different  $u'_{LL}$  values limit fault conditions allowing correct results for faults positioned at the midst of each line

Figure 4-17 shows the method performance for phase-to-ground faults in the case of untransposed overhead lines in the network. The method performs well also in this configuration of the conductors, as it can be seen by comparing Figures 4-17 and 4-14.

The results relevant to both cases agree, except for the opposite dependence of the limit value of  $R_f$  on the lines length.

#### **4.2.4.4. Phase-to-phase short circuit - Untransposed lines**

Figure 4-18 reports the maximum value of  $R_f$  in function of the line-to-line voltage instead of the phase voltage given that phase-to-phase short circuits are considered. For this type of fault no remarkable difference can be found in the results when the main feeder or one lateral line is faulted.

#### **4.2.4.5. Variations in the network topology**

##### **Disconnection of lines**

Simulations have then been run under different operating conditions. First of all the performance of the method have been tested for phase-to-ground faults with disconnected lines respect to the configuration of the network registered in the master database.

The system configurations taken into account for simulations are the following:

Fault on line L1 when the line L6 is not connected;

Fault on line L2 when the line L6 is not connected;

Fault on line L2 when the line L7 is not connected;

Fault on line L3 when the line L6 is not connected;

Fault on line L3 when the line L8 is not connected;

Fault on line L4 when the line L8 is not connected;

Fault on line L5 when the line L9 is not connected;

Fault on line L4 when the line L9 is not connected;

Fault on line L6 when the line L7 is not connected;

Fault on line L8 when the line L7 is not connected.

By analyzing the obtained results different behaviour of the method can be drawn: i) if the faulted line is not connected to a node where also the disconnected lateral ends, no difference in the results can be appreciated; ii) if the fault affects a line that feeds a load bus, and hence connected to a transformer in its end, the maximum value of  $R_f$  leading to a correct location is almost identical; iii) if the fault occurs on the main feeder the boundary value of  $R_f$  is lowered of around 40% respect to the value relevant to the same fault case in normal operating conditions. Considerations ii) and iii) are valid independently of which line having one common end with the faulted one is disconnected.

**Table 4-8** Fault parameters relevant to the points represented in Figure 4.18

	L1	L2	L3	L4	L5	L6
$u'_{LL}[V]$	$R_f[\Omega]$	$R_f[\Omega]$	$R_f[\Omega]$	$R_f[\Omega]$	$R_f[\Omega]$	$R_f[\Omega]$
1,54E+04						2,85E+03
1,55E+04	3,00E+03					
1,49E+04			7,40E+03			
1,47E+04				7,40E+03		
1,47E+04					3,00E+03	
1,52E+04		8,40E+03				
8,77E+03						1,70E+03
4,44E+03						750
8,84E+03	1,90E+03					
4,48E+03	800					
8,66E+03		5,40E+03				
4,34E+03		2,70E+03				
8,49E+03			4,70E+03			
4,28E+03			2,30E+03			
8,41E+03				4,70E+03		
4,28E+03				2,40E+03		
8,52E+03					1,90E+03	
4,41E+03					900	

### Disconnection of load busses

Some simulations of phase to ground fault in the case of loads not connected to their busses have been run. The performance of the proposed fault location method are identical to the ones shown above, both if the fault occurs on the lateral without load at its end and if the fault affects a line connected to the unloaded lateral.

### Variations of loads power

Simulations results have shown that decreasing the values of resistance and inductance of any three phase load till 50% can lead to variations of the boundary value of  $R_f$  relevant to a grounded fault of some Ohms (whereas  $R_f$  is in the order of some kiloOhms). The same can be said if the power of the load is increased of 50%. In order to obtain appreciable variations in the performance of the fault location method (anyway  $R_f$  values decreased only of some points %) the load power has to be varied of one order of magnitude. Finally, the simulations results lead to conclude that the method is not influenced by variations of the power absorbed by the loads.

### Non linear loads – harmonic distortion

The effect of non-linear loads has also been considered. Odd harmonic frequency components up to 11<sup>th</sup> order have been simulated in the network and the boundary magnitude levels described in [6] have been assumed for each order. As a matter of fact, in the IEC standard the highest tolerated level of harmonic current pollution corresponds for every frequency component to the value  $I_1/h$ , where  $I_1$  is the nominal RMS of the fundamental component of the current and  $h$  is the harmonic order of the frequency component.

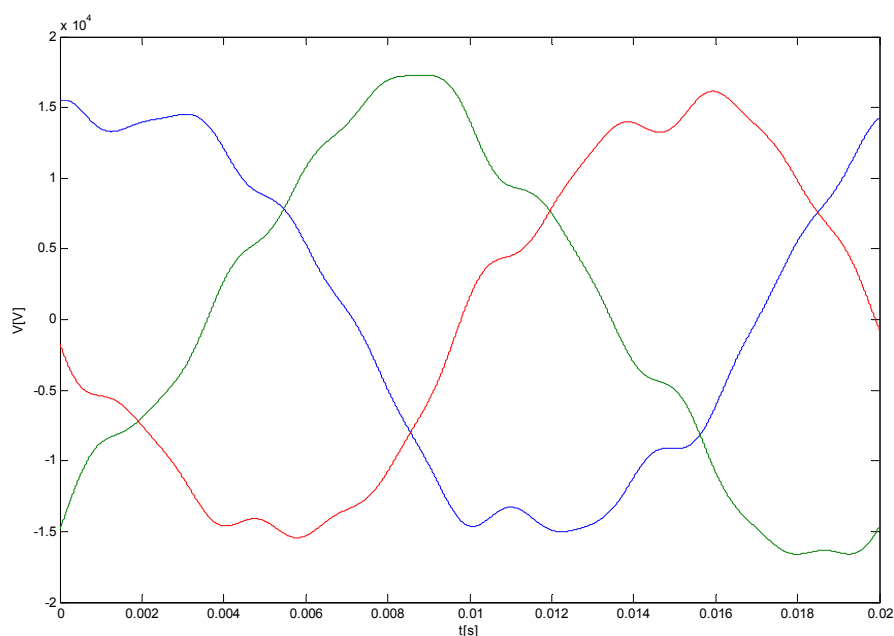


**Figure 4-19** voltage waveforms when non linear loads are present in the network.

Ideal current sources have been connected in parallel to each load bus to generate harmonics to check whether the slaves could always distinguish the transient disturbance generated by a fault from harmonic distortion (periodic disturbance). For example, Figure 4-19 reports the voltage waveforms acquired by the slave unit S2 when non linear loads are present in the electric system.

As expected, no meaningful difference in the performance of the detection and location system can be found, in fact the EDB installed in each slave unit is immune to any frequency component of the voltage signal lower than 10 kHz, and hence no fake event detection can happen in the presence of periodic distortion. At the same time, the transient disturbance is always distinguished by the harmonics superposed to the 50 Hz phase voltage and immediately registered by the remote stations.

### 4.3. Implementation of a radial distribution network to test the version of the fault location procedure integrated with DWT analysis

Simulations have been run in EMTP-RV [3] environment to obtain the voltage waveform on a distribution network when the electromagnetic transient due to a fault propagates through the lines. The signals acquired in different points of the network under test have been imported in MatLab environment, where proper scripts emulate all the instrumentation required by the distributed system. These scripts process the set of digital waveforms relevant to one case of fault simulation (as if they were the data acquired by the DAQ board and sent from slave units) and implement the fault detection and location algorithm.

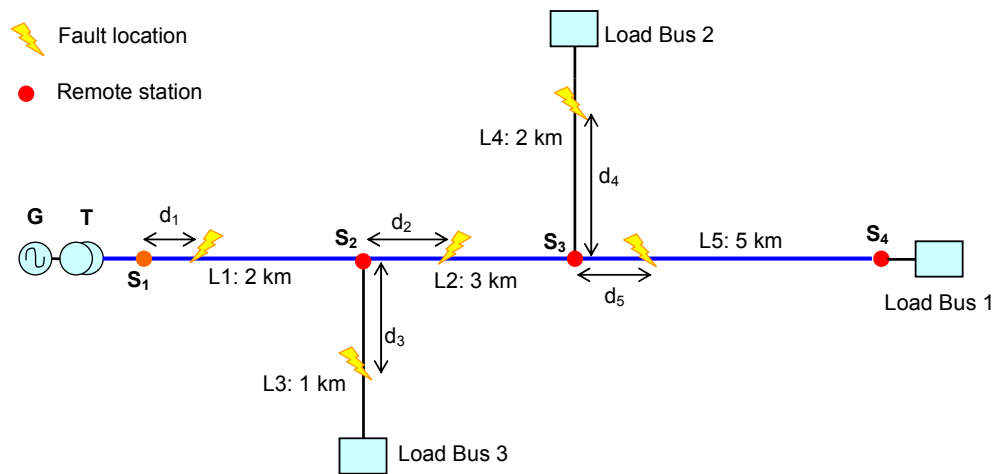


**Figure 4-20** The power distribution network used for tests (not in scale)

Figure 4-20 is a map of the power distribution system implemented in EMTP simulations. It consists in a 10-km long main feeder (lines L1, L2 and L5) and in two laterals: L4 (2-km long) and L3 (1-km long). In the system three-phase overhead lines are used. The model adopted for the lines is the Constant Parameters Line Model, i.e. an equivalent circuit with uniformly distributed parameters  $R$ ,  $L$ ,  $C$  and  $G$  per unit length. The radial distribution network is fed by a 150/20 kV substation  $G$ , where the transformer  $T$  is of the  $Y_g/d$  connection type. All the load busses are modeled as a three-phase balanced impedance. Each load is connected to the relevant lateral through a 20/0.4 kV transformer. As suggested in literature [4] capacitors are connected in parallel to each wiring of the EMTP transformer model; this way a first order approximation of its behavior when signals include frequency components around 100 kHz. Three-phase and single phase-to-ground short circuits have been simulated at different locations, shown by flashes in Figure 4-20, by using ideal switches. Four slave units of the distributed measurement system, denoted by  $S_1$ ,  $S_2$ ,  $S_3$  and  $S_4$ , are placed in correspondence of the black bullets in Figure 4-20.

The integration time for all the faulted network simulations has been set to 100 ns, equivalent to the nominal resolution in time performed by the measurement chain of a slave unit. The values of  $T_{nk_{ref}}$  relevant to the propagation along the main feeder have been obtained by dividing the nominal length of each section by the propagation speed of the  $\alpha$  mode.

The proposed algorithm detects correctly the line affected by the fault for the positions considered and grounded faults are distinguished from ungrounded ones. The main feeder is assumed to be faulted in the case of lines  $L_1$ ,  $L_2$ ,  $L_5$  affected by short circuits, whereas not faulted if the event occurs on lines  $L_3$  and  $L_4$ . As a consequence, the location of the fault is estimated by different algorithms for the two set of positions, and the relevant results are shown in Table 4-9.

**Table 4-9** Estimated and actual distance of the fault from the nearest measurement unit

Kind of fault	$d_1$ (m)		$d_2$ (m)		$d_3$ (m)		$d_4$ (m)		$d_5$ (m)	
	Estim.	Ref.	Estim.	Ref.	Estim.	Ref.	Estim.	Ref.	Estim.	Ref.
Three phase	500.50	500.00	1299.20	1300.00	706.00	700.00	1500.40	1500.00	999.60	1000.00
Phase to ground	500.50	500.00	1299.30	1300.00	356.00	700.00	1262.00	1500.00	999.60	1000.00

As far as symmetric short circuits are concerned, it can be stated that the fault is located with very good accuracy by both the procedures, whereas in case of phase-to-ground faults the analysis based on the traveling waves theory features worse accuracy in locating the short circuit along the faulted lateral. This is due to the difficulty in detecting in the transient waveform the correct spike used to compute the distance between fault point and line head, corresponding to the wave reflected from the fault point that has to be distinguished by all the other simultaneous reflections coming from the nodes of the network. moreover, losses along the line dump quite quickly the magnitude of the oscillations, hence if the fault is not very heavy for the network it does not give rise to a disturbance much higher than the usual noise level affecting phase signals. Analysis of the DWT decomposed signals under different points of view have been performed investigating on the chance to overcome the problem. For example other levels of details have been analyzed, the energy contribution of the levels have been compared, since each decomposition level is relevant to a frequency subband and the equivalent frequency of the oscillations in the transient depends on the distance fault-node. The signals have also been reported in the time domain by applying the inverse wavelet transform only to the highest levels so that only the waveshape of the disturbance is obtained. Finally, the DWT has been applied to the modal voltages instead of the phase ones, since grounded short circuits as dissymmetric conditions lead to a



higher zero mode coupling respect to the three phase ones. All such approaches do not lead to a significant improvement of performance.

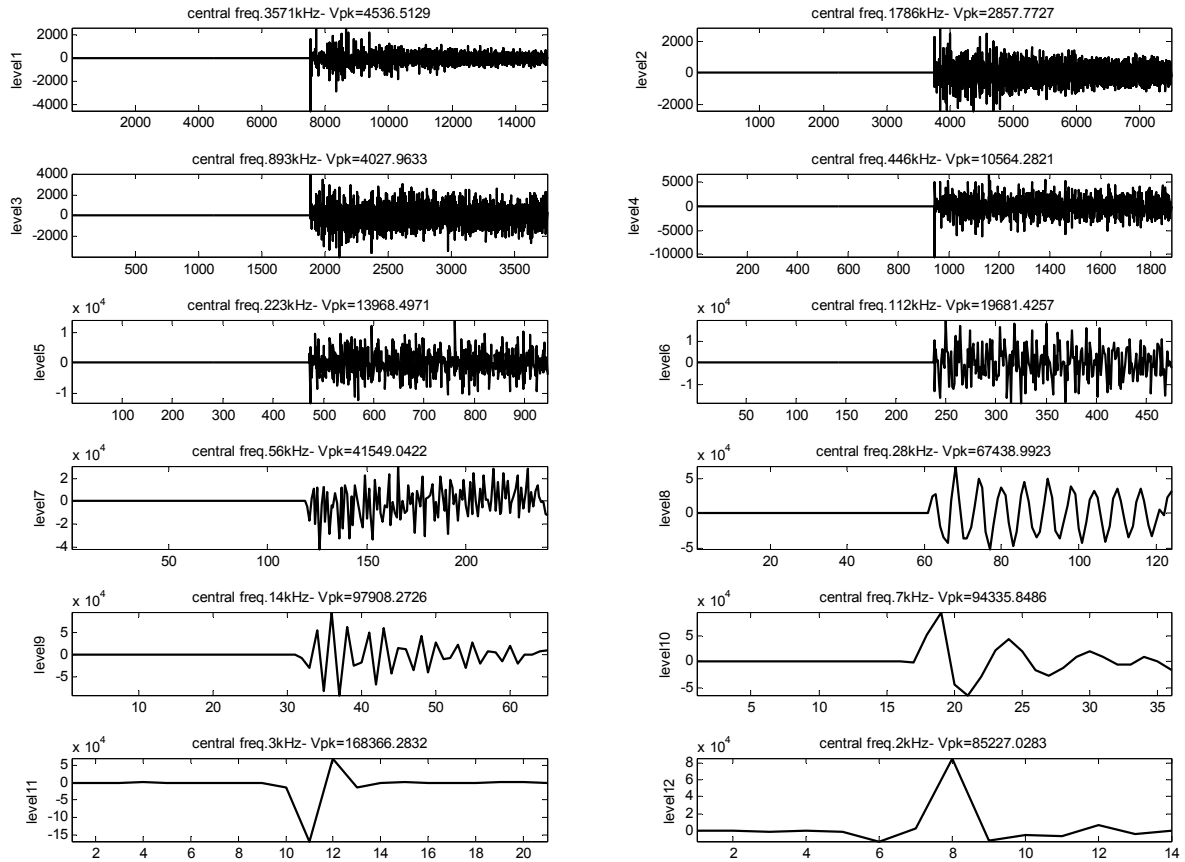


**Figure 4-21** Phase-to-ground fault in the line  $L_4$ : details coefficients obtained by processing the voltage signal measured in  $S_3$

## References

- [1] IEEE Distribution planning WG report, "Radial distribution test feeders", *IEEE Trans. on Power Systems*, vol.6, n.3, pp. 975-985, August 1991;
- [2] IEC 60050-161 "International Electrotechnical Vocabulary – Electromagnetic Compatibility", International Electrotechnical Commission, Geneva, Switzerland, 1997;
- [3] J. Mahseredjian, L. Dubé, L. Gérin-Lajoie, "New advances in the Simulation of Transients with EMTP: Computation and Visualization Techniques", *Electrimacs*, 19 August 2002;
- [4] A. Borghetti, S. Corsi, C.A. Nucci, M. Paolone, L. Peretto, R. Tinarelli, "On the use of continuous-wavelet transform for fault location in distribution power networks", *International Journal of Electrical Power & Energy Systems*, vol. 28, n. 9, November 2006, pp. 608-617;
- [5] Nakada K.; Yokota T.; Yokoyama S.; Asakawa A.; Nakamura M.; Taniguchi H.; Hashimoto A., "Energy Absorption of Surge Arresters on Power Distribution Lines due to direct lightning strokes effects of an overhead ground wire and installation position of surge arresters", *IEEE Trans. On Power Delivery*, Vol. 12, No. 4, October 1997, pages 1779 – 1785;
- [6] EN 61000-2-4 "Electromagnetic Compatibility (EMC) Part 2-4: Environment – Compatibility levels in industrial plants for low-frequency conducted disturbances", CENELEC, Bruxelles, Belgium, 2002.

## **5. The distributed measurement system for transients detection**

The measurement techniques of the main indexes of PQ have been the subject of specific standard definitions in order to let experimental results of different measurement campaigns be comparable. Thanks to the new hardware and software technologies, the instrumentation is more and more efficient, as well as less easy for the operator to use and to interpret the result goodness. A single instrument can be set to measure different type of disturbance just by changing the elaboration algorithm of the input data.

The issue is not finding the right instrument, usually available for each application, but the best device for conditioning the input signals. In fact transducers have to transfer voltage and/or current to the measurement instrumentation without modifying the main characteristics of their frequency spectrum.

Usual commercial instrumentation is multi-purpose, for example display in real time the frequency spectrum of the input under the hypothesis of periodic signals; give statistical parameters regarding transient disturbances; can log data for limited time intervals. The most significant bandwidth of the signal to be transduced can be in the order of some kilohertz as well as hundred of kilohertz according to the phenomena to be monitored.

The dynamic range of the input signals can be order of magnitude greater than the electronic equipment aimed at elaborating them, hence the adequate isolation level has to be granted by the transducer interposed between the two blocks. The traditional TA and TV (i.e. current and voltage transformers) feature a too low frequency bandwidth. In this context nowadays electronic devices, such as Hall-effect probe and Rogowski coil, are substituting passive transducers.

When Digital Signal Processing (DSP) is involved, a basic aspect is the choice of the sampling technique according to the measurement conditions. The sampling frequency has to be chosen in a range that avoids aliasing error, i.e. the birth of fake low frequency components due to a too low sampling frequency respect to the input spectrum. The time interval for the acquisition of the signal has to be extended in function of the desired frequency resolution: high resolution in the signal spectrum requires a long time window, but such a condition is achieved only in case of stable signals. The choice of the measurement strategy is not so easy and experience is needed, even because commercial instrumentation is characterized by the manufacturer without declaring all the operating conditions.

The measurement system designed to monitor the voltage quality of a distribution power system and to implement the method for the location of the transient source described in

chapter 3 is a distributed measurement system. The architecture chosen for the application is master – slave, where a set of slave stations are installed in the network nodes and are aimed at registering data at the occurrence of a transient event and send them to the master unit via GPRS. In practice the communication net let each slave station send data in real-time to the master unit in case of anomalous working conditions of the power system, but also the master unit send information to any slave for diagnosis purposes or check up of the hardware.

Every slave unit is a stand-alone device, in the sense that a microprocessor is programmed to control the system settings, the acquisition of data and the communication with the master. Let's recall the block diagram of a remote unit (slave), reported in Figure 5-1. It both acquires the starting instant and the waveform of a transient. The former information is then sent to the master unit which locates the source of the transient by processing the data received from all the slaves. The dashed box in Figure 5-1 contains the blocks performing the measurement of the transient starting instant. Only by way of example let us consider the problem of locating the source of a transient voltage. The voltage  $u(t)$  at the monitored point is conditioned by a Voltage-to-Voltage Transducer (VVT), whose output  $u_{VVT}$  feeds an Event Detection Block (EDB). The EDB output  $u_{out}$  is a logic signal that, as a transient occurs, triggers both a Data Acquisition board (DAQ) and a GPS-based device, which provides the relevant "time stamp". The time stamp is determined with an uncertainty that propagates through the algorithm which the proposed measurement procedure relies on, and affects the estimate of the transient source location.

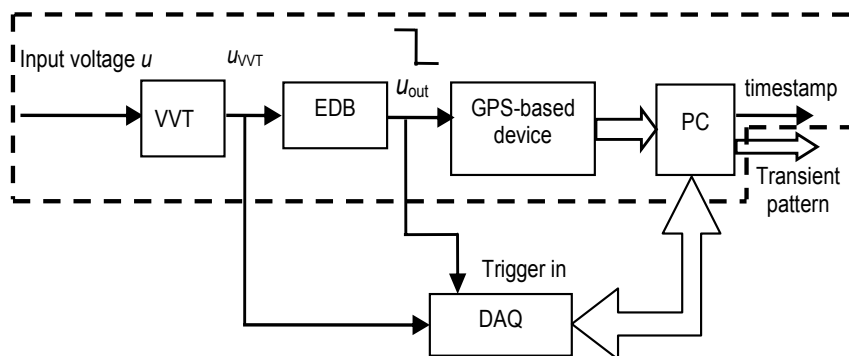


**Figure 5-1.** Block diagram of a remote unit (slave).

In a quite similar way the measurement system can also locate the source of transient currents. In such a case the output of a suitable current-to-voltage transducer in place of  $u_{VVT}$  has to be considered.

In the following the blocks of one measurement channel are considered one by one and described.

### 5.1. *The voltage transducer*

The voltage to voltage transducer chosen for the system is a capacitive voltage divider made by Pearson Electronics, the model VD305A (see Figure 5-2). The reason why such a device has been chosen for power quality measurement in distribution networks are: large bandwidth, high accuracy and linear input-output characteristic for a wide range of input voltages, low delay on the output signal respect to the input one, immunity to electromagnetic disturbances. Such a performance let the transient disturbance affecting the high voltage signal be correctly transduced on the low voltage side, feeding both the Event Detection Block and the DAQ board. It is not hard to understand that the characteristics of the conditioning block are of primary importance in the design of the measurement chain.

The Model VD-305A capacitive voltage divider is intended for the measurement of voltage amplitude and wave-shape of ac signals at high potential [1]. It has a nominal division ratio of 5000:1, and the exact measured ratio is printed on the name-plate. This ratio is measured in insulating oil at 35°C, and is accurate to  $\pm 5\%$ . The division ratio is temperature compensated to  $\pm 1\%$  over the range of 20° to 80°C. The unit consists of two capacitors connected in series. The high voltage center electrode forms a capacitor with a guarded pickup ring located in the lower metal cylinder. This pickup ring is connected to the center conductor of the output connector via a 50 Ohm resistor. The low-voltage capacitor connects the pickup ring to the outer conductor of the connector. The output voltage is thus a fraction of the input voltage determined by the ratio of the capacitances. The standard calibration is for use in oil, which has a dielectric constant of about 2.3. If the unit is used in air, its division ratio will be approximately 11500:1, but if this is the intended use, a factory calibration of 5000:1 in air would be more accurate and desirable. The maximum pulse voltage rating for use in air is 50 kV. These ratings are for pulses up to 5  $\mu$ s duration.



Maximum Pulse Voltage, in oil	300 kilovolt
Maximum Pulse Voltage, in air	50 kilovolt
Voltage Division Ratio, in oil	5000:1
Frequency Range, into 1M $\Omega$ load	30 Hz to 4 MHz
Droop Rate, into 1 M $\Omega$ load	0.02 % / $\mu$ second
Usable Rise-time	100 nanosecond
Capacitance added to circuit	18 pF (approximate)

**Figure 5-2.** The capacitive voltage divider.

## 5.2. The event detection block

The Event Detection Block is an analog circuit based upon two comparators. In order to detect in real time any transient distortion affecting a signal, both impulsive or oscillatory, the input  $u_{in}$  is compared to the signal obtained by filtering  $u_{in}$  itself and by superposing to the filtered signal  $u_f$  a bias. The block diagram of the EDB is shown in Figure 5-3. the offset component summed to  $u_f$  is positive in one case and negative in the other case, leading to  $u_f^+$  and  $u_f^-$  respectively. In practice the pattern of the original signal  $u_{in}$  is instantaneously included within a couple of signals that represent a double threshold for its high frequency content. The signals at the input and output of the two comparators are represented in Figure 5-4.

Comparator #1 changes the level of its output  $u_{out}^+$  when a surge starting with a rising front affects the input voltage, whereas comparator #2 turns its level down when the transient presents a falling front. An And-gate is used to make the logic signal at the EDB output change its level for any commutation of  $u_{out}^+$  and  $u_{out}^-$ , i.e. in correspondence of the first peak of the disturbance, independently of its derivative sign. Since the transients are most of the times of the oscillatory type, it is easy to understand that such an operating principle would lead to pulse sequences on  $u_{out}$  because it would commute in correspondence of every oscillation of the disturbance. By considering the entire measurement chain of a channel, this behaviour would correspond to give a repetitive trigger to the DAQ board and the GPS station, as if more than one event occurred at once. Moreover, the devices are busy for a time interval much longer respect to the period of oscillations, time needed to acquire, convert and save the waveform and the timestamp, but also the PC takes time to save the data in its memory support, compress and send them to the master via GPRS.

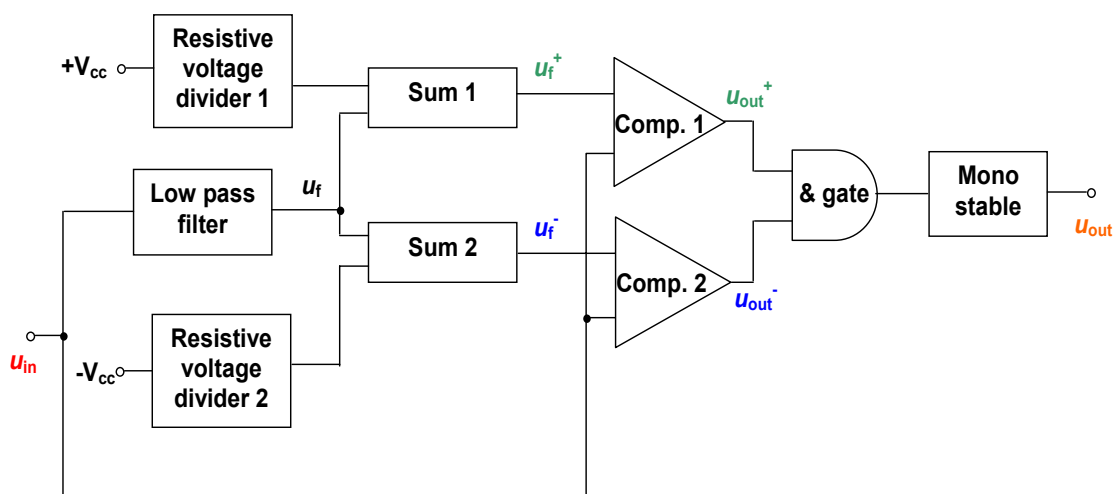
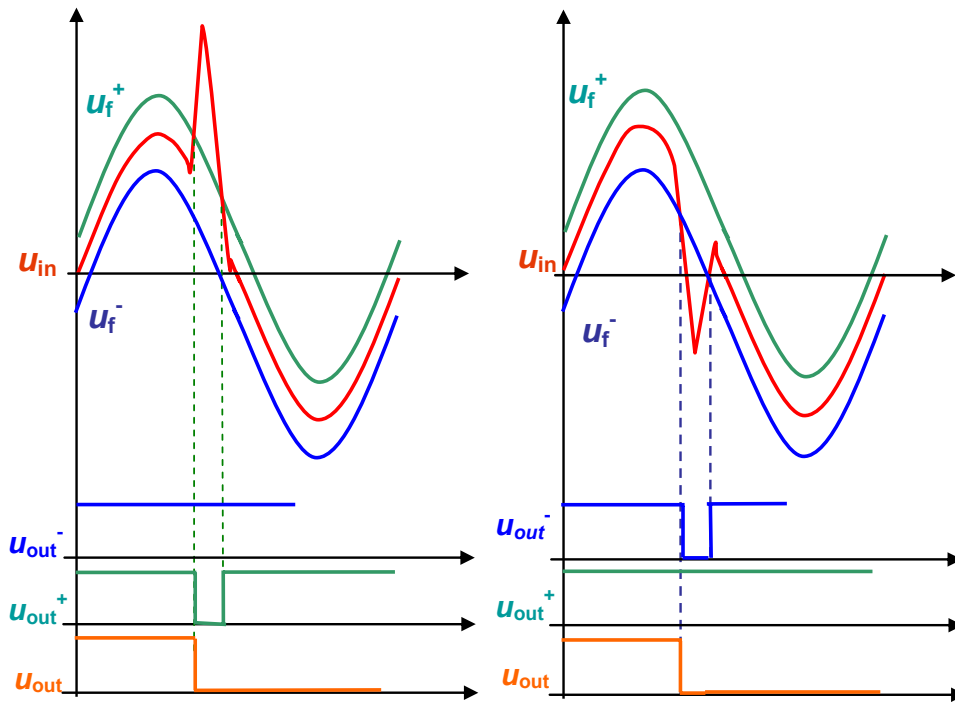


Figure 5-3. Block diagram of the analog circuit of the EDB.



**Figure 5-4.** Signals on the EDB circuit at the occurrence of a positive or negative surge on  $u_{in}$ .

On the basis of these considerations, the EDB is blinded for a time interval corresponding to 1,5 s after each detection of an event. To this purpose, a monostable multivibrator is connected at the output of the And gate. Finally,  $u_{out}$  commutes to low level synchronously with the first commutation of one of the two comparators and keeps that value for 1,5 s. In this way the electronic equipment is triggered once by  $u_{out}$  and can carry out the acquisition process.

A basic step in the design of the circuit is the choice of the cut-off frequency of the low-pass filter. This frequency has to be much greater than the maximum harmonic component that can affect the power system voltage, but at the same time lower than the typical spectrum associated to transient disturbances. In this way the logic signal  $u_{out}$  triggers the GPS and DAQ board only in case of non periodic disturbances, and detects any type of transient. Under such operating conditions the cut-off frequency should be just a few greater than 2 kHz, i.e. the value corresponding to the 40<sup>th</sup> harmonic order of the 50 Hz component, so that even the slowest transients are taken into account by the slave.

By considering the signals  $u_f^+$  and  $u_f^-$  compared to  $u_{in}$ , the positive and negative bias superposed to each of them to shift signals along the vertical axis can be seen as the real threshold of the EDB. Setting the magnitude of such biases turns into setting the sensitivity of the detector; the ideal configuration of the circuit would be making the EDB more sensible as possible, decreasing the bias till a value near zero; in real applications it is not possible to reach such performance of the transient detector, because the input signal in steady state is not a perfectly clean sinusoidal waveform. Hence, in order to

avoid fake detections and acquisitions of the measurement system, the threshold has to be greater than the maximum peak that can be seen in the white noise affecting the network voltages. By considering the definition of noise according to the standards and at the same time voltage waveforms acquired during similar measurement campaigns carried out on distribution networks, the noise reveals to be in the order of 1% of the magnitude of the fundamental component, and its frequency content is lower than 300 kHz. The bias in the EDB has been set equal to 2% of  $u_{in}$  amplitude; it should be noted that the frequency spectrum of the noise covers all the frequency range in which EM transients can be found, so finally it can be said that the presence of noise leads to worse performance of the measurement system by putting a higher boundary for its sensitivity.

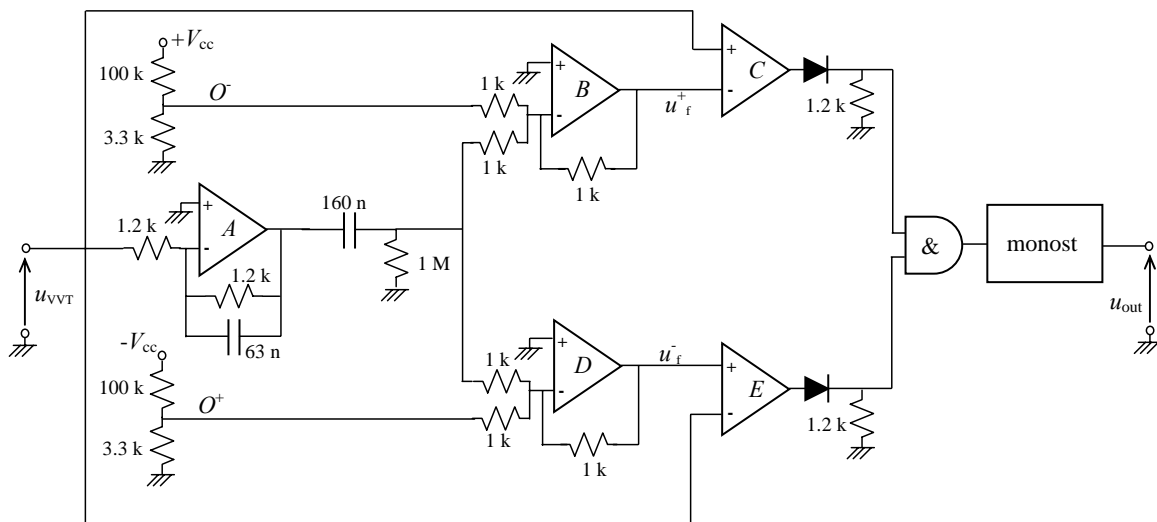


**Figure 5-5.** Scheme of the Event Detection Block.

The entire procedure above described and implemented in the analog circuit of the block works correctly and makes sense only if the signals  $u_f$  compared to  $u_{in}$  are always in phase with it. This is a crucial aspect of the practical realization of the device, in fact the cut-off frequency adopted for the low-pass filter is not so high respect to the fundamental component of the input, hence the output of the filter is affected by a not negligible phase delay. As explained in section 3.5, the input signal  $u_{in}$  has to be compared to a signal reproducing only its low frequency content, eliminating as much as possible the transient disturbance superposed to it. If this condition is not respected, the detection of the beginning of the transient is affected by an error that leads to wrong results when the fault location algorithm is applied. Finally, the cut-off frequency of the low-pass filter cannot be incremented to reduce the phase-shift affecting the 50 Hz component, because the efficiency of the filter itself would be strongly compromised. To bring back to zero the delay between input and output a different solution has been then adopted: a high-pass



filter in cascade with the low-pass one has been added, having its same order. The cut-off frequency of the high-pass filter, much lower than 50 Hz, is chosen so that the phase of the global output  $u_f$  is null referred to  $u_{in}$ .

The diodes inserted at the output of each comparator are used to limit the dynamic of the logic signal. In fact the comparator commutes from +5 V to -5 V whereas the TTL compatible signal that has to be sent to the sequent devices as external trigger has to change level from +5 V to 0 V in negative logic.

### **5.3. The GPS-based device**

#### **5.3.1. What is GPS?**

The first satellite of the GPS was launched into orbit in 1977. The aim of the GPS was to replace the old, inaccurate, and inconvenient system of satellite navigation called transit, put into operation in 1959 to control Polaris rockets. In March 1994 the U.S. Department of Defense announced a preliminary permission to use the GPS and it was declared fully operational on July 1995 [2].

The GPS constellation consists of 24 solar-powered satellites that orbit the earth in 12 hours. They are equally spaced on six circular orbits, 60° apart, about 20,183 km above the earth's surface. The orbits are inclined at about 55° respect to the equatorial plane. This constellation allows concurrent communication with at least four satellites at any one-time, enabling to assess the coordinates (latitude and longitude for sea vessels and land vehicles) or three coordinates (additionally altitude for aircrafts). In this way also the accuracy of the estimation is allowed.

In practice, GPS receivers located between 80° N and 80° S not occluded by cliffs, mountains, skyscrapers, etc. can simultaneously receive signals from five to nine satellites. The signal transmitted by satellites comprises its identification code, a GS time stamp and location information, such as location of other satellites. The receiver analyzes the data and rejects records from satellites that are less than 10 to 15° above the horizon and then uses the transmission from the satellites in the optimal geometric configuration to calculate the maximum positioning accuracy. The receiver then displays the result as geographical coordinates.

The geographical position calculation is based on the precise measurement of a distance between a GPS receiver and the satellites. The locations of the satellites are constantly tracked by ground stations and are known exactly at all times. The distance measurement is based upon the accurate measurement of intervals between signal transmission from a satellite and its receipt by a receiver, which is installed, for example, on a ship or a car whose position is being computed. Each satellite of the system is

equipped with four atomic clocks which automatically correct the quartz clock of the GPS receivers

Until May 2000, two GPS positioning services of different precision were available. The more accurate one, called Precise Positioning Service, was based on an encrypted signal called P-Code transmitted at a carrier frequency of 1227,60 MHz. the position estimation error was not greater than 18 m horizontally and 23 m vertically. PPS was available only for the U.S. military. The less precise service, called Standard Positioning Service (SPS), was available for all civil users worldwide without charge or restrictions. A coarse acquisition code was transmitted from a satellite at 1575,42 MHz. the accuracy of the SPS was intentionally degraded by the U.S. Department of Defense. An abundance of error estimation methods for satellite navigation systems in general makes their comparison and evaluation difficult. Some sources cite root-mean-squared error of consecutive measured positions; others rely on selective measurements in a given period. Above all, this error is often calculated with a different confidence level, it may refer to the real receiver's position (from a chart) or to the average position of all the conducted measurements. The error values are given as inaccuracy in latitude and longitude or as a distance between real and determined position. According to the U.S. Department of Defense, the SPS horizontal accuracy is  $\pm 100$  m at 99.5% confidence level and  $\pm 300$  m at 99.9%. the main component of GPS positioning inaccuracy results from time and space varying conditions of radio wave propagation, which both depend on atmospheric, disturbances in the satellites, orbit stability, and so on. The error due to the transmitter and receiver operation precision or time measurement accuracy is negligible.

A method for GPS precision enhancement commonly used by civil users is the Differential Global Positioning System. It is based on additional GPS measurements of a precise position from a nearby correcting station. The error, which is characteristic for a large region around the station, is radio transmitted and taken into account by the DGPS receivers as a position correction.

### **5.3.2. The GPS station**

The operation of the device relies on a programmable GPS 168 PCI card by Meinberg. The station is made of two devices: the GPS antenna (see Figure 5-6) and a PCI board (see Figure 5-7) linked by a BNC cable. In the rear panel of the board, a part from the BNC connector, two led and a DB9 connector are found. The red led turns on every time the board is started and turns off only at the end of the synchronization process carried out by the receiver, whereas the green led turns on when the position of the receiver is computed.



**Figure 5-6.** The antenna of the GPS station.      **Figure 5-7.** The PCI board of the GPS system.

The DB9 connector, whose pins are reported in Table 5-1, cannot be connected to a serial port of the PC because in this case the voltage level is  $\pm 12$  V, whereas the radio clock for example operates with a TTL logic (0 – 5 V). the DB9 connector is useful to let input and output of the station be available for the operator.

**Table 5-1.** GPS DB9 connector.

Pin	Signal	Dil2
1	+5V	1
2	RxD	-
3	TxD	-
4	P_MIN	5
4	10MHz	10
5	GND	-
6	CAP0	2
7	CAP1	3
8	P_SEC	4
9	DCF_OUT	6

By using the corresponding DIL switch, some input (such as User Capture 0 and 1) and output (such as Pulse per Second/Minute) of the PCI board can be activated. The signals without a DIL switch are always available. In the case of interest, the two Time Capture Input and the Pulse per Second output have been turned on. The first ones are aimed at detecting events; in doing this the time resolution of the GPS is 100 ns. The event is detected according to the TTL logic by the User Capture in its falling front and then saved in a buffer. Once it has been saved, the event data can be sent via the Com Port of the GPS or read by the PCI bus in order to be reported in the monitoring software. Meinberg

Radio Clock is the name of the program given by the manufacturer for monitoring and diagnostic of the GPS unit.

For the application in the distributed measurement system, in order to have a complete list of all the times when an event occurred, the relevant data have been saved in a text file by using Hyper terminal of Windows.

The data are transmitted through a GPS COM Port with a FIFO strategy immediately after the event occurrence, thus there is no risk of saturation for the memory buffer of the unit. It should be noted that the GPS station cannot detect two consecutive events separated by less than 1.5 ms of delay; in this case a warning message is displayed in the software interface: 'capture overrun'. The Pulse per Second, reported in Figure 5-8, is a signal with 1s period. The high level (5 V) last 200 ms, then the low level (0 V) last the remaining 800 ms; the signal features its best accuracy,  $\pm 250$  us, after the synchronization and 20 minutes of continuative working. In the first experimental phase for the development of the measurement chain this logic signal played a main role as time reference for the calibration procedures.

Hyper Terminal of Windows is a software that lets data be acquired through the Serial Port of a PC, so a particular connector has been realized to link the GPS Com Port to the RS-232 Port of the PC. In order to let Hyper Terminal acquire data, a session configured in the following way must be started: i) data transmission speed = 19200 bps; ii) bit number per single data = 8; stop bit = 1; flux control = none. Coherent configuration has to be set in the GPS Com Port.

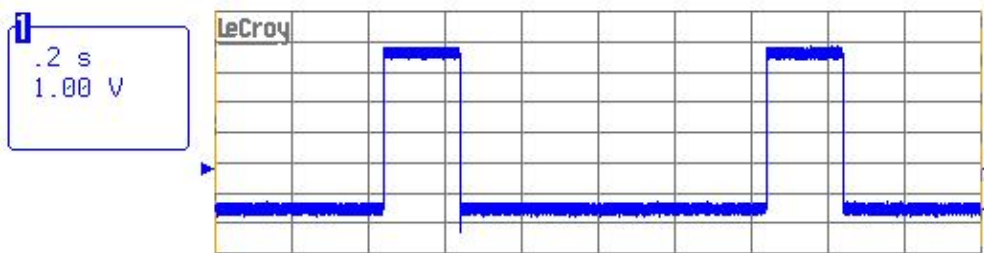


**Figure 5-8.** The Pulse per Second signal acquired by the DSO.

Meinberg Radio Clock Monitor is an application that let the operator check the status of the reference clock, i.e. the time reference of the PC and the time adjustment service. The latter one gives information about the correction factor applied to the PC time reference to synchronize it with the radio Clock.

#### **5.4. The DAQ Board**

The waveshape of each transient disturbance affecting the voltage signal is saved into a file by an acquisition and digital conversion board. The model chosen for the purpose is

the ADC-212/100 by Picotech (see Figure 5-9). Two different software can be installed on the PC in order to control and communicate with the DAQ board:

Picoscope, which enables the desktop PC to work as a Digital Storage Oscilloscope high-end, a spectrum analyzer and a multimeter; PicoLog Player, which allows to use the DAQ board as a device to acquire data in a fast way. The main specifications of the device are reported in Table 5-2. the DAQ board can be connected to the PC through the parallel port or by using an adaptor Pico/USB port.

**Table 5-2.** Picotech ADC-212/100 data sheet.

<b>Channels</b>	2 BNC + 1 external trigger
<b>Frequency bandwidth</b>	50 MHz
<b>Sampling Frequency (single channel)</b>	100 MS/s
<b>Sampling Frequency (dual channel)</b>	50 MS/s
<b>Sampling Rate (repetitive signals)</b>	5 GS/s
<b>Resolution</b>	12 bit
<b>Buffer Size</b>	128 K
<b>Dynamic range</b>	80 dB
<b>Scope timebase</b>	100ns/div to 50s/div
<b>Spectrum range</b>	0 to 50 MHz
<b>Trigger Modes</b>	Free run, Auto, Repeat, Single
<b>Pre/post trigger</b>	±100%
<b>Voltage range</b>	± 50mV to ±20V in nine steps
<b>Overload protection</b>	±100 V
<b>Input Impedance</b>	1 MΩ
<b>Coupling</b>	AC, DC
<b>Accuracy</b>	±1%
<b>Power supply</b>	500 mA @ 12 V (main adaptor supplied)
<b>Output connector</b>	D25 to PC parallel port (cable supplied)
<b>Dimensions</b>	(140 x 190 x 45) mm

The configuration and control of the board can be carried out by using the dedicated software provided by the manufacturer as well as programs developed in LabView environment.



**Figure 5-9.** Acquisition and Analog to Digital conversion board.

### **5.5. The GSM protocol**

Global System for Mobile communications (GSM: originally from Groupe Spécial Mobile) is the most popular standard for mobile phones in the world. Its promoter, the GSM Association, estimates that 82% of the global mobile market uses the standard. GSM is used by over 2 billion people across more than 212 countries and territories. GSM differs from its predecessors in that both signalling and speech channels are digital call quality, and so is considered a second generation mobile phone system. This has also meant that data communication were built into the system using the 3rd Generation Partnership Project [18].

The ubiquity of the GSM standard has been advantageous to both consumers and also to network operators, who can choose equipment from any of the many vendors implementing GSM. GSM also pioneered a low-cost alternative to voice calls, the Short message service (SMS), which is now supported on other mobile standards as well. Newer versions of the standard were backward-compatible with the original GSM phones. For example, Release '97 of the standard added packet data capabilities, by means of General Packet Radio Service (GPRS). Release '99 introduced higher speed data transmission using Enhanced Data Rates for GSM Evolution (EDGE).

GSM is a cellular network, which means that mobile phones connect to it by searching for cells in the immediate vicinity. GSM networks operate in four different frequency ranges. Most GSM networks operate in the 900 MHz or 1800 MHz bands. Some countries in the Americas (including Canada and the United States) use the 850 MHz and 1900 MHz bands because the 900 and 1800 MHz frequency bands were already allocated. The rarer 400 and 450 MHz frequency bands are assigned in some countries, notably Scandinavia, where these frequencies were previously used for first-generation systems.

In the 900 MHz band the uplink frequency band is 890–915 MHz, and the downlink frequency band is 935–960 MHz. This 25 MHz bandwidth is subdivided into 124 carrier frequency channels, each spaced 200 kHz apart. Time division multiplexing is used to allow eight full-rate or sixteen half-rate speech channels per radio frequency channel. There are eight radio timeslots (giving eight burst periods) grouped into what is called a TDMA frame. Half rate channels use alternate frames in the same timeslot. The channel data rate is 270.833 kbit/s, and the frame duration is 4.615 ms. The transmission power in the handset is limited to a maximum of 2 watts in GSM850/900 and 1 watt in GSM1800/1900.

GSM has used a variety of voice codecs to squeeze 3.1 kHz audio into 5.6 to 13 kbit/s. Originally, two codecs, named after the types of data channel they were allocated, were used, called Half Rate (5.6 kbit/s) and Full Rate (13 kbit/s). These used a system based upon linear predictive coding. In addition to being efficient with bitrates, these codecs also made it easier to identify more important parts of the audio, allowing the air interface layer to prioritize and better protect these parts of the signal.

GSM was further enhanced in 1997 with the Enhanced Full Rate (EFR) codec, a 12.2 kbit/s codec that uses a full rate channel. Finally, with the development of UMTS, EFR was re-factored into a variable rate codec called AMR-Narrowband, which is high quality and robust against interference when used on full rate channels, and less robust but still relatively high quality when used in good radio conditions on half-rate channels.

There are four different cell sizes in a GSM network—macro, micro, pico and umbrella cells. The coverage area of each cell varies according to the implementation environment. Macro cells can be regarded as cells where the base station antenna is installed on a mast or a building above average roof top level. Micro cells are cells whose antenna height is under average roof top level; they are typically used in urban areas. Picocells are small cells whose coverage diameter is a few dozen meters; they are mainly used indoors. Umbrella cells are used to cover shadowed regions of smaller cells and fill in gaps in coverage between those cells. Cell horizontal radius varies depending on antenna height, antenna gain and propagation conditions from a couple of hundred meters to several tens of kilometers. The longest distance the GSM specification supports in practical use is 35 kilometres. There are also several implementations of the concept of an extended cell, where the cell radius could be double or even more, depending on the antenna system, the type of terrain and the timing advance.

Indoor coverage is also supported by GSM and may be achieved by using an indoor picocell base station, or an indoor repeater with distributed indoor antennas fed through power splitters, to deliver the radio signals from an antenna outdoors to the separate indoor distributed antenna system. These are typically deployed when a lot of call

capacity is needed indoors, for example in shopping centers or airports. However, this is not a prerequisite, since indoor coverage is also provided by in-building penetration of the radio signals from nearby cells.

The modulation used in GSM is Gaussian minimum-shift keying (GMSK), a kind of continuous-phase frequency shift keying. In GMSK, the signal to be modulated onto the carrier is first smoothed with a Gaussian low-pass filter prior to being fed to a frequency modulator, which greatly reduces the interference to neighbour channels (adjacent channel interference).

### **5.5.1. The GPRS protocol**

General Packet Radio Service (GPRS) is a Mobile Data Service available to users of GSM and IS-136 mobile phones. It provides data rates from 56 up to 114 Kbps. GPRS data transfer is typically charged per kilobyte of transferred data, while data communication via traditional circuit switching is billed per minute of connection time, independent of whether the user has actually transferred data or has been in an idle state. GPRS can be used for services such as Wireless Application Protocol (WAP) access, SMS, MMS and for Internet communication services such as email and World Wide Web access.

Such a technology provides moderate speed data transfer, by using unused Time division multiple access (TDMA) channels in, for example, the GSM system. Originally there was some thought to extend GPRS to cover other standards, but instead those networks are being converted to use the GSM standard, so that GSM is the only kind of network where GPRS is in use. GPRS is integrated into GSM Release 97 and newer releases. It was originally standardized by European Telecommunications Standards Institute (ETSI), but now by the 3rd Generation Partnership Project.

The multiple access methods used in GSM with GPRS are based on frequency division duplex and TDMA. During a session, a user is assigned to one pair of up-link and down-link frequency channels. This is combined with time domain statistical multiplexing, i.e. packet mode communication, which makes it possible for several users to share the same frequency channel. The packets have constant length, corresponding to a GSM time slot. The down-link uses first-come first-served packet scheduling.

GPRS originally supported (in theory) Internet Protocol (IP) and Point-to-Point Protocol (PPP). GPRS is new technology which speed is a direct function of the number of TDMA time slots assigned, which is the lesser of what the particular cell supports and the maximum capability of the mobile device expressed as a GPRS Multislot Class. Transfer speed depends also on the channel encoding used. The least robust, but fastest, coding scheme (CS-4) is available near a base transceiver station (BTS), while the most robust



coding scheme (CS-1) is used when the mobile station is further away from a BTS. Using the CS-4 it is possible to achieve a user speed of 20.0 kbit/s per time slot. However, using this scheme the cell coverage is 25% of normal. CS-1 can achieve a user speed of only 8.0 kbit/s per time slot, but has 98% of normal coverage. Newer network equipment can adapt the transfer speed automatically depending on the mobile location. GPRS is packet based. When TCP/IP is used, each phone can have one or more IP addresses allocated. GPRS will store and forward the IP packets to the phone during cell handover (when you move from one cell to another). A radio noise induced pause can be interpreted by TCP as packet loss, and cause a temporary throttling in transmission speed.

### **5.6. Metrologic characterization of the measurement system - The Supplement 1 to the G.U.M.**

The Supplement to the “*Guide to the expression of Uncertainty in Measurement*” (GUM) is concerned with the propagation of probability distributions through a mathematical model of measurement as a basis for the evaluation of uncertainty of measurement, and its implementation by a Monte Carlo method. The treatment applies to a model having any number of input quantities, and a single output quantity.

The described Monte Carlo method is a practical alternative to the GUM uncertainty framework. It has particular value when:

- i) linearization of the model provides an inadequate representation of the measurement process, or
- ii) the probability density function (PDF) for the output quantity departs appreciably from a Gaussian distribution or a scaled and shifted t-distribution, e.g. due to marked asymmetry. In the former case the estimate of the output quantity and the associated standard uncertainty provided by the GUM uncertainty framework might be unreliable.

In case ii), unrealistic coverage intervals (a generalization of “expanded uncertainty” in the GUM uncertainty framework) might be the outcome.

The GUM [3] provides a framework for assessing uncertainty, which is based on the use of the law of propagation of uncertainty and the characterization of the output quantity by a Gaussian distribution or a scaled and shifted t-distribution. Within that framework, the law of propagation of uncertainty provides a means for propagating uncertainties through the model. Specifically, it evaluates the standard uncertainty associated with an estimate of the output quantity, given

- a) best estimates of the input quantities,
- b) the standard uncertainties associated with these estimates, and, where appropriate,
- c) degrees of freedom associated with these standard uncertainties, as well as
- d) any nonzero covariance associated with pairs of these estimates.

Also within the framework, the PDF taken to characterize the output quantity is used to provide a coverage interval, for a stipulated coverage probability, for that quantity.

The best estimates, standard uncertainties, covariances and degrees of freedom summarize the information available concerning the input quantities. With the approach considered in the Supplement 1 [4], the available information is encoded in terms of PDFs for the input quantities. The GUM uncertainty framework does not explicitly refer to the assignment of PDFs to the input quantities. However a Type A standard uncertainty is

obtained from a probability density function derived from an observed frequency distribution, while a Type B standard uncertainty is obtained from an assumed probability density function based on the degree of belief that an event will occur. Both approaches employ recognized interpretations of probability.

The approach operates with the PDFs of the input quantities in order to determine the PDF for the output quantity. Whereas there are some limitations to the GUM uncertainty framework, the propagation of distributions will always provide a PDF for the output quantity that is consistent with the PDFs for the input quantities.

This PDF for the output quantity describes the knowledge of that quantity, based on the knowledge of the input quantities, as described by the PDFs assigned to them. Once the PDF for the output quantity is available, that quantity can be summarized by

- a) its expectation, taken as an estimate of the quantity, and
- b) its standard deviation, taken as the standard uncertainty associated with the estimate. Further, the PDF can be used to obtain
- c) a coverage interval, corresponding to a stipulated coverage probability, for the output quantity.

The PDF for a quantity expresses the state of knowledge about the quantity, i.e. it quantifies the degree of belief about the values that can be assigned to the quantity based on the available information. The information usually consists of raw statistical data, results of measurement or other relevant scientific statements.

The propagation of distributions has wider application than the GUM uncertainty framework. It works with richer information than that conveyed by best estimates and the associated standard uncertainties (and degrees of freedom and covariances when appropriate). Given the model relating the input quantities and the output quantity and the PDFs characterizing the input quantities, there is a unique PDF for the output quantity. Generally, the latter PDF cannot be determined analytically. Therefore, the objective of the approach described in [4] is to determine (a), (b), and (c) above to a prescribed numerical tolerance. The uniqueness of the PDF for the output quantity depends on the model defining the output quantity uniquely in terms of the input quantities. In [4] are not considered models that do not define the output quantity uniquely (for example, involving the solution of a quadratic equation, without specifying which root is to be taken).

### **5.6.1. Main stages of uncertainty evaluation**

The main stages of uncertainty evaluation constitute formulation, propagation, and summarizing:

a) Formulation:

- 1) define the output quantity, the quantity intended to be measured (the measurand);

- 2) determine the input quantities upon which the output quantity depends;
  - 3) develop a model relating the output quantity to these input quantities;
  - 4) on the basis of available knowledge assign PDFs—Gaussian (normal), rectangular (uniform), etc.—to the input quantities. Assign instead a joint PDF to those input quantities that are not independent;
- b) Propagation:  
propagate the PDFs for the input quantities through the model to obtain the PDF for the output quantity;
- c) Summarizing: use the PDF for the output quantity to obtain
- 1) the expectation of that quantity, taken as an estimate of the quantity,
  - 2) the standard deviation of that quantity, taken as the standard uncertainty associated with the estimate [3],
  - 3) a coverage interval containing the output quantity with a specified probability (the coverage probability).

### 5.6.2. Propagation of distributions

When  $Y$  is the result of an indirect measurement, i.e. it is obtained as a function of  $N$  direct measurements  $X_1, X_2, \dots, X_N$ , a formal definition for the PDF for  $Y$  is:

$$g_Y(\eta) = \int_{-\infty}^{\infty} \dots \int_{-\infty}^{\infty} g_X(\xi) \delta(\eta - f(\xi)) d\xi_N \dots d\xi_1 \quad (5.1)$$

where  $\delta(\cdot)$  denotes the Dirac delta function. The multiple integral (5.1) cannot generally be evaluated analytically. A numerical integration rule can be applied to provide an approximation to  $g_Y(\eta)$ , but this is not an efficient approach.

In [4] a generally efficient approach for determining (a numerical approximation to) the distribution function  $G_Y(\eta) = \int_{-\infty}^{\eta} g_Y(z) dz$  for  $Y$  is considered. It is based on applying a Monte Carlo method (MCM) as an implementation of the propagation of distributions. An estimate of  $Y$  is the expectation  $E(Y)$ . The standard uncertainty associated with this estimate is given by the standard deviation of  $Y$ , the positive square root of the variance  $V(Y)$  of  $Y$ . A coverage interval for  $Y$  can be determined from  $G_Y(\eta)$ . Let denote any numerical value between zero and  $(1-p)$ , where  $p$  is the required coverage probability. The endpoints of a  $100p\%$  coverage interval for  $Y$  are  $G_Y^{-1}(\alpha)$  and  $G_Y^{-1}(p + \alpha)$  i.e. the  $\alpha$ - and  $(p+\alpha)$ - quantiles of  $G_Y(\eta)$ .

The choice  $\alpha=(1-p)/2$  gives the coverage interval defined by the  $(1-p)/2$ - and  $(1+p)/2$ -quantiles, providing a probabilistically symmetric  $100p\%$  coverage interval. A numerical value of  $\alpha$  different from  $(1-p)/2$  may be more appropriate if the PDF is asymmetric. The shortest  $100p\%$  coverage interval can be used in this case. It has the property that, for a

unimodal (singlepeaked) PDF, it contains the mode, the most probable value of  $Y$ . It is given by the numerical value of  $\alpha$  such that  $G_Y^{-1}(p + \alpha) - G_Y^{-1}(\alpha)$  is a minimum.

The probabilistically symmetric  $100p\%$  coverage interval and the shortest  $100p\%$  coverage interval are identical for a symmetric PDF, such as the Gaussian and scaled and shifted t-distribution used within the GUM uncertainty framework [3]. Therefore, in comparing the GUM uncertainty framework with other approaches, either of these intervals can be used.

The propagation of distributions can be implemented in several ways:

- a) analytical methods, providing a mathematical representation of the PDF for  $Y$ ;
- b) uncertainty propagation based on replacing the model by a first-order Taylor series approximation — the law of propagation of uncertainty;
- c) as b), except that contributions derived from higher-order terms in the Taylor series approximation are included;
- d) numerical methods that implement the propagation of distributions, specifically using MCM.

Analytical methods are ideal in that they do not introduce any approximation. They are applicable in simple cases only, however. MCM as considered here is regarded as a means for providing a numerical representation of the distribution for the output quantity, rather than a simulation method per se. In the context of the propagation stage of uncertainty evaluation, the problem to be solved is deterministic, there being no random physical process to be simulated.

Approaches to uncertainty evaluation other than the GUM uncertainty framework are permitted by the GUM. The approach advocated in [4], based on the propagation of distributions, is general. For linear or linearized models and input quantities for which the PDFs are Gaussian, the approach yields results consistent with the GUM uncertainty framework. However, in cases where the conditions for the GUM uncertainty framework to be applied do not hold, the approach of this Supplement can generally be expected to lead to a valid uncertainty statement.

The conditions necessary for the GUM uncertainty framework to give valid results hold, then that approach can be used. If there are indications that the GUM uncertainty framework is likely to be invalid, then another approach should be employed. A third situation can arise in which it is difficult to assess whether or not the GUM uncertainty framework will be valid. In all three cases, MCM provides a practical (alternative) method. In the first case, MCM may sometimes be easier to apply due to difficulties in calculating sensitivity coefficients, for example. In the second, MCM can generally be expected to give valid results, since it does not make approximating assumptions. In the third, MCM

can be applied either to determine the results directly or to assess the quality of those provided by the GUM uncertainty framework.

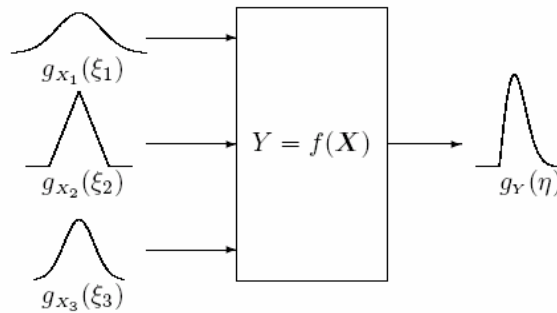


**Figure 5-10.** Illustration of the propagation of distributions for  $N=3$  independent input quantities. The propagation of the PDFs  $g_{X_i}(\xi_i)$ ,  $i=1, \dots, N$ , for the input quantities  $X_i$  through the model to provide the PDF  $g_Y(\eta)$  for the output quantity  $Y$  is illustrated in Figure 5-10 for  $N = 3$  independent  $X_i$ . The  $g_{X_i}(\xi_i)$ ,  $i = 1, 2, 3$ , are Gaussian, triangular, and Gaussian, respectively.  $g_Y(\eta)$  is indicated as being asymmetric, as generally arises for non-linear models or asymmetric  $g_{X_i}(\xi_i)$ .

### 5.6.3. Monte Carlo approach to the propagation

MCM provides a general approach to obtain an approximate numerical representation  $G$  of the distribution function  $G_Y(\eta)$  for  $Y$ . The heart of the approach is repeated sampling of the PDFs for the  $X_i$  and the evaluation of the model in each case. Since  $G_Y(\eta)$  encodes all the information known about  $Y$ , any property of  $Y$  such as expectation, variance and coverage intervals can be approximated using  $G$ . The quality of these calculated results improves as the number of times the PDFs are sampled increases. Expectations and variances (and higher moments) can be determined directly from the set of model values obtained. The determination of coverage intervals requires these model values to be ordered.

If  $y_r$ ,  $r = 1, \dots, M$ , represent  $M$  model values sampled independently from a probability distribution for  $Y$ , then the expectation  $E(Y)$  and variance  $V(Y)$  can be approximated using the  $y_r$ . In general, the moments of  $Y$  (including  $E(Y)$  and  $V(Y)$ ) are approximated by those of the sampled model values. Let  $M_{y_0}$  denote the number of  $y_r$  that are no greater than  $y_0$ , any prescribed number. The probability  $P_r(Y < y_0)$  is approximated by  $M_{y_0}/M$ . In this way, the  $y_r$  provide a step function (histogram-like) approximation to the distribution function  $G_Y(\eta)$ .

Each  $y_r$  is obtained by sampling at random from each of the PDFs for the  $X_i$  and evaluating the model at the sampled values so obtained.  $G$ , the primary output from MCM, constitutes the  $y_r$  arranged in monotonically increasing order.

MCM as an implementation of the propagation of distributions is shown diagrammatically in Figure 5-11 for  $M$  provided in advance. MCM can be stated as a step-by-step procedure:

- a) select the number  $M$  of Monte Carlo trials to be made;
- b) generate  $M$  vectors, by sampling from the assigned PDFs, as realizations of the set of  $N$  input quantities  $X_i$ ;
- c) for each such vector, form the corresponding model value of  $Y$ , yielding  $M$  model values;
- d) sort these  $M$  model values into non-decreasing order, using the sorted model values to provide  $G$ ;
- e) use  $G$  to form an estimate  $y$  of  $Y$  and the standard uncertainty  $u(y)$  associated with  $y$ ;
- f) use  $G$  to form an appropriate coverage interval for  $Y$ , for a stipulated coverage probability  $p$ .

Mathematically, the average of the  $M$  model values is a realization of a random variable with expectation  $E(Y)$  and variance  $V(Y)/M$ . Thus, the closeness of agreement between this average and  $E(Y)$  can be expected to be proportional to  $M^{-1/2}$ .

Step e) can equally be carried out by using the  $M$  model values of  $Y$  unsorted. It is necessary to sort these model values if the coverage interval in step f) is required.

The effectiveness of MCM to determine  $y$ ,  $u(y)$  and a coverage interval for  $Y$  depends on the use of an adequately large value of  $M$  (step a). The propagation of distributions implemented using MCM can validly be applied, and the required summary information subsequently determined, in terms of the information provided in [4], under the following conditions:

- ✓  $f$  is continuous with respect to the elements  $X_i$  of  $X$  in the neighbourhood of the best estimates  $x_i$  of the  $X_i$ ; no condition on the derivatives of  $f$  is required;
- ✓ the distribution function for  $Y$  is continuous and strictly increasing.

These two conditions are necessary to ensure that the inverse of the distribution function is unique and hence coverage intervals can be determined. Only the first condition is needed if a coverage interval is not required.

- ✓ the PDF for  $Y$  is continuous over the interval for which this PDF is strictly positive, unimodal (single-peaked), strictly increasing (or zero) to the left of the mode and strictly decreasing (or zero) to the right of the mode.

Such condition is necessary to ensure that the shortest coverage interval corresponding to a stipulated coverage probability is unique. The mode may occur at an endpoint of the interval over which this PDF is strictly positive, in which case one of the two above conditions is vacuous.

- ✓  $E(Y)$  and  $V(Y)$  exist; this condition is needed for convergence of MCM as the number  $M$  of trials increases.
- ✓ a sufficiently large value of  $M$  is used.

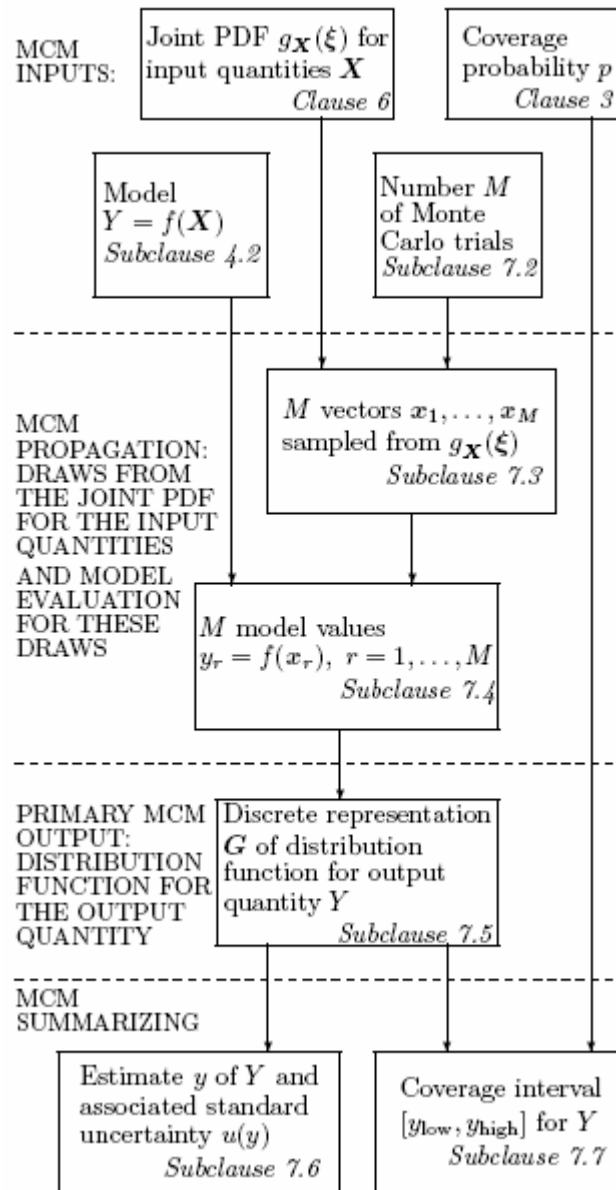


**Figure 5-11.** The propagation and summarizing stages of uncertainty evaluation using MCM to implement the propagation of distributions.

When using the principle of maximum entropy, introduced by Jaynes [5], a unique PDF is selected among all possible PDFs having specified properties, e.g. specified central moments of different orders or specified intervals for which the PDF is non-zero. This method is particularly useful for assigning PDFs to quantities for which a series of indications is not available or to quantities that have not explicitly been measured at all. In applying the principle of maximum entropy, to obtain a PDF  $g_{\mathbf{X}}(\xi)$  that adequately characterizes incomplete knowledge about a quantity  $\mathbf{X}$  according to the information



available, the functional  $S[g] = -\int g_X(\xi) \ln g_X(\xi) d\xi$ , i.e. the “*information entropy*”, is maximized under constraints given by the information.

If the only available information regarding a quantity  $X$  is a lower limit  $a$  and an upper limit  $b$  with  $a < b$ , then, according to the principle of maximum entropy, a rectangular distribution  $R(a, b)$  over the interval  $[a, b]$  would be assigned to  $X$ . the PDF for  $X$  is then:

$$\begin{aligned} g_X(\xi) &= \frac{1}{b-a} \rightarrow a \leq \xi \leq b \\ g_X(\xi) &= 0 \rightarrow \textit{otherwise} \end{aligned} \tag{5.2}$$







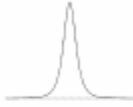
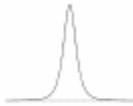


$X$  expectation and variance are respectively:

$$E(X) = \frac{a+b}{2} \tag{5.3}$$

$$V(X) = \frac{(b-a)^2}{12} \tag{5.4}$$

Table 5-3 reports the criteria suggested by the Guide to assign a certain PDF to each input quantity  $X_i$  to be considered for using the Monte Carlo approach to estimate the PDF of  $Y$  and hence the combined standard uncertainty on it.

**Table 5-3.** PDF assigned on the basis of available information.

Available information	Assigned PDF and illustration (not to scale)	
Lower and upper limits $a, b$	Rectangular: $R(a, b)$	
Inexact lower and upper limits $a \pm d, b \pm d$	Curvilinear trapezoid: $CTrap(a, b, d)$	
Sum of two quantities assigned rectangular distributions with lower and upper limits $a_1, b_1$ and $a_2, b_2$	Trapezoidal: $Trap(a, b, \beta)$ with $a = a_1 + a_2,$ $b = b_1 + b_2,$ $\beta =  (b_1 - a_1) - (b_2 - a_2)  / (b - a)$	
Sum of two quantities assigned rectangular distributions with lower and upper limits $a_1, b_1$ and $a_2, b_2$ and the same semi-width ( $b_1 - a_1 = b_2 - a_2$ )	Triangular: $T(a, b)$ with $a = a_1 + a_2, b = b_1 + b_2$	
Sinusoidal cycling between lower and upper limits $a, b$	Arc sine (U-shaped): $U(a, b)$	
Best estimate $x$ and associated standard uncertainty $u(x)$	Gaussian: $N(x, u^2(x))$	
Best estimate $\mathbf{x}$ of vector quantity and associated uncertainty matrix $U_{\mathbf{x}}$	Multivariate Gaussian: $N(\mathbf{x}, U_{\mathbf{x}})$	
Series of indications $x_1, \dots, x_n$ sampled independently from a quantity having a Gaussian distribution, with unknown expectation and unknown variance	Scaled and shifted $t$ : $t_{n-1}(x, s^2/n)$ with $\bar{x} = \sum_{i=1}^n x_i/n,$ $s^2 = \sum_{i=1}^n (x_i - \bar{x})^2 / (n - 1)$	
Best estimate $x$ , expanded uncertainty $U_p$ , coverage factor $k_p$ and effective degrees of freedom $\nu_{\text{eff}}$	Scaled and shifted $t$ : $t_{\nu_{\text{eff}}}(x, (U_p/k_p)^2)$	
Best estimate $x$ of non-negative quantity	Exponential: $Ex(1/x)$	
Number $q$ of objects counted	Gamma: $G(q + 1, 1)$	

### **5.7. Evaluation of the combined uncertainty on the position of the transient source**

To complete an exhaustive analysis of the proposed method, the measurement system needs to be characterized in terms of uncertainty on the position of the fault. Hence, each block of a voltage channel of a remote unit (slave) is characterized to evaluate all the contributions to the uncertainty on the captured time stamp. In fact, the uncertainty on the position of the fault depends on the uncertainty affecting the time stamps captured by the slaves and then processed by the master unit.

The propagation of the uncertainty source effects through the fault location algorithm has been analyzed. The combined standard uncertainty  $u(t_{ij})$  on the time stamp  $t_{ij}$  is due to the random effects of the uncertainty sources located in all the devices of the measurement hardware, whereas the biases are assumed to be known; hence, compensated.

Experimental tests for the metrological characterizations of the VVT, the EDB and the GPS station have been carried out: the effects of the uncertainty sources located in the measurement chain have been obtained and expressed as PDFs; then, a numeric technique, i.e. the Monte Carlo Simulation (MCS) procedure, has been run to evaluate  $u(t_{ij})$ . In this connection, two assumptions were taken: i) the statistical mean value of the random variable is the bias affecting  $t_{ij}$  itself; ii) all the time stamps that can be captured by any channel of any slave have similar frequency distribution. The MCS procedure is applied to phase-to-ground voltage signals previously obtained by the EMTP-RV simulations described in Section 4.2; the voltage monitored in each node of the considered network in different fault cases is used as input. The accuracy performance of the fault location method has been tested in realistic working conditions.

#### **5.7.1. Metrological Characterization of the voltage transducer**

The transducer transfer function has been determined to build up the equivalent model of the conditioning block used in the MCS procedure. In the experiments, both magnitude- and phase- frequency response have been obtained by processing the data simultaneously acquired at the input and output of the VVT, as shown in Figure 5-12. The calibrator Wavetek Datron 4800A has been used to feed the VVT. It can provide up to 1000 V for frequencies up to 33 kHz, 100 V for frequencies up to 100 kHz and 10 V up to 1 MHz. Its nominal accuracy specifications are: 50 ppm for AC voltage; zero-to-full-range linearity < 0.1 ppm of full scale. The calibrator has been configured to generate a sinusoidal waveform in the range 50 Hz - 1 MHz. For each frequency, 100 measurements of the RMS of both the input and output signals were taken along with their phase shift.

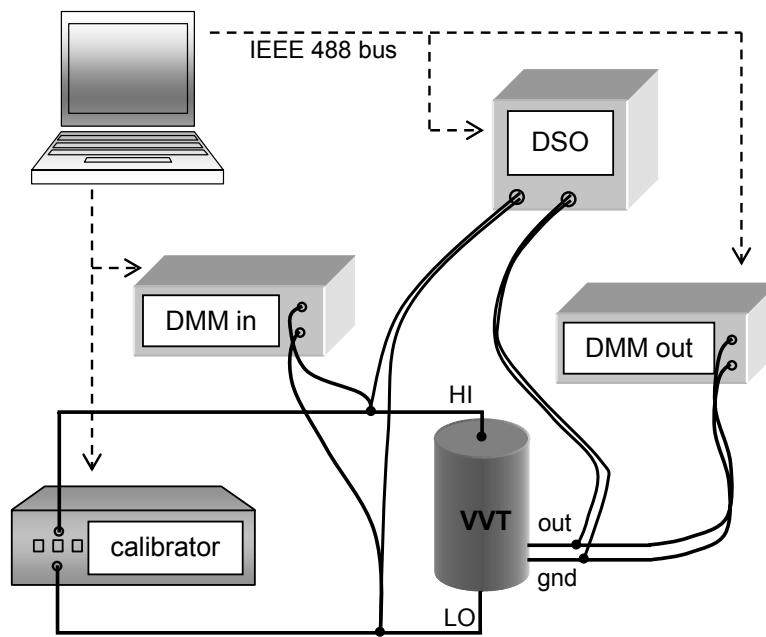


Figure 5-12. Test bank for the VVT characterization.

Table 5-4. Expected value and standard uncertainty of  $K$  and  $\Delta\varphi$  of the VVT in function of frequency.

freq [Hz]	50	100	200	500	1000	2000	5000
$\mu(K)$	3.816767 E+03	3.776311 E+03	3.773185 E+03	3.762691 E+03	3.769573E +03	3.760425 E+03	3.768550 E+03
$\sigma(K)$	2.320323	1.903766	3.816121 E-01	2.100704	5.625032 E-01	1.665146	8.187730 E-01
$\mu(\Delta\varphi)$	2.685629 E-02	1.185071 E-02	3.639100 E-04	2.636453 E-02	5.124309 E-02	7.291264 E-02	6.090281 E-02
$\sigma(\Delta\varphi)$	2.954740 E-03	3.234570 E-03	3.561580 E-03	3.130740 E-03	3.192580 E-03	3.269770 E-03	3.249960 E-03

freq [Hz]	10000	20000	50000	100000	200000	500000	1000000
$\mu(K)$	3.777446 E+03	3.797845 E+03	3.966952 E+03	4.430782 E+03	5.918742 E+03	1.572539 E+03	2.816077 E+02
$\sigma(K)$	8.393617 E-01	1.421423	3.349240	1.088968	2.441792 E+02	3.424351 E+02	2.501426 E+01
$\mu(\Delta\varphi)$	4.272287 E-02	3.565416 E-02	1.904711 E-02	7.089267 E-02	5.237120 E-01	3.275576 E-01	1.170569
$\sigma(\Delta\varphi)$	3.553780 E-03	4.070260 E-03	6.340950 E-03	5.703560 E-03	3.377108 E-02	2.793566 E-01	8.552284 E-02

This way, the probability density functions of the random variables representing the gain  $K$  and the phase error  $\Delta\varphi$  of the transducer have been determined vs. frequency. For the above tests, two highly-accurate Digital Multi Meters (DMMs) HP3458A are used for RMS measurements of the VVT input and output signals. The HP3458 model has been widely

used as reference sampling device, see e.g. [6, 7]; despite, its use for computing the signals RMS and phase-shift is not possible given that its maximum sampling rate is not compatible with the frequency range of interest.

This DMM supports three techniques for RMS measurement, each offering specific capabilities: a) synchronously sub-sampled computed RMS technique, b) analog computing RMS conversion technique, c) random sampled computed RMS technique. The a) technique features very high linearity and the highest accuracy; it requires a repetitive input signal in the bandwidth 1 Hz – 10 MHz. The b) mode is the default one and ensures the fastest measurement speed in the range 10 Hz – 2 MHz. Finally, the c) solution features high linearity as a) but the lowest accuracy in the bandwidth 20 Hz – 10 MHz. Being the calibrator output repetitive and stable, the a) mode seems to be the most suitable for our purpose. The time delay introduced by the VVT vs. frequency is evaluated by acquiring the input and output signals with a Digital Storage Oscilloscope (DSO) whose channels feature nominal simultaneous acquisition with high sampling rate. The delay between the input and output signals can be directly measured by the DSO as “time skew” between two input channels. This procedure is automatically run by controlling the instruments through a PC via an IEEE 488-based interface. The measurement results are stored in the PC and then processed to obtain the frequency distributions of the amplitude- and phase- transfer functions.

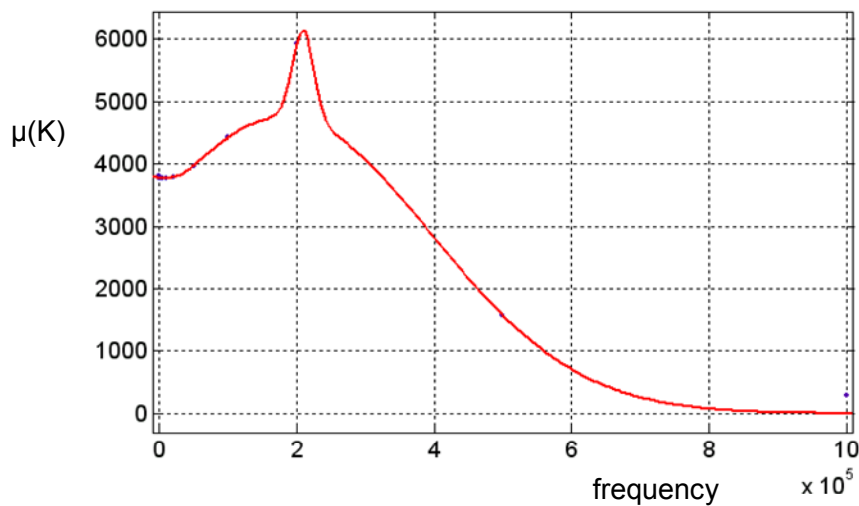


**Figure 5-13** Expected value of  $K$  of the VVT in function of frequency (red curve = best fit to experimental results)

In Figure 5-13 and Figure 5-14 are reported the mean value of the gain  $K$  and of the phase error  $\Delta\phi$ , respectively, in function of frequency. The red curves are obtained by fitting experimental results with polynomial interpolating expressions. In this way  $\mu(K)$  and  $\mu(\Delta\phi)$  can be considered continuous functions in the frequency domain in the whole

range of interest for the characterization. The results on whose basis the curves are obtained are reported in Table 5-4.

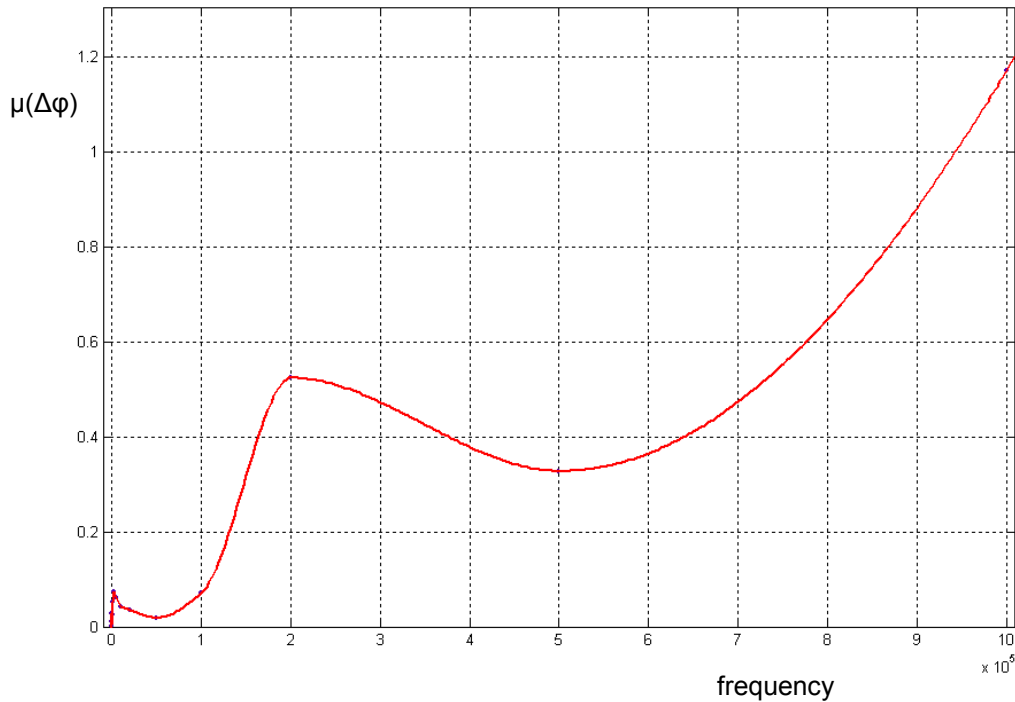


**Figure 5-14** Expected value of  $\Delta\phi$  of the VVT in function of frequency (red curve = best fit to experimental results)

### 5.7.2. Metrological characterization of the Event Detection Block

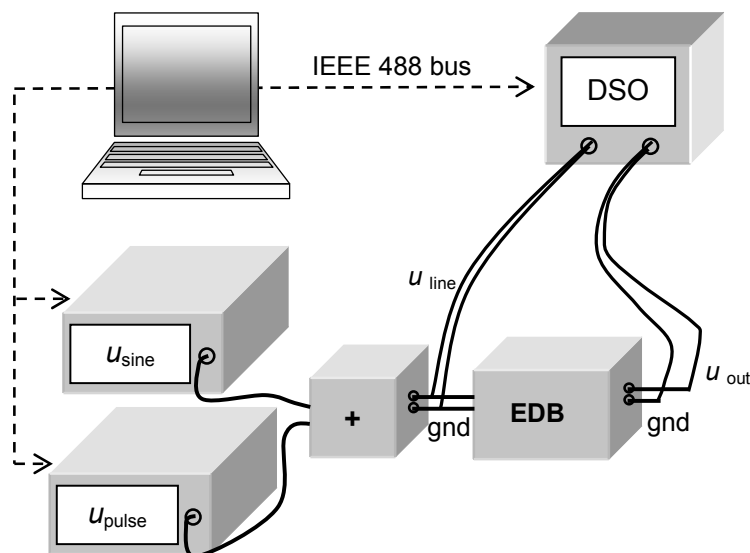


**Figure 5-15** Automatic test bench for the EDB characterization

The uncertainty contribution of the EDB to  $t_{ij}$  has to be evaluated as the time delay between the occurrence of the transient and the corresponding change of the logic level of the EDB output. To this purpose, an automatic test procedure has been developed by

using two function generators and the DSO (see Figure 5-15). One of the sources is configured to generate a sinusoidal waveform  $u_{\text{sine}}$  at power frequency with amplitude 10 V. The second function generator is configured to give a 1 V-peak pulse waveform  $u_{\text{pulse}}$ . The rising-front time and the duration of  $u_{\text{pulse}}$  are randomly extracted in the intervals [5 ns – 100 ns] and [500 ns – 10 us]. The former parameter corresponds to setting the derivative of the first surge of the event, while the latter parameter is equivalent to half period of the oscillations in case of oscillatory transient, or to the duration of the surge in case of impulsive transient. This way, the frequency content of the signal is different in each test and ranges through the entire frequency range associated to EM transient disturbances affecting power networks.

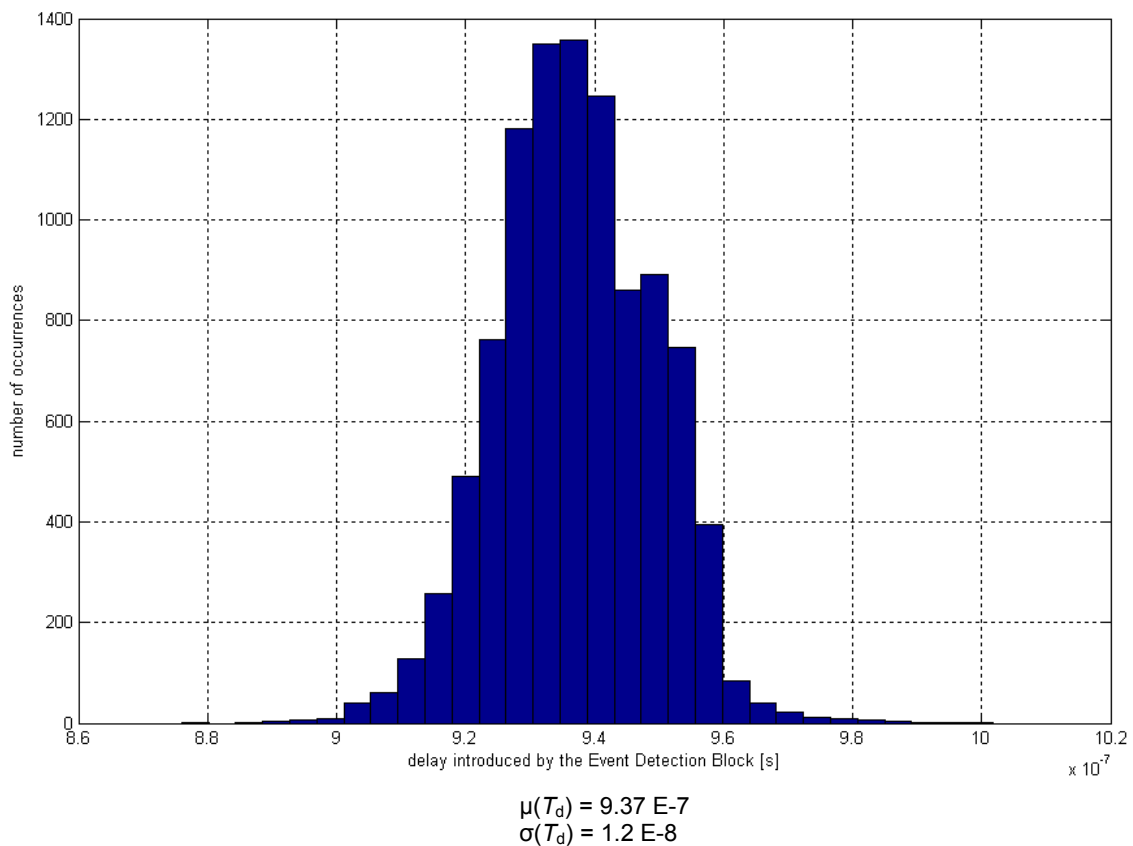


**Figure 5-16** Frequency distribution of  $T_d$  introduced by the EDB

The signal  $u_{\text{line}}$  at the input of the EDB has been obtained by adding  $u_{\text{sine}}$  and  $u_{\text{pulse}}$ . For each value of the rising time of  $u_{\text{pulse}}$ , the DSO acquires  $u_{\text{line}}$  and  $u_{\text{out}}$  to measure the “time skew” between the beginning of the rising front of the former signal and the commutation from high to low level of the latter one. Ten thousand measurements of the time skew have been carried out to get a probability distribution featuring a standard deviation that reasonably takes into account all the combination of rising fronts and durations that can be found in transients scenario. The results are reported in Figure 5-16 by means of a 30 classes histogram.

### 5.7.3. Metrological characterization of the GPS station

The GPS station is the GPS168 PCI by Meinberg, whose nominal accuracy specification are: time resolution equal to 100 ns; standard uncertainty on the captured time lower than 250 ns. In this case, only a type-B uncertainty evaluation can be done. Therefore, according to [3], a uniform probability density function with zero expected value and 250 ns standard deviation is assumed to represent the GPS contribution to  $u(t_{ij})$ .

### 5.7.4. Monte Carlo Method to evaluate the combined uncertainty on the fault location

The results of the metrological characterization carried out for the blocks of the measurement system are used to evaluate the uncertainty affecting the position of a fault occurring within the power network monitored by the system itself. According to the above described probabilistic approach, the procedure takes into account both bias and random uncertainty contributions of the devices, and corrupts the input voltage of the emulated slave unit by applying their effects to each acquired sample. In practice a Matlab script loads as input the set of voltage waveforms obtained in correspondence of all the slave stations present in the simulated distribution network when one particular case of short circuit occurs. The magnitude and phase spectrum of each line-voltage are corrupted by means of the characteristics of gain  $K$  and phase error  $\Delta\varphi$ , respectively; every frequency component is distorted in amplitude, under the effect of both the bias  $\mu(K)$ , (see Figure 5-13) and a random contribution to  $K$  assumed to have a Gaussian PDF with mean value  $\mu(K)$  and as  $\sigma(K)$  the maximum value of the experimental standard deviation, i.e. the one measured at  $f = 500$  kHz (see Table 5-4). The same happens to the phase of the frequency component, affected by both the bias contribution  $\mu(\Delta\varphi)$  (see Figure 5-14) and a random variable having uniform PDF, expected value  $\mu(\Delta\varphi)$  and amplitude 2 times the  $\sigma(\Delta\varphi)$  measured at  $f = 500$  kHz (see Table 5-4). In this way the worst operating conditions are assumed for the VVT. The frequency spectrum of the input voltage “filtered” by the VVT model is then brought back in the time domain, so that the transduced signal is obtained. This is the waveform that in each slave is given as input to the EDB.

The Event Detection Block described in Section 5.2 has been reproduced in Matlab, where the filters used to obtain  $u_f$  have been implemented in the time domain. The logic signal at the output of the EDB function changes its level when the difference between the transduced voltage waveform and its low frequency content is greater than the EDB threshold. The timestamp corresponding to the commutation is then corrupted by adding the delay measured during the characterization of the EDB (see Figure 5-16), assumed as a random variable  $T_d$  having a Gaussian PDF with  $\mu(T_d)=9.37e-7$  and  $\sigma(T_d)=1.2e-8$ .



Finally, the effect of the uncertainty of the GPS station is taken into account, and to each timestamp obtained by the previous step a random contribution is superposed, according to what described above.

### 5.7.5. Experimental results

The MCM described above has been applied to the set of voltage waveforms obtained at the end of an EMTP simulation carried out in the distribution network described in Section 4.2. In particular, the considered case of fault was a phase *a*-to-ground short circuit affecting line L6 and distant 2000 m from node S7 (see Figure 4.8). One thousand MC trials have been run to obtain the set of results used for the evaluation of the combined uncertainty on the fault location. At the end of each trial the information relevant to the line assumed as faulted, the slave node considered the nearest one to the fault point and the estimated distance of the fault position from the latter node were saved. In 100% of the trials run the faulted line and the nearest node to fault have been correctly identified as L6 and S7, respectively.

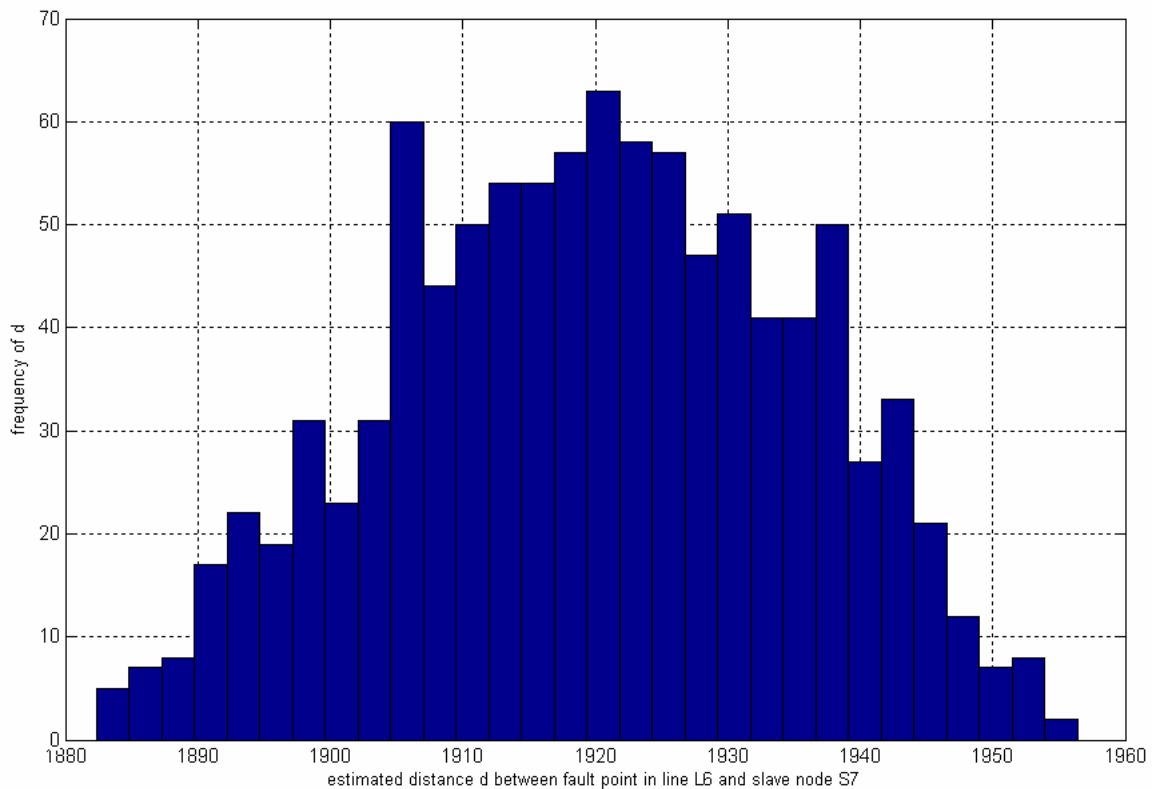


**Figure 5-17** Histogram of the fault location method results in case of line-to-ground short circuit. The frequency distribution of the distance  $d$  computed to locate the short circuit along the line at the end of each trial is represented in Figure 5-17 by means of a 30 classes histogram. The expected value of  $d$  corresponds to 1920 m, affected by an error of 80 m respect to the actual fault position, whereas the standard uncertainty on  $d$  is equal to 15.2 m. It should be noted that, according to [3], the bias uncertainty contribution, once it is

known, has to be compensated to carry out the characterization of the system, hence the final uncertainty on the fault location can be associated to the only random contribution. A second MCM procedure has been run to evaluate to dispersion of results in the case of phase a to phase c short circuit affecting line L8, 1 km distant from slave S9. The results of the 1000 trials are reported in Figure 5-18 in terms of frequency distribution of the estimated distance  $d$  of the fault point from node S9. Even in this case an histogram featuring 30 classes has been created. The expected value of  $d$  corresponds to 1013.3 m, hence it is affected by a bias of 13 m respect to the actual value, and the standard uncertainty is equal to 13.2 m, just a few lower than the standard deviation obtained in the previous fault case. The different accuracy affecting the fault location in the two analyzed cases turns into a different polarization of the frequency distributions; the expected value of the distance  $d$  is affected by a greater bias in the case of grounded short circuit respect to the ungrounded one maybe because the propagation speed assumed by the master for the travelling waves is more correct in the latter fault condition than in the former one. Moreover, a grounded fault is usually less heavy for the power system than a fault between phase conductors, and thus the surge rising at the fault point and propagating through the lines is more dumped.

By considering the application of the fault location procedure, as already explained in previous sections, this fact leads to a more difficult and consequently less accurate location of the fault.

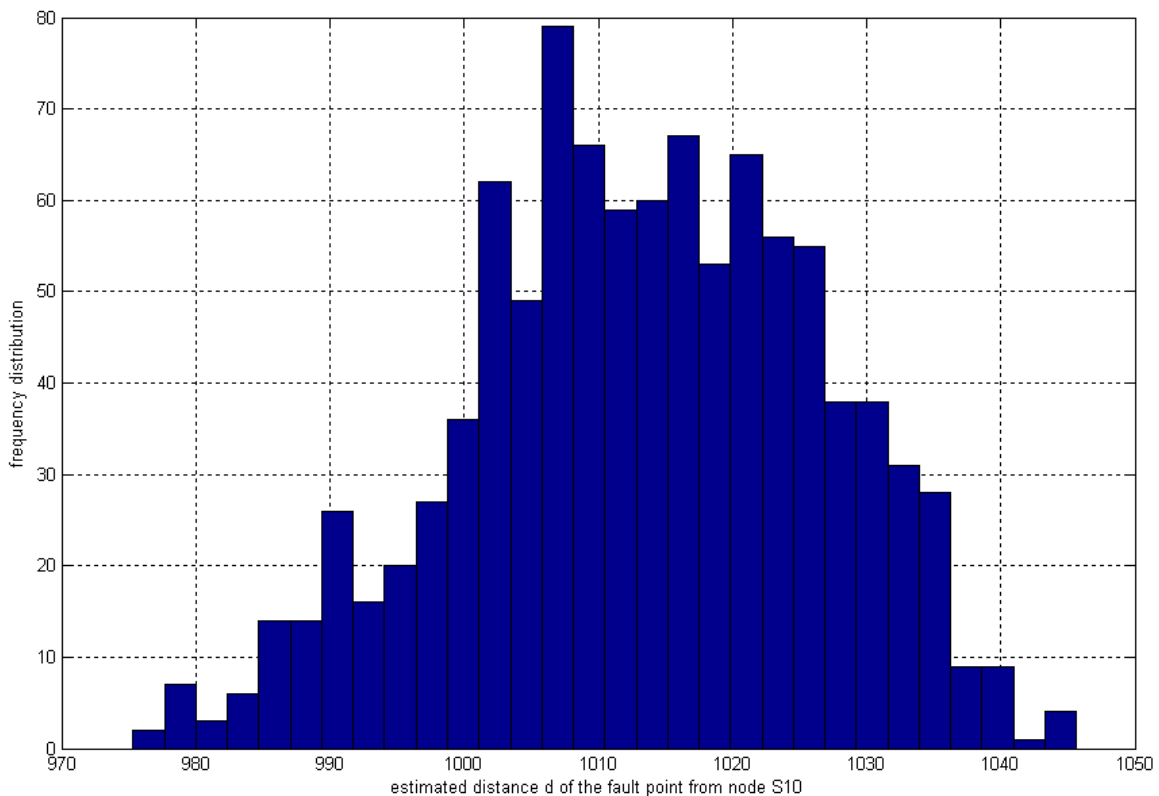


**Figure 5-18** Histogram of the fault location method results in case of line-to-line short circuit

## **5A. Appendix: Uncertainty Contribution of the Analog Conditioning Block in DSP-based Instruments**

The type-B evaluation of the uncertainty affecting the measurements provided by any instrument could be done by properly processing the nominal accuracy specifications of each functional block in the instrument. In DSP-based measurements, the implementation of such a procedure faces the difficulty arising from the fact that the usual accuracy specifications of the input analog conditioning block cannot be used to determine the uncertainty affecting each sample of the block output signal. A calibration procedure has been developed to try to tackle this issue. It is based on the use of high-accuracy data acquisition boards and the simultaneous acquisition of the signals at the input and output of the analog block. Basically, any measuring instrument based on Digital Signal Processing (DSP) techniques consists of three blocks: an input block, which contains transducers and analog conditioning circuits; a data acquisition and A/D conversion (DAQ) block; a control and data processing block. The uncertainty estimation in DSP-based measurements requires that the uncertainty affecting each acquired data is known. A problem immediately arises in this estimation, because of the different characterization procedures of the analog conditioning blocks and DAQ boards. As a matter of fact, the accuracy specifications of a DAQ board are defined with reference to a generic sample, whereas the parameters given to specify the accuracy of the input analog block devices do not allow the estimate of the uncertainty affecting the samples of the block output. For instance, the traditional instrument transformers are characterized by means of the ratio and phase angle errors (see, e.g. the International Standards [8, 9]). Even in the case of electronic voltage transformers which feature a digital output section, no parameter characterizing the accuracy of the samples is defined by IEC Std. 60044-7 [10].

The method for the characterization of the analog input blocks, which allows determining the uncertainty affecting each sample of the block output, is based on the comparison between samples simultaneously acquired at the block input and output by means of highly-accurate acquisition and A/D conversion systems. Such a procedure provides a calibration curve which takes into account all the effects of the uncertainty sources located in the block. The information derived from the curve can then be used, along with the accuracy specifications of the DAQ block, to evaluate the uncertainty affecting the estimate of the measurand.

The method could be used by the manufacturer to test a significant statistical sample of a given block model, in order to provide accuracy specifications characterizing each output sample of any device of that type. In the case of voltage transducers, the method can be implemented by means of the measurement setup described in the following.

### 5A.1. The calibration method

The method can be implemented under both AC and DC conditions, and allows the estimate of the uncertainty affecting each output sample of the instrument analog conditioning block.

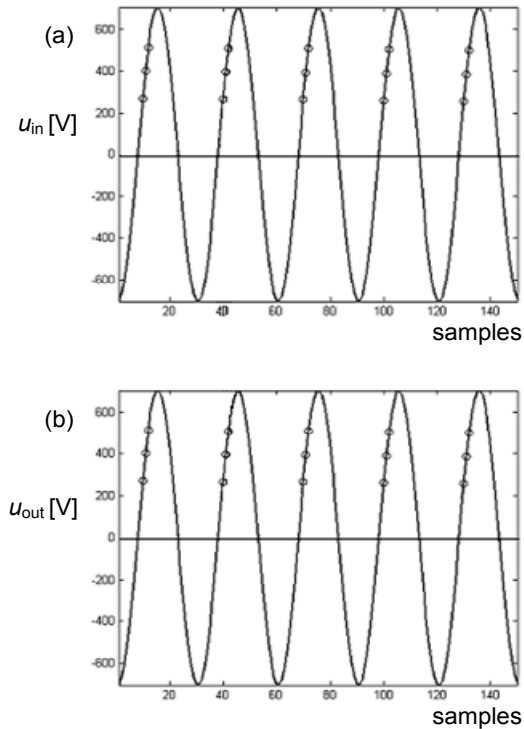


**Figure 5-19** Some of the corresponding samples of the input and output waveforms used to build up the calibration curve

Let us assume, only by way of example, that the AC signal is sinusoidal and the input block is a voltage-to-voltage transducer. Moreover, let us refer to Figure 5-19, where both the input and output voltages denoted by  $u_{in}(t)$  and  $u_{out}(t)$ , respectively, are simultaneously acquired over  $N_p$  periods, thus obtaining two sequences of length  $N_s$ . Let us denote their generic elements by  $u_{in}[n]$  and  $u_{out}[n]$ , respectively.

As for the example in the above figure, it is  $N_p = 5$ ,  $N_s = 150$ . In both Figure 5-19 and what follows, the output signal is multiplied by the ratio  $R_U$  between the transducer nominal input and output. Hence, the waveforms only differ because of the transducer uncertainty. The figure qualitatively shows the process of building up the two above sequences. Of course, due to the plot scale, Figure 5-19 cannot show the differences between the input and output signals; therefore, the two graphs seem identical. Two periodic sequences of length  $N_s/N_p$  are then built up. Their generic element is denoted by  $\bar{u}_{in}[n]$  and  $\bar{u}_{out}[n]$ , respectively. They are defined as follows:

$$\bar{u}_{in}[n] = \frac{1}{N_p} \sum_{k=0}^{N_p-1} u_{in}\left[n + k \frac{N_s}{N_p}\right] \quad (5A.1)$$

$$\bar{u}_{out}[n] = \frac{1}{N_p} \sum_{k=0}^{N_p-1} R_U \cdot u_{out}\left[n + k \frac{N_s}{N_p}\right] \quad (5A.2)$$

i.e., they are the mean value of the samples having the same position in each period of the observation interval. This averaging procedure reduces the random effects that could affect the data acquired.

As for the tests under DC conditions, a sequence of DC signals is applied and their amplitude is increased up to the transducer under test (TUT) full scale; the TUT input and output are acquired and averaged. Both in AC and DC conditions, the averaged samples of the input and output signals are the x-domain and y-domain, respectively, of the calibration curve.

The curve takes into account all the effects of the uncertainty sources located in the TUT; then a linear fitting process is used to obtain a suitable best fit straight line (BSL). Three well-known linearization criteria are exemplified in Figure 5-20: (a) the BSL is obtained by means of a linear regression technique, which determines slope and offset of the line itself; (b) the linear regression technique is applied to get a BSL through zero (i.e. without offset); (c) the BSL through the end points of the calibration curve is considered. After that, the device can be characterized by means of indexes derived from: the comparison between the slopes of the BSL and the ideal characteristic of the device itself; the worst deviation of the calibration curve from the BSL; the BSL offset (if any).

## 5A.2. Characterization indices

Two indices are used to characterize the deviation of the actual behaviour of the TUT from the ideal one.  $\alpha$  and  $\beta$  are defined as follows:

$$\alpha = \frac{\Delta}{\left| \frac{g - g_n}{g_n} \right|} \quad (5A.3)$$

$$\beta = \frac{\Delta \max\left\{ \left| \bar{u}_{out}[n] - g \cdot \bar{u}_{in}[n] \right| \right\}}{\max\left\{ \left| \bar{u}_{out}[n] \right| \right\}} \quad (5A.4)$$

In (5A.3) and (5A.4)  $|\cdot|$  denotes the absolute value of “•”. In (5A.3),  $g$  is the angular coefficient of the BSL and is computed with reference to Figure 5-20 b by applying the least square method, whereas  $g_n$  (which is unity in suitable coordinates) is the slope of the ideal characteristic. Hence,  $\alpha$  is a gain error. As for  $\beta$ , it is similar to the integral non-linearity of a DAC, as endorsed by [11].

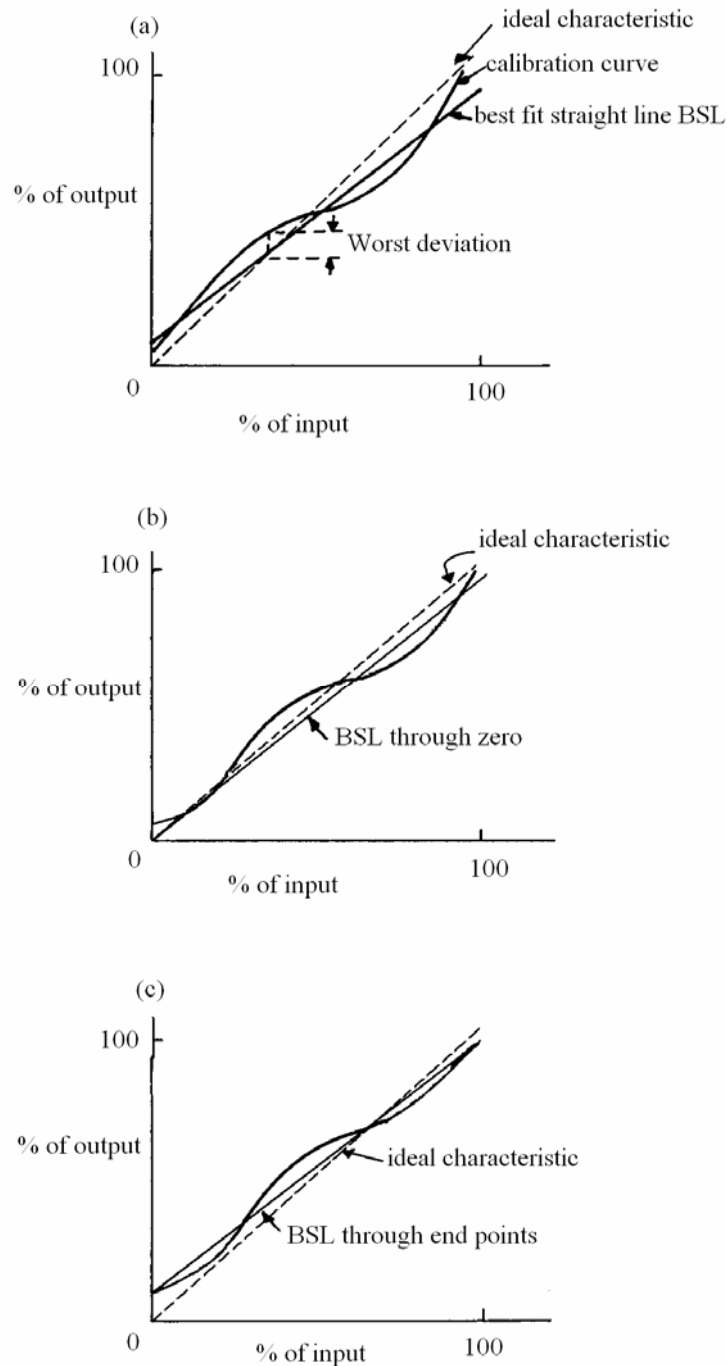


**Figure 5-20** Linearization criteria

If the device can be considered linear, the two indexes can be used also in non-sinusoidal conditions. The procedure proposed could be difficult to implement in common laboratories (where high-accuracy sampling devices may not be available), but can easily be implemented in a manufacture laboratory. Moreover, if a significant statistical sample of a given transducer model is characterized according to this procedure, the maximum values  $A_{U-U}$  and  $B_{U-U}$  found for  $\alpha$  and  $\beta$ , could then be given in the data sheet to qualify that transducer model.

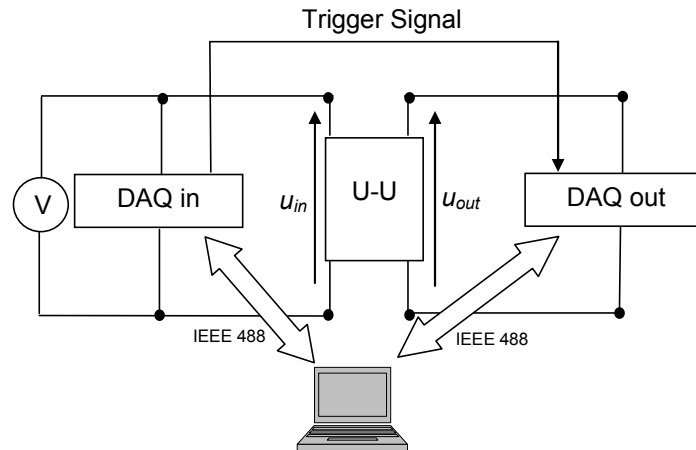


**Figure 5-21** Block diagram of the calibration setup

Figure 5-21 is the schematic block diagram of the setup used to characterize the TUT by means of the proposed procedure. U-U denotes the voltage-to-voltage transducer under test, V refers to a suitable reference voltage source (which must feature high short-term stability) and DAQ refers to a high-accuracy data acquisition device. Two HP 3458A have been used as high-accuracy sampling devices. HP 3458A features 0.02% of reading, plus an offset voltage varying from 8 mV at 10 V to 0.8 V at 1 kV.

**Table 5-5** Values of  $A_{U-U}$  and  $B_{U-U}$ , along with their relevant standard uncertainties  $u(A_{U-U})$  and  $u(B_{U-U})$ , respectively, vs. frequency (input voltage RMS value: 250 V)

Frequency [Hz]	DC	50	1000	3000
$A_{U-U}$	$1.2 \cdot 10^{-3}$	$3.23 \cdot 10^{-3}$	$2.8 \cdot 10^{-3}$	$1.31 \cdot 10^{-2}$
$u(A_{U-U})$	$7 \cdot 10^{-4}$	$9 \cdot 10^{-5}$	$1 \cdot 10^{-4}$	$5 \cdot 10^{-4}$
$B_{U-U}$	$3.0 \cdot 10^{-3}$	$4.8 \cdot 10^{-3}$	$5.82 \cdot 10^{-2}$	$1.75 \cdot 10^{-1}$
$u(B_{U-U})$	$2 \cdot 10^{-4}$	$7 \cdot 10^{-4}$	$7 \cdot 10^{-4}$	$1 \cdot 10^{-3}$

The method requires the simultaneous sampling of  $u_{in}$  and  $u_{out}$ , otherwise the contribution of the transducer delay to  $\alpha$  and  $\beta$  gets lost. To this purpose, the A/D conversion start of DAQ<sub>in</sub> has been used to trigger the operation of DAQ<sub>out</sub>. Active transducers LEM LV-25P have been characterized by means of the above setup. They basically are current transducers, but behave as voltage transducers by adding suitable resistors in series with their input and output. The tested transducers feature the following nominal specifications: maximum input voltage: 400 V; conversion voltage ratio  $R_U = 40.7 : 1$ ; overall accuracy: 0.8% at full scale; offset voltage: 30 mV.

In the DC tests, input signals having amplitude varying in steps of 50 V from -250 V to 250 V have been applied. As for the AC tests, the RMS value of the sinusoidal input has been kept constant at 250 V, whereas the signal frequency has been varied in the interval [50 Hz, 3 kHz]. The maximum frequency has been chosen according to the requirements

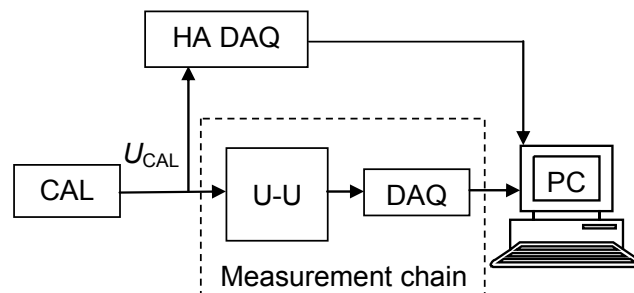
of the IEEE Standard 1159–1995 [12] for harmonics evaluation. The above frequency range also contains the one endorsed by the European Standard EN-50160 [13].

Table 5-5 refers to the characterization of three voltage transducers LEM LV 25-P and reports, vs. some test frequencies, the maximum absolute values  $A_{U-U}$  and  $B_{U-U}$  characterizing the considered set, along with the relevant standard uncertainty.

### 5A.3. Application example

The purpose of this application example is verifying whether the above indexes  $A_{U-U}$  and  $B_{U-U}$ , taken to characterize the considered transducer set, can be used to evaluate the uncertainty affecting a parameter measured by a DSP-based measurement chain containing any transducer belonging to the set. In affirmative case,  $A_{U-U}$  and  $B_{U-U}$  could be determined, and then reported in the transducer data sheet, by testing a significant statistical sample of them in the manufacture laboratory. The problem has been seen by the point of view of a transducer manufacturer on the one hand and of a user on the other hand, under the assumption that they built up two similar measurement chains based on a voltage transducer and a DAQ board for the measurement of a RMS voltage. The manufacturer is assumed to have already characterized a significant statistical sample of transducers of the same type used in the chain, by means of the described procedure. He would like to verify the usefulness of the indexes obtained. As for the user, he wants to determine the uncertainty affecting the RMS measurement.

As explained in chapter 5, the uncertainty can be estimated by applying the GUM [3] or other approaches that can be found in the literature, see e.g. [14 - 16]. When the measurand is not directly measured, the GUM endorses the Law of Propagation of Uncertainty which relies on the linearization of the functional relationship between the measurand and the input quantities. Recently, the ISO document [4] has endorsed the use of a MCM to evaluate the uncertainty by means of numerical methods for the propagation of probability distributions through the measurement process.



**Figure 5-22** Block diagram of the setup used for the application example

Figure 5-22 shows the block diagram of the setup implemented to run the application example. CAL refers to the reference voltage source Wavetek 4800, whose nominal



accuracy, in terms of expanded uncertainty with 95%-confidence level, is 40 ppm. The measurement chain consists of a transducer LEM LV 25-P and a DAQ board NI PCI 6070 having the following nominal specifications [17]: offset  $O_{\text{DAQ}} = 6.38$  mV; percentage of reading  $\alpha_{\text{DAQ}} = 0.0714\%$ ; noise + quantization  $Q_{\text{DAQ}} = 6.10$  mV. A Personal Computer (PC) controls both the setup operation and provides estimates of the measurand. It also performs offline estimates of the relevant uncertainties by processing the data acquired by the DAQ board and the high-accuracy sampling device HA DAQ, along with the parameters characterizing the accuracy of the data at the output of each device of the measurement chain. The tests have been carried out in sinusoidal conditions by setting the calibrator output  $u_{\text{CAL}}(t)$  at the RMS voltage  $U_{\text{CAL}} = 230$  V, with frequency  $f = 50$  Hz.

Two MCS procedures have therefore been implemented, according to the ISO document [4]. In both cases the acquired data have been corrupted by the effects, treated as random variables, of the uncertainty sources located in U-U and the DAQ board. Then, the data have been processed to obtain an estimate of the measurand and of its type-B uncertainty, which, in accordance with [4], has been expressed as the shortest coverage interval associated to the confidence level of 95%. In any case, let us denote by  $\alpha_U$  and  $\beta_U$ , respectively, the random variables characterizing the effects of the uncertainty sources located in the voltage transducer. They have uniform distribution within the intervals  $[-A_U, +A_U]$  and  $[-B_U, +B_U]$ . Moreover, as for the DAQ board, let us denote by  $o_{\text{DAQ}}$ ,  $\alpha_{\text{DAQ}}$ ,  $q_{\text{DAQ}}$  the random variables relevant to the uncertainty sources located in the board itself. They have uniform distribution within the intervals  $[-O_{\text{DAQ}}, +O_{\text{DAQ}}]$ ,  $[-A_{\text{DAQ}}, +A_{\text{DAQ}}]$ ,  $[-Q_{\text{DAQ}}, +Q_{\text{DAQ}}]$ , respectively.

In both series of simulations, the values reported in Table 5.5 and relevant to 50 Hz, i.e.  $A_U = 3.3 \cdot 10^{-3}$  and  $B_U = 4.8 \cdot 10^{-3}$ , have been considered for the transducers, whereas for the DAQ board the values of  $O_{\text{DAQ}}$ ,  $A_{\text{DAQ}}$  and  $Q_{\text{DAQ}}$  found in the data-sheet (reported above) have been used. It is worthwhile highlighting that all the above random variables show different statistical properties. Among them,  $q_{\text{DAQ}}$  and  $\beta_U$ , are assumed to be totally uncorrelated; the other variables are assumed to be totally correlated. When different measurements (or trials, in the case of simulations) are performed, the values of the latter random variables are constant in a single trial, but randomly vary from one trial to another.

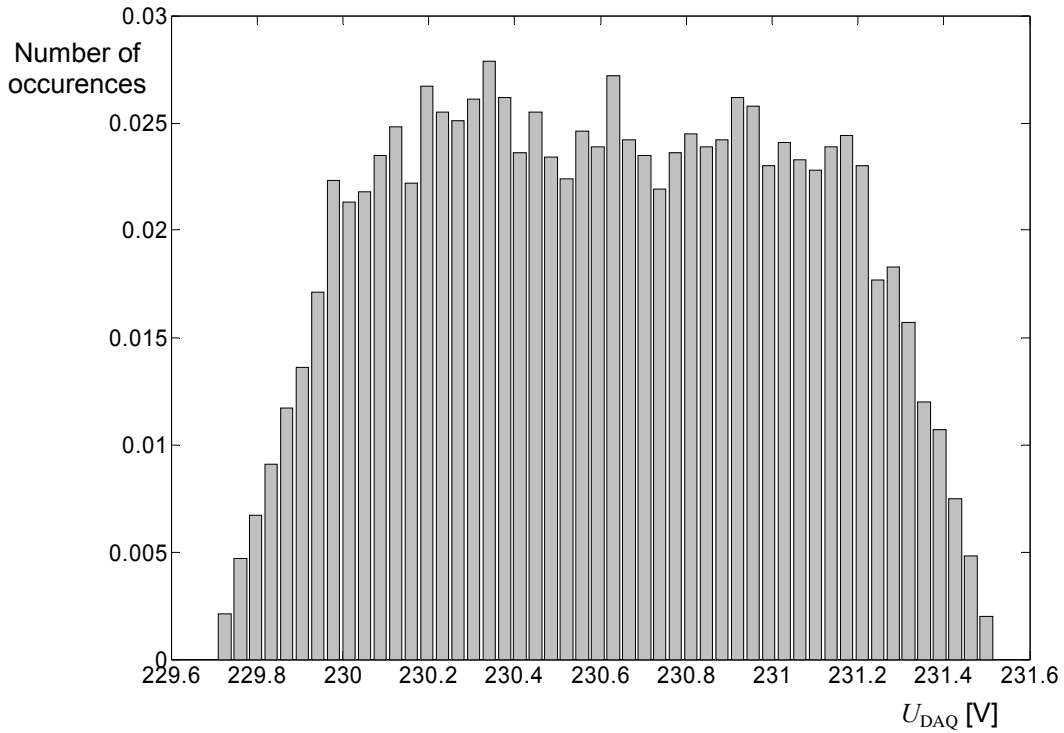


**Figure 5-23** Frequency distribution of the  $U_{\text{DAQ}}$  values provided by the Monte Carlo simulation procedure.

Now, consider the problem as if it should be tackled by the user, assumed to be provided by the transducer manufacturer of the values of  $A_U$  and  $B_U$ . The  $N$ -length sequence acquired by the DAQ board presents  $u[n]$  as generic element; finally the MCS procedure is implemented. The RMS value  $U_{\text{DAQ}_m}$  measured in the  $m$ -th trial ( $1 \leq m \leq M$ ) of the MCS has been computed as follows:

$$U_{\text{DAQ}_m} = \sqrt{\frac{1}{N} \sum_{n=1}^N \left\{ u[n] + \alpha_{U_m} \cdot u[n] + \beta_U \cdot \max\{u[n]\} + \alpha_{\text{DAQ}_m} \cdot u[n] + q_{\text{DAQ}} + o_{\text{DAQ}_m} \right\}^2} \cdot R_U^2 \quad (5A.5)$$

$M = 10^4$  trials have been carried out; the distribution in Figure 5-23 of the obtained values of  $U_{\text{DAQ}_m}$  has been found to be symmetrical. The statistical mean value  $\tilde{U}_{\text{DAQ}}$  of the distribution, which is the estimate of the expected value of the measurand, along with the estimate of the relevant uncertainty, can therefore be derived at the end of the MCS procedure. The RMS values:  $U_{\text{CAL}}$  set by the voltage reference source;  $U_{\text{DAQ}}$  measured by the chain in Figure 5-22; and  $\tilde{U}_{\text{DAQ}}$  provided by the MCS procedure have been reported in Fig. 6. Both  $U_{\text{DAQ}}$  and  $\tilde{U}_{\text{DAQ}}$  are centred in the interval representing the uncertainty, and there is compatibility between  $\tilde{U}_{\text{DAQ}}$  and  $U_{\text{CAL}}$  (whose 95%-confidence level is plot).

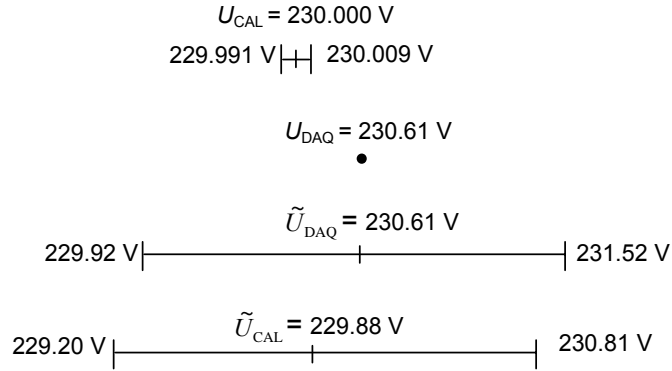


**Figure 5-24** Measurement results (not in scale).  $U_{\text{DAQ}}$ : voltage RMS measured by the chain in Figure 5-22;  $U_{\text{CAL}}$ : voltage reference source RMS, with its 95%-confidence interval;  $\tilde{U}_{\text{DAQ}}$  and  $\tilde{U}_{\text{CAL}}$ : statistical mean RMS values gauged by applying the MCS procedures to DAQ- and HA DAQ-output data, respectively, with their 95%-coverage intervals.

If the digital signal at the DAQ output is seen as the board reading, the evaluation procedure of the type-B uncertainty affecting  $U_{\text{DAQ}}$ , i.e. processing the data corrupted by the effects of the uncertainty sources located in U-U and DAQ, is quite similar to the one usually performed to estimate the uncertainty affecting an instrument reading by applying the accuracy specification to the reading itself.

Another series of  $M = 10^4$  trials (which could easily be implemented in a manufacture laboratory, where high accuracy sampling devices are available) have been run by processing the data acquired by HA DAQ corrupted by the effects of the uncertainty sources located in U-U and the DAQ board in order to estimate the expected value of  $U_{\text{CAL}}$ , which we denote by  $\tilde{U}_{\text{CAL}}$ , and the relevant uncertainty.  $\tilde{U}_{\text{CAL}}$  represents another measurand estimate. The effects of the uncertainty sources in HA DAQ have reasonably been neglected. Also this procedure has provided a symmetrical distribution of RMS values. The resulting statistical mean value, along with the relevant uncertainty, has been reported in Figure 5-24 too, where it can be seen that there is compatibility between  $\tilde{U}_{\text{CAL}}$  and the other measurand estimates. The coverage interval, which in accordance with [4] represents the uncertainty, is not centred on  $U_{\text{DAQ}}$ ; this is due to the fact that the bias introduced by HA DAQ is negligible if compared to the one caused by the measurement chain. Therefore the indexes derived by the proposed characterization procedure seems to be useful for the contribution estimation of that kind of voltage transducer to the uncertainty in the measurement of  $U_{\text{DAQ}}$ .

### 5A.4. An Equipment for Voltage Transducers Calibration

The above method has been implemented in the case of voltage transducers. The indexes (5A.3) and (5A.4) are computed for more than one transducer belonging to the same model, obtaining intervals of values for both of them. If the number of transducers under test corresponds to a consistent statistical sample, the obtained calibration results can be extended to any same-model transducer.

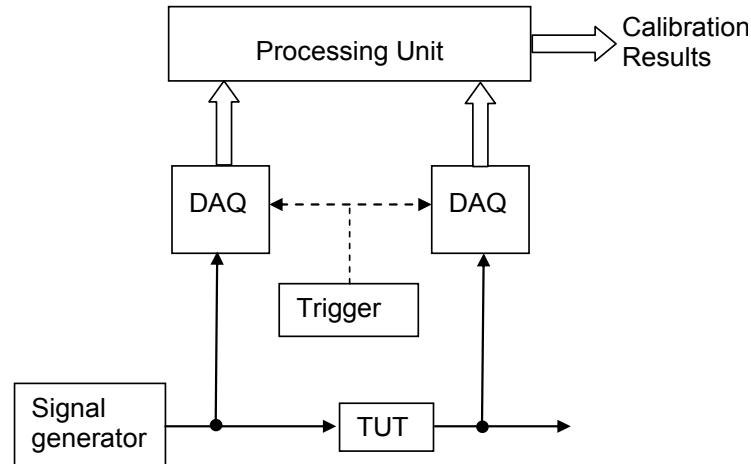


**Figure 5-25** Block diagram describing the proposed method

In Figure 5-25 the calibration procedure is recalled. A high-stability generator applies the signal to the Transducer Under Test (TUT). The method relies on the comparison between signals simultaneously acquired at the input and output of the TUT; hence, an external signal is used to trigger the sampling process of two data acquisition boards (DAQ). The uncertainty affecting the estimates of  $\alpha$  and  $\beta$ , which are mostly due to the DAQ contribution, need to be at least one order of magnitude lower than the  $\alpha$  and  $\beta$  values.

For DC tests, an increasing sequence of DC signals up to the TUT full scale is applied, and the TUT input and output are acquired. As for AC conditions, a suitable number  $N_p$  of periods of both the input and output quantities are acquired, then two periodic sequences of length  $N_s$ , whose generic elements are denoted by  $x[i]$  and  $y[i]$  respectively, are built up. Finally, a proper averaging procedure is applied to reduce the random effects on the above elements. Two sequences of length  $N_s/N_p$  are then obtained, whose generic elements  $\bar{x}[i]$  and  $\bar{y}[i]$  are defined as follows:

$$\bar{x}[i] = \frac{1}{N_p} \sum_{k=0}^{N_p-1} x\left[i + k \frac{N_s}{N_p}\right] \quad (5A.6)$$

$$\bar{y}[i] = \frac{1}{N_p} \sum_{k=0}^{N_p-1} y\left[i + k \frac{N_s}{N_p}\right] \quad (5A.7)$$

The calibration curve relates the two sequences. A regression technique is used to fit the curve with a straight line forced to cross the axes origin; finally the indexes  $\alpha$  and  $\beta$  are computed.

When the TUT is a voltage transducer, the block diagram in Figure 5-25 turns into the circuit in Figure 5-26. U-U denotes the voltage-to-voltage transducer under test, V refers to a suitable voltage source and DAQ<sub>in</sub> and DAQ<sub>out</sub> refer to digital multimeters (DMM) used as high-accuracy data acquisition boards. The calibrator Wavetek Datron 4800 has been used as voltage source. It can provide 1000 V at 33 kHz and its nominal accuracy specifications are: 6 ppm for DC voltage; 50 ppm for AC voltage. The zero-to-full-range linearity is lower than 0.1 ppm of full scale. Two HP3458A have been used as DAQ boards.

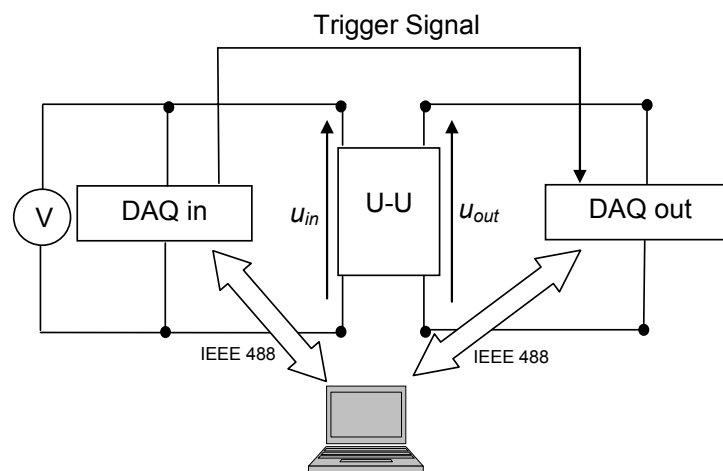


**Figure 5-26** Schematic block diagram of the calibration setup in case of voltage transducers. Each DMM is controlled by a personal computer (PC) via an IEEE 488-based interface. The digital signals are stored, in 16-bit format, in the PC in order to be processed. The storing format is compatible with a limit of the protocol used. The DMMs can feature two real-time sampling procedures: direct sampling and DCV digitizing. Direct-sampling operation is characterized by a maximum sampling rate of 50 kSa/s with 16-bit resolution; the input range can vary from 10 mV to 1000 V. In case of direct sampling the nominal best accuracy is 0.02% of reading and the offset voltage is 8 mV and 800 mV in the 10V-range and 1000V-range, respectively, which are the ones used in the experiments. The nominal accuracy specifications of DCV digitizing are: 0.005% of reading; offset voltage 500  $\mu$ V in the 1000-V range and 5  $\mu$ V in the 10V-range. The time jitter on the sampling period is lower than 50 ps for both configurations. DCV digitizing features lower noise level, higher resolution and double maximum sampling rate (100 kSa/s) respect to direct sampling. Its drawbacks are: greater jitter on the trigger arm and lower input bandwidth (30 kHz vs. 2 MHz for direct-sampling mode). Direct-sampling mode has been preferred

due to the following two main reasons: (i) the better resolution of DCV is lost by storing the data in 16-bit format; (ii) the bandwidth of 30 kHz did not fit the tests performed.

A master-slave configuration has been adopted to grant a nominally simultaneous sampling of the input and output waveforms during the tests. Figure 5-26 shows that DAQ<sub>in</sub> is set as master, whereas DAQ<sub>out</sub> is set as slave. Thus, the acquisition process of DAQ<sub>out</sub> starts simultaneously with the A/D conversion of DAQ<sub>in</sub>. To do this, DAQ<sub>in</sub> is programmed to trigger DAQ<sub>out</sub> when the A/D conversion starts. Of course, the DAQ<sub>out</sub> trigger is set as “external”, whereas the DAQ<sub>in</sub> one is set as internal and “level” (zero crossing). This way, the simultaneous acquisition is independent of the delay introduced by the analog conditioning blocks of both instruments. The nominal trigger latency, i.e. the time delay between the trigger and the beginning of the measurement, is specified to be lower than 125 ns for an external trigger and lower than 700 ns for zero crossing; the nominal jitter standard deviation is lower than 2 ns.

A time skew between the starting instant of the acquisition at the two sides of the TUT is expected to occur due to the following reasons: (i) different DMMs feature different latencies; (ii) there is a time delay between the beginning of the A/D conversion of the master and the output of the external trigger signal; (iii) a time delay occurs between the trigger-in and the start of the acquisition performed by the slave. The time skew has been measured according to the procedure described in what follows.

Voltage transducers LEM CV 3-1000 have been calibrated by means of the equipment implemented. They feature the following nominal specifications: 1000-V maximum input voltage; 500-kHz bandwidth (-1 dB); 1000 V : 10 V conversion ratio; accuracy (referred to as overall accuracy in the data sheets) 0.2% at full scale; 5-mV offset.

### 5A.5. Uncertainty sources in the equipment

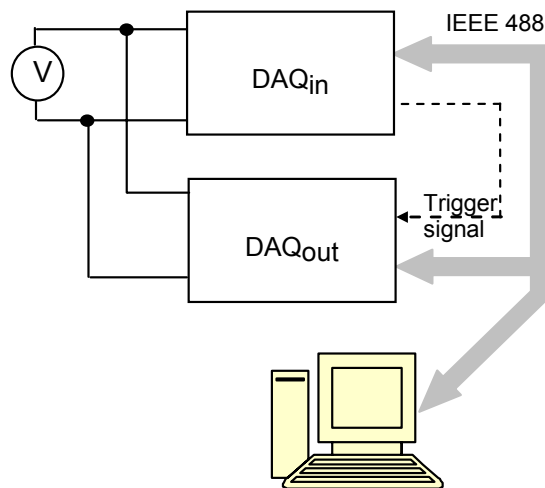


Figure 5-27 Circuit for the measurement of the time delay  $T_d$

The simultaneous sampling of the TUT input and output signals is the main task in the proposed calibration procedure, given that the acquisition processes are only nominally simultaneously performed by the two DAQs. A time delay  $T_d$  between their starting instants has been evaluated by means of the system in Figure 5-27 by applying the same sinusoidal signal to both the sampling devices, which are connected and controlled as described in the previous Section. Different values of the signal amplitude and frequency, along with different input ranges of the DAQs, have been used in the tests. 30 tests have been performed for each test condition in order to understand whether there is a relationship between  $T_d$  and the above parameters.

The value of  $T_d$  has been determined by measuring the phase shift between the two acquired sinusoidal waveforms. Table 5-6 reports both its statistical mean value  $\mu(T_d)$  and the relevant sampling standard deviation  $s(T_d)$  vs. the test frequencies. The values in Table 5-6 have been confirmed by the results of tests performed at different input ranges and not reported here just for the sake of simplicity. They lead to conclude that  $T_d$  can be assumed constant and equal to 12  $\mu\text{s}$ , since in all cases  $s(T_d)$  is at least two order of magnitude lower than  $\mu(T_d)$ . Hence,  $\mu(T_d)$  is a bias; it has been corrected by means of an ad-hoc algorithm before evaluating  $\alpha$  and  $\beta$ . Of course, the uncertainty  $u(T_d) = s(T_d)$  in the bias estimation also affects  $\alpha$  and  $\beta$ .

**Table 5-6**  $\mu(T_d)$  and  $s(T_d)$  for some of the different test conditions

Frequency [Hz]	$\mu(T_d)$ [s]	$s(T_d)$ [s]
50	$1.17 \cdot 10^{-5}$	$1 \cdot 10^{-7}$
1000	$1.18 \cdot 10^{-5}$	$0.4 \cdot 10^{-7}$
3000	$1.18 \cdot 10^{-5}$	$0.3 \cdot 10^{-7}$

Now, let us analyze the effects of the uncertainty sources located in the hardware of the calibration equipment and how their effects propagate in the algorithm used to compute  $\alpha$  and  $\beta$ . This way, the standard uncertainties  $u(\alpha)$  and  $u(\beta)$  can be estimated. In addition to  $u(T_d)$ , the following effects of the other uncertainty sources have to be analyzed:

- the offset of both the DAQs, whose values we denote by  $O_{in}$  and  $O_{out}$ , respectively;
- the percentage of reading of  $DAQ_{in}$  as well as  $DAQ_{out}$ , whose values we denote by  $R_{in}$  and  $R_{out}$ , respectively;
- the time jitter on the sampling period.

A Monte-Carlo simulation procedure consisting of 10,000 trials has been performed to evaluate the expanded uncertainty on  $\alpha$  and  $\beta$ . Such parameter is expressed as the shortest coverage interval corresponding to the confidence level of 95% [4].

The measurement algorithm evaluates in each trial: a) the average periods of both input and output signals; b) the best-fit straight line by applying the least square method; c)  $\alpha$

and  $\beta$  by means of (5A.3) and (5A.4). According to the accuracy specifications formerly reported, the time jitter on the sampling period is some ppm of the period itself and, hence, negligible. In the simulations, the effects of the remaining uncertainty sources have been assumed to be independent random variables with uniform distribution and zero expected value. They are denoted by  $o_{in}$ ,  $o_{out}$ ,  $r_{in}$ ,  $r_{out}$ ,  $t_d$ , hence,  $o_{in} \in [-O_{in}, O_{in}]$ ,  $o_{out} \in [-O_{out}, O_{out}]$ ,  $r_{in} \in [-R_{in}, R_{in}]$ ,  $r_{out} \in [-R_{out}, R_{out}]$ ,  $t_d \in [-u(T_d)\sqrt{3}, u(T_d)\sqrt{3}]$ .

The time delay  $T_d$  is constant in each trial. Indeed,  $t_d$  belongs to a set of totally correlated random variables. The same condition is assumed for  $o_{in}$ ,  $o_{out}$ ,  $r_{in}$ ,  $r_{out}$ , given that the offset is a constant contribution to all the samples of the considered data set whereas the percentage of reading leads to a contribution proportional to the sample value, with constant proportionality factor. The values of the above random variables are constant in a single trial but randomly vary over the whole range of test.

The equipment described has been used for the metrological characterization of a statistical sample of nine voltage-to-voltage transducers LEM CV 3-1000. In the case of DC tests, input signals varying from 50 V to 750 V by steps of 50 V have been used. For each magnitude value, the averaging procedure recalled in the previous Section has been applied to 200 samples acquired with 2000 Sa/s frequency. As for AC tests, the RMS value of the sinusoidal input was kept constant, equal to 500 V, whereas the signal frequency has been varied in the interval [50 Hz, 3 kHz]. The maximum frequency has been chosen according to the requirements of both the IEEE Standard [12] and the European Standard [13] relevant to the harmonics evaluation. In each test, the above averaging procedure has been applied to five periods of the input signal.

Table 5-7 a) and b) reports the maximum absolute values  $A$  and  $B$  of  $\alpha$  and  $\beta$  vs. frequency, along with the relevant coverage intervals associated to the 95% coverage probability. The confidence intervals reported in Table 5-7 are effects of the uncertainty sources located in the equipment hardware on the estimation of the indexes  $\alpha$  and  $\beta$ .

**Table 5-7** Values of  $A$  and  $B$  and relevant confidence intervals for different input frequencies (RMS input value: 500 V; coverage probability 95%)

**5-7 a)**

Frequency	$A$	confidence interval
DC	$1.8 \cdot 10^{-3}$	$[1.5, 2.1] \cdot 10^{-3}$
50 Hz	$1.2 \cdot 10^{-3}$	$[0.9, 1.5] \cdot 10^{-3}$
1000Hz	$1.4 \cdot 10^{-3}$	$[1.0, 1.7] \cdot 10^{-3}$
3000 Hz	$9.0 \cdot 10^{-3}$	$[8.7, 9.5] \cdot 10^{-3}$

**5-7 b)**

Frequency	$B$	confidence interval
DC	$0.7 \cdot 10^{-3}$	$[0.54, 1.0] \cdot 10^{-3}$



50 Hz	$3.7 \cdot 10^{-3}$	$[2.2, 5.7] \cdot 10^{-3}$
1000Hz	$6.6 \cdot 10^{-3}$	$[5.1, 8.5] \cdot 10^{-3}$
3000 Hz	$20 \cdot 10^{-3}$	$[18, 23] \cdot 10^{-3}$

Figure 5-28 and Figure 5-29 show the histograms of the relative occurrences of  $\alpha$  and  $\beta$ , respectively. The histograms have been determined for the transducers corresponding to the data reported in the 50-Hz row of Table 5-7. Both frequency distributions are triangular and are valid for all the characterized transducers. This is due to the limited number of random variables considered (assumed to have uniform density functions), on the basis of the Central Limit Theorem.

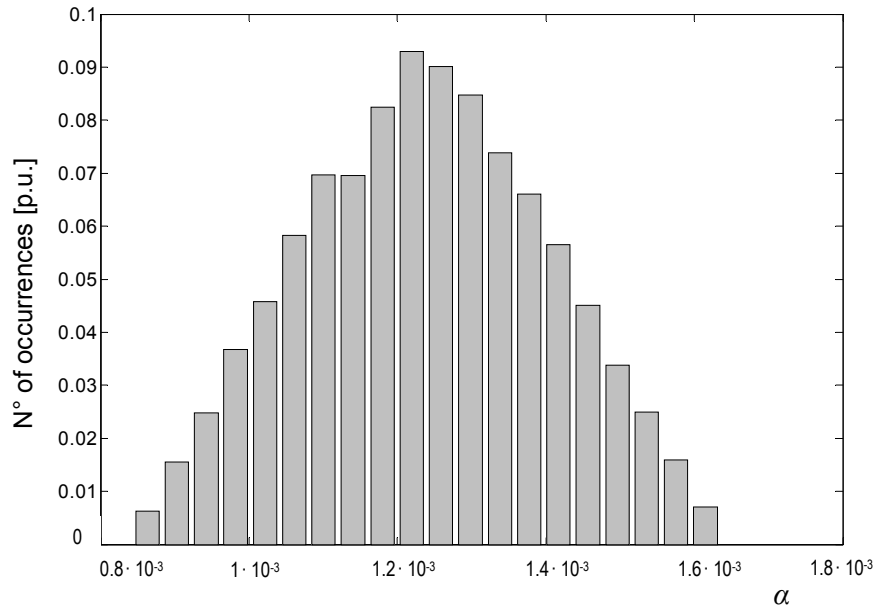


Figure 5-28 Histogram of the relative occurrences of  $\alpha$  at 50 Hz (p.u.: per unit)

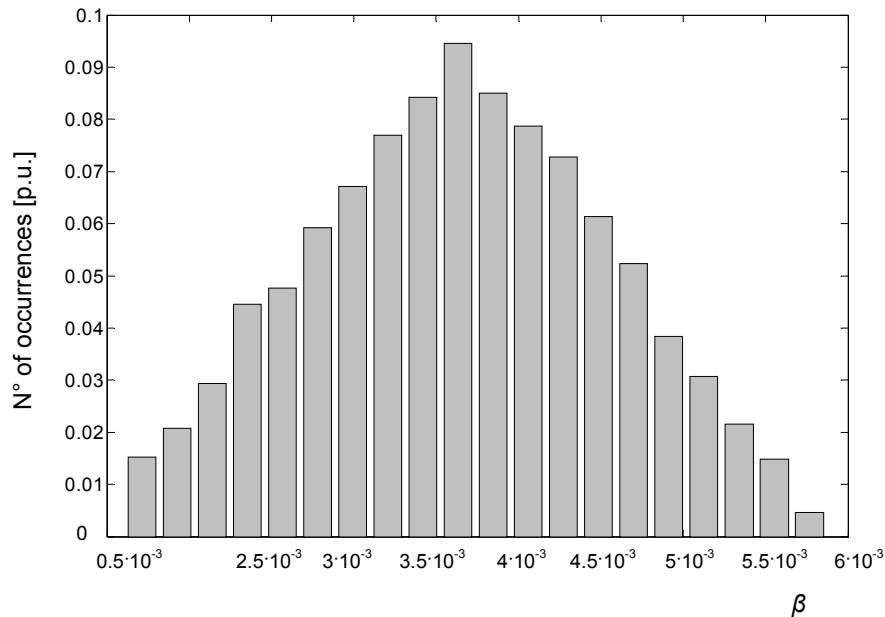


Figure 5-29 Histogram of the relative occurrences of  $\beta$  at 50 Hz (p.u.: per unit)

The standard deviations  $\sigma_\alpha$  and  $\sigma_\beta$  of the random variables  $\alpha$  and  $\beta$  can be expressed as functions of independent random variables with uniform distribution:

$$\sigma_\alpha = \sqrt{\text{Var}\{\alpha\}} = \sqrt{\left(\frac{\sum_i x_i y_i}{\sum_i x_i^2}\right)^2 \frac{(R_{in}^2 + R_{out}^2)}{3}} \cong R_{in} \sqrt{\frac{2}{3}} \quad (5A.8)$$

$$\sigma_\beta = \sqrt{\text{Var}\{\beta\}} = \frac{1}{y_{FS}} \sqrt{\frac{2}{3}} \sqrt{4(x_j R_{in})^2 + O_{in}^2} \quad (5A.9)$$

Such expressions can be demonstrated as follows. Recalling (5A.3):  $\alpha = (g - g_n) / g_n$ , by assuming  $g_n = 1$  provides:  $\alpha = g - 1$ .

If  $g$  is evaluated through the least mean square method, then it is:

$$\alpha = \frac{\sum_i x_i y_i}{\sum_i x_i^2} - 1 \quad (5A.10)$$

For the sake of simplicity, only the random variables  $o_{in}$ ,  $o_{out}$ ,  $r_{in}$ ,  $r_{out}$  are taken into account for each DAQ. Under these assumptions, the following expression for  $\alpha$  holds:

$$\begin{aligned} \alpha &= \frac{\sum_i [x_i + (r_{in} x_i + o_{in})] \cdot [y_i + (r_{out} y_i + o_{out})]}{\sum_i [x_i + (r_{in} x_i + o_{in})]^2} - 1 \cong \\ &\cong \frac{\sum_i x_i y_i + \sum_i x_i (r_{out} y_i + o_{out}) + \sum_i y_i (r_{in} x_i + o_{in})}{\sum_i x_i^2 + 2 \sum_i x_i (r_{in} x_i + o_{in})} - 1 \end{aligned} \quad (5A.11).$$

In (5A.11) the second-order contributions are neglected. By also assuming that the input signal is alternative, we get:

$$\alpha \cong \frac{\sum_i x_i y_i + r_{out} \sum_i x_i y_i + r_{in} \sum_i x_i y_i}{\sum_i x_i^2 + 2r_{in} \sum_i x_i^2} - 1 = \frac{[1 + r_{in} + r_{out}] \sum_i x_i y_i}{(1 + 2r_{in}) \sum_i x_i^2} - 1 \quad (5A.12)$$

(5A.12) can be rewritten as follows:

$$\begin{aligned} \alpha &= \frac{[1 + r_{in} + r_{out}] \sum_i x_i y_i}{(1 + 2r_{in}) \sum_i x_i^2} \frac{(1 - 2r_{in})}{(1 - 2r_{in})} - 1 = \frac{[1 + r_{in} + r_{out} - 2r_{in}] \sum_i x_i y_i}{\sum_i x_i^2} - 1 = \frac{[1 + r_{in} + r_{out}] \sum_i x_i y_i}{\sum_i x_i^2} - 1 \\ \alpha &= \frac{\sum_i x_i y_i}{\sum_i x_i^2} + \frac{(r_{in} + r_{out}) \sum_i x_i y_i}{\sum_i x_i^2} - 1 \end{aligned} \quad (5A.13)$$

Under the assumption of independent random variables with uniform distribution, the expression of the standard deviation  $\sigma_\alpha$  of  $\alpha$  is:

$$\sigma_{\alpha} = \sqrt{\text{Var}\{\alpha\}} = \sqrt{\left(\frac{\sum_i x_i y_i}{\sum_i x_i^2}\right)^2 \frac{(R_{in}^2 + R_{out}^2)}{3}} \cong \sqrt{\frac{2}{3} R_{in}^2} \quad (5A.14)$$

which is identical to (5A.8) under the assumptions:  $R_{in} = R_{out}$  (given that the two DAQs are of the same model), and:  $\sum_i x_i y_i / \sum_i x_i^2 \cong 1$ . Equation (5A.8) allows to estimate the

uncertainty affecting  $\alpha$  on the basis of the nominal accuracy specifications of the DAQs.

As far as the standard deviation  $\sigma_{\beta}$  of the random variable  $\beta$  is concerned, let us recall

$$(5A.4): \beta = \frac{\max\left\{\left|\bar{u}_{out}[n] - g \cdot \bar{u}_{in}[n]\right|\right\}}{\max\left\{\left|\bar{u}_{out}[n]\right|\right\}}. \text{ By taking into account the uncertainty contributions}$$

that affect the generic samples  $x_i$  and  $y_i$ , it becomes:

$$\begin{aligned} \beta &= \frac{\max_i \left| (y_i + r_{out} y_i + o_{out}) - \left[ \frac{\sum_i x_i y_i}{\sum_i x_i^2} + \frac{\sum_i x_i y_i}{\sum_i x_i^2} (r_{in} + r_{out}) \right] (x_i + r_{in} x_i + o_{in}) \right|}{y_{FS} + r_{out} y_{FS} + o_{out}} \cong \\ &\cong \frac{\max_i \left| \left( y_i - \frac{\sum_i x_i y_i}{\sum_i x_i^2} x_i \right) + r_{out} y_i + o_{out} - \frac{\sum_i x_i y_i}{\sum_i x_i^2} r_{out} x_i - 2 \frac{\sum_i x_i y_i}{\sum_i x_i^2} r_{in} x_i - \frac{\sum_i x_i y_i}{\sum_i x_i^2} o_{in} \right|}{y_{FS} + r_{out} y_{FS} + o_{out}}. \end{aligned} \quad (5A.15)$$

The approximations  $x_i = y_i$  and  $\sum_i x_i y_i / \sum_i x_i^2 = 1$ , lead to:

$$\begin{aligned} \beta &\cong \frac{\max_i \left| \left( y_i - \frac{\sum_i x_i y_i}{\sum_i x_i^2} x_i \right) + o_{out} - 2r_{out} x_i - 2r_{in} x_i - o_{in} \right|}{y_{FS} + r_{out} y_{FS} + o_{out}} = \\ &= \frac{\max_i \left| \left( y_i - \frac{\sum_i x_i y_i}{\sum_i x_i^2} x_i \right) - 2x_i (r_{out} + r_{in}) + o_{out} - o_{in} \right|}{y_{FS} + r_{out} y_{FS} + o_{out}} \end{aligned} \quad (5A.16)$$

The term  $r_{out} \cdot (y_{FS} + o_{out})$  can reasonably be neglected, in fact one could easily show that it only provides second-order contributions. Hence, the final expression for  $\beta$  becomes:

$$\beta = \frac{\max_i \left| \left( y_i - \frac{\sum_i x_i y_i}{\sum_i x_i^2} x_i \right) - 2x_i (r_{out} + r_{in}) + o_{out} - o_{in} \right|}{y_{FS}}. \quad (5A.17)$$

The expression of the standard deviation  $\sigma_\beta$  of  $\beta$  can then be obtained by considering the value  $j$  of the index  $i$  that provides  $\beta$ .

$$\sigma_\beta = \sqrt{\text{Var}\{\beta\}} = \sqrt{\frac{4x_j^2(R_{out}^2 + R_{in}^2) + O_{out}^2 + O_{in}^2}{3y_{FS}^2}}. \quad (5A.18)$$

Finally, if we take  $R_{in} = R_{out}$  and  $O_{in} = O_{out}$ , then (5A.18) becomes:

$$\sigma_\beta = \sqrt{\text{Var}\{\beta\}} = \frac{1}{y_{FS}} \sqrt{\frac{2}{3}} \sqrt{4(x_j R_{in})^2 + O_{in}^2}, \quad (5A.19)$$

which is identical to (5A.9). It depends on the value of  $x_j$ . However, if  $x_j = y_{FS}$  is taken, then:

$$\sigma_\beta \leq \sqrt{\frac{2}{3}} \sqrt{4R_{in}^2 + \frac{2}{3y_{FS}^2} O_{in}^2} = \max(\sigma_\beta), \quad (5A.20)$$

Also the maximum value of  $\sigma_\beta$  only depends on the accuracy specifications of the sampling devices.

Actually, the effect of the delay contribution  $u(T_d)$  has not been taken into account in (5A.8) and (5A.9); anyway, by assuming  $x_j = y_{FS}$ ,  $\sigma_\beta$  has been overestimated. The results of (5A.8) and (5A.9) are compared in Table 5-8 with the sampling standard deviations  $s_\alpha$  and  $s_\beta$  of the distributions in Figure 5-28 and Figure 5-29, respectively. The comparison shows that (5A.8) and (5A.9) are useful to foresee the uncertainty affecting  $\alpha$  and  $\beta$  without heavy computations. Hence, an equipment implementing the method described can be properly designed. Moreover, forecasting the values of  $s_\alpha$  and  $s_\beta$  provides information on the minimum values of  $\alpha$  and  $\beta$  that the equipment can measure. Finally, Table 5-8 also confirms that  $u(T_d)$  at 50 Hz is negligible.

**Table 5-8** Comparison between  $s_\alpha$ ,  $s_\beta$ , and  $\sigma_\alpha$ ,  $\sigma_\beta$  of the random variables in Figure 5-28 and in Figure 5-29

$s_\alpha$	$\sigma_\alpha$	$s_\beta$	$\sigma_\beta$
$1.634 \cdot 10^{-4}$	$1.631 \cdot 10^{-4}$	$9.07 \cdot 10^{-4}$	$9.64 \cdot 10^{-4}$

**References:**

- [1] Model VD305A capacitive voltage divider, 2006 Pearson Electronics, Inc.
- [2] J. Czajewski, "The Accuracy of the Global Positioning Systems", IEEE Instrumentation and Measurement Magazine, March 2004, pp. 56-60.
- [3] ISO "Guide to the expression of uncertainty in Measurement", International Standardization Organization, Geneva (Switzerland), 1995.
- [4] Evaluation of Measurement data - Supplement 1 to the "Guide to the Expression of Uncertainty in Measurement" – propagation of distribution using a Monte Carlo method, Joint Committee for Guides in Metrology, Final Draft September 2006.
- [5] Jaynes, E. T. Information theory and statistical mechanics. Phys. Rev 106 (1957), 620–630.
- [6] U. Pogliano, "Use of integrative analog-to-digital converters for high precision measurement of electrical power", *IEEE Trans. on Instr. Meas.*, vol. 50, no. 5, pp. 1315-1318, Oct. 2001.
- [7] M. Kampik, H. Laiz and M. Klonz, "Comparison of three accurate methods to measure AC voltage at low frequencies", *IEEE Trans. on Instr. Meas.*, vol. 49, no. 2, pp. 429-433, Apr. 2000.
- [8] IEC Std. 60044-1, "Instrument transformers – Part 1: Current transformers", International Electrotechnical Commission, Geneva (Switzerland), 1996.
- [9] IEC Std. 60044-2, "Instrument transformers – Part 2: Inductive voltage transformers", International Electrotechnical Commission, Geneva (Switzerland), 1997.
- [10] IEC Std. 60044-7, "Instrument transformers – Part 7: Electronic voltage transformers", International Electrotechnical Commission, Geneva (Switzerland), 1999.
- [11] IEEE Std. 1241-2000, "IEEE Standard for terminology and test methods for analog-to-digital converters", The IEEE, New York (USA), 2001.
- [12] IEEE Std. 1159-1995, "Recommended practice for monitoring electric power quality", The IEEE, Piscataway (USA), November 1995.
- [13] EN 50160, "Voltage characteristics of electricity supplied by public distribution systems", CENELEC, Bruxelles (Belgium), 1999.
- [14] A. Ferrero, M. Lazzaroni, S. Salicone, "A calibration procedure for a digital instrument for power quality measurement", *IEEE Trans. on Instr. Meas.*, vol. 51, no. 4, pp. 716-722, August 2002.
- [15] N. Locci, C. Muscas, E. Ghiani, "Evaluation of uncertainty in digital processing of quantized data", *Measurement*, vol. 32, no. 4, December 2002, pp. 265-272.
- [16] A. Ferrero, S. Salicone, "An innovative approach to the determination of uncertainty in measurement based on fuzzy variables ", *IEEE Trans. Instr. Meas.*, vol.52, no. 4, pp. 1174-1181, 2003.
- [17] National Instruments, "The measurement and automation catalog, 2004", Austin (USA), 2004.
- [18] 3GPP specification 45.002 "Multiplexing and Multiple Access on the Radio path".



## **6. Design and Characterization of an Electric field based Medium-Voltage Transducer**

Power quality measurement instruments, especially those in portable packages, are generally provided with inputs designed for low-voltage applications. Some permanently installed PQ measurement instruments are mounted at a distance from the point of the circuit where the parameters are to be measured. In both cases, a suitable transducer might be needed, to step down the voltage, to isolate the input circuits from the system voltage, or to transmit the signals over some distance. To accomplish any of these functions, a transducer may be used, provided that its characteristics are suitable for the parameter of interest.

In low-voltage systems, PQ measurement instruments are generally connected direct to the voltage point of interest, but transducers are often used for current measurements. In medium- and high-voltage systems, transducers are used for both voltage and current PQ measurements.

There are two important concerns using transducers: – signal levels: signals levels should use the full scale of the instrument without distorting or clipping the desired signal; – frequency and phase response: these characteristics are particularly important for transient and harmonic measurements.

In order to avoid incorrect measurements the full-scale rating, linearity, frequency and phase response, and burden characteristics of the transducer should be carefully considered [1].

### **6.1. Voltage transducers**

The most common voltage transducer is the voltage transformer. Two types of voltage transformers can be considered: those used by protective relay circuits, and those used by metering circuits. The first type is sized so as to provide a correct response even in the case of overvoltages due to an unbalanced short circuit. The second, in contrast, is designed to protect meters from network overvoltages. In the latter category, in case of saturation, distortion of the delivered signal will occur. Where monitoring is attached to a voltage transformer which is also used for other functions (for example, metering), one must be careful that the additional burden do not affect the calibration or uncertainty of such other functions. One should be careful when making connections to the secondary circuit of a transformer used for a protective relay. Connection errors might cause the relay to inadvertently trip.

In general, transformer-type electromagnetic voltage transducers have frequency and transient responses suitable up to typically 1 kHz; but the frequency range may

sometimes be limited to well below 1 kHz, and sometimes may extend to a few kilohertz. Simple capacitor dividers can have frequency and phase responses that are suitable up to hundreds of kilohertz or even higher; however, in many applications a resonant circuit is intentionally added, making the frequency response of the capacitive divider unsuitable for measurements at any frequency other than the fundamental. Resistive voltage dividers may have frequency and phase response suitable up to hundreds of kilohertz. However, they may introduce other problems, for example, the capacitive load of the measurement instrument can influence the frequency and phase response of the resistive voltage dividers.

There are two important concerns that must be addressed when selecting transducers for a.c. mains transients. First, signal levels should use the full scale of the instrument without distorting or clipping the desired signal. Second, the frequency response (both amplitude and phase) of the transducer should be adequate for the expected signal.

Voltage transducers should be sized to prevent measured disturbances from inducing saturation. For low-frequency transients, this requires that the knee point of the transducer saturation curve be at least 200 % of the nominal system voltage. The frequency response of a standard metering class Voltage transducer depends on its type and the burden applied. With a high impedance burden, the response is usually adequate to at least 2 kHz, but it can be less. Capacitive-coupled voltage transformers generally do not provide accurate representation of any higher frequency components. High-frequency transient measurements require a capacitor divider or pure resistive divider. Special purpose capacitor dividers can be obtained for measurements requiring accurate characterization of transients up to at least 1 MHz.

For both voltage and current, the spectra of common test waveforms for a.c. mains transients (see Figure 6-1) contain frequencies that range up to approximately 10 MHz (lasting for 200  $\mu$ s), with large amplitudes up to 1 MHz (lasting for 2 ms). For end-use a.c. mains connections, the amplitudes of common test waveforms range up to 6 kV, and up to 5 kA. The sampling rate must therefore be at least twice the maximum frequency of the waveform; also, the corresponding anti-alias filter must have appropriate characteristics.

On the one hand, for low voltage power systems there are different solutions to measure power quality, in fact the market offers several commercial transducers featuring wide bandwidth and linear characteristic for reasonable costs. Most of the transducers include an electronic circuit, hence they can be considered “active” devices: current transformers exploit Hall-effect based sensors or Rogowski coil followed by the analog conditioning circuit, whereas active voltage transformers can be made of resistive dividers combined with suitable isolating amplifiers or use the same Hall-effect probe with a shunt resistor at



the input of the conditioning stadium. Passive current transformers improving performance respect to the traditional ones are windings with compensating capacitors.

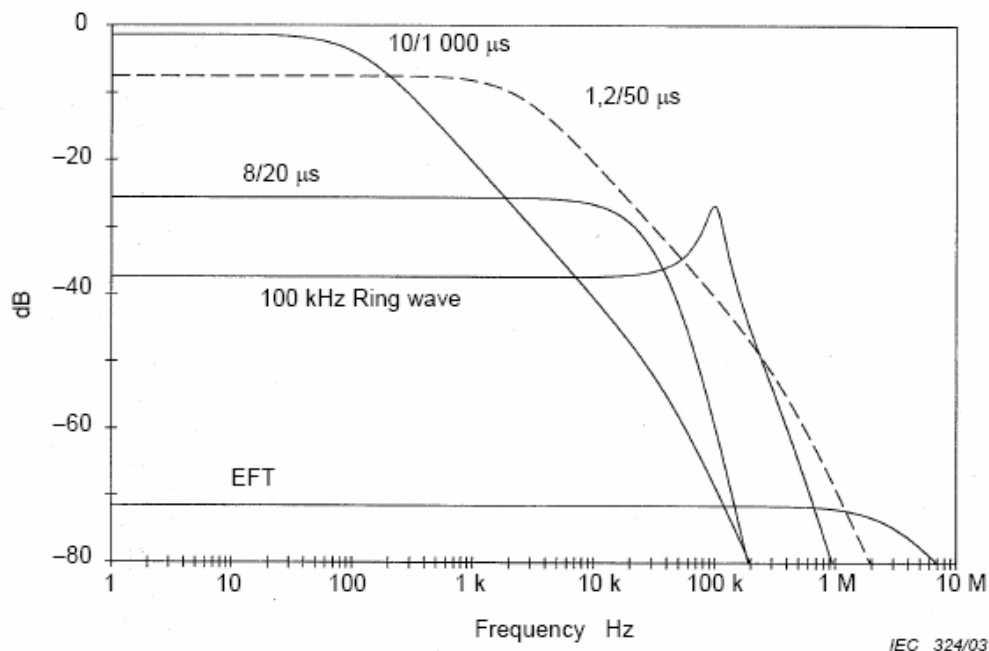


**Figure 6-1** Frequency spectrum of typical representative transient test waveforms

On the other hand, as a consequence of the recent recommendations of national regulators [2, 3], some utilities have shown increasing interest in power quality measurements, with reference to transmission and especially distribution lines. Presently, Italy, Norway, Portugal and Slovenia are using so-called “*voltage quality monitoring system*” on both distribution and transmission lines. In Hungary only distribution lines are monitored whereas Czech Republic and Spain are planning measurement activities. Unfortunately, wideband commercial transducers suitable for such applications are expensive and hard to install in usual medium-voltage substations. Therefore, measurement campaigns are often limited to a very small portion of network. As far as the scientific community proposals are concerned, the use of optical voltage transducers is dealt with in some papers [4 - 6]. An interesting solution to optically supply active voltage transducers is proposed in [7].

In order to decrease significantly the cost of the distributed measurement system developed during the PhD research activity, a part from reducing the number of remote units to be installed on the network by adopting the wavelet-based algorithm, it is important to find the cheapest version of the hardware needed in each channel of a slave station. The most expensive block in the measurement chain described in cap 5a is the voltage transducer, i.e. the capacitive voltage divider by Pearson Electronics. The research has then been focused to develop a different transducer which could perform similarly but cost much less than it. The main requirements to be fulfilled were: a)

bandwidth suitable also for transient measurements; b) good accuracy; c) isolation level suitable for MV systems; d) easy and fast installation on the line to be monitored.

The solution adopted is an active voltage transducer obtained as combination of an electric field probe and the suitable conditioning circuit, so that no electric contact is needed between the device input and the conductor of the line on which it is installed. In this case the IEC Standard 60044-7 [8] relevant to Electronic Voltage Transformers has been taken into account as reference document for: ratings setting (standard values of primary voltage and output voltage); accuracy class designation (according to the voltage error and phase displacement introduced by the instrument); insulation requirements; and the corresponding tests.

### **6.2. *Electric field strength meters***

The purpose of IEEE Standard 644-1994 [9] is to establish uniform procedures for the measurement of power frequency electric and magnetic fields from alternating current overhead power lines and for the calibration of the meters used in these measurements. A uniform procedure is a prerequisite to comparisons of electric and magnetic fields of various ac overhead power lines. These procedures apply to the measurement of electric and magnetic fields close to ground level, but even to electric field measurements near an energized conductor or structure.

Electric field strength meters consist of two parts: the probe or field sensing element and the detector which processes the signal from the probe and indicates the RMS value of the electric field strength in units of V/m using an analog or digital display. For commercially available free-body meters, the detector is usually contained in, or is an integral part of, the probe. The probe and detector are introduced into an electric field on an insulating handle. The detector measures the steady-state induced current or charge oscillating between the conducting halves (electrodes) of the probe. In Standard IEEE 1308-1994 [10] the following three types of electric field meters are considered:

- a) The free-body meter
- b) The ground reference meter
- c) The electro-optic meter.

When measurements of the electric field strength are performed, the observer must be sufficiently removed from the probe to avoid significant perturbation of the field at the location of the probe. Free-body and electro-optic type meters should be sufficiently small so that the size of the probe does not significantly perturb the charge distributions on boundary surfaces generating the electric field, i.e., energized and grounded surfaces. Although field meters are calibrated in nearly uniform electric fields, the field that is measured need not be very uniform. Electric field meters measure the projection of the

oscillating (linearly polarized) or rotating (elliptically or circularly polarized) electric field vector onto the electrical axis of the probe (the axis of greatest electric field sensitivity). The three types of meters used to measure the electric field strength from ac power lines are described in the following.

### 6.2.1. Free-Body meter

It measures the steady-state induced current or charge oscillating between two halves of an isolated conductive body in an electric field. The free-body meter is suitable for survey-type measurements because it is portable, allows measurements above the ground plane, and does not require a known ground reference. Therefore, this type of meter is recommended for outdoor measurements near power lines. The size of the probe should be such that charge distributions on the boundary surfaces generating the electric field (energized and ground surfaces) are, at most, weakly perturbed when the probe is introduced for measurement. The electric field should be approximately uniform in the region where the probe will be introduced. Probes can be of any shape; however, meters commercially available are generally in the shape of rectangular boxes, with side dimensions ranging from ~7 to ~20 cm, as represented in Figure 6-2. The meters are calibrated to read the RMS value of the power frequency electric field component along the electrical axis (the axis of greatest electric field strength sensitivity).

There also exist free-body meters designed for remote display of the electric field strength. In this case, a portion of the signal processing circuit is contained in the probe and the remainder of the detector is in a separate enclosure with a digital display. A optic-fibre link connects the probe to the display unit. This type of probe is also introduced into an electric field on an insulating handle.

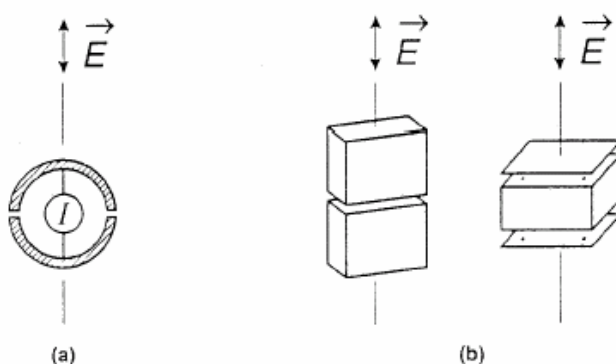


**Figure 6-2** Geometries of E-field probes: (a) spherical probe (b) commercial probes

In order to characterize the instrumentation adequately, the manufacturer should provide a detailed description of the electronics, as well as other relevant information. For example, if the field meter reading has a temperature dependence, the temperature coefficient should be provided. This permits the operator to correct E-field readings made outdoors using an instrument calibrated at room temperature. If the electrical axis of the

field strength meter is not coincident with the geometric axis, the departure in degrees and direction shall be specified.

Briefly, the theory of operation of free-body meters can be understood by considering an uncharged conducting free body with two separate halves introduced into a uniform field  $E$ . The charge induced on one of the halves is:

$$Q = \int_{S/2} \vec{D} \cdot d\vec{A} \quad (6.1)$$

Where  $\vec{D}$  is the electric displacement and  $d\vec{A}$  is an area element on half of the body with total surface area  $S$ . The case of spherical geometry (Figure 6-2) yields the result

$$Q = 3\pi a^2 \varepsilon_0 E \quad (6.2)$$

where  $a$  is the radius of the sphere and  $\varepsilon_0$  is the permittivity of free space.

The surface charge density is given by  $3\varepsilon_0 E \cos\theta$ . Integration over the hemisphere gives the previous equation. For less symmetric geometries, the result can be expressed as:

$$Q = k\varepsilon_0 E \quad (6.3)$$

where  $k$  is a constant dependent on geometry. Sensing electrodes resembling cubes and parallel plates (Figure 6-2) have been employed. If the electric field strength has a sinusoidal dependence, for example,  $E_0 \sin\omega t$ , the charge oscillates between the two halves and the current is given by:

$$I = \frac{dQ}{dt} = k\omega\varepsilon_0 E_0 \cos\omega t \quad (6.4)$$

If there are harmonics in the electric field, there will be an additional term on the right side of equation (6.4) for each harmonic. Because of the differentiation operation in equation (6.4), each of the additional terms will be weighted by the associated harmonic number. As for the magnetic field meter case, it is necessary for the detector to perform the inverse mathematical operation, namely integration, to recover the electric field waveform. This is accomplished by introducing a stage of integration. For example, an integrating amplifier or a passive integrating circuit combined with a voltmeter could be used as a detector. The frequency response of the probe-integrating detector combination should be made flat over the frequency range of interest. Filters should be used to exclude signals outside of the frequency range of interest.

It should be noted that the uniform  $E$ -field direction serves as an alignment axis for the field probe and that during field measurements this axis should be aligned with the field component of interest. The constant  $k$  can be thought of as a field strength meter constant and is determined by calibration. For more exact results, a second term not shown should be added to the right-hand side of equation (6.4) because of the presence of the dielectric handle held by the observer. The influence of the handle, representing a leakage

impedance, and the perturbation introduced by the observer are taken to be negligible in the above discussion.

The detector, although calibrated to indicate the RMS value of the power frequency field, may, depending on the detector circuit design, measure a) a quantity proportional to the average value of the rectified power frequency signal from the probe; b) The true RMS value of the signal.

The response of the detector to harmonic components in the  $E$ -field also depends on the design of the detector circuit. For example, in case a), because of the signal-averaging feature, an analog display will not necessarily indicate the RMS value of the composite  $E$ -field waveform (fundamental plus harmonics). For case b), the true RMS value of the electric field strength with harmonics could be observed if the detector circuit contained a stage of integration.

The frequency response of the free-body meter can be determined experimentally by injecting a known alternating current at various frequencies and observing the response.

The rated accuracy of the detector at power frequency is a function of the stability of its components at a given temperature and humidity and is generally high (<0.5% uncertainty).

### 6.2.2. Ground-Reference-Type meter

Such a device measures the current-to-ground from a flat probe introduced into an electric field. Flat ground-reference-type meters can be used only under special conditions. Electric field strength meters intended for characterization of radio-frequency electric fields should not be used to measure the electric field strength from ac power lines.

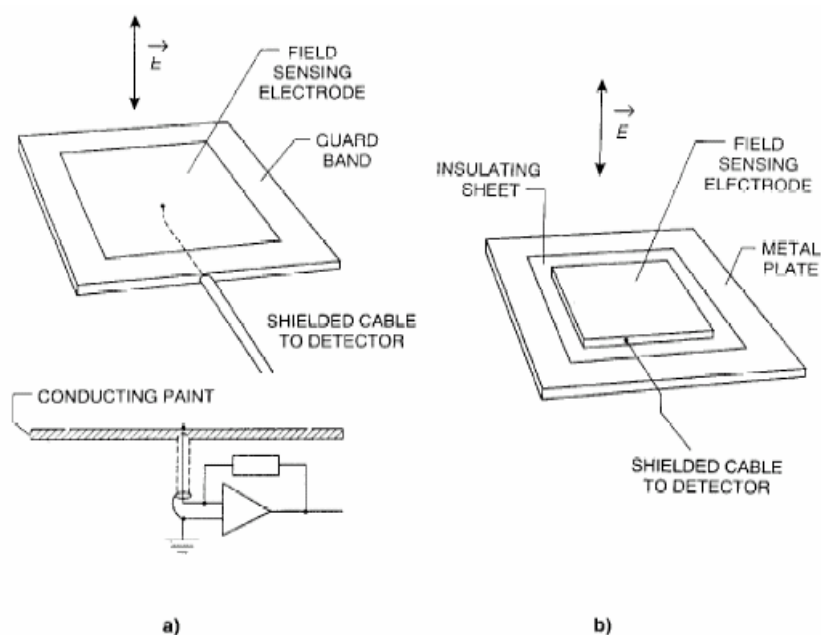


**Figure 6-3** Two designs for flat probes used with ground-referenced electric field meters.

Ground reference meters determine the electric field strength by measuring the current or charge on the sensing surface of a flat probe. Such meters are normally used to measure the electric field at ground level or on flat conducting surfaces that are at ground potential. Two probe designs, drawn in Figure 6-3 have been employed. One design makes use of a single flat conductor with an isolated central section that serves as the sensing surface. Small versions of this type of probe have been made with double-clad printed circuit board. A second design consists of two parallel plates separated by a thin sheet of insulation, with the top plate acting as the sensing surface. From Gauss Law, the charge,  $Q$ , induced on a sensing surface with area  $A$ , is:

$$Q = \epsilon_0 EA \quad (6.5)$$

where  $E$  is the average electric field strength across the sensing surface;  $\epsilon_0$  is the permittivity of free space.

Assuming that  $E$  varies sinusoidally with angular frequency  $\omega$ , i.e.,  $E = E_0 \sin \omega t$ , the resulting induced current is given by:

$$I = \omega \epsilon_0 EA \cos \omega t \quad (6.6).$$

### 6.2.3. Electro-optic meter

The probe used in this case is subject to the Pockels effect when it is introduced into the electric field to be measured. Electro-optic field meter is similar to the free-body meter in that it is suitable for survey type measurements, allows measurements at most points above the ground plane, and does not require a ground reference potential. The probe, which is separate from the detector, can be supported in the field with an insulating handle. The probe and detector are connected with optical fibers through which light from the detector is routed to and from the probe. In general, the probes are small in dimension (~2 cm) compared to free-body meter probes and this permits measurements closer to conducting surfaces because of the smaller interactions with the surface charge distributions. However, while smaller in size, Pockels effect probes have less sensitivity to electric fields (~5 kV/m and higher) compared to freebody meters (~1 V/m and higher) and are more expensive to fabricate.

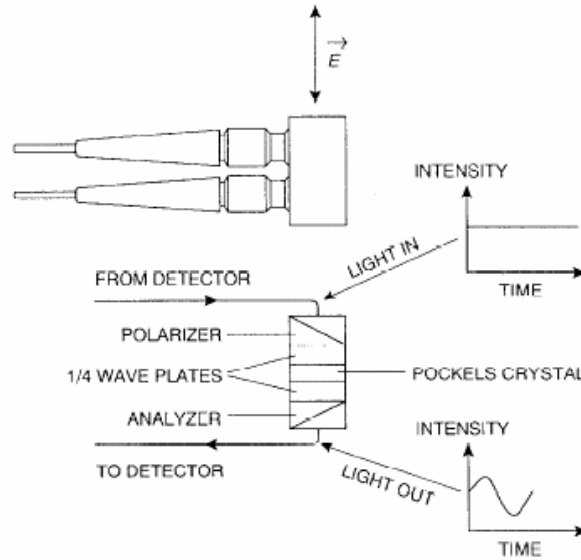


**Figure 6-4** Probe for Pockels-effect electric field meter - The amplitude of the modulation as light passes through the Pockels crystal and other optical elements provides a measure of the electric field  $E$ .

Figure 6-4 shows a sketch of a Pockels effect probe and its constituent components. Light originating in the detector is sent to and from the probe via optical fibers. The electric field  $E$  induces a birefringence in an appropriately oriented dielectric (Pockels) crystal that causes the intensity of the linearly polarized light to be modulated according to the relation

$$\frac{I_t}{I_i} = \frac{[1 + \sin(E'/F)]}{2} \quad (6.7)$$

where:

$I_t$  is the transmitted light

$I_i$  is the incident light

$E'$  is the electric field in the crystal

$F$  is equal to  $\lambda / 2\pi n^3 c_e l$ ;  $\lambda$  is the wavelength of light;  $n$  is the index of refraction;  $l$  is the crystal thickness;  $c_e$  is the electro-optic coefficient of the crystal.

For equation (6.7) to hold, it is assumed that the crystal has no intrinsic optical activity. Equation (6.7) shows that the amplitude of light modulation is a function of the electric field in the crystal that, in turn, is dependent on the external field  $E$ . Because the light transmission tracks the waveform of the electric field, a stage of integration is unnecessary in the detector to appropriately process signals due to harmonics that may be in the electric field. The Pockels crystal is sometimes coated with transparent electrodes to permit measurements of voltage using the Pockels effect. Electro-optic meters may be battery or mains operated.

### 6.2.4. Calibration of electric field strength meters

Parallel plate structures, single ground plates with guard rings, and current injection circuits have all been used for calibration purposes. Each is now briefly described.

#### **Parallel plates**

Uniform field regions of known magnitude and direction can be created for calibration purposes with parallel plates, provided that the spacing of the plates, relative to the plate dimensions, is sufficiently small. The uniform field value  $E_0$  is given by  $V/t$ , where  $V$  is the applied potential difference and  $t$  is the plate spacing. As a guide for determining plate spacing, the magnitudes of the electric field strength  $E$ , normalized by the uniform field, that is  $E/E_0$ , at the plate surface and midway between semi-infinite parallel plates are plotted as a function of normalized distance  $x/t$  from the plate edge in Figure 6-5.

Because nearby ground surfaces are always present, grading rings have been employed to grade the field at the perimeter of the structure and to provide isolation from surrounding perturbations. No exact theoretical treatment of the problem is available for rectangular geometries, but analytical solutions do exist for structures of cylindrical symmetry.

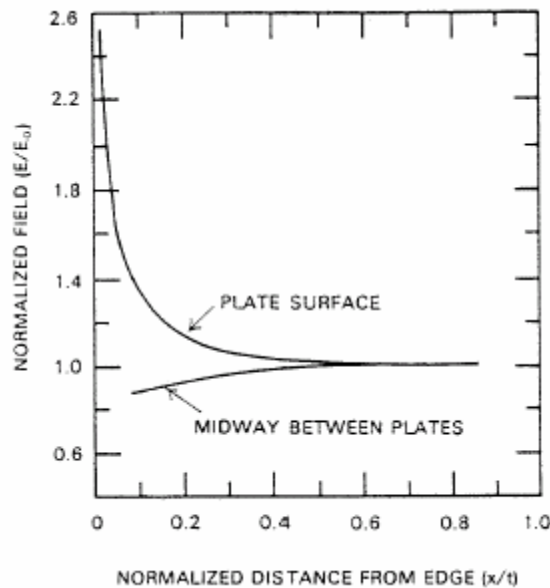


**Figure 6-5** Calculated normalized electric field at plate surfaces and midway between plates as function of normalized distance from edge of plate

Parallel plate structures can be energized with one plate at zero potential or both plates can be energized using a center tapped transformer. For example, stretched metal screens on 3 m x 3 m frames with a 1 m separation and four grading rings have been used to form a parallel plate structure. Potentials are applied to the grading rings using a resistive divider. Resistors that effectively “short out” stray capacitance between the grading rings and nearby surfaces are used. Theoretical considerations and experimental measurements indicate that energization of the plates using a center tapped transformer



provides a field that is more immune from nearby sources of perturbation than other energization schemes.

The electric field strength meter shall be calibrated periodically, with the frequency of calibrations depending in part on the stability of the meter. The meter shall be placed in the center of a parallel plate structure with the insulating handle normally used during measurements. The dimensions of the structure should be 1.5 m x 1.5 m x 0.75 m spacing. With these dimensions, no grading rings (or resistor dividers) are necessary to obtain a calibration field that is within 1% of the uniform field value  $V/t$ . It is assumed that the largest diagonal dimension of the electric field strength meter to be calibrated is no larger than 23 cm. The distance to nearby ground planes (walls, floors, etc.) shall be at least 0.5 m. The dimensions of the calibration apparatus may be scaled upward or downward for calibration of larger or smaller electric field strength meters.

### **6.2.5. Main sources of measurement uncertainty**

The measurement uncertainty during practical outdoor measurements using commercially available free-body meters is typically near 10%, although this figure can be reduced under more controlled conditions. The most likely sources of major errors are difficulty in positioning the meter, reading errors, handle leakage in some cases, temperature effects, and observer proximity effects. Because of interactions that can occur between the field meter probe and surface charge distributions on nearby conducting surfaces, the electric field measurement can be significantly perturbed if the probe is brought too close to the surface. Calculations show that this perturbation for a spherical probe is reduced to near 0.5% when the distance between a ground plane and the probe centre is three probe radii. Therefore, a spherical probe is not expected to have significant measurement error if a distance of two probe diameters is maintained between the probe and conducting surfaces. The diameter of probes with rectangular geometries can be conservatively estimated as the largest diagonal dimension of the probe.

Asymmetries in the design of an electric field meter probe can change the direction of the electrical axis (axis with greatest electrical sensitivity) with respect to the geometrical axis. Measurements performed with such an instrument may be more or less immune to observer proximity effects. In such cases, the observer proximity effect should be quantified before the field meter is used for measurements.

Because magnetic fields are typically produced at the same time as electric fields, electric field meters should be designed so that they are not significantly affected by magnetic fields at the levels anticipated in a given measurement environment. The coil system described in standard IEEE 1308 [10] for producing magnetic fields can be used to check for immunity to magnetic fields.

Electrical leakage via a grounded observer and surface contamination on the insulating handle of the meter may perturb the electric field beyond the normal geometric perturbation produced by the electrically floating probe. To check for handle leakage, the electric field meter should be oriented with its axis perpendicular to the direction of a known field. Significant electrical leakage would cause a nonzero reading. Such a reading, expressed as a percent of the actual field, would represent the order of magnitude of the uncertainty that could be caused by this mechanism. It is assumed for this check that the electrical and geometrical axes coincide.

Under high humidity conditions, a layer of surface condensation may form on parts of an electric field meter. The major source of uncertainty comes from handle leakage through the mounting insulation to one of the electrodes. If significant, this leakage will greatly increase the currents induced in the probe and the resulting field meter reading. A much smaller uncertainty is associated with leakage between the two sensing electrodes, which would reduce the reading of the field meter. The field meter, its handle assembly, and its internal insulation should be kept clean and dry to minimize errors due to leakage currents. The influence of ambient humidity on the performance of field meters can be determined by applying the current injection technique (free-body meters) or voltage injection technique (electro-optic meters) with the field meter in an environmental chamber. The dependence on humidity can be determined by monitoring the field meter response as a function of humidity while holding the injected current (voltage) constant.

Environmental chamber tests of free-body meters with analogue displays have shown that the field meter reading can change by as much as 8% over the temperature range 0°C to 40°C. As for the magnetic field meter case, if extreme differences in temperature are anticipated at a measurement site compared to the temperature at the time of calibration, the effects of temperature should be known or may need to be quantified.

In order to determine the total uncertainty associated with RMS measurements of the electric field strength in different measurement environments, there should be an appropriate accounting of the various sources of uncertainty. Possible sources of uncertainty have been identified above. Many sources of uncertainty can be made negligible or, depending on the type of meter, may not apply in a given measurement situation. In any event, the combined uncertainty of the significant sources of uncertainty should be taken as the square root of the sum of the squares.

### 6.3. The voltage transducer

#### 6.3.1. Operating principle

The voltage transducer relies on the measurement of the electric field irradiated by the considered conductor. To do this, a device based on the schematic block diagram in Figure 6-6 was implemented.

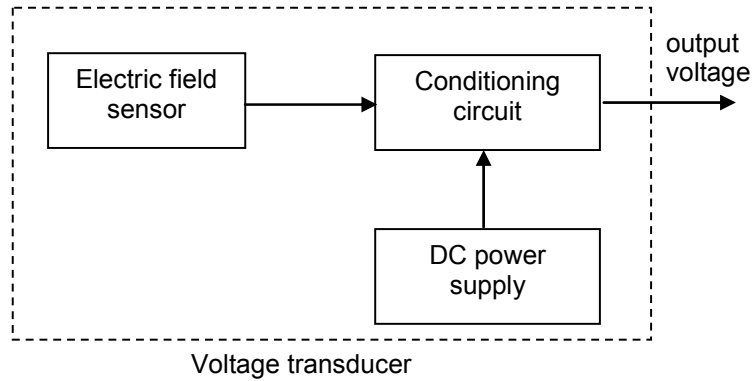


**Figure 6-6** Schematic block diagram of the voltage transducer

It consists in three main elements: a) an electric field probe; b) a conditioning circuit; c) a dc bipolar power source.

According to what reported in previous Section, the electric field sensor can be considered as a “Ground-reference” and “un-isotropic” type. The probe is a metallic surface normal to the incident electric field component and connected to ground through a proper shunt resistance. A current  $i(t)$  flows from the plate draining to ground the free charges cumulated on its surface. As recalled in previous section, in other words  $i(t)$  is proportional to the first derivative of the incident electric field. Moreover, if i) the distance between the conductor and the probe is constant, ii) the dielectric mean interposed between them is fixed and iii) the influence of external electric field sources can be neglected, the current  $i(t)$  can be assumed also proportional to the first derivative of the voltage  $u(t)$  to be measured, i.e. to the source of the electric field:

$$i(t) \propto \frac{du(t)}{dt} \quad (6.8)$$

Therefore, the conditioning circuit integrates  $i(t)$  providing an output voltage proportional to  $u(t)$ . Suitable impedance matching and signal amplification are also operated.

#### 6.3.2. Prototype realization

To fulfil (6.8), three issues must be tackled in designing the transducer prototype: i) ensure the recommended electrical insulation between the transducer and the voltage source; ii) shield the device from other electric field sources; iii) keep constant the distance between the conductor and the sensor.

As for i) the solution adopted consists in placing the voltage transducer into an insulator-like case so that it is installed directly on the conductor (Figure 6-7). This way, also problem iii) is solved given that the distance between the probe and the source is fixed. Moreover, in this conditions also the dielectric interposed between the electric field probe and source is known and stable as far as electrical and environmental influences are concerned.

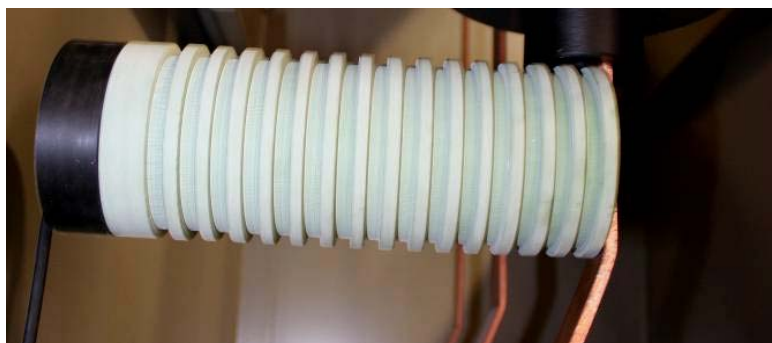


**Figure 6-7** The insulator-like case containing the electric-field based transducer

The same could not be said with air interposed between them, in fact in this case temperature, dirt and humidity, just to give an example of the main environmental factors, can affect strongly the performance of the sensor.

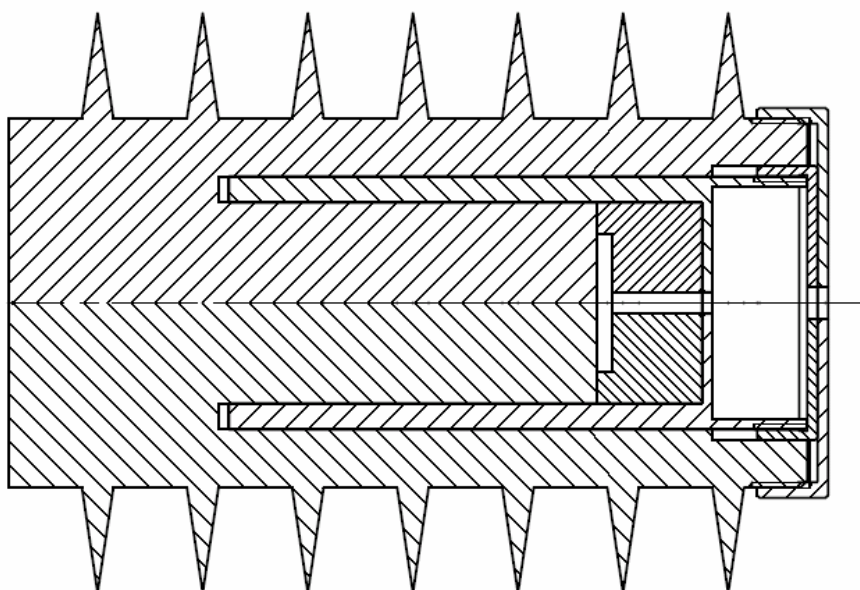


**Figure 6-8** Section of the voltage transducer: the shielded probe and circuit are covered by the insulator-shaped resin.

The insulator was sized for a nominal RMS voltage of 17.5 kV, which is a typical value in Italian distribution networks. In accordance with [8], the corresponding rated insulation level requires to pass tests with a rated lightning-impulse of 95 kV and a power-frequency withstand voltage of 38 kV for 60 s.

As for ii), both the sensor and the conditioning circuit were shielded by a grounded metallic case, included inside the insulator-like one. The shielding box has been provided

with a suitable aperture facing the MV copper bar in order to let only the electric strength lines generated by the source of interest enter the shield.

As far as the conditioning circuit is concerned, the easy principle of operation does not turn into an immediate correct realization of it. First of all, the input buffer has to be chosen with very high input impedance, so that the probe is not loaded and also the value of the shunt resistance in parallel to the input pins is not significantly modified. The gain of the first stadium does not need to be higher than 10, and this improves the stability of the circuit. Since the voltage measured as input is proportional to the first-order time derivative of the primary voltage, the equivalent model of the sequence electric field probe - shunt resistor corresponds to an ideal derivative-operator. Despite, the analog circuit used to obtain the output voltage cannot be an ideal integrator, because any bias currents and offset voltage of the operational amplifier used in the integrator or non-white noise superposed to the input would lead the output to saturation. In fact, the integrator gain increases as frequency decreases, thereby amplifying the low-frequency random noise and zero-frequency offset drift. The integrator gain needs to be reduced for frequencies below which the measurement accuracy is not significantly affected. A large resistor  $R_2$  is put across the capacitor  $C_1$  in order to provide DC feedback for stable biasing. The effect of such configuration is to roll off the integrator action at very low frequencies ( $f < 1/R_2C_1$ ). The transfer function of the integrator shown in Figure 6-9 is given by the following expression:

$$\frac{V_{out}}{V_{in}} = \frac{R_2}{R_1} \cdot \frac{1}{(1 + j\omega R_2 C_1)} \quad (6.9)$$

The integrator design, i.e. the choice of suitable values for  $R_1$ ,  $R_2$  and  $C_1$ , is actually a trade off between gain and integrating pole position. The accuracy of the integration is strongly affected by the value of the integrator pole, placed at  $f=1/2\pi R_1 C_1$ . In this application the pole corresponds to a nominal frequency of 50 mHz, so that the performance of the transducer are not degraded: the phase displacement introduced by the circuit at 50 Hz is lower than 3 mrad. As above explained, an operational amplifier configured to work as integrator greatly attenuates the input AC signal. To compensate such strong reduction of the component of interest, the DC gain of the amplifier, i.e.  $A=R_2/R_1$ , is set equal to 100. A higher value would give rise to wrong results because both the stability of the stadium would not be assessed and the bias components would be too much amplified respect to the AC input signal.

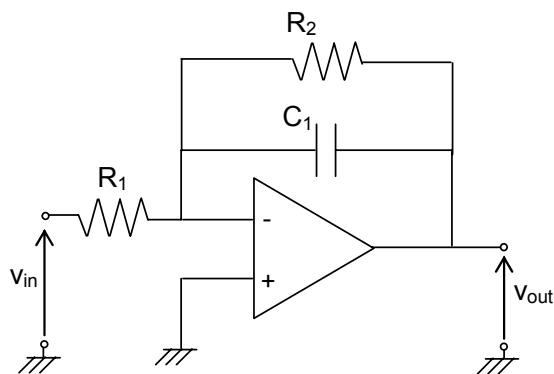


**Figure 6-9** Operational amplifier configured as integrator

Finally, the last amplifier has been used to regulate the overall gain of the conditioning circuit, obtaining a standard rated secondary voltage equal to  $1.625/\sqrt{3}$  V [10], i.e. when the primary phase-to-ground voltage is  $17.5/\sqrt{3}$  kV (phase-to-phase voltage equal to 17.5 kV) the output is  $1.625/\sqrt{3}$  V.

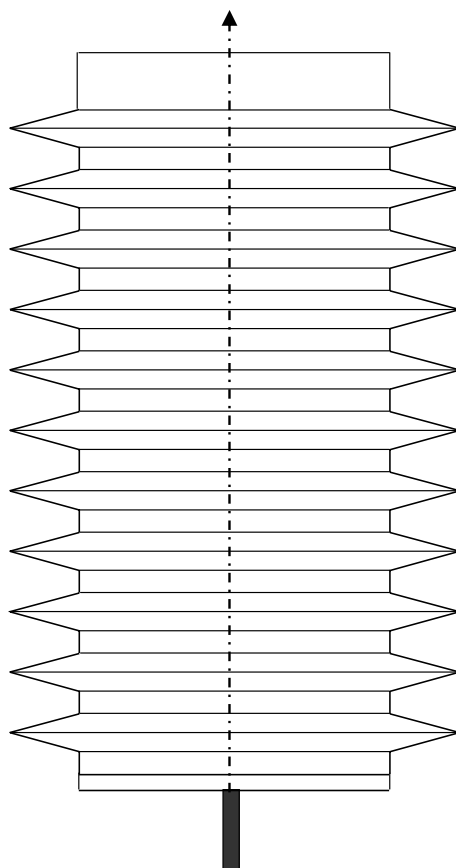


**Figure 6-10** Direction of the electric axis of the field probe, coincident with the geometrical axis of the transducer.

### 6.3.3. Experimental setup

The experimental campaign was programmed to investigate on four main characteristics of the device performance: a) voltage error; b) phase displacement; c) bandwidth; d) immunity to other voltage sources present in any three-phase MV/lv cabin. The relevant setups are described in the following.

### 6.3.3.1. Voltage error

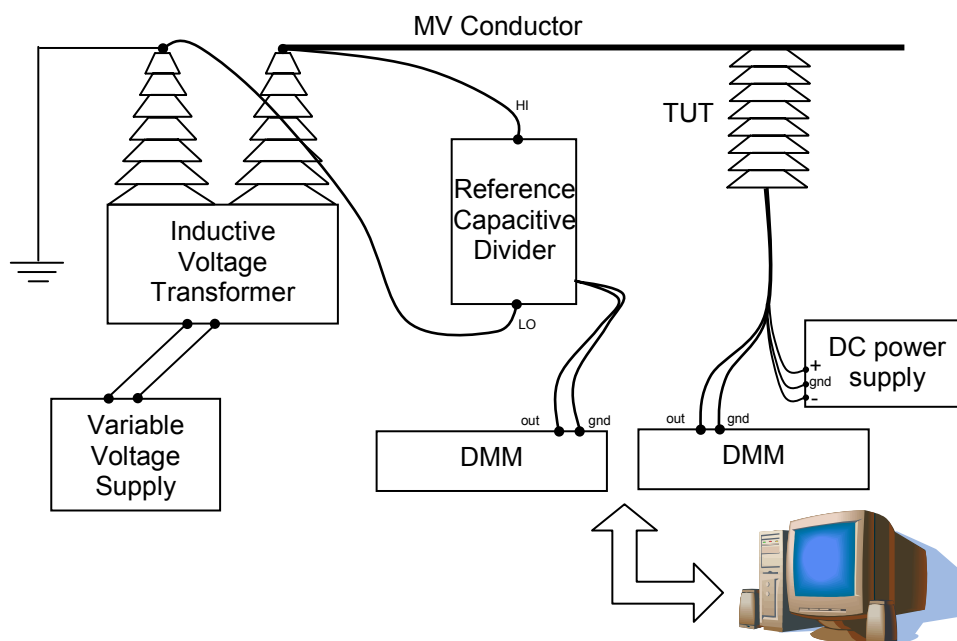


**Figure 6-11** Schematic representation of the circuit for the voltage error evaluation

The circuit shown in Figure 6-11 was implemented, where TUT denotes the voltage transducer under test and DMM an HP 3458A digital multimeter. The DMM nominal accuracy specifications in the considered range  $U_{FS}=10$  V and for  $f=50$  Hz, are  $\alpha=0.09\%$  of reading plus  $\beta=0.06\%$  of range [11].

The low-voltage side of a standard inductive voltage transformer (70 kV/100 V) is supplied with a sinusoidal 50-Hz voltage waveform. The transformer output (high-voltage side) fed both a plain copper bar, where the TUT is installed, and a reference capacitive divider made by Pearson Electronics, i.e. the transducer that should be substituted by the one under test. Its specifications (in oil and into  $1M\Omega$  load) are: nominal ratio = 5000:1, bandwidth = 30 Hz – 4 MHz, droop rate = 0.02% /  $\mu$ s, usable rise-time = 100 ns. The outputs of both the capacitive divider and the TUT were measured by the DMMs, controlled by a personal computer via IEEE 488 interface. The control program configured each DMM to carry out 100 measurements of RMS for every value of the test voltage ( $U_{test}$ ); in order to minimize the random uncertainty contribution of the test bank, the DMM gives as output the mean value of 10 subsequent RMS readings.

**Table 6-1** Measurements of primary and secondary voltages

$U_{test}$ [kV]	$U_{in}$ [kV]	$u(U_{in})$ [kV]	$U_{out}$ [V]	$u(U_{out})$ [V]
2	2.001	0.002	0.1858	0.0002
5	4.977	0.003	0.4619	0.0002
8	8.022	0.006	0.7444	0.0006
10	9.952	0.008	0.9233	0.0007
12	12.008	0.006	1.1133	0.0006

In accordance with Figure 6-11, one hundred measurements of both the TUT and the capacitive divider output were taken for each testing voltage. It must be noted that  $U_{in}$  refers to a phase-to-ground voltage. As a consequence, 10 kV corresponds at a phase-to-phase voltage of about 17.5 kV, which is the rated primary voltage of our device. Table 6-1 shows the obtained results, where  $u(\cdot)$  denotes the standard uncertainty affecting  $(\cdot)$ , evaluated according to [13] by taking into account both the instrument accuracy and the standard deviation of the 100 measurements. On the basis of the tests results reported in Table 6-1, the transformation ratio  $K$  of the transducer to be characterized is computed according to the following expression:

$$K = \frac{U_{out}}{U_{in}} = \frac{U_{out} \cdot K_{nref}}{U_{ref}} \quad (6.10)$$

where  $U_{in, out}$  are the RMS of the voltage signals at the input and output of the TUT, whereas  $U_{ref}$  is the RMS voltage measured at the output of the capacitive divider and  $K_{nref}$  its nominal ratio.

The results obtained for each  $U_{test}$  feature very similar frequency distributions; for example Figure 6-12 reports the 20 classes histogram relevant to  $U_{out}$  measured for  $U_{test} = U_n = 10\text{kV}$ .

According to [8] the voltage error of the transducer under test, expressed in percent, is defined as:

$$\varepsilon_U = \frac{K_n \cdot U_{out} - U_{in}}{U_{in}} \cdot 100 \quad (6.11)$$

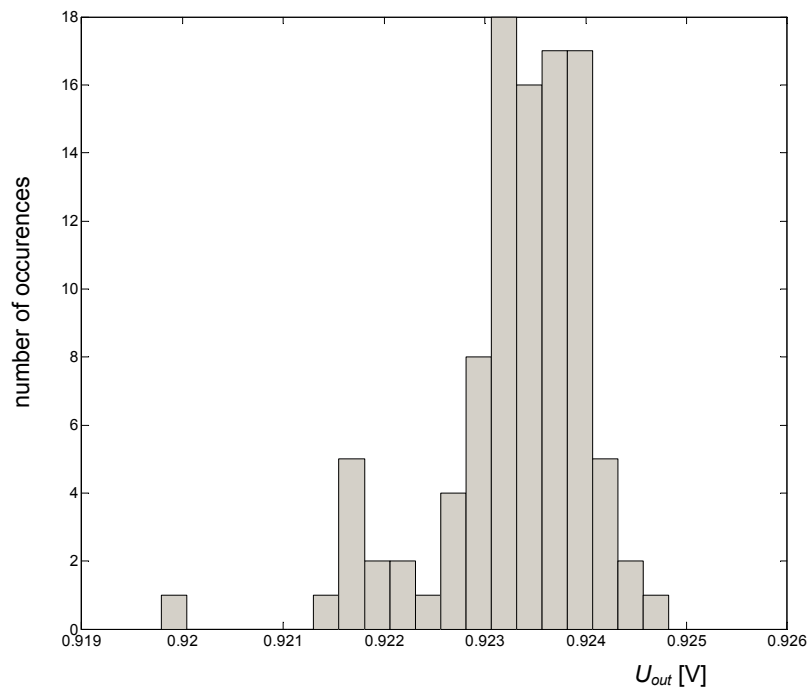


**Figure 6-12** Frequency distribution of the secondary  $U_{out}$  measured for  $U_{test} = U_n$



As it can be drawn from Figure 6-12 the main contribution to  $u(U_{out})$  is due to the experimental standard deviation, i.e. around 80% of the standard uncertainty. Similar considerations hold for all the primary voltages and also for  $u(U_{in})$ .

**Table 6-2** Evaluation of the Voltage Error  $\varepsilon_u$  for the different test voltages.

$U_{test}$ [kV]	$\varepsilon_u$ [%]	$u(\varepsilon_u)$ [%]
2	-0.23	0.06
5	-0.25	0.05
8	-0.27	0.05
10	-0.29	0.04
12	-0.36	0.03

Table 6-2 shows the voltage error values for different primary voltages along with their relevant standard uncertainties  $u(\varepsilon_u)$ . As well known, ISO document [8] classifies voltage transducers according to their accuracy evaluated on the basis of the voltage and phase error. The first one is required to be lower than a given value (according to the accuracy class) for any voltage between 80% and 120% of the rated primary voltage, that is between 8 kV and 12 kV in the case of the prototype under test. Results reported in Table 6-2 lead to conclude that, at least for the voltage error, the transducer can be considered as belonging to class 0.5.

### 6.3.3.2. Phase error

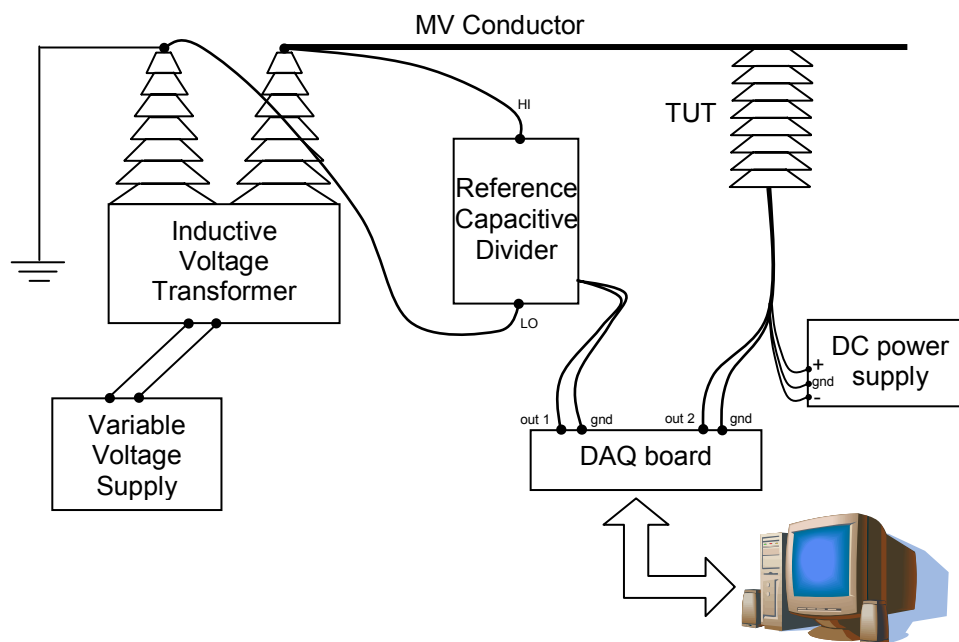


**Figure 6-13** Schematic representation of the circuit for the phase error evaluation

The circuit shown in Figure 6-13 was implemented, where DAQ board refers to a 16-bit digital acquisition board featuring a simultaneous sampling. This way, no additional delay is added to that of the TUT.

The outputs of both the capacitive divider and TUT were simultaneously acquired by the DAQ board. A sampling frequency of 200 kSa/s and an observation interval of 200 ms (40,000 samples) were used. The personal computer ran a simple algorithm to extract the 50-Hz components and to compute the phase error.

The measurement procedure was carried out 1,000 times aiming at taking into account the effect of random contributions to the uncertainty. Fourier analysis was used to extract the 50-Hz components, thus avoiding the contribution of eventual primary voltage distortions. The phase error  $\varphi_u$  is given by [8]:

$$\varphi_u = \varphi_{out} - \varphi_{in} \tag{6.12}$$

**Table 6-3** Results of tests for the phase error evaluation of the TUT

$U_{test}$ [kV]	$\varphi_u$ [mrad]	$u(\varphi_u)$ [mrad]
<b>2</b>	5.23	0.02
<b>5</b>	4.33	0.02
<b>8</b>	3.89	0.03
<b>10</b>	3.21	0.02
<b>12</b>	3.14	0.02

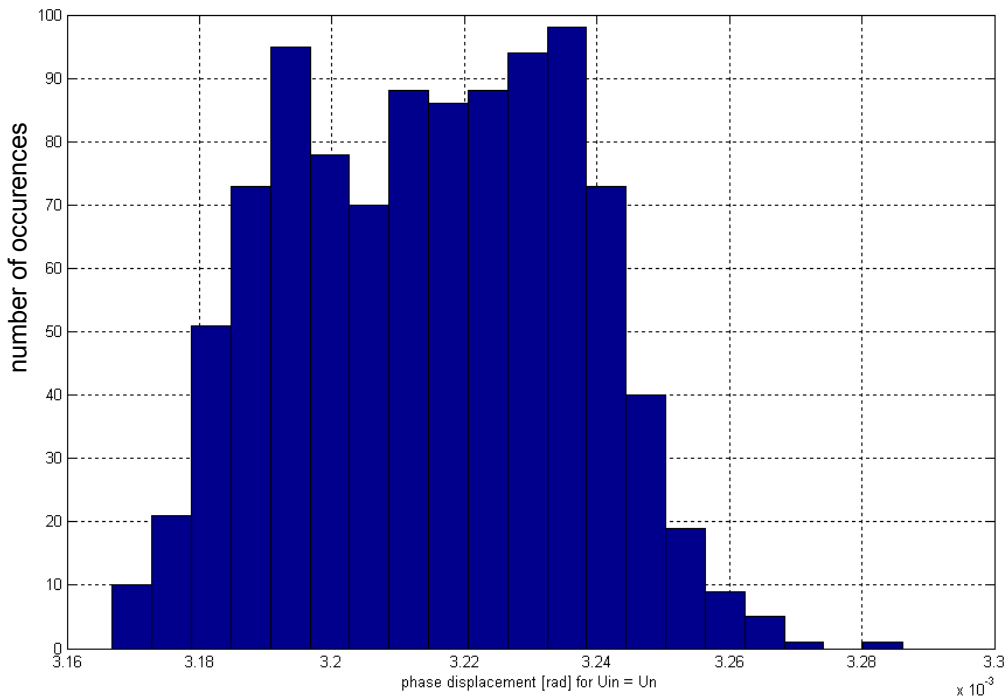


**Figure 6-14** Frequency distribution of the phase displacement between input and output of the TUT obtained in the case of  $U_{test} = U_n = 10$  kV

Table 6-3 shows the obtained values of  $\varphi_u$  along with their relevant standard uncertainties  $u(\varphi_u)$ . As an example, Figure 6-14 is the histogram of the phase displacement measured when  $U_{test} = U_n$ . According to [14], the positive sign of the phase error denotes that the output voltage leads the input one. From the results in Table 6-3, it can be concluded that the proposed transducer belongs to class 0.5 also for phase error, in fact it always holds [8]:  $\varphi_u < 6$  mrad.

### 6.3.3.3. Bandwidth

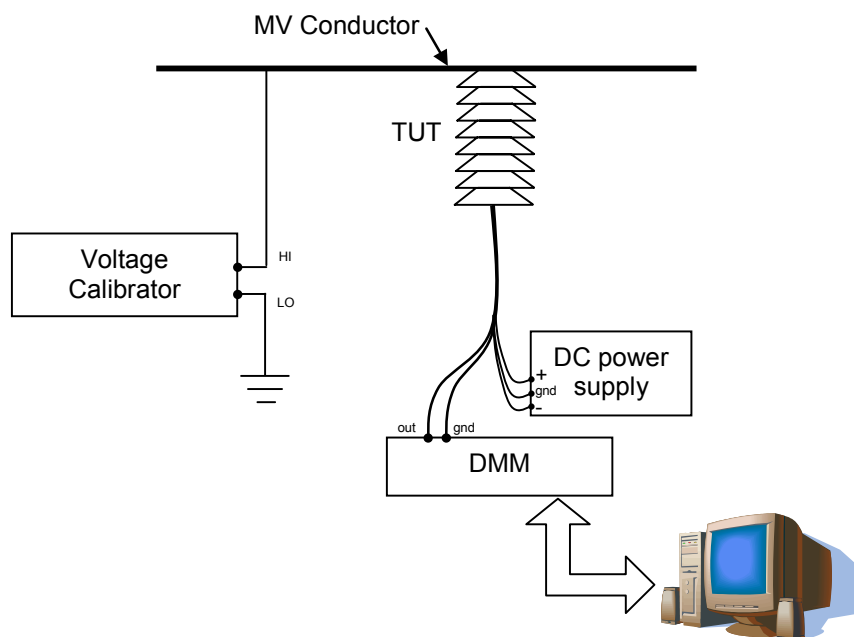


**Figure 6-15** Schematic representation of the circuit for the bandwidth evaluation

The circuit in Figure 6-15 was built up for the TUT bandwidth evaluation. Voltage Calibrator refers to Wavetek Datron 4800A. Its sinusoidal voltage output is  $1000 V_{rms}$  up to 33 kHz and  $100 V_{rms}$  up to 1 MHz. The Calibrator fed the TUT through the MV bar whereas the DMM measured the TUT output voltage. The test have been carried out by varying the frequency of the signal generated by the Calibrator from 10 Hz to 50 kHz, and by measuring 100 times the RMS of the TUT output for each test frequency. The RMS given by the DMM is obtained even in this case as the mean value of 10 measurements carried out automatically by the device itself. The value of the output considered to characterize the transducer ratio versus frequency is the mean value of the 100 RMS measurements corresponding to the same frequency. The parameter to be taken into account is the attenuation of the TUT, i.e.  $A = 1/K = U_{out}/U_1$ , where  $U_1$  is the Calibrator output voltage. The procedure described was implemented automatically by controlling the DMM with the PC. Figure 6-16 is the curve obtained by interpolating the experimental points: it can be seen that the cut-off frequency of the transducer corresponding to -3dB attenuation is around 30 kHz. It should be noted that such a value is coherent with the

estimated bandwidth of the analog circuit used to integrate the signal coming from the electric field probe. In fact, the circuit bandwidth depends on the nominal performance declared for the operational amplifiers and on the DC gain at which each stadium is configured to work. The bandwidth of the transducer seems to be satisfactory wide to the purpose of acquiring line voltages affected by transient disturbances, but in case the cut-off frequency may not be high enough to avoid distortion of the high frequency content of the input signals, a new design of the circuit can be faced in order to improve its performance, featuring the electric field probe no significant limit in the frequency range of interest.

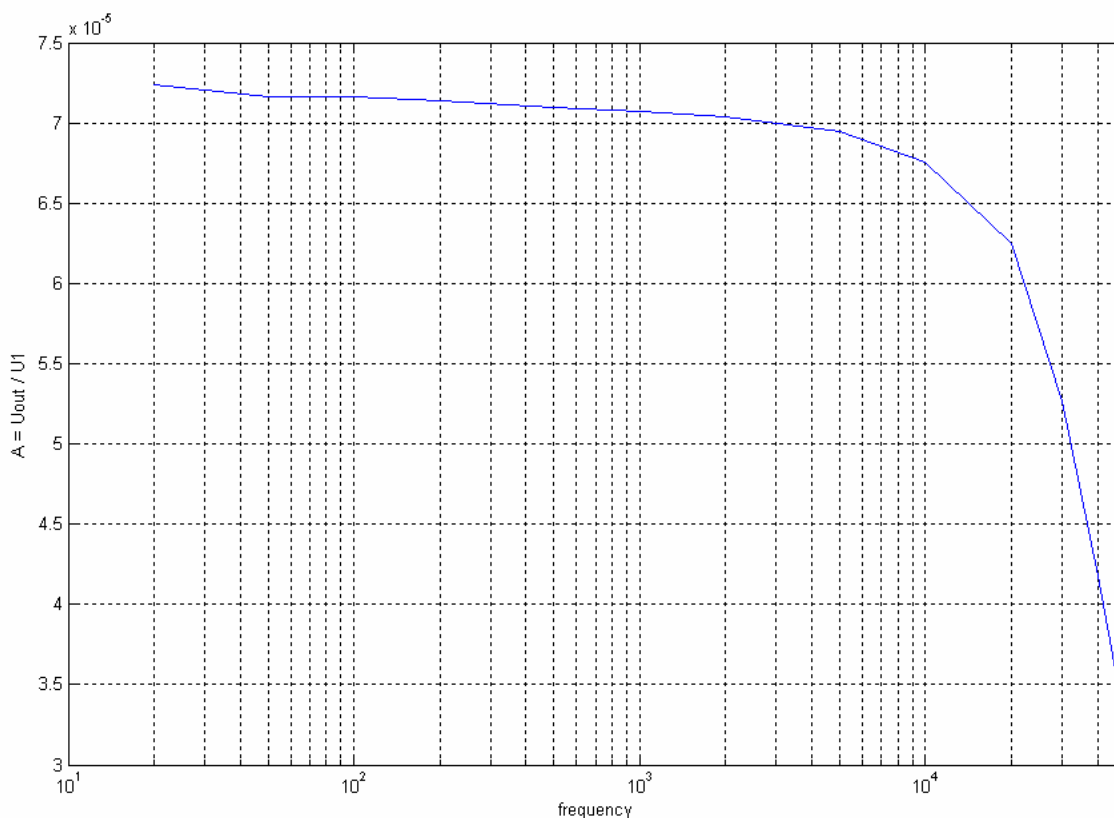


**Figure 6-16** Attenuation  $A$  of the TUT in function of frequency

**Table 6- 4** Experimental results of the bandwidth evaluation of the TUT

Frequency [Hz]	10	20	50	100	200	500	1000
$A (10^{-5})$	7.24	7.16	7.17	7.14	7.10	7.07	7.04
$u(A) (10^{-5})$	0.03	0.02	0.02	0.02	0.02	0.02	0.02

Frequency [kHz]	2	5	10	20	30	40	50
$A (10^{-5})$	6.95	6.66	6.24	5.26	4.17	3.3	2.4
$u(A) (10^{-5})$	0.02	0.02	0.03	0.03	0.03	0.1	0.1

### 6.3.3.4. Immunity to other electric field contributions

The circuit in Figure 6-11 was used, but the position of the TUT with respect to the MV conductor was changed in order to check the influence on the measurement result of voltage sources not aligned with the TUT sensitivity axis. As a matter of fact, due to both the anisotropy of the electric field sensor and the geometry of the shield, the transducer is designed to feature the maximum sensitivity for strength lines normal to the sensor top surface (Figure 6-10).

Figure 6- 17 shows the adopted test configurations. In ideal conditions, positions of the TUT other than the correct one (# 1) should lead to zero output voltage. The procedure to test the sensitivity of the electric field probe to the effect of electric field sources different from the one of interest, i.e. the one positioned in correspondence of configuration #1, has been carried out as follows: the TUT was positioned in one of the other configurations (#2, #3 and #4 in Figure 6- 17) with respect to the MV copper bar connected to the voltage source. For each position of the TUT within the MV cabin, the voltage generated by the Inductive Transformer has been varied from 80% to 120% of the nominal RMS value of the primary voltage. For each level of the primary voltage applied to the bar, the automatic measurement bench carried out 100 RMS measurements of both the primary and the output of the TUT, so that its sensitivity to the electric field generated by the MV conductor is evaluated. Such a parameter has been quantified as the ratio between the output of the TUT reported to the corresponding input value and the primary voltage applied to the bar. As a matter of fact, a complete immunity of the transducer to MV conductors positioned outside the correct area cannot be granted, as it can be seen by considering the results reported in Table 6-5. On the basis of the 100 measurements carried out for each position and test voltage level, the expected value of the sensitivity coefficient as well as its standard uncertainty are evaluated.

**Table 6-5** Expected value of the sensitivity coefficient  $s$  and relevant standard uncertainty measured vs. position of the TUT and MV level applied to the copper bar.

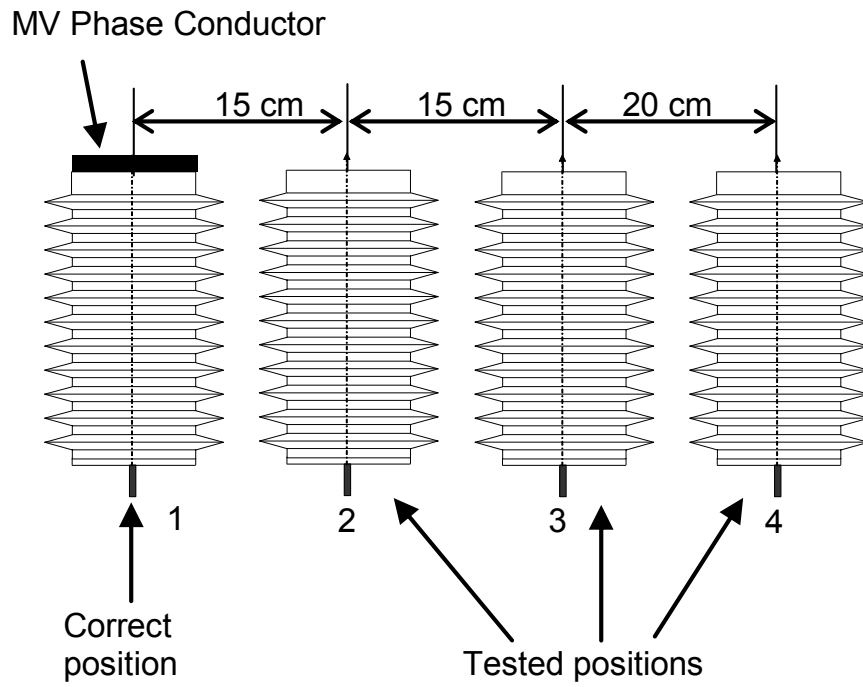
#2	80% $U_{1n}$	100% $U_{1n}$	120% $U_{1n}$
$\mu(s)$	$3.85 \cdot 10^{-2}$	$3.98 \cdot 10^{-2}$	$3.849 \cdot 10^{-2}$
$\sigma(s)$	$1 \cdot 10^{-4}$	$4 \cdot 10^{-4}$	$8 \cdot 10^{-5}$

#3	80% $U_{1n}$	100% $U_{1n}$	120% $U_{1n}$
$\mu(s)$	$1.83 \cdot 10^{-2}$	$1.833 \cdot 10^{-2}$	$1.845 \cdot 10^{-2}$
$\sigma(s)$	$1 \cdot 10^{-4}$	$6 \cdot 10^{-5}$	$3 \cdot 10^{-5}$

#4	80% $U_{1n}$	100% $U_{1n}$	120% $U_{1n}$
$\mu(s)$	$7.8 \cdot 10^{-3}$	$7.8 \cdot 10^{-3}$	$8.6 \cdot 10^{-3}$
$\sigma(s)$	$2 \cdot 10^{-4}$	$1 \cdot 10^{-4}$	$3 \cdot 10^{-4}$



**Figure 6- 17** Position of the TUT with respect to the MV copper bar during sensitivity tests to electric field sources not aligned with the electric axis of the TUT

## References:

- [1] IEC 61000-4-30, "Electromagnetic compatibility (EMC) – Part 4-30: Test and Measurements techniques – Power quality measurements methods";
- [2] Italian Regulator for Electrical Energy and Gas, "Monitoring of voltage quality in medium voltage network" (in Italian), Milano, Italy, July 2005;
- [3] Electricity Working Group: Quality of Supply Task Force, "Third benchmarking report on quality of electricity supply", Council of European Energy Regulators, Bruxelles, Belgium, 2005;
- [4] T.W.Cease, J.G. Driggans, S.J. Weikel, "Optical voltage and current sensors used in a revenue metering system", *IEEE Trans. on Power Delivery*, vol. 6, n. 4, October 1991, pp.1374-1379;
- [5] A. Cruden, Z.J. Richardson, J.R.McDonald, I. Andonovic, W. Laycock, A. Bennett, "Compact 132 kV combined optical voltage and current measurement system", *IEEE Trans. on Instrumentation and Measurement*, vol. 47, n. 1, February 1998, pp. 219-223;
- [6] F.Rahmatian, P.P Chavez, N.A.F. Jaeger, "230 kV optical voltage transducers using multiple electric field sensors", *IEEE Trans. on Power Delivery*, vol. 17, n. 2, April 2002, pp. 417-422;
- [7] C.Svelto, R. Ottoboni, A.Ferrero, "Optically-supplied voltage transducer for distorted signals in High-Voltage systems", *IEEE Trans. on Instrumentation and Measurement*, vol. 49, n. 3, June 2000, pp. 550-554;
- [8] IEC Std. 60044-7, "Instrument transformers Part 7: Electronic voltage transformers", International Electrotechnical Commission, Geneva, CH, 1999;
- [9] IEEE Std. 644-1994, "IEEE Standard Procedures for Measurement of Power Frequency Electric and Magnetic Fields From AC Power Lines", The Institute of Electrical and Electronics Engineers, NY, USA, 1995;
- [10] IEEE Std. 1308-1994, "IEEE recommended practice for instrumentation: specifications for magnetic flux density and electric field strength meters-10 Hz to 3 kHz", The Institute of Electrical and Electronics Engineers, NY, USA, 1995;
- [11] Hewlett Packard, "HP3458A User Manual", September 1988.
- [12] IEC Std. 60050-321, "International Electrotechnical Vocabulary (IEV) - Chapter 327: Instrument transformers", International Electrotechnical Commission, Geneva, CH, 1986;
- [13] ISO "Guide to the expression of uncertainty in Measurement", International Standardization Organization, Geneva (Switzerland), 1995;
- [14] IEC Std. 60050-321, "International Electrotechnical Vocabulary (IEV) - Chapter 327: Instrument transformers", International Electrotechnical Commission, Geneva, CH, 1986.





## 7. Conclusions

The present work is relevant to measurements for power quality evaluation, in particular the subject is a distributed measurement system to be installed in Medium Voltage distribution networks. The system is designed to monitor continuously the power system signals in strategic points and to detect in real time the non periodic disturbances affecting line voltages. At any occurrence of an electromagnetic transient, the remote measurement stations installed in the network nodes register the instant corresponding to the beginning of the disturbance on each voltage, i.e. the arrival time of the transient propagating along the various lines. Such information are then used to estimate the position of the source of the transient disturbance within the monitored power system.

The research activity has been firstly focused on studying an approach to estimate the position of the transient source, then to design the distributed measurement system that could allow reliable detection and time referring process of such disturbances. Once the hardware belonging to each input channel of the three phase remote stations was chosen, the method has been tested by means of simulations.

The first simulations were aimed at verifying the performance of the fault location method considered as working in ideal operating conditions, and thus deduce the accuracy and the limits of the procedure itself. Then, a second simulation campaign has been carried out with the purpose of testing the procedure in actual conditions of the power system; the fault type, position and parameters were systematically varied, as well as the configuration of loads and lines. The results obtained case by case have been used to both improve the algorithm robustness and above all to analyze the performance of the method in actual applications.

In the light of the good performance featured by the developed method, an alternative algorithm has been developed and tested to reduce drastically the number of measurement units to be installed on the monitored power system. In particular, the lack of information on the propagation times of the transient event has been compensated by analyzing with time-frequency mathematical tools the voltage waveforms acquired at its occurrence in the monitored nodes.

In order to complete the research activity on the developed system, the measurement hardware has been characterized by means of experimental tests. All the uncertainty contributions that can affect the result of the procedure have been taken into account. In this sense, the metrological characterization of each block of the measurement chain has been used to estimate the combined uncertainty affecting the position of a fault implementing a numeric statistic approach.

## 7. CONCLUSIONS

---

Finally, in order to reduce the global cost of the studied distributed measurement system, a Medium Voltage transducer based on an electric field sensor has been developed, realized and characterized in order to check if there was the opportunity to substitute the more expensive capacitive voltage divider present in the conditioning block at the input of each channel of every measurement station.